FRA/ORD-76/305

DESIGN AND TESTING OF A 12,000 KVA LINEAR INDUCTION MOTOR AND POWER CONVERTER

J. COLMERY
R. DAY
G. KALMAN
S. MITCHELL

RELEASED
JUNE 1977

FINAL REPORT

Prepared for

U.S. DEPARTMENT OF TRANSPORTATION

FEDERAL RAILROAD ADMINISTRATION
Office of Research and Development
400 Seventh Street, SW
Washington, DC 20590

Technical Report Documentation Page

1. Report No.	2. Government Accession No.	3. Recipient's Catalog No.
FRA/ORD-76/305		

4. Title and Subtitle	5. Report Date
DESIGN AND TESTING OF A 12,000 KVA LINEAR INDUCTION MOTOR AND POWER CONVERTER	June 1977
	6. Performing Organization Code: 70210
7. Author(s): G. Kalman, J. Colmery, R. Day, S. Mitchell	8. Performing Organization Report No.: 76-12916
9. Performing Organization Name and Address: AiResearch Manufacturing Company of California, 2525 West 190th Street, Torrance, CA 90509	10. Work Unit No. (TRAIS)
	11. Contract or Grant No.: DOT-FR-40016
12. Sponsoring Agency Name and Address: U.S. Department of Transportation, Federal Railroad Administration, Office of Research and Development, 400 Seventh Street, SW, Washington, DC 20590	13. Type of Report and Period Covered: Final, July 1970 to April 1976
	14. Sponsoring Agency Code

15. Supplementary Notes

16. Abstract

This report presents pertinent technical data on the design, development, fabrication, and testing of the linear induction motor propulsion system (LIMPS). The LIMPS is designed to convert constant-voltage, constant-frequency, 3-phase, 60-Hz, 8250-V, wayside electrical power to a variable-voltage, variable-frequency output, to power an integral linear induction motor capable of providing to 33,300 N (7600 lbf) propulsive thrust at speeds up to 134 m/s (300 mph). The LIMPS produces continuously variable thrust in the forward and reverse directions, and includes such features as automatic startup, regenerative braking, and automatic failure/malfunction detection and shutdown. Further, the system incorporates high-voltage, water-cooled components to achieve a power density of more than 0.67 kW/kg (0.3 kW/lb).

The LIMPS program comprised three major phases: design/development, static test, and field test. This report describes the events and results of each program phase. Measured performance results are compared with theoretical results for field test data obtained during pulsed-mode tests, start-to-run-mode transition tests, low-speed braking tests, reaction rail temperature-rise tests, and LIMPS influence on the wayside power system tests.

17. Key Words	18. Distribution Statement
Linear induction motor (LIM) Tracked levitated research vehicle (TLRV) Ground transportation Propulsion system Power conversion	Document is available to the public through the National Technical Information Service, Springfield, Virgina 22151

19. Security Classif. (of this report)	20. Security Classif. (of this page)	21. No. of Pages	22. Price
UNCLASSIFIED	UNCLASSIFIED	237	

Form DOT F 1700.7 (8-72) Reproduction of completed page authorized

PREFACE

This report presents pertinent technical data on the design, development, fabrication, and testing of the linear induction motor propulsion system (LIMPS), developed by the AiResearch Manufacturing Company for the Federal Railroad Administration, Department of Transportation. The LIMPS is designed to convert constant-voltage, constant-frequency, 3-phase, 60-Hz, 8250-V, wayside electrical power, to a variable-voltage, variable-frequency output, to power an integral linear induction motor capable of providing up to 33,300 N (7500 lbf) propulsive thrust at speeds up to 134 m/s (300 mph). The LIMPS produces continuously variable thrust in the forward and reverse direction, and includes such features as automatic startup, regenerative braking, and automatic failure/malfunction detection and shutdown. Further, the system incorporates high-voltage, water-cooled components to achieve a power density of more than 0.67 kW/kg (0.3 kW/lb).

Basically, the LIMPS comprises two major subsystems: (1) a high power density, multimegawatt power conditioning unit (PCU), and (2) a linear induction motor (LIM). The former functions as a variable-voltage, variable-frequency power supply, with potential applications for both LIM electric propulsion as well as ac electric traction systems. In line with this dual capability the overall program objectives are to:

- Develop multimegawatt solid-state power conversion equipment, capable of supplying ac electric machines over a wide speed range.
- Demonstrate that ac propulsion systems are viable alternatives, in terms of performance, to conventional dc traction equipment.
- Demonstrate the feasibility and practicability of line-commutated, as opposed to field-commutated, inverters as variable-frequency

power supplies for large ac induction (asynchronous) motors, for both the linear and rotary versions.

- Investigate the compatibility of the ac propulsion system with the wayside electrified power system.
- Establish a technical base on which a policy decision can be made regarding choice of ac propulsion systems for the next generation of ground transportation equipment.

To provide a better perspective of these objectives the background of the overall program is briefly described below.

Interest in linear induction motors as possible propulsion means for modern railway equipment was shown relatively early by the Department of Transportation. A study[1]* program was funded in 1966 to determine the feasibility of using such motors for high speed ground transportation. By 1969 a special test vehicle, the linear induction motor research vehicle had been built and tested at low speed.[2] The vehicle was moved to the Transportation Test Center, Pueblo, CO, a government facility established for testing ground transportation vehicles and associated propulsion systems. Subsequently the LIMRV has been operated at speeds up to 113.5 m/s (254 mph) and has provided a wealth of baseline data on the operation of such systems.[3]

As the LIMRV program progressed, interest in the LIM and the associated power conversion equipment widened and therefore a second generation LIM was developed. This new LIM and the associated propulsion system operated from high-voltage, fixed-frequency, wayside electrical power. Coincident with this interest in electrical propulsion systems, DOT was already developing a vehicle intended as a primary test bed for air cushion and high-speed vehicle

*Numbers in parentheses denote References, which are listed at the end of this program summary.

suspension research. In the interest of economy and shortened development time it was decided to configure the new LIMPS[4] to interface with the new air cushion vehicle, which became known as the tracked levitated research vehicle (TLRV).[5] A companion development was the wayside power system[6] to feed the LIMPS.

The LIMPS program began in mid-1970. By early 1976, with only a 500-m long electrified guideway completed, field testing at TTC commenced, but principally due to a shift in emphasis on air cushions and high-speed vehicles, further LIMPS development was restricted and testing was limited to low speed. Because of this waning interest in the test bed vehicle the TLRV program was halted by mid-1976. This, however, did not imply lack of interest in the LIMPS concept. In fact the TLRV operation was continued beyond its planned termination just to allow limited LIMPS field tests. All of the above-mentioned LIMPS program objectives could not be demonstrated due to the limitations imposed by the curtailment of the TLRV program. However, the field test did demonstrate satisfactory operation of the LIMPS in all operating modes. Though testing was limited, propulsive thrust greater than 20,000 N (4500 lbf) was attained as low-speed performance data was acquired. The LIMPS tests confirm the effectiveness of the variable-voltage, variable-frequency concept; and as a consequence, this type of large, multimegawatt power conversion equipment continues to be of considerable interest for the more conventional transportation system.

The LIMPS program comprised three major phases: design/development, static test, and field test. This report describes the events and results of these three program phases.

REFERENCES

(1) C.H. Lee, "Study of Linear Induction Motor, Its Feasibility for High-Speed Ground Transportation, "U.S. Clearinghouse, Springfield, VA, Rep. PB-174886.

(2) NTIS Report No. FRA-RT-73-2-5, "Final Report, Linear Induction Motor Research," October 1971.

(3) NTIS Report No. FRA-OR&D 76-165, "LIM Electrical Performance Test," March 1976.

(4) NTIS Report No. FRA-RT-72-35, "Development and Manufacture of a Linear Induction Motor Propulsion System for the Tracked Air Cushion Research Vehicle," April 1971.

(5) G. Grubelich, "Tracked Air Cushion Research Vehicle Design and Test Plan," presented at the AXCE/ASME National Transportation Engineering Conference, Seattle, Washington, July 1971.

(6) NTIS Report No. FRA-ORD&D 74-25, "Design, Development and Test of a Wayside Power Distribution and Collection System for the Tracked Levitated Research Vehicle," April 1974.

CONTENTS

Section		Page
1	SYSTEM DESIGN	1
	Operation	5
	START Mode	7
	RUN Mode	7
	BRAKE mode	8
	Primary Controls	8
	Thrust Loop	12
	Jerk Limit	12
	Inverter Regulator	12
	Absolute Value Circuit	12
	Current Regulator	13
	Speed Error	13
	Field Current Command	13
	Direction Command	14
	Frequency and Current Zero Detectors	14
	Sequence Change	16
	Start Logic	17
	Current Zero Cycle	17
	Protection Circuitry	18
	Performance	19
	Reactive Power	19
	Real Power	19
	Maximum Power Envelope	20
	System Mass (Weight)	20
	Schematic/Wiring Diagram	20
	Subsystems and Components	24
	Linear Induction Motor	24
	Synchronous Condenser and Field Power Supply	29
	Phase Delay Rectifier, Inductor, and Inverter	39
	Phase Delay Rectifier	39
	Inductor	39
	Inverter	42
	Load Break Switch	44
	Auxiliary Power Transformer	44
	Controls, Displays, and Instrumentation	47
	Cooling System	51
2	MOCKUP ASSEMBLY	66
3	STATIC TEST INTRODUCTION	71
	Objective	71
	Conclusions	71

CONTENTS (Continued)

Section		Page
4	TEST FACILITIES	74
	Data Acquisition	74
	Instrumentation	79
	Voltage	79
	Current	79
	Flow	79
	Thrust	79
	Vibration	80
	Temperature	80
	LIM Frequency	80
	Power	80
	Reactive VA	80
	Data Display/Presentation	80
	Problems	82
5	TESTS PERFORMED	84
	Preliminary Subsystem Tests	84
	Cooling System	84
	Instrumentation and Control System	87
	PCU Control and Protection System	87
	System Tests at 480 V	87
	Basic No-Load Testing	87
	Operation in Brake Mode	88
	Deceleration Testing	88
	System Tests at 4160 V	97
	Tests with LIM Disconnected	97
	No-Load, High-Speed Testing	97
	Speed Limit Mode Testing	102
	Locked-Rail Testing	102
	Run No. 1	106
	Run No. 2	106
	Run No. 3	108
	Run No. 4	108
	Locked-Rail Tests with External Resistors in Series with the LIM	117
	System Tests at 8250 V	119
	Test Statistics	131
6	FIELD TEST INTRODUCTION	132
	Test Progression	133
	Pulsed Mode Tests	133
	Start/Run Transition Tests	133
	Performance Tests	134

CONTENTS (Continued)

Section		Page
	Background	134
	Objectives	135
	System Performance during Start Mode	135
	System Performance during Start-to-Run Transition	136
	Low-Speed Run-Mode Performance	137
	Low-Speed Braking Characteristics	139
	Influence of Vehicle Operation on Wayside Power System	139
	Temperatures and Cooling System Performance	140
	Conclusions	140
7	TEST FACILITIES	143
	Vehicle Facilities	143
	Wayside Electric Power System Facilities	145
8	DATA ACQUISITION AND PROCESSING	148
	Instrumentation	148
	Data Acquisition	148
	Data Van Equipment	158
	Data Acquired	159
	Data Processing	161
	Instrumentation Accuracy	161
	Instrumentation Description	161
	Current Measurements	161
	Voltage Measurements	163
	LIM Thrust Parameters	163
	Temperature Measurements	164
	Vibration Measurements	164
	Current Measurement Accuracy	164
	Voltage Measurement Accuracy	165
	Thrust Measurement Accuracy	170
	Temperature Measurement Accuracy	171
	Power and Reactive Power Measurement Accuracy	171
9	DATA ANALYSIS	173
	Pulsed-Mode Tests	173
	Inverter Commutation	173
	Pulsed-Mode Performance	178
	Synchronous Condenser Filtering Capability	184
	Starting Time	185

CONTENTS (Continued)

Section		Page
	Start-to-Run-Mode Transition Tests	189
	Successful Transition	189
	Effects Encountered during Transition Tests	189
	Insufficient Synchronous Condenser Speed	191
	LIM Propulsion System Reversion to Pulsed Mode	191
	Transition Followed by Commutation Failure and Quick Shutdown	191
	Inverter Firing with Respect to the Synchronous Condenser Rotor Position	194
	Run-Mode Tests	196
	Steady-State Performance	196
	Run Profiles	204
	Synchronous Condenser Filtering Capability	218
	Synchronous Condenser Grounding	218
	LIM Performance	218
	Low-Speed Braking Tests	222
	Electrical Braking Characteristics	222
	Regenerative Braking	222
	Dynamic Braking	224
	Reaction Rail Temperature Rise Tests	226
	Summary	226
	Test Conducted	226
	Reaction Rail Temperature Rise	227
	Measured Temperature Rise	227
	Calculated Temperature Rise	231
	Tests Related to the Wayside Power System	234
	Conducted EMI	234
	Radiated EMI	234

ILLUSTRATIONS

Figure		Page
1-1	LIMPS Installation in Tracked Levitated Research Vehicle	3
1-2	LIMPS Block Diagram	4
1-3	LIMPS Simplified Schematic Diagram	6
1-4	Control System Functional Schematic Diagram	9
1-5	Propulsion Logic Functional Block Diagram	10
1-6	Field Current Command Schedule	15
1-7	Power Conditioning Unit Power Envelope	21
1-8	LIMPS Electrical Schematic Wiring Diagram	23
1-9	Linear Induction Motor	26
1-10	Predicted LIM Performance	30
1-11	Synchronous Condenser	32
1-12	Field Power Supply	38
1-13	Phase Delay Rectifier	40
1-14	Brooks Coil Inductor	40

Figure		Page
1-15	PDR/Inverter Thyristor Module	43
1-16	Inverter	45
1-17	Static Test Mockup Showing Component Locations	45
1-18	Load Break Switches	46
1-19	TLRV Cockpit Controls/Displays	49
1-20	Typical Control/Instrumentation Cabinet Drawers	50
1-21	LIMPS Liquid Cooling System Schematic	62
1-22	Cooling System Components	63
2-1	PCU Compartment Mockup	68
2-2	PCU Mockup Awaiting Shipment	68
2-3	Cooling System Plumbing Layout	69
2-4	PCU Mockup during Trial Fitting of Cooling System Plumbing	69
2-5	PCU Mockup in Test Cell	70
4-1	Mockup with LIMPS Components Installed in the Test Cell during Static Tests	75
4-2	Facility Power Distribution	76
4-3	LIMPS Data Acquisition System	77
4-4	Typical Computer Program Printout of Power Flow Diagram	83
5-1	Facility Deionization System	85
5-2	System 480-V Test Setup	87
5-3	Inverter Output Voltage (Frequency = 10.4 Hz)	89
5-4	SC Performance, 480-V No-Load (No Rail) Test	90
5-5	Coast Mode Test at 480 V	92
5-6	Brake Mode Test at 480 V	94
5-7	Synchronous Condenser Deceleration	96
5-8	System 4160-V Test Setup	98
5-9	Ninety-Four Percent Synchronous Speed Test	99
5-10	Synchronous Condenser Frequency vs Field Current	103
5-11	Speed Limit Mode Test, No Load	104
5-12	Reaction Rail Cooling System Flow Diagram	107
5-13	Quick Shutdown Immediately Following Transition	114
5-14	Transition Mode Oscillogram Showing Quick Shutdown	115
5-15	Successful Transition From Start Mode to Run Mode, 1.2-Ohm External Resistors	120
5-16	Run Mode, 31.7-mm (1.25-in.) Airgap, 1.2-Ohm External Resistors	121
5-17	Run Mode, 38.1-mm (1.5-in.) Airgap, 0.6-Ohm External Resistors	122
5-18	System 8250-V Test Setup	125
5-19	Successful Test Run at 8250 V without External Resistors	127
5-20	System 8250-V Test, Commutation Failure	129
7-1	LIM Air Supply Characteristics	144
7-2	Overall LIMPS-Supply Electrical Schematic	146
7-3	Wayside Power Collector Engaged in the Wayside Power Rails	147

Figure		Page
8-1	Simplified Schematic of LIMPS, Showing Key Elements and Instrumentation	162
8-2	Resistive Voltage Divider Equivalent Circuit	167
9-1	Start Mode Control Logic Block Diagram	174
9-2	Inverter Commutation, Pulsed Mode	176
9-3	Inverter Voltage and Current Phase Relation during Start Mode	177
9-4	Dc Link Current Waveshape, Pulsed Mode	179
9-5	Pulsed-Mode Performance Data, 50-Percent Thrust Command	180
9-6	Pulsed-Mode Performance Data, 90-Percent Thrust Command	181
9-7	LIMPS Power Flow Diagram, Pulsed Mode	183
9-8	Synchronous Condenser Filtering Capability, Pulsed Mode	185
9-9	LIMPS Dynamic Response during Start Mode	188
9-10	Start-to-Run-Mode Transition Performance Data	190
9-11	Reversion-to-Pulsed-Mode Performance Data	192
9-12	Commutation-Failure-after-Transition Performance Data	193
9-13	Thrust Command Transfer Function	197
9-14	Run-Mode Steady-State Performance, 100-Percent Thrust Command	199
9-15	Run-Mode Steady-State Performance, 50-Percent Thrust Command	200
9-16	Inverter Delay Angle, Dc Link Current Transfer Function	202
9-17	Normalized Dc Link Current as a Function of Overlap Angle	203
9-18	LIMPS Power Flow Diagram, 100-Percent Thrust Command	205
9-19	LIMPS Power Flow Diagram, 50-Percent Thrust Command	206
9-20	LIMPS Efficiency	207
9-21	Typical Thrust Command Settings	208
9-22	Typical Speed Profiles	209
9-23	Typical Dc Link Current Profiles	210
9-24	Typical Elapsed Time Profiles	211
9-25	Typical Corrected Thrust Profiles	212
9-26	Typical Acceleration Profiles	213
9-27	Typical Dc Link Power Usage	214
9-28	Typical LIM Power Usage	215
9-29	Typical LIM Reactive Power Usage	216
9-30	Typical Synchronous Condenser Reactive Power Usage	217
9-31	Synchronous Condenser Filtering Capability, Run Mode	219
9-32	Synchronous Condenser Neutral-to-Ground Voltage	220
9-33	LIM Thrust Performance Data	221
9-34	Regenerative Braking	223
9-35	Dynamic Braking	225
9-36	Reaction Rail Temperature Rise vs Thrust Command	228
9-37	Strip Chart Record of Reaction Rail Temperature	229
9-38	Phase Delay Rectifier Current Harmonics	235
9-39	LIMPS Broadband Radiated Emissions	237

TABLES

Table		Page
1-1	LIMPS Specification at Design Point	2
1-2	Inverter Operating Sequences	16
1-3	LIMPS Mass (Weight)	22
1-4	LIM Design Data	25
1-5	Synchronous Condenser Design Data	31
1-6	Field Power Supply Characteristics	37
1-7	PDR and Inverter Design Data	41
1-8	Inductor Characteristics	42
1-9	LIM Parameters Available for Recording	52
3-1	LIMPS Static Tests Summary	72
5-1	Partial Summary of 4160-V, No-Load System Tests	101
5-2	Partial Summary of 4160-V, Locked-Rail System Tests	110
5-3	Partial Summary of 4160-V, Locked-Rail System Tests with External Resistors in Series with LIM	118
5-4	Static Test Statistics	131
8-1	Digital Instrumentation	149
8-2	Parameters Available for Analog Recording	156
8-3	Oscillograms Acquired	160
8-4	Current Parameters Accuracy	166
8-5	PDR Net Transformer Voltage Ratio Measurements	169
8-6	Voltage Parameters Accuracy	170
8-7	Three-Sigma Deviation from Line of Best Fit for LIM Thrust Calibration	171
8-8	Temperature Measurement Accuracy	171
8-9	Accuracy of Power and Reactive Power Measurements	172
9-1	Inverter Firing Order	175
9-2	Power Analysis (Run 221, Thrust Command 50 Percent)	184
9-3	Pulsed-Mode Harmonic Content (Run 221, Thrust Command 50 Percent, Frequency 1.5 Hz)	187
9-4	LIMPS Run-to-Start-Mode Transition Criteria	191
9-5	Parameters with Test Range Limited	196
9-6	Parameters with Test Range Near Rated Values	198
9-7	Inverter Commutation Margin Requirements	201
9-8	Typical Acceleration Performance Summary	204
9-9	Measured Reaction Rail Temperature Rise	230
9-10	Measured Reaction Rail Temperature Data	231

SECTION 1

SYSTEM DESIGN

During the initial design phase of the program the linear induction motor propulsion system (LIMPS) was conceived as comprising two basically identical propulsion system modules, each utilizing its own autonomous linear induction motor and power conditioning unit, but sharing certain other common ancillary subsystems/components. In implementing this approach it was deemed judicious to proceed, at first, with only one of the propulsion system modules (i.e., a "half-system") and acquire the second module when the test results and program requirements would justify such action. The design described herein was, thus, composed solely of hardware incident to a half-system configuration. Principal design point specifications of the LIMPS, with the half-system configuration, are summarized in Table 1-1.

Most of the system components were installed in the body of the test bed vehicle. The power conditioning unit and most of the associated ancillary subsystems were accommodated in the 2.3 by 4.4 by 1.5 m (92 by 172 by 58 in.) equipment bay, with sufficient room left for onboard maintenance and repair. The LIM was fitted to the vehicle chassis. Figure 1-1 shows the general arrangement of the hardware, as fully installed. All parts illustrated are components of the LIMPS. Figure 1-2, a simplified block diagram, shows the general functional arrangement of the components. The LIMPS comprises:

One linear induction motor (LIM)

One synchronous condenser (SC)

One synchronous condenser field power supply (FPS)

One static inverter (INV)

One Brooks coil inductor (IND)

One static phase delay rectifier (PDR)

TABLE 1-1

LIMPS SPECIFICATION AT DESIGN POINT

Parameter	Value
Propulsive thrust	22,000 N (5000 lbf)
Rated speed	135 m/s (300 mph)
Output power	2970 kW (4000 hp)
Input power	4200 kW
Input power factor	94 percent
Design point efficiency	80 percent

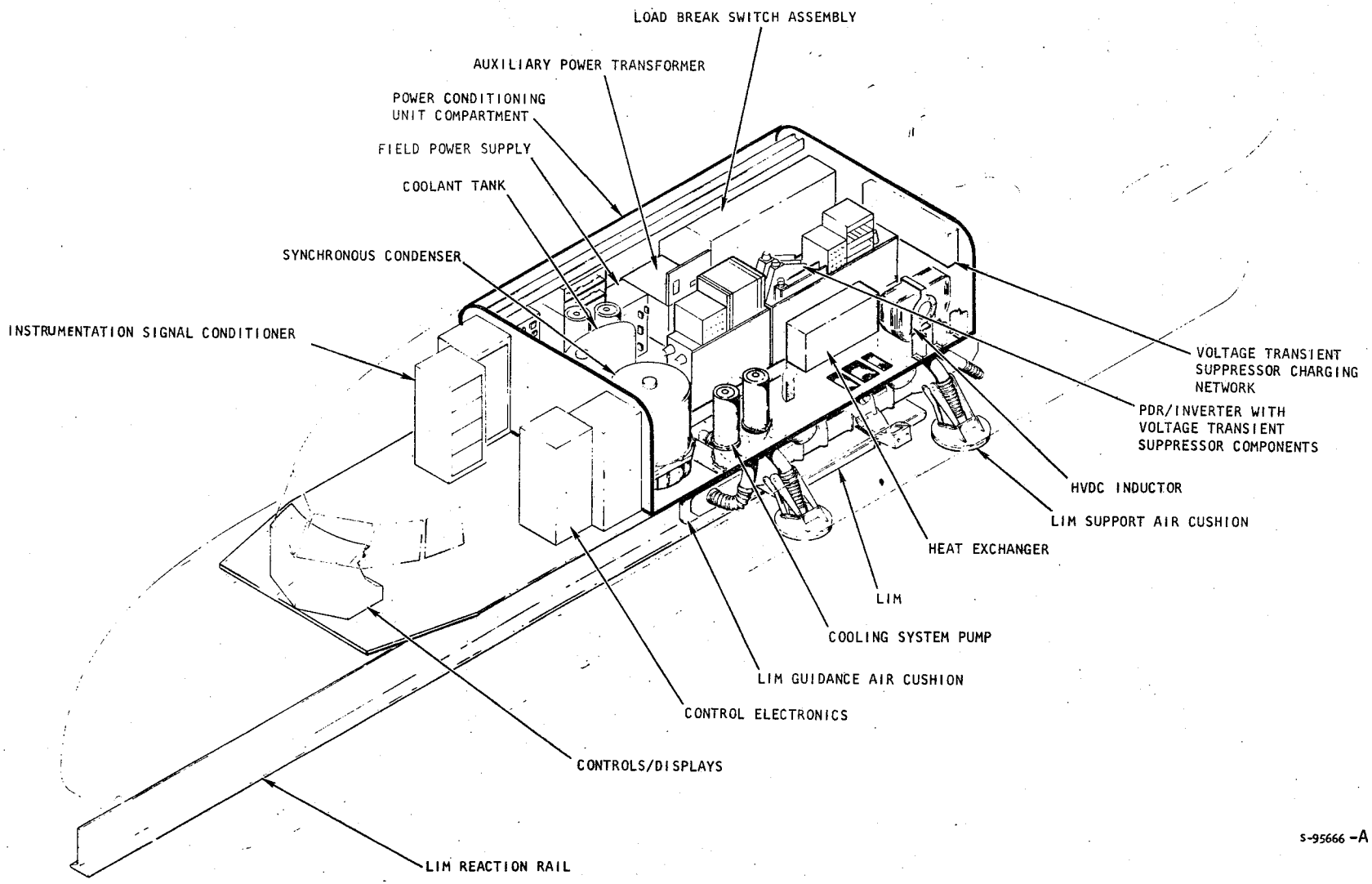

Figure 1-1. LIMPS Installation in Tracked Levitated Research Vehicle

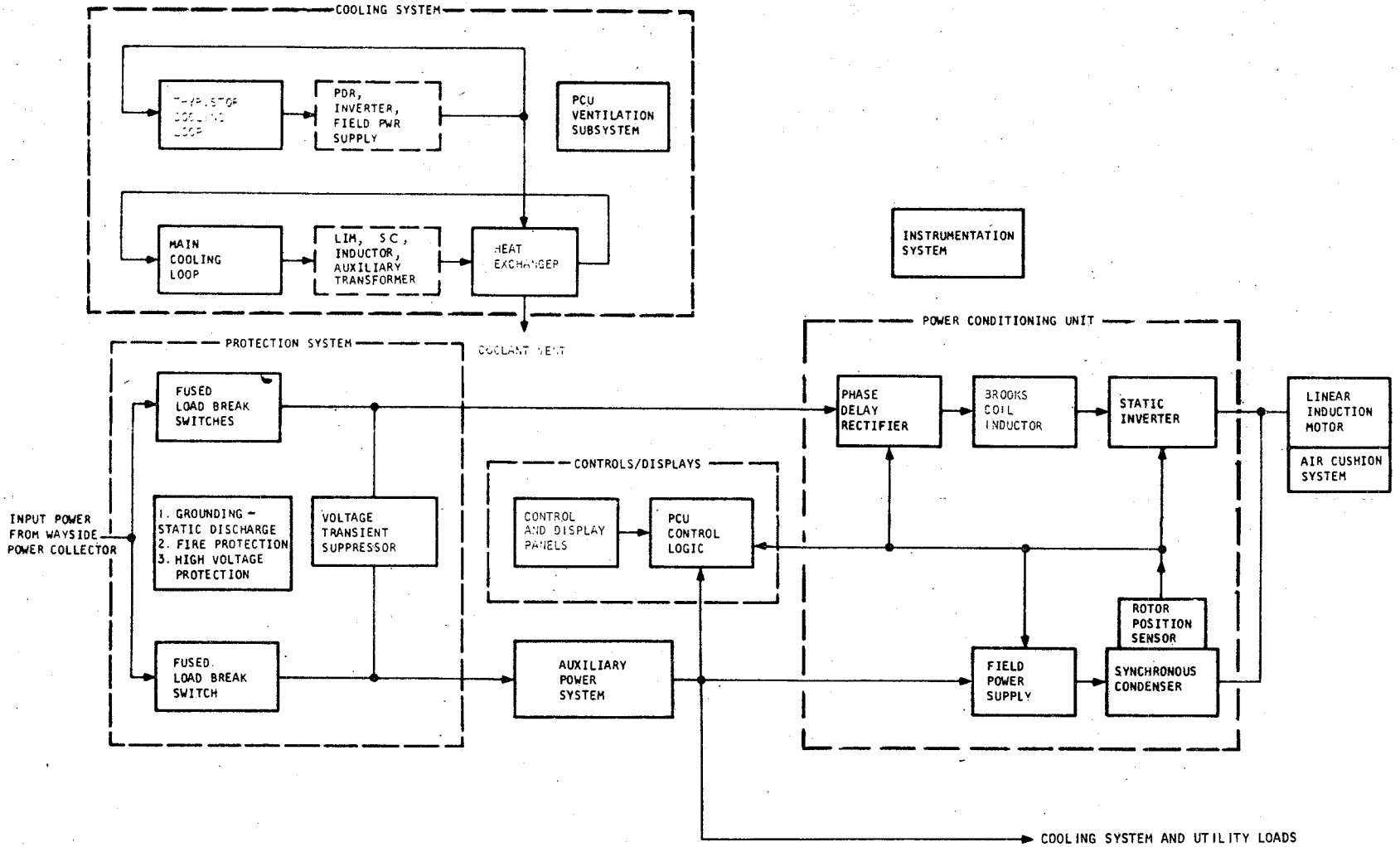

Figure 1-2. LIMPS Block Diagram

One auxiliary power transformer (APT)

One set of controls and displays

Two fused load-break switches in one enclosure (LBS)

One liquid cooling system

One ventilation system

One instrumentation system

Various other ancillary components/subsystems

OPERATION

In operation, 60-Hz wayside power is converted by the PCU, which functions as a variable-voltage, variable-frequency power supply for the LIM. In the propulsive mode, the 60-Hz wayside power is supplied to the input of a phase-delay rectifier (PDR) from which the variable dc output (filtered by an inductor) is applied, through the dc link, to the input of an inverter (INV). The inverter output is connected to the parallel terminals of the LIM and the synchronous condenser (SC), which provides line commutation at the inverter and power-factor correction for the LIM. The PDR, INV, inductor, and SC are the principal electrical components of the PCU. The simplified circuitry is shown schematically in Figure 1-3.

LIM speed is approximately proportional to dc link voltage, while LIM thrust is approximately proportional to dc link current. The function of the inductor is to smooth out current undulations. For most practical considerations, the inductor can be assumed to be so large that the dc current waveform has a negligible ripple content.

The SC function is to provide back emf for inverter commutation and to supply lagging reactive power needed by the converter over its normal operating range. In addition, the LIM also imposes a lagging reactive power demand that

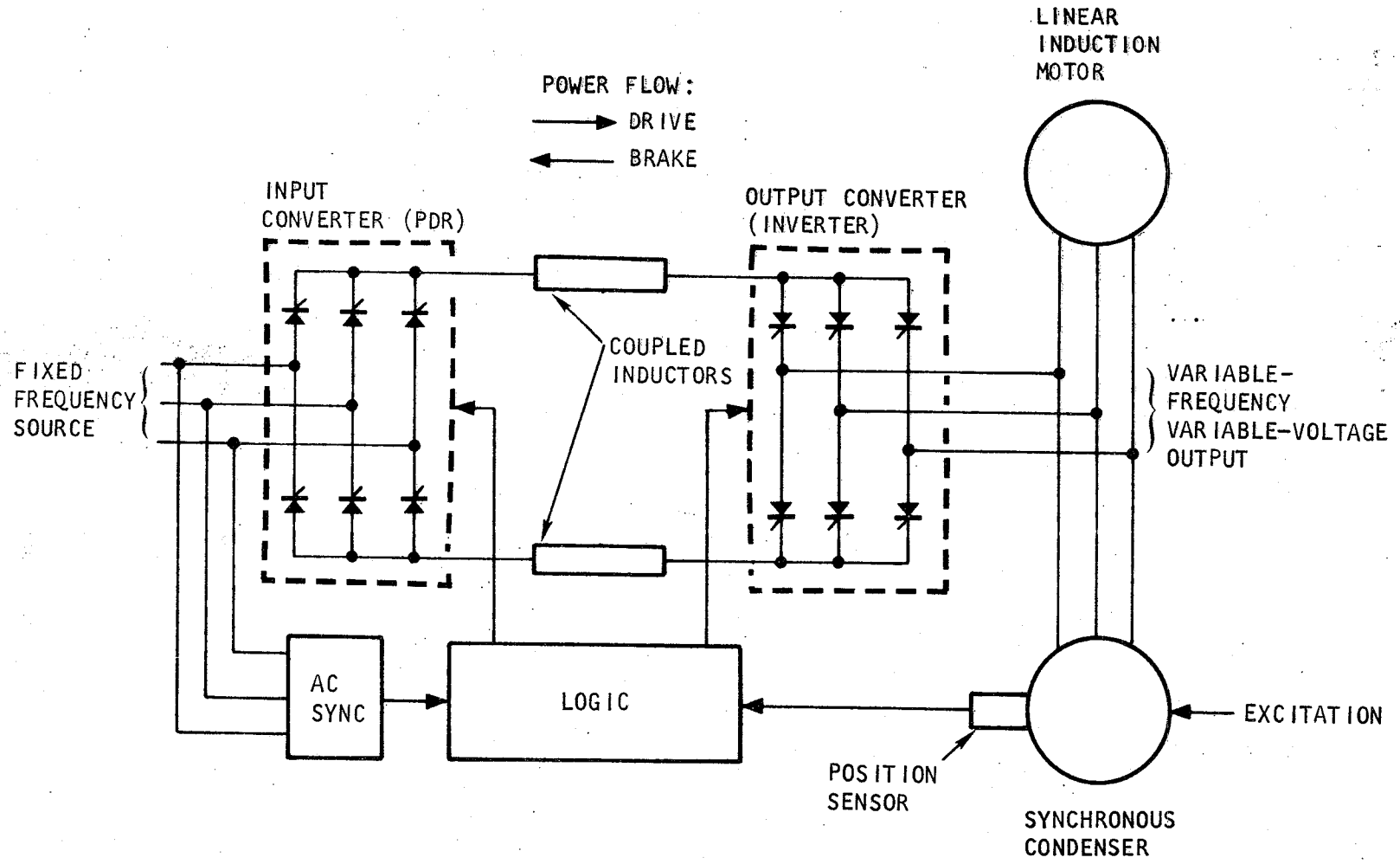

Figure 1-3. LIMPS Simplified Schematic Diagram

must be supplied by the SC. The SC may be regarded as a large, continuously adjustable capacitor in parallel with the ac supply.

The three basic operating modes of the system are briefly described below.

START Mode

Because the INV, output stage of the PCU, cannot line commutate until sufficient back emf is available from the synchronous machine, a special start mode is necessary to bring the SC up to a minimum operating speed. This is accomplished by selectively pulsing sets of machine windings through the INV, which causes the machine to accelerate until a speed is reached where the generated back emf will permit normal operation of the INV (synchronous or line commutation). During the START mode, INV commutation is achieved through current quenching by the PDR. This starting operation is accomplished automatically by special logic and shaft position/speed sensors.

RUN Mode

The RUN mode is the principal mode of operation and actually comprises three regimes of operation, propulsive drive (acceleration), cruise (speed maintenance), and coast. During acceleration the PDR is operated in the rectifier region to deliver dc link voltage and current consonant with the desired thrust and speed commands. The INV and SC deliver, respectively, real and reactive power to the LIM, and the SC also line commutates the INV. The speed maintenance (or cruise) operating regime is very similar to the drive regime except the PDR thyristor control commands are automatically phased back to reduce the dc link level whenever the sensed speed exceeds the manually set speed limit. Coasting is implemented by manually reducing the thrust command to a null setting. In the coast mode the dc link current and the output of the inverter are zero, and the SC essentially idles, supplying the reactive power to the LIM.

BRAKE Mode

In this mode of operation the roles of the two static converters are reversed. The PDR functions as an inverter and the INV functions as a controlled rectifier. The role reversal is accomplished by varying the thyristor commands to produce reverse dc link power flow by reversing the average dc line voltage. The LIM produces the desired braking effort through regeneration.

PRIMARY CONTROLS

The propulsion logic manipulates the propulsion system to achieve feedback signals consistent with manual control settings. Deviations from the control settings occur only in transition or protective modes where attempts to comply with the control settings would result in undesirable propulsion characteristics or equipment malfunctions. Figure 1-4 shows a functional schematic diagram of the control system. A detailed block diagram of the propulsion logic is shown in Figure 1-5.

The propulsion logic operates with six control inputs and seven feedback signals:

Control Inputs	Feedback Signals
Thrust control	Dc link current (I_{dc})
Forward direction control	PDR ac current (PDR I_{ac})
Reverse direction control	INV ac current (INV I_{ac})
Speed limit control	Ac synchronization
Quick shutdown (QSD)	SC shaft position
Quick shutdown reset	Input ac voltage
	SC field current (I_{field})

Primary control of the propulsion effort is established with the thrust control. The control command is produced by the manual thrust control level, which provides a voltage proportional to displacement from a center (zero-thrust) null

1. POWER COLLECTOR
2. FUSED LOAD-BREAK SWITCH
3. SURGE ARRESTER
4. TRANSIENT SURGE SUPPRESSOR
5. AUXILIARY TRANSFORMER
6. PHASE DELAY RECTIFIER
7. SMOOTHING INDUCTOR
8. INVERTER
9a. LINEAR INDUCTOR MOTOR
9b. REACTION RAIL
10a. SYNCHRONOUS CONDENSER
10b. FIELD COIL
10c. ROTOR POSITION SENSOR
11. FIELD POWER SUPPLY
12. DC CURRENT SENSOR
13. THYRISTOR FIRING CIRCUIT
14. LOGIC CIRCUIT
15. THRUST COMMAND
15a. JERK LIMITER
15b. ABSOLUTE VALUE GENERATOR
15c. REGULATOR
16. SPEED CONTROL
16a. SPEED ERROR
16b. REGULATOR
17. FIELD CURRENT COMMAND
17a. FIELD BOOST
17b. REGULATOR
18. INVERTER ANGLE
19. DIRECTION CONTROL
20. START LOGIC

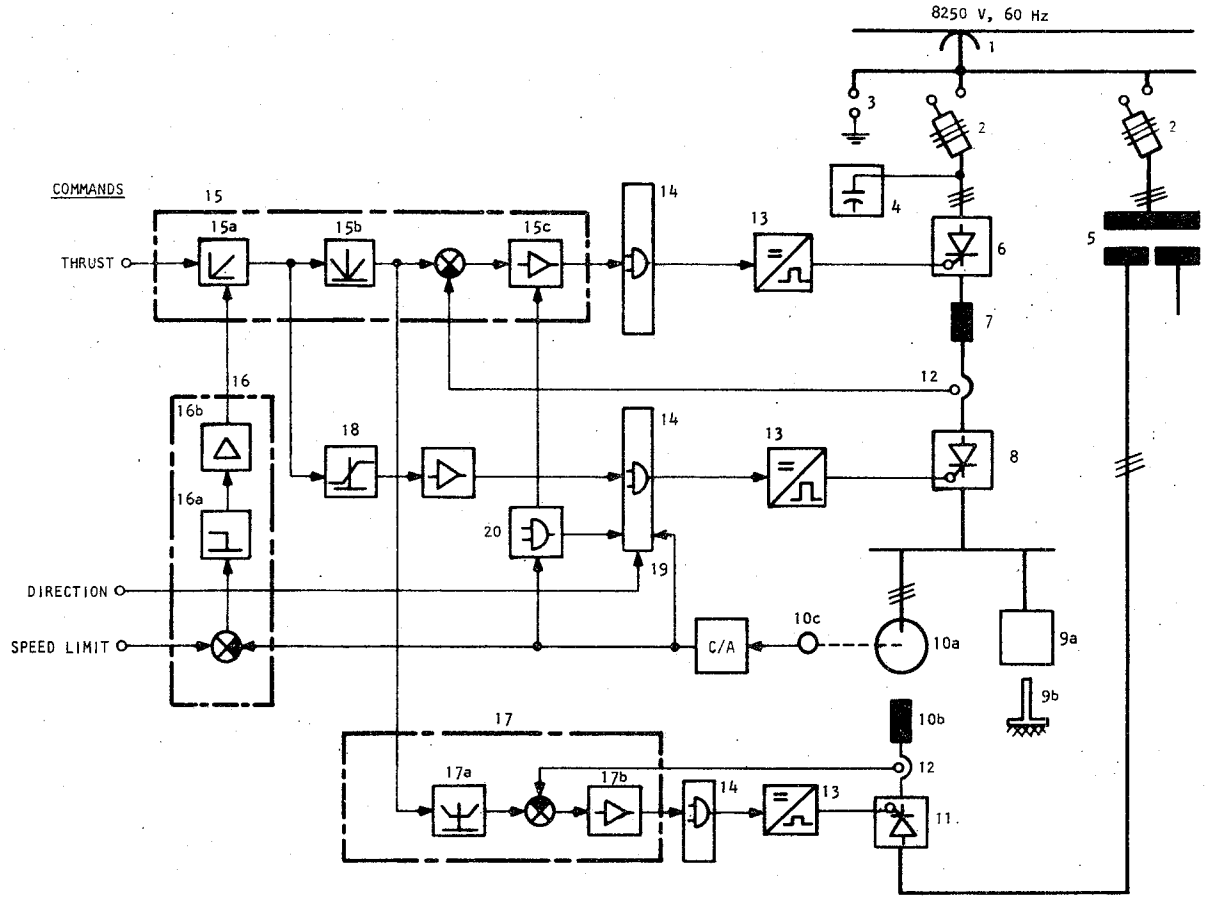

Figure 1-4. Control System Functional Schematic Diagram

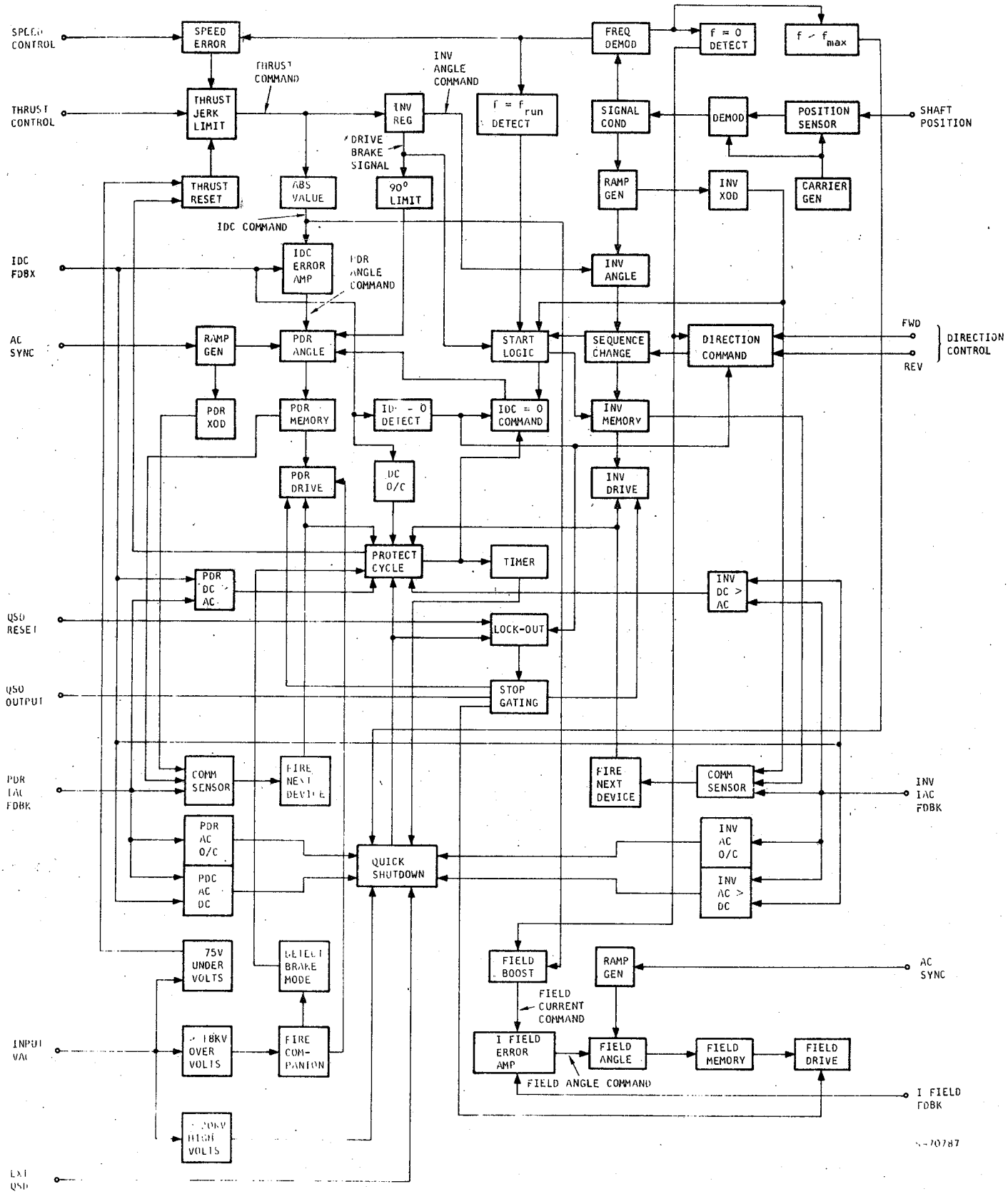

Figure 1-5. Propulsion Logic Functional Block Diagram

position. Positive voltage from this control represents a request for positive acceleration (drive) while negative voltage represents a request for negative acceleration (brake). The thrust control determines only acceleration, not vehicle direction.

The direction control is a pushbutton switch on the control panel that indicates a request for forward or reverse vehicle movement. The control is effective only when the vehicle is at rest. Any change in the direction control while the vehicle is in motion is overridden (ignored) by the propulsion logic.

The manual speed limit control lever establishes a maximum electrical frequency that may be applied to the LIM. Propulsion effort at any frequency below this setting is determined solely by the thrust control. When the selected maximum frequency is approached, the available accelerating thrust is automatically reduced so that the selected frequency will not be exceeded. An upward change in this setting when the system is operating in the speed limit mode will produce acceleration as chosen by the thrust control. A downward change is this setting will reduce the thrust to zero until the vehicle coasts to the new speed limit.

The quick shutdown (QSD) control will produce cessation of all electrical propulsion effort (drive or brake) as rapidly as possible. Once activated, control of the vehicle using the LIM system can be achieved only with a manual resetting procedure.

The QSD reset will unlock the propulsion system from a QSD mode unless the parameter that caused the shutdown is still in evidence and inhibiting operation to prevent subsequent malfunctions.

Thrust Loop

1. Jerk Limit

The thrust control input is directed to the jerk limit circuitry. This circuit has a 1:1 transfer function but a limited slew rate (rate of change of thrust-jerk). Hence, any rapid change by the thrust control will be translated at a specific rate as a new thrust command. The output of the jerk limit circuitry is the thrust command signal, which is delivered to an inverter regulator and an absolute value circuit.

2. Inverter Regulator

The inverter regulator determines whether the thrust command is positive or negative. If positive (drive mode), the regulator requests an inverter firing angle of approximately 150 deg. If the inverter regulator recognizes a negative thrust command (brake mode), it requests an inverter firing angle of approximately 30 deg. The change between the two firing angle positions, although relatively rapid, is smoothly controlled to prevent transients in the power system.

When the inverter regulator has detected a thrust command for the brake mode, a signal is delivered to a 90-deg limit circuit. This circuit prevents the PDR firing angle from operating in a rectifier mode. Without this limit circuit the PDR angle would advance to the rectifier mode in an effort to maintain the command current when the vehicle reaches a low speed. At relatively low speeds the LIM may be unable to regenerate sufficient current, and the 90-deg limit circuit prevents the system from making up the difference with power flow into the vehicle.

3. Absolute Value Circuit

The absolute value circuit receives the thrust command and derives the absolute value of this signal with a 1:1 transfer function. The output of this circuit is the command level for the dc link current, approximately proportional to vehicle thrust.

4. Current Regulator

The dc link current command is then compared with the dc link current feedback. The amplified difference between the two levels is termed angle command and is used to request a firing angle from the PDR that will tend to minimize the feedback/command error.

5. Speed Error

The speed error detector compares the frequency feedback signal with the speed limit input signal and develops an appropriate error signal. If the speed error indicates a speed limit setting greater than the operating frequency, no action is taken. If the speed error indicates an operating frequency greater than the speed limit, an output is created that operates, through the jerk limit circuitry, to reduce the thrust command toward zero until the error between speed limit and operating frequency is minimized. Inherent in this speed override loop is the need for acceleration bias. To achieve a speed limit without overshoot or thrust jerk, the thrust must be reduced before the speed reaches the desired limit. As the acceleration rate is increased, the thrust reduction must begin at an increasingly lower speed below the limit. This permits a smooth approach to a speed limit mode of operation. Both the unidirectional correction and the acceleration bias are included in the speed error circuitry.

6. Field Current Command

The current delivered to the SC field is controlled by a separate full-wave thyristor converter (the field power supply) that receives firing information from the propulsion logic. The normal field current command is generated by the field boost circuitry acting in response to inputs from the I_{dc} command and a zero frequency detector. Depending upon the conditions of the two inputs, the field current command can be in any of the four control modes defined below.

This particular method of field current control has been implemented to protect the SC field sliprings from spot heating when the rotor is stationary.

Mode 1--SC at rest; zero dc current command; field command = zero ($f < 0$; $I_{dc} = 0$)

Mode 2--SC at rest; dc current command greater than zero; field command = 25 percent of rated field current ($f < 0$; $I_{dc} > 0$)

Mode 3--SC rotating; dc current command less than 100 percent; field command = 100 percent of rated field current ($f > 0$; $I_{dc} < 100$ percent)

Mode 4--SC rotating; dc current command greater than 100 percent; field command is proportional to dc current command ($f > 0$; $I_{dc} > 100$ percent)

The relationship between the field current and the thrust command is shown in Figure 1-6 for the two possible conditions of SC frequency (f).

Direction Command

The six pulse trains resulting from the INV ramp-to-angle command comparisons are delivered to a sequence change circuit on their route to the INV memory. This circuitry directs the pulses to the INV memory by using one of two possible sequences. The choice of sequence is based on the direction command (ABC sequence = forward; ACB sequence = reverse).

1. Frequency and Current Zero Detectors

The direction command receives information from the direction controls, the frequency zero detector, and a zero current detector associated with the dc link current feedback. A change in direction command will not be activated until the frequency indicates zero and the dc link current indicates zero. These conditions assure that the vehicle is at rest with zero thrust.

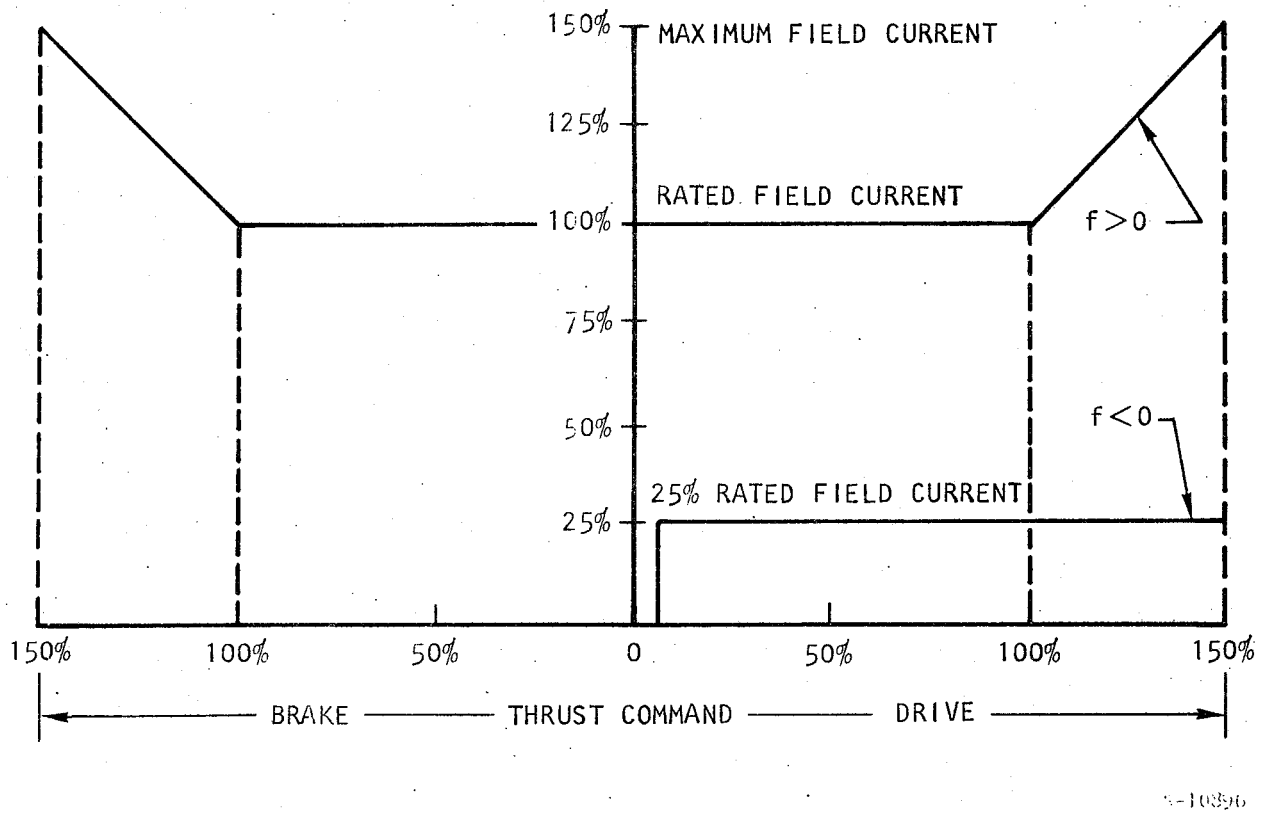

Figure 1-6. Field Current Command Schedule

2. Sequence Change

When the six pulse trains are arranged in a particular sequence they are used to control the state of six flip-flops in the INV memory circuit. Each flip-flop is associated with a particular leg of thyristors in the INV. When a flip-flop to toggled by the appropriate pulse, the output directs a particular set of drive circuitry to be activated. The two possible operating sequences are summarized in Table 1-1.

TABLE 1-2

INVERTER OPERATING SEQUENCES

ABC Rotation (Forward Direction): Firing Pulse Sequence	Flip-Flops Set	Flip-Flops Reset	Resultant Drive
A+	A+	C+	A+ and B-
C-	C-	B-	A+ and C-
B+	B+	A+	B+ and C-
A-	A-	C-	B+ and A-
C+	C+	B+	C+ and A-
B-	B-	A-	C+ and B-
ACB Rotation (Reverse Direction): Firing Pulse Sequence	**Flip-Flops Set**	**Flip-Flops Reset**	**Resultant Drive**
A+	A+	B+	A+ and C-
B-	B-	C-	A+ and B-
C+	C+	A+	C+ and B-
A-	A-	B-	C+ and A-
B+	B+	C+	B+ and A-
C-	C-	A-	B+ and C-

Start Logic

Whenever the INV regulator indicates that the thrust command requires drive mode and the frequency is recognized to be below f_{run} (the value necessary for line commutation of the inverter), the start logic circuitry is activated. This circuitry bypasses the normal firing angle circuitry for the INV and uses information from the INV synchronizing crossover detector (XOD) to force a full 180-deg firing angle position into the INV memory. In addition, the start logic produces an input to the $I_{dc} = 0$ command circuit. Since the INV power bridge should operate by changing the flow of current every 60 electrical degrees, the start logic activates the $I_{dc} = 0$ command each time the end of a particular 60-deg interval is indicated by the crossover detector circuit. Once activated, the $I_{dc} = 0$ command circuit forces an immediate maximum fourth quadrant position of the PDR angle such that the dc link current is rapidly forced to zero. At the same time the start logic advances, the INV gate drive proceeds to the next configuration in the normal sequence determined by the direction command.

Current Zero Cycle

When the dc link current is zero, the off-going INV power devices regain their voltage blocking capability. The zero current condition is recognized by an $I_{dc} = 0$ detector, and the output from this detector cancels the command for $I_{dc} = 0$. The magnitude of the dc current then rises again to the value determined by the thrust loop. This current zeroing cycle occurs every 60 deg of output frequency during the start mode. These actions enable the SC to accelerate from a rest position to the frequency (f_{run}) where line commutation of the INV power devices is possible. At this point the start mode is terminated. One final dc link current zero cycle is commanded and the INV drive reverts to the normal drive mode firing angle of approximately 150 deg. After

this transition the vehicle thrust and speed parameters are determined by the settings of the operator's thrust and speed controls.

Protection Circuitry

There are 15 system-protection sensors that may cause deviation from normal operation into a protection mode. These sensors are divided into two distinct groups:

System Failure Sensors

PDR ac overcurrent

INV ac overcurrent

PDR $I_{ac} > I_{dc}$

INV $I_{ac} > I_{dc}$

Ac input voltage very high

External QSD

Output overfrequency

Incipient System Failure Sensors

DC link overcurrent

PDR commutation failure

INV commutation failure

PDR $I_{dc} > I_{ac}$

INV $I_{dc} > I_{ac}$

Ac input undervoltage

Ac input overvoltage

PERFORMANCE

Actual system performance is constrained by the real and reactive power limitations of the different components. In this connection it is pointed out that the LIM input power is actually supplied from two separate sources. The real power is provided through the PDR, Brooks coil inductor, and static INV, and the reactive power is furnished by the SC.

Reactive Power

At the maximum operating frequency, 165 Hz, the SC output is limited by its field current rating. The overload field current is 2665 A. The corresponding SC overload current at rated voltage is 809 A.

Real Power

For maximum power transfer through the dc link, the INV should be phased back as little as possible. Phasing back the INV is necessary to allow sufficient time for commutating, i.e., transferring the current from one phase to the next. During the first portion of this time interval, the currents in the two commutating phases rise and decay at a rate that is dictated by the component reactances and by the dc link current value. During the remainder of the time interval, usually referred to as the thyristor turnoff time, the current carriers in the semiconductor devices stabilize. The turnoff time for the particular thyristors used is about 200 sec, which represents 12 electrical degrees at an operating frequency of 165 Hz. The inverter is nominally phased back (i.e., its thyristor firing angle is retarded) by a constant, but adjustable, value of 30 degrees.

Maximum Power Envelope

Based on the assumption that the inverter thyristors are fired at their minimum angle of retardation, the maximum real and reactive currents available from the power conditioning unit to the LIM are as shown in Figure 1-7. The current through the dc link supplies both the LIM and SC real power requirements. As a result, the sloping horizontal line corresponds to a constant dc link current where the slope represents that portion of the real power that supplies the SC losses.

The dc link output is thermally limited by the thyristor current rating at approximately 680 A.

In addition to supplying the reactive power requirements of the LIM, the SC also is the source of reactive power associated with phasing back the inverter. The near-vertical line in Figure 1-7 corresponds to the maximum reactive current available from the SC overload field current. The slope of the line is proportional to the reactive current required to commutate the inverter.

The LIM, as part of the TLRV propulsion system, must operate within this envelope, limited on one side by the dc link, and on the other side by the SC output. The original LIM design point is also shown in Figure 1-7; it lies within these limiting boundaries.

SYSTEM MASS (WEIGHT)

Table 1-3 is a breakdown of LIMPS mass (weight).

SCHEMATIC/WIRING DIAGRAM

Figure 1-8 is the system electrical schematic/wiring diagram for the primary electrical loads (i.e., the instrumentation, control, and some protection systems wiring are not shown). In addition to the primary propulsion components, the motor/pump loads for cooling provisions, and switches, relays, contactors, junction boxes, terminal strips, and connectors are also shown.

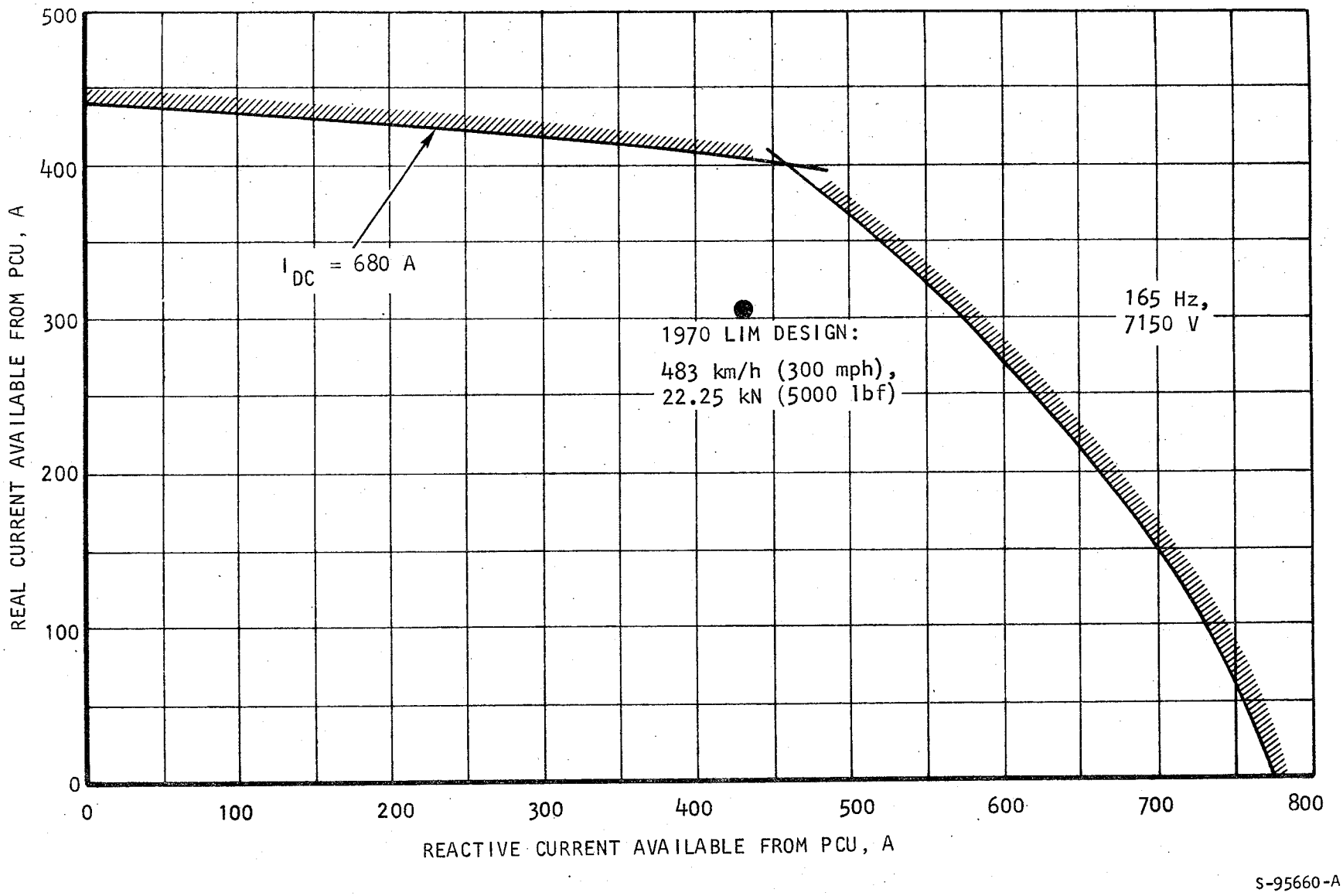

Figure 1-7. Power Conditioning Unit Power Envelope

TABLE 1-3

LIMPS MASS (WEIGHT)

Subsystem/Component	Mass, kg	Weight, lb
Linear Induction Motor	2223	4900
Basic motor	1610	3551
Air cushion system	417	920
Ancillary hardware	195	429
Power Conditioning Unit	3171	6991
Inverter	226	498
Inductor	277	611
Phase delay rectifier	280	617
Synchronous condenser	1898	4185
Field power supply	58	127
Cabling, connectors, bus bars protection	432	953
Auxiliary Power System	839	1850
Auxiliary power transformer	701	1546
Power distribution panels	61	135
Cabling, connectors, bus bars, etc.	77	169
Controls/Displays	320	705
Control/display panels	14	31
Control cabinet	124	274
Cabling, connectors, etc.	181	400
Instrumentation System	272	599
Instrumentation cabinet	163	360
Instrumentation cabinet cables, junction boxes, etc.	108	239
Protection System	555	1223
Load break switch assembly	469	1035
Bushings, buses, etc.	23	51
Voltage transient suppressor	33	72
Fire protection	29	65
Cooling System	1355	2987
Ventilation components	181	400
Pumps	450	993
Boiler	195	430
Tank (full)	272	600
Plumbing and ullage	201	444
Pressurization components	54	120
LIMPS Total	8734	19,255
Vehicle borne	6511	14,355
Guideway borne	2223	4900

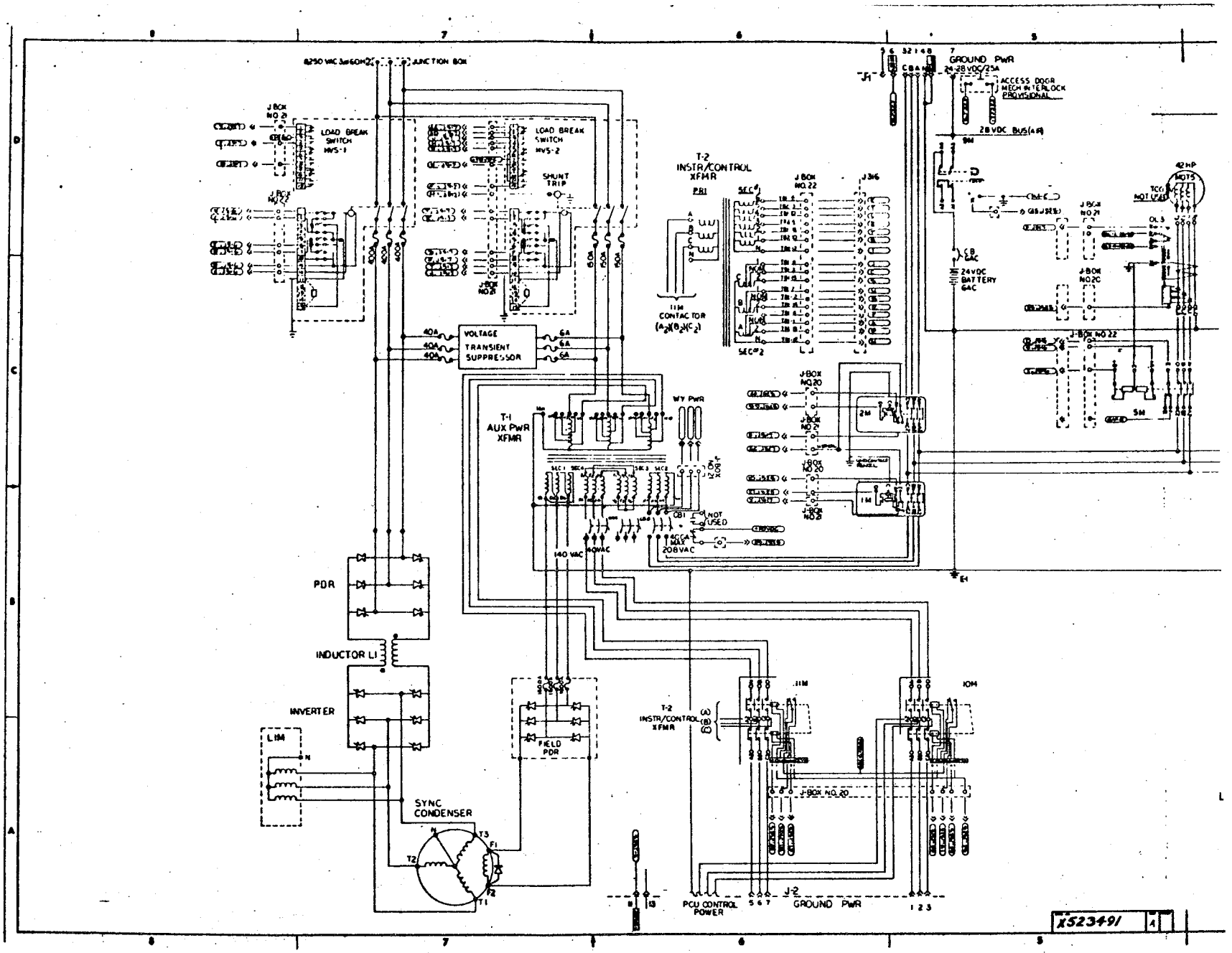
8250 VAC 3ø60HZ
JUNCTION BOX
LOAD BREAK SWITCH MVS-1
LOAD BREAK SWITCH MVS-2
SHUNT TRIP
T-2 INSTR/CONTROL XFMR
PRI
SEC #1
SEC #2
11M CONTACTOR
VOLTAGE TRANSIENT SUPPRESSOR
T-1 AUX PWR XFMR
WY PWR
CB1
NOT USED
140 VAC
40VAC
PDR
INDUCTOR L1
INVERTER
L1M
FIELD PDR
SYNC CONDENSER
T1
T2
T3
F1
F2
GROUND PWR
24-28 VDC/25A
ACCESS DOOR MECH INTERLOCK PROVISIONAL
28 VDC BUS(4A)
24VDC BATTERY 6AC
42HP MOTS
TCC NOT USED
J-BOX NO.20
J-BOX NO.21
J-BOX NO.22
J-BOX NO.23
J-BOX NO.24
J-BOX NO.25
J-BOX NO.26
J-BOX NO.27
J-BOX NO.28
J-BOX NO.29
J1
J2
J3
J4
J36
PCU CONTROL POWER
GROUND PWR
X523491

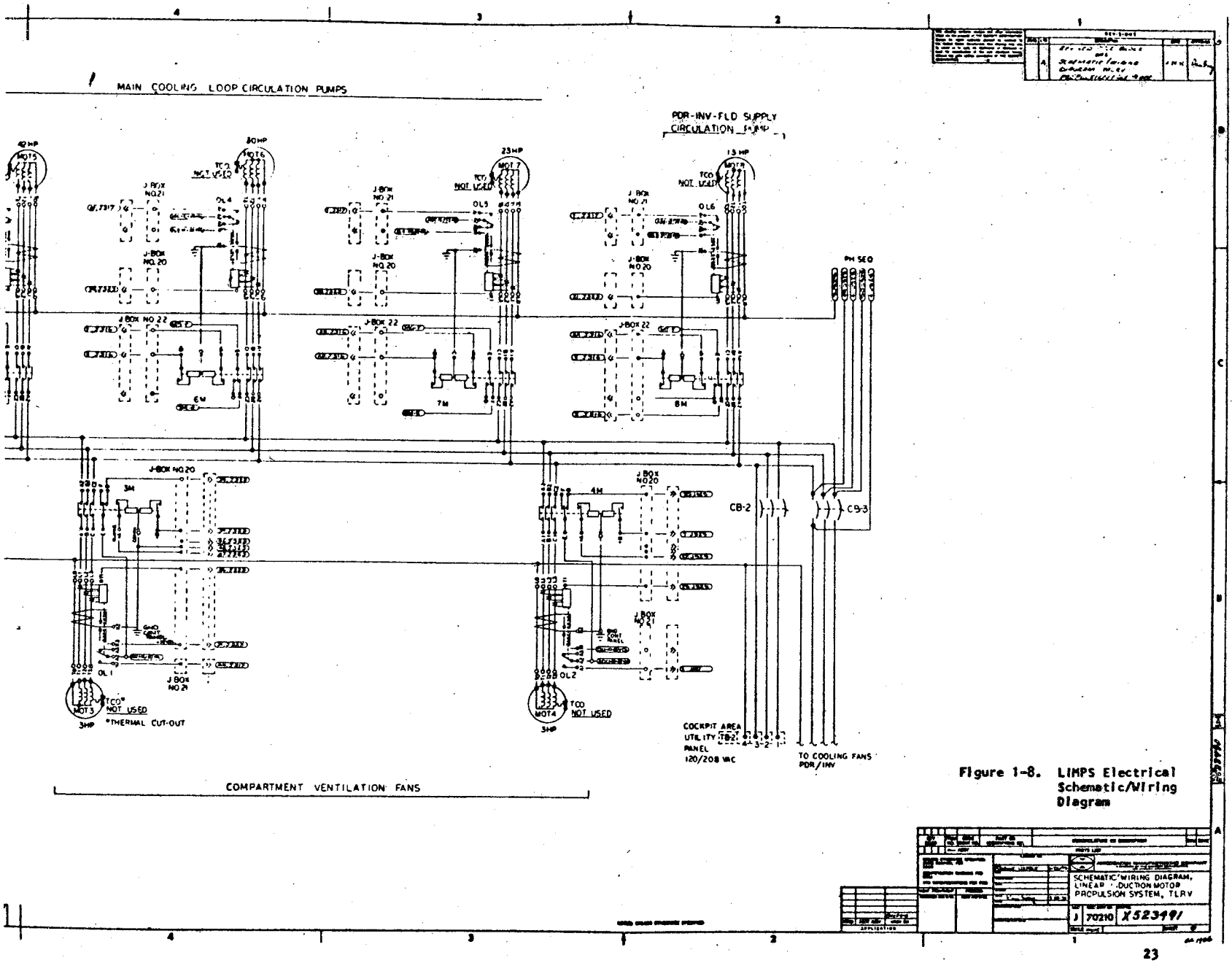

Figure 1-8. LIMPS Electrical Schematic/Wiring Diagram

SCHEMATIC/WIRING DIAGRAM, LINEAR INDUCTION MOTOR PROPULSION SYSTEM, TLRV

J 70210 X523491

SUBSYSTEMS AND COMPONENTS

The following paragraphs describe the LIMPS subsystems and components. Numerous photographs of the hardware are also provided.

Linear Induction Motor

The LIM is a double-primary machine that straddles and reacts electromagnetically with a stationary reaction rail vertically mounted in the center of the guideway. Table 1-4 summarizes the salient characteristics of the LIM. Basically, the LIM comprises five subassemblies: stack assembly, primary winding assembly, housing, utilities, and air cushions. Figure 1-9 shows several views of the LIM hardware during fabrication and assembly.

The LIM stack is an assemblage of 2576-mm (101.4-in.) long, 0.355-mm (0.014-in.) thick M19 silicon steel laminations and a suitable structural channel for their support. The laminations are stacked and assembled in a U-shaped channel made of titanium to minimize weight, and secured by insulated bolts. The resulting box structure provides good torsional rigidity for this application. Also, electrical loss due to end leakage flux is minimized by the high electrical resistance of titanium.

Boron-dexodized copper with silver content for high-temperature strength retention is used for the primary windings. Insulation is mica-based preimpregnated tape with asbestos wrapping in the slot portion and glass taping in the end-turn region for mechanical protection. A conducting varnish is applied over the asbestos tape for corona protection. The insulated coil will withstand operating temperatures to 200°C (392°F). A two-layer coil assembly of 75 diamond-shaped coils is used for each of the two LIM primaries. These 75 coils are inserted in 85 slots in the primary stack; the first 10 slots and the last 10 slots contain only one coil side to reduce end effect.

TABLE 1-4

LIM DESIGN DATA

Nominal Design Point	
Thrust	22,200 N (5000 lbf)
Speed	134 m/s (300 mph)
Voltage	4120 VRMS, line-to-neutral, 3-phase
Current	530 ARMS
Frequency	165 Hz
LIM Primary Stack*	
Material	AISI M-19C-4 silicon steel
Height	190 mm (7.5 in.)
Length	2576 mm (101.4 in.)
LIM Primary Winding*	
Poles	5
Pole pitch	450.8 mm (17.75 in.)
Slots	85 per side
Slot pitch	30.05 mm (1.183 in.)
Conductors per slot	2 (10 slots at each end are half-filled)
Slots per pole	15
Coil pitch	2/3
Conductors	6.553 mm (0.258 in.) square with 3.632 mm (0.143 in.) dia hole
Coils	75 per side, double-layer, diamond, lower end bent 90 deg to minimize height
Water flow	2.84 l/s (4.5 gpm)
Water pressure drop	448 kPa (65 psi)
LIM Secondary (Reaction Rail)	
Material	Aluminum alloy, 6061-T6
Conductivity	27.6 MS/m (20°C)
Overall width	15.875 mm (0.625 in.)
Effective thickness	7.07 mm (0.278 in.)
Nominal Airgap	
Primary-to-primary	38.1 mm (1.5 in.)
Primary-to-secondary	11.1 mm (0.4375 in.) each side

*LIM configuration, double-sided, on a per-side basis

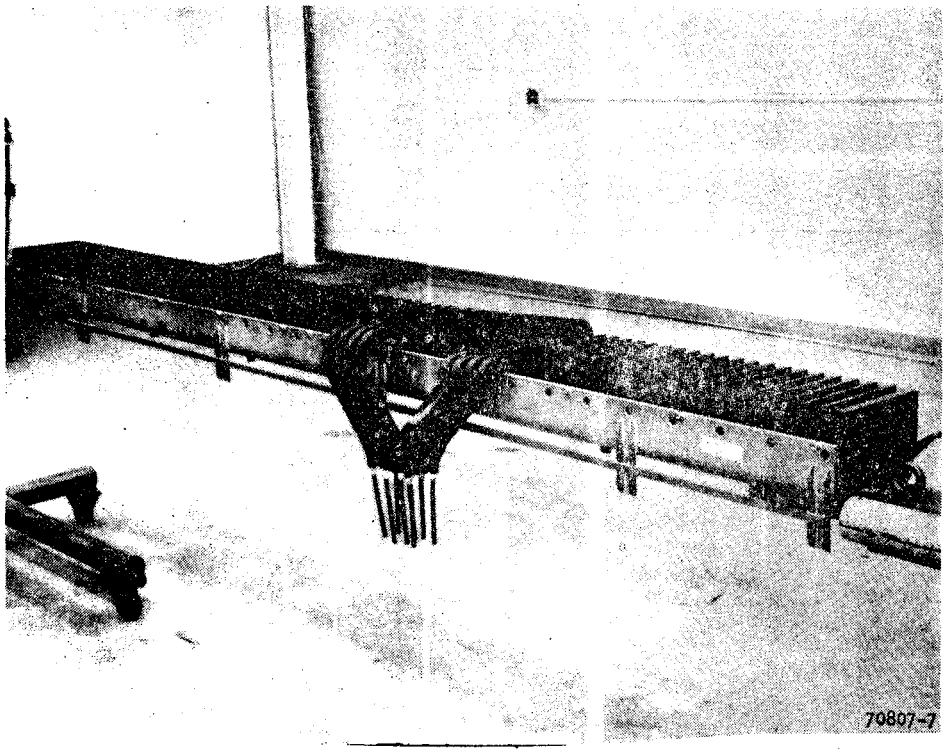

a. STACK ASSEMBLY WITH FOUR COILS FITTED

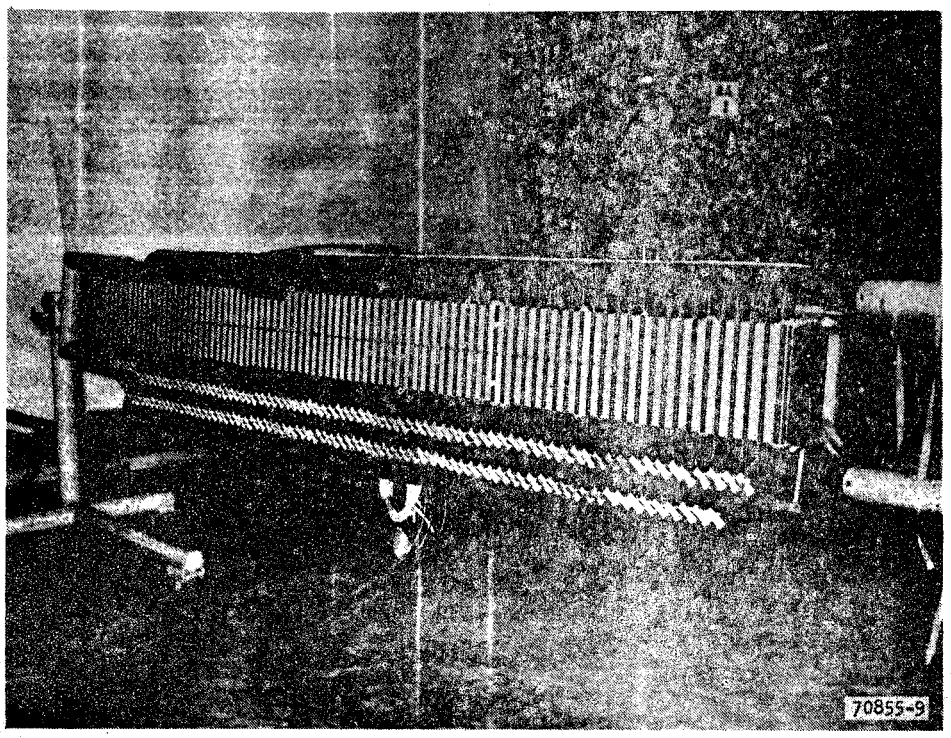

F-21420

b. PRIMARY WINDING ASSEMBLY (ONE SIDE)

Figure 1-9. Linear Induction Motor

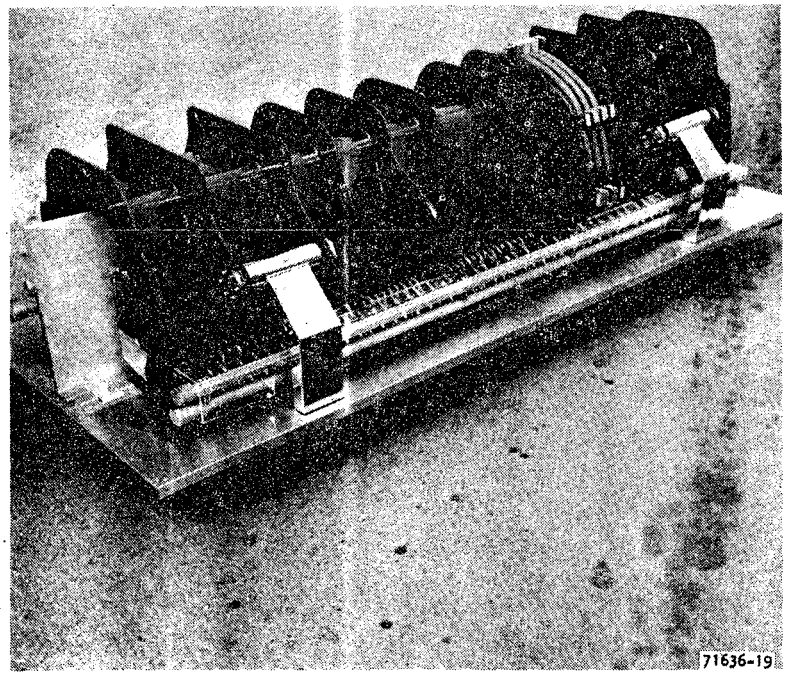

c. BARE MACHINE ASSEMBLY (WITHOUT UTILITIES AND AIR CUSHIONS) ON GROUND CART

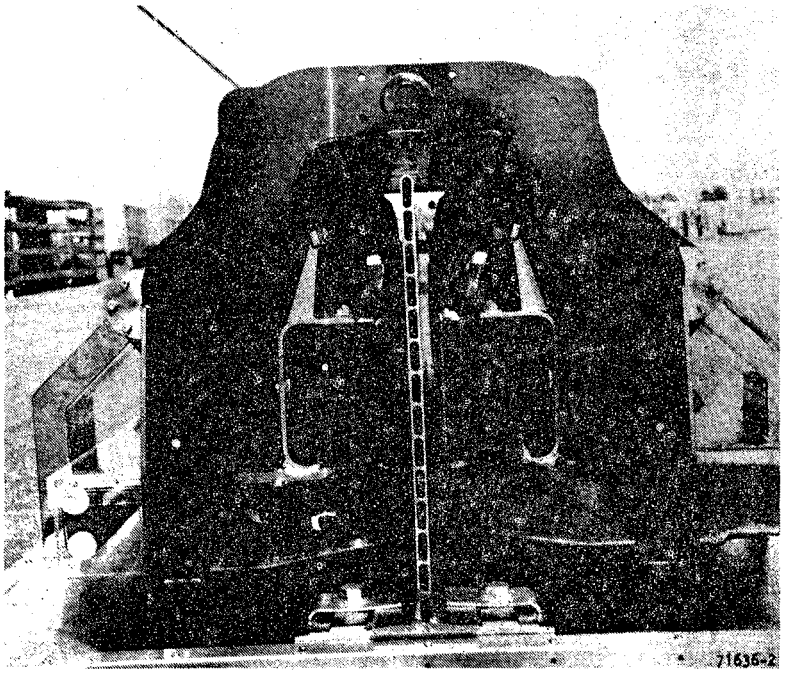

d. END VIEW OF BARE MACHINE WITH REACTION RAIL

F-21422-A

Figure 1-9. (Continued)

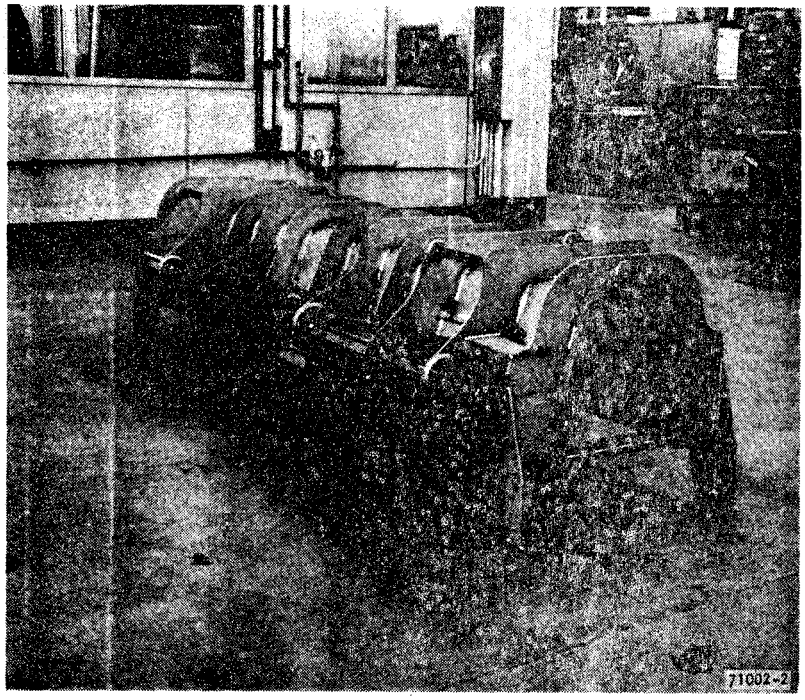

a. HOUSING

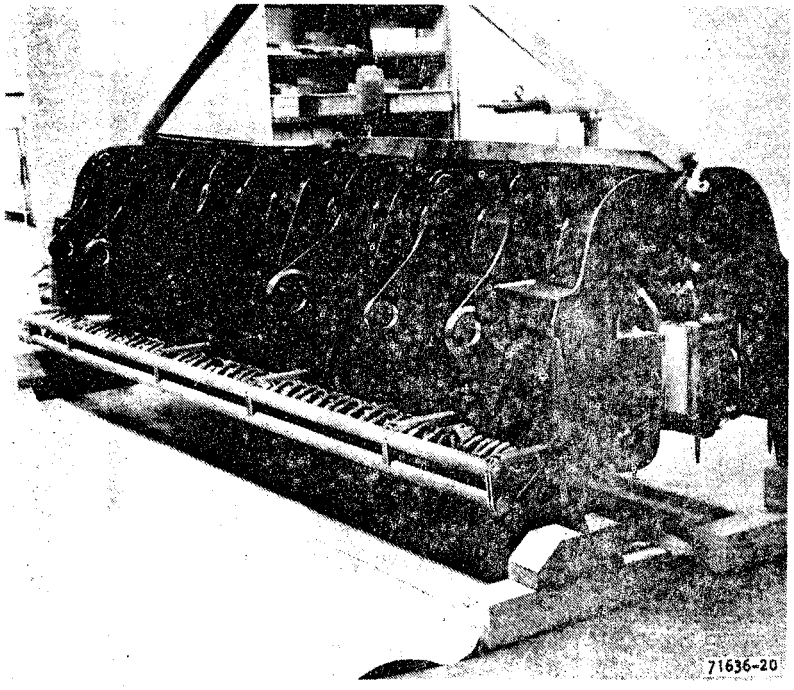

F-21421

b. HOUSING WITH BOTH PRIMARY WINDING ASSEMBLIES AND LIQUID COOLING MANIFOLDS

Figure 1-9. (Continued)

The LIM housing provides the support and restraining structure for the two LIM primary sides. It is a semimonocoque structure made of titanium and designed primarily for high stiffness.

The LIM air cushion system comprises an air plenum, a vertical support system, and a lateral guidance system; it provides restoring forces in vertical, lateral, roll, yaw, and pitch movements.

Predicted LIM performance (1970) at rated frequency and voltage is shown in Figure 1-10.

Synchronous Condenser and Field Power Supply*

The SC electrically parallels the LIM and the inverter, and is operated as an overexcited synchronous motor to: correct the low power factor of the LIM over the range of operating frequency and thrust, and line commutate the inverter thyristors by providing a sinusoidal back-emf and leading reactive current. A resolver, mounted on top of the machine and connected to the rotor shaft, provides a phase-position signal that is used by the power conditioning unit (PCU) controls to pulse the inverter through the PDR during the LIMPS start mode. Table 1-5 lists the design characteristics of the machine. Figure 1-11 shows several views of the machine during fabrication and assembly.

The SC is a high-voltage, vertically-mounted, 3-phase machine. The stator is four-wire, wye-connected with the neutral grounded through a 10-kilohm resistance. The wound-rotor field (four nonsalient poles) is excited through a brush-slipring connection to a low-voltage power supply. A freewheeling (clamping) diode is connected across the field winding to provide transient protection.

---

* NTIS Report No. FRA-OR&D 76-266, "Design, Development, Fabrication, and Testing of a Synchronous Condenser for the Tracked Levitated Research Vehicle," June 1976.

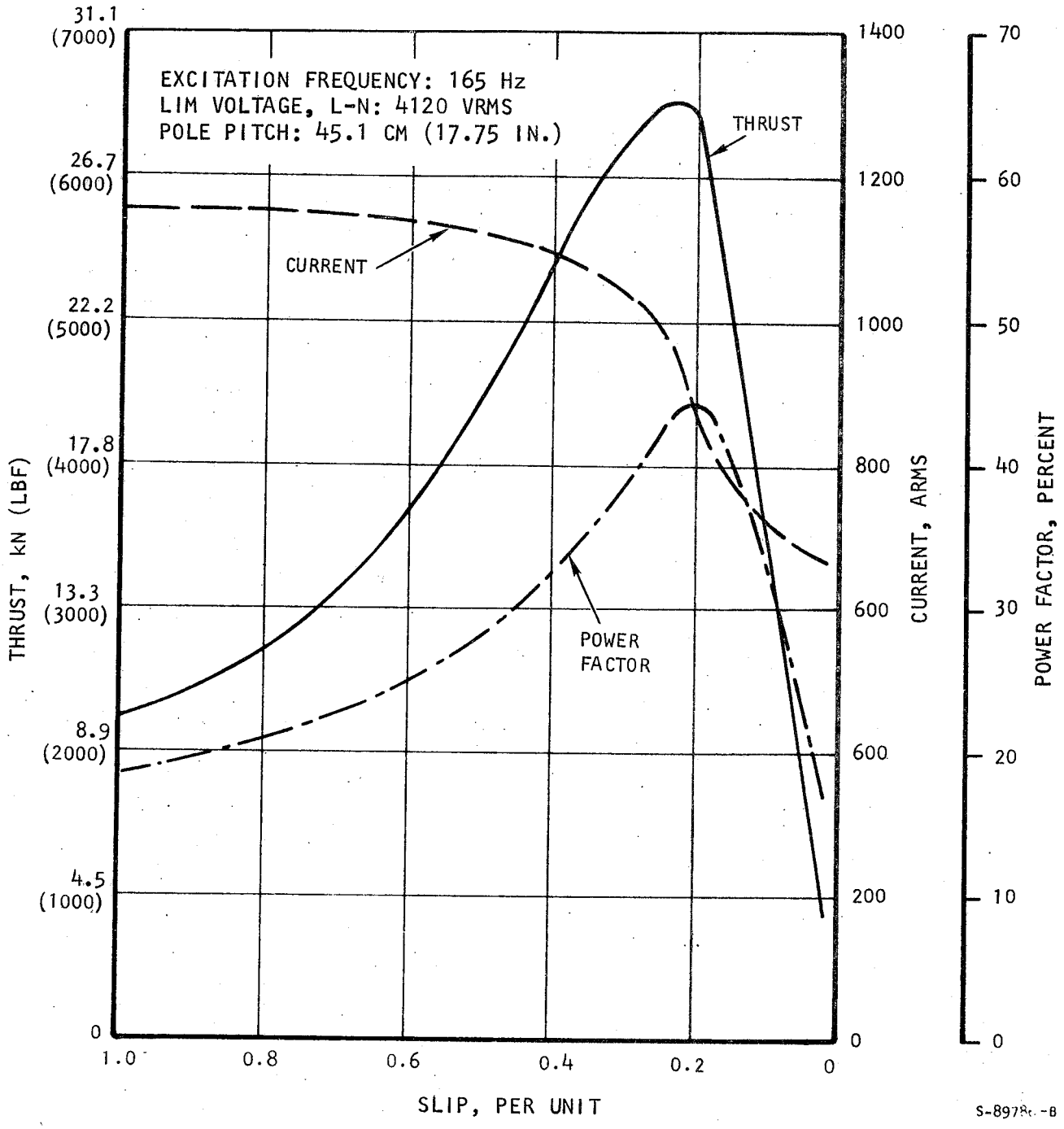

Figure 1-10. Predicted LIM Performance

TABLE 1-5

SYNCHRONOUS CONDENSER DESIGN DATA

Design Point	
Rated speed, rad/s (rpm)	518 (4950), 4 poles
Rated power, MVA	7 continuous, 10 overload (0 power factor, 165 Hz)
Voltage	7150 VRMS, line-to-line
Mass, kg (weight, lb)	1906 (4202)
Power density, kVA/kg (kVA/lb)	3.7 (1.7) at continuous rating 5.3 (2.4) at overload rating
Rotor diameter, m (in.)	0.545 (21.5)
Mounting	Vertical
Cooling	Direct water
Load Condition	
Armature density, A/mm^2 ($A/in.^2$)	28.9 (18,700) nominal, 41.8 (27,000) max.
Field density, A/mm^2 ($A/in.^2$)	24.6 (15,900) nominal, 36.5 (23,600) max.
Armature	
Phase resistance, ohms (180°C)	0.218
Base impedance, ohms	7.38
Synchronous reactance, per unit (unsaturated)	3.44
Transient reactance, per unit (unsaturated)	0.496
Subtransient reactance, per unit (unsaturated)	0.316
Negative sequence (X_2) reactance, per unit	0.316
Stator leakage reactance, per unit	0.174
Field leakage reactance, per unit	0.358
Zero sequence reactance, per unit	0.102
Damper leakage reactance, per unit	0.142
Mean turn length, m (in.)	2.10 (82.6)
Strands per turn	2
Turns per phase	72
Turns per slot	3
Field	
Resistance, ohms (180°C)	0.0481
Inductance, mH (unsaturated)	16.9
Mean turn length, m (in.)	1.56 (61.4)
Strands per turn	1
Turns per pole	20
Turns per slot	5

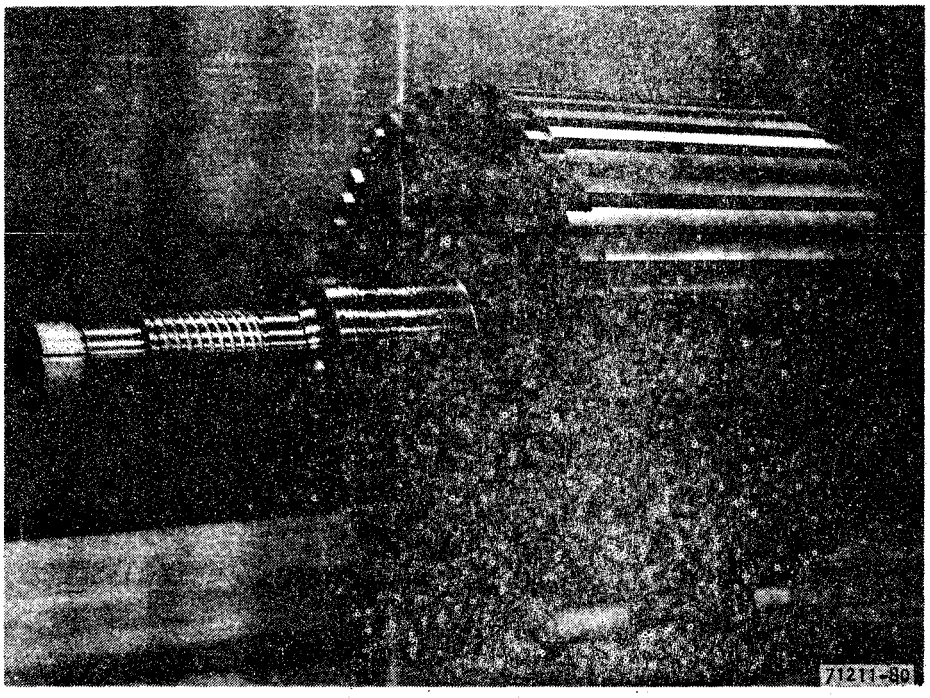

a. ROTOR AFTER FINISH MACHINING

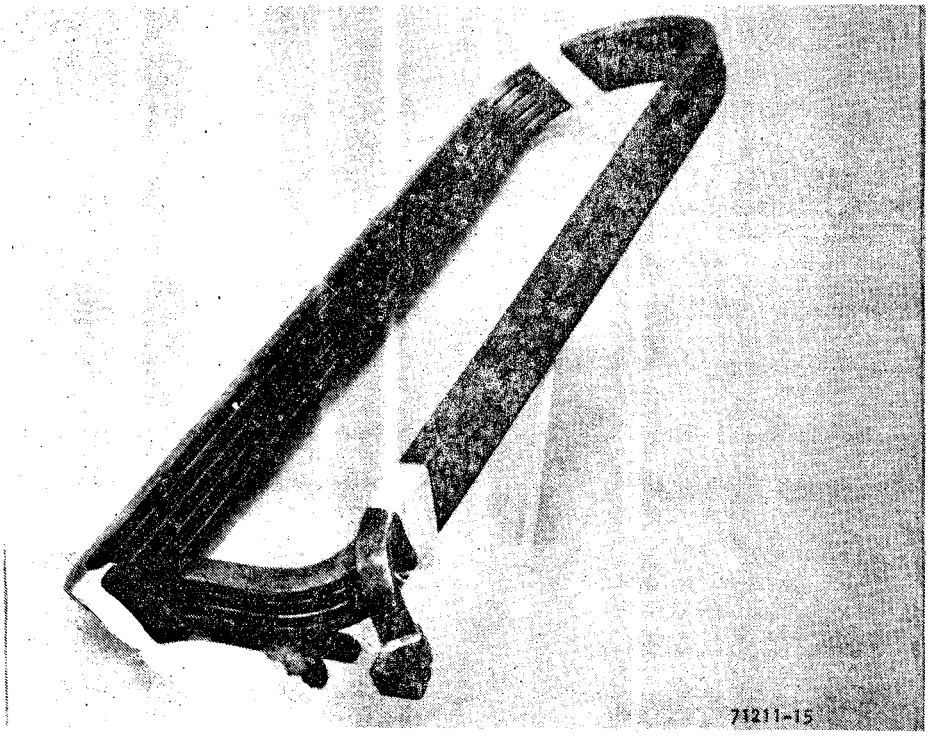

F-21425

b. ROTOR COIL

Figure 1-11. Synchronous Condenser

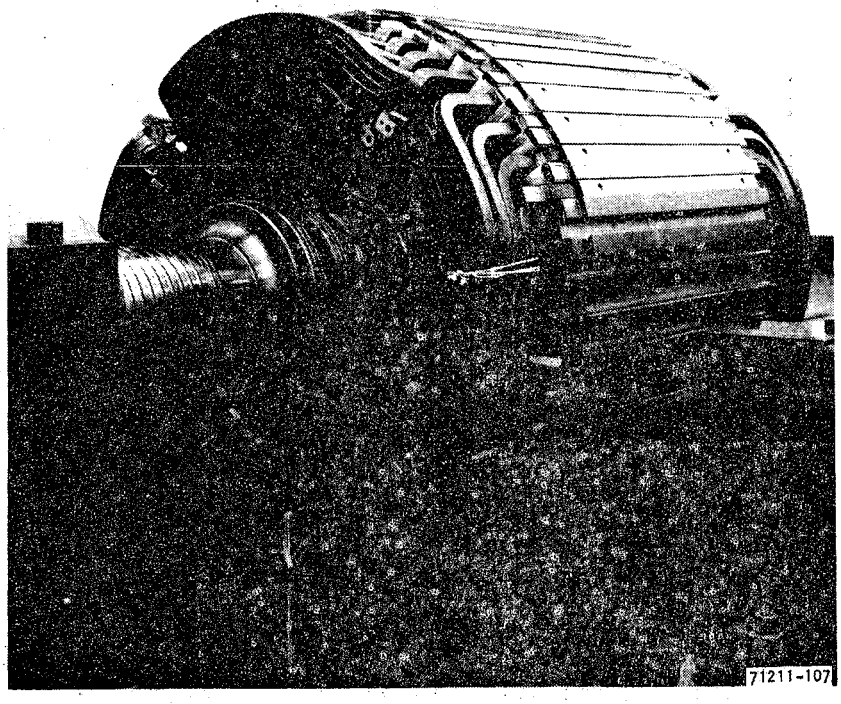

c. ROTOR WITH COILS ASSEMBLED

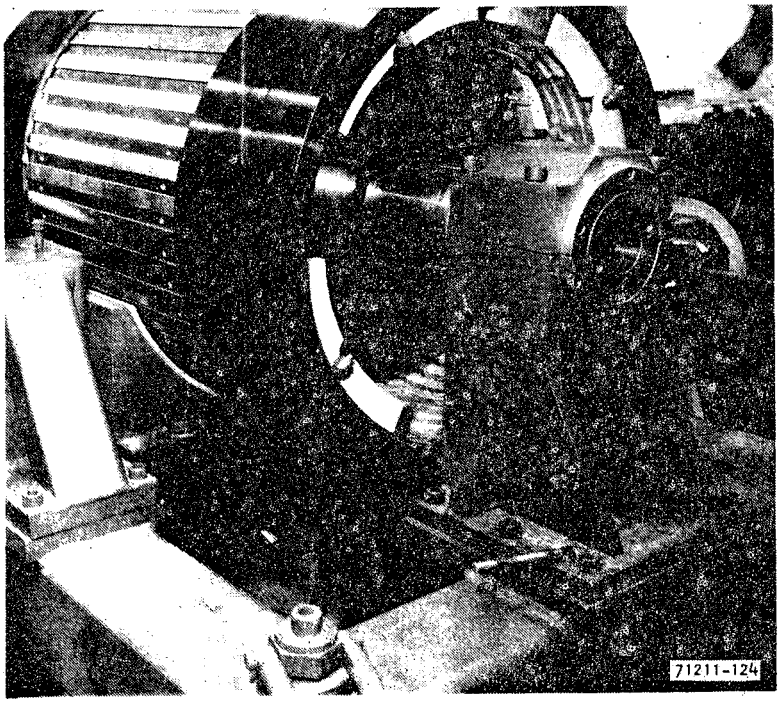

F-21427

d. FINISHED ROTOR

Figure 1-11. (Continued)

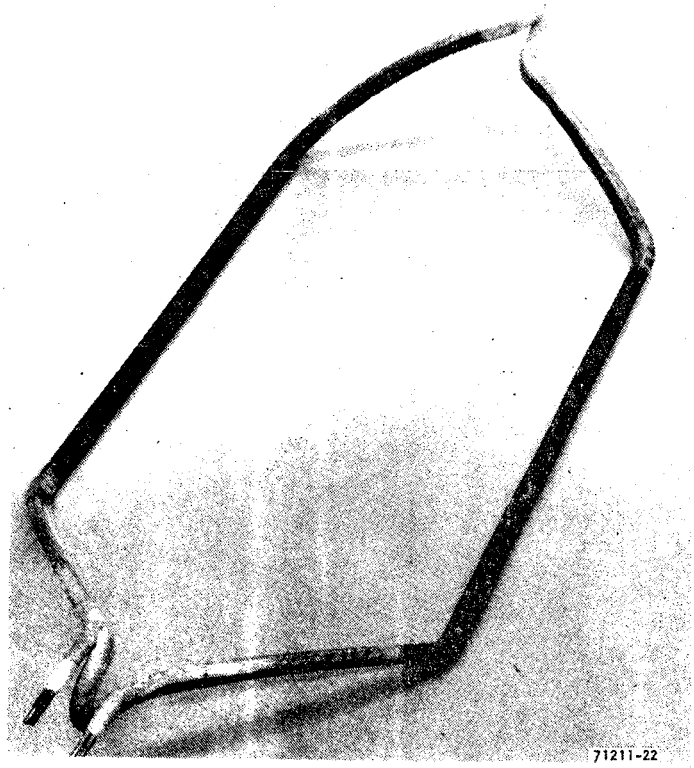

e. STATOR COIL

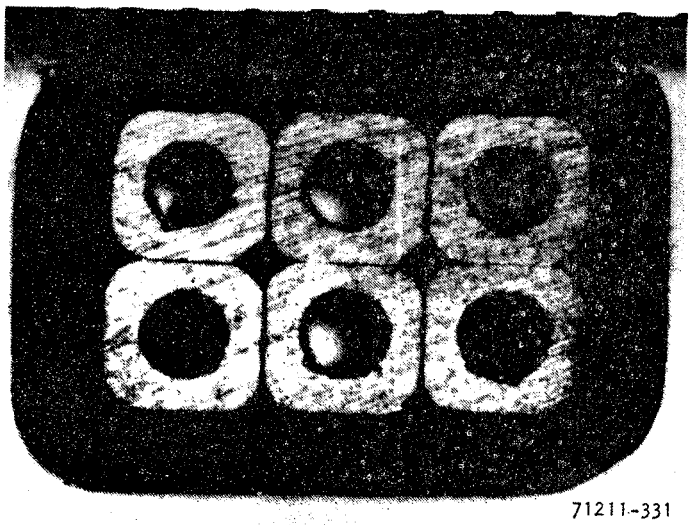

F-21426

f. STATOR COIL CROSS-SECTION SHOWING LIQUID COOLING PASSAGES

Figure 1-11. (Continued)

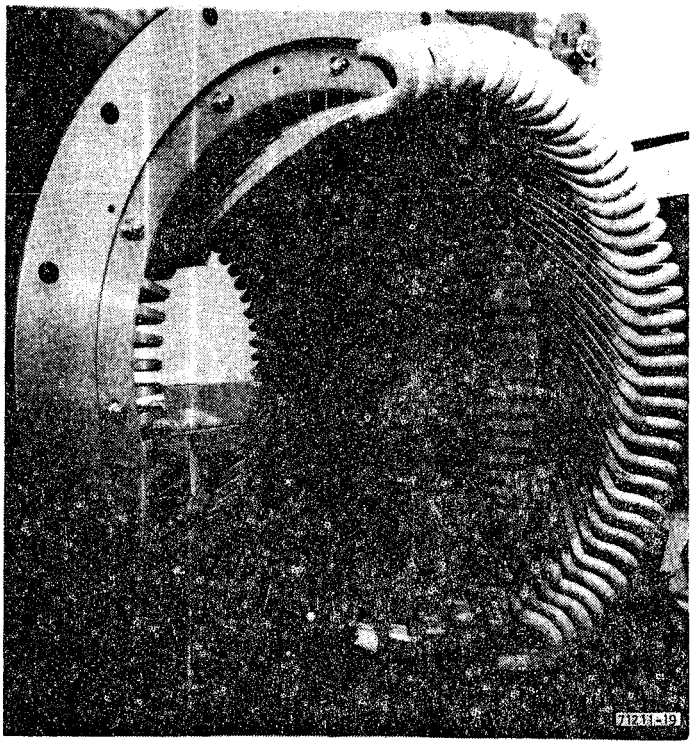

g. STATOR ASSEMBLY PARTIALLY COMPLETED

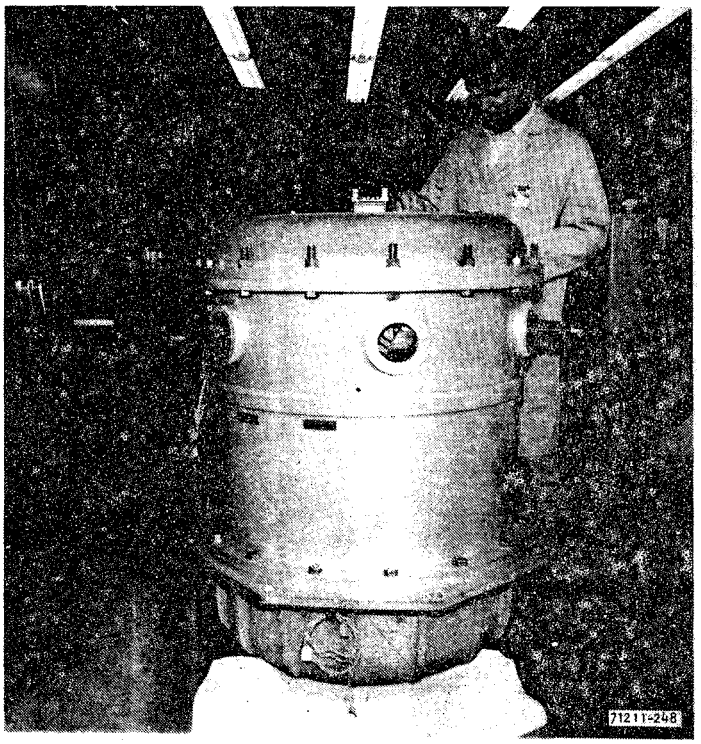

F-21435

h. FINAL ASSEMBLY

Figure 1-11. (Continued)

The machine is operated at essentially constant flux density (fixed voltage per cycle) down to zero frequency and speed. The rotor is capable of safe overspeed operation to 630 rad/s (6000 rpm).

The SC design is unique in that the machine is completely liquid cooled, including both rotor field and damper windings, stator windings, bearings, seals, sliprings, brushes, and field protection diode. In addition, provisions for liquid cooling of the stator core and lower end-bell outer diameter are incorporated. The high coolant temperatures--up to 177°C (350°F)-- and pressures--3103 kPa (450 psi)--required use of novel approaches in electrical insulation, sealing, and coolant flow connections.

Each stator conductor, produced from boron-deoxidized copper with silver content, is designed for a continuous 28.9 A/mm^2 (18,700 $A/in.^2$) current density and is insulated with a fused Kapton tape and glass wrapping, followed by sealed tape layers of mica and a final corona shield of asbestos/graphite to form a stator coil assembly. The stator coils are assembled into the stack assembly with the coils parallel. The hollow copper conductors, liquid cooled, are electrically insulated from metallic manifolds through nonconductive hoses.

The rotor is high-strength forged steel with slots machined into the core section to receive the coils. The rotor field conductor, designed for a continuous 24.6 A/mm^2 (15,900 $A/in.^2$) current density, has conventional low-voltage Class H insulation. Again, all coils are connected electrically in series and hydraulically in parallel. The motor damper winding is identical to that of the rotor field, but is, of course, uninsulated. Damper conductors join to electrically conductive end-ring manifolds to form a squirrel cage damper winding. High-strength Inconel rings restrain the rotor end windings against radial forces acting on the rotor surface peripheral speed.

The machine rating is the sum of the reactive power for the LIM and that required for the inverter, including phase-back and overlap considerations.

Field excitation for the SC is provided by the field power supply (FPS), which produces low-voltage dc power in accordance with commands received from the LIMPS control electronics.

The control logic commands the firing circuits within the FPS to step the dc output from zero field excitation at zero thrust/zero speed to 25 percent of field excitation at threshold thrust/zero speed, and to 100 percent of field excitation for all rated-load thrust commands. Dc output will then vary continuously from 100 to 150 percent of field excitation in direct proportion to overload thrust commands.

Figure 1-12 shows the FPS prior to assembly and installation in the mockup. Table 1-6 lists major FPS characteristics.

TABLE 1-6

FIELD POWER SUPPLY CHARACTERISTICS

	H x W x L:
Dimensions	29.36 x 32.07 x 73.66 cm
	(11-9/16 x 12-5/8 x 29 in.)
Mass (weight)	57.6 kg (127 lb)
Power controlled	368 kW
Input voltage	114.5 to 140 VRMS, line to line, 60 Hz, 3-phase wye or delta
Output voltage	85 Vdc (rated load), 133 Vdc (overload)
Input current	0 to 2255 ARMS
Output current	1750 Adc (rated load), 2760 Adc (overload)

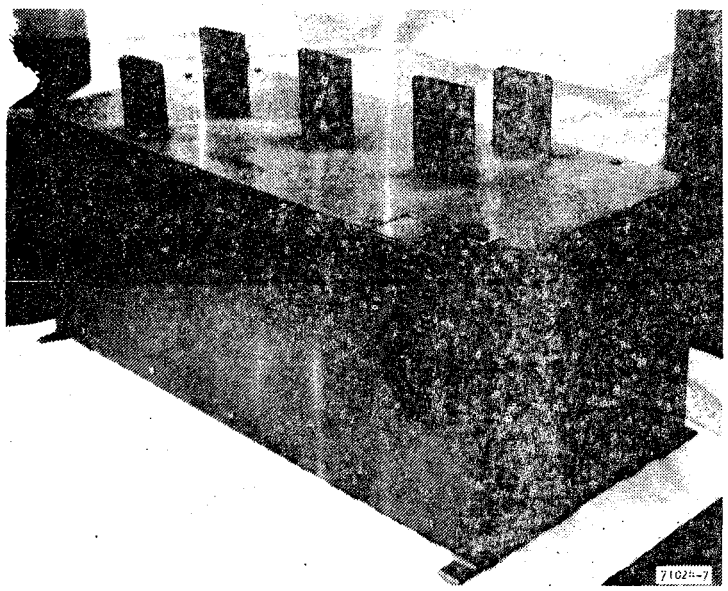

a. FULLY ASSEMBLED PRIOR TO INSTALLATION IN MOCKUP

F-21447-A

b. INSTALLED IN MOCKUP, FPS COVER AND AUXILIARY POWER TRANSFORMER ENCLOSURE PANELS REMOVED

Figure 1-12. Field Power Supply

Phase Delay Rectifier, Inductor, and Inverter

The main components involved in converting the fixed-voltage, fixed-frequency input to a variable-voltage, variable-frequency supply for the SC/LIM load are the phase delay rectifier, Brooks coil inductor, and inverter.

1. Phase Delay Rectifier

The PDR comprises a phase-controlled, 3-phase, full-wave rectifier bridge with 12 identical thyristors in series in each leg. The thyristors are rated at 2000 VRMS and 600 ARMS. Each thyristor is shunted with both a dc leakage resistance and a nonlinear snubber network comprising resistance, capacitance, and diode elements to minimize the effects of fast forward voltage rise across the thyristor and also to provide dynamic voltage sharing. Gating of the thyristors is controlled by a logic and control unit through a high-frequency carrier system designed to provide high-voltage isolation between the thyristor gates and the control unit. The actual gating circuit for the various thyristors is packaged integrally with its respective device.

Figure 1-13 shows the PDR fully assembled, but without the side covers in place. Table 1-7 lists major characteristics of the PDR and the inverter.

2. Inductor

The rectified output of the PDR passes through an inductor. The high-voltage inductor provides: (1) surge current protection for the PDR and inverter thyristors, and (2) smoothing of the dc link ripple voltage. Basically an air-core Brooks coil, it is liquid cooled to minimize size and weight. The coil inductance was selected primarily to limit surge currents to values within the capability of the selected PDR and inverter thyristors. Also, this inductance provides adequate ripple current smoothing. THe nominal inductance of the coil in free air is 22 mH. Figure 1-14 shows one coil of the inductor, ready for final assembly. Table 1-8 lists major inductor characteristics.

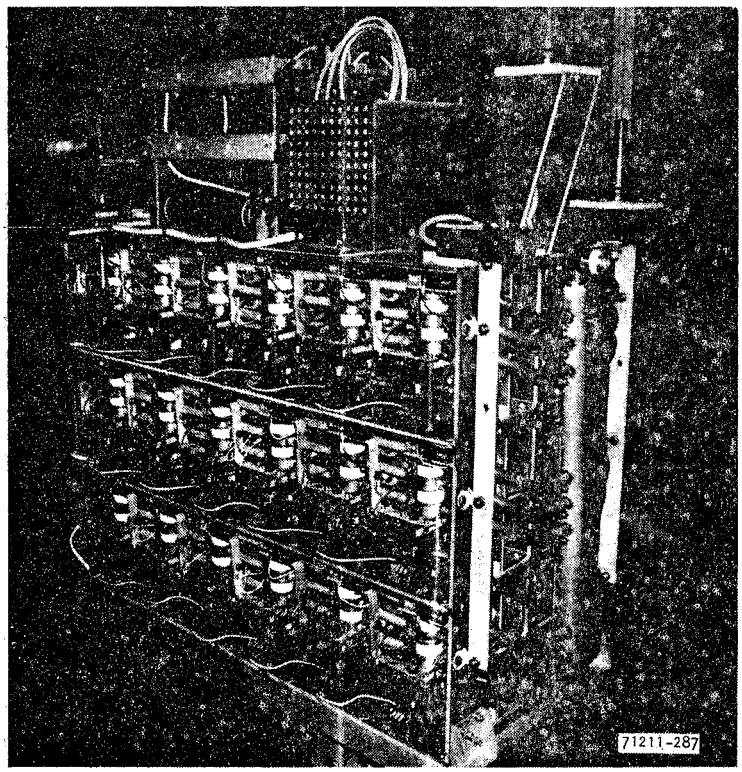

Figure 1-13. Phase Delay Rectifier

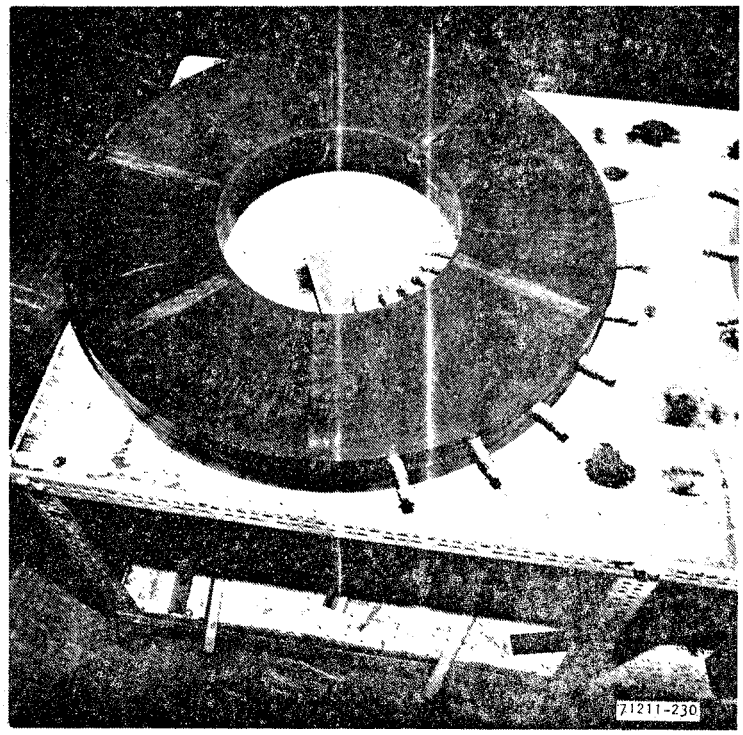

F-21424

Figure 1-14. Brooks Coil Inductor

TABLE 1-7

PDR AND INVERTER DESIGN DATA

Design Point	PDR	Inverter
Dimensions, m (in.)	1.22 H x 0.56 W x 1.24 L (48.0 H x 48.0 W x 48.8 L)	1.22 H x 0.56 W x 1.07 L (48.0 H x 22.0 W x 42.2 L)
Mass, kg (Weight, lb)	280 (617)	226 (498)
Connection	Three-phase, full-wave, bridge	Three-phase, full-wave, bridge
Power controlled, MW	6.0	6.0
Input voltage	7000 to 8250 VRMS	0 to 8890 Vdc
Peak transient voltage	28,800 V	24,000 V
Output voltage	0 to 8890 Vdc	0 to 7125 Vac
Frequency, Hz	60	0 to 165
Input current	0 to 550 Aac	0 to 680 Adc
Output current	0 to 680 Adc	0 to 550 Aac
Thyristors		
Type	C602, GE	C602, GE
Voltage rating, VRMS	2000	2000
Current rating, ARMS	600	600
Number per module	2, in series	2, in series
Number modules/phase	12, in series	10, in series
Total number	72	60
Gate firing	Continuous	Continuous
Turnoff time, μs	200	200
Delay time, μs	4	4
Cooling		
Water cooling load, kW	24.5	25.2
Water temperature, °C	74	74
Water flow, l/s (gpm)	2.3 (36)	2.3 (36)
Air cooling load, kW	13.7	11.4
Air temperature, °C	74	74
Airflow, l/s (cfm)	850 (1800)	850 (1800)

TABLE 1-8

INDUCTOR CHARACTERISTICS

Parameter	Value
Dimensions	H x W x L: 1.03 x 0.28 x 0.84 m (40.6 x 11.2 x 33 in.)
Mass (Weight)	277 kg (611 lb)
Inductance	22 mH, free air
Current	0 to 680 Adc
Voltage capability	0 to 8890 Vdc
Power dissipation	28 kW rated, 60 kW overload
Ripple current	13 percent of rated load, RMS
Surge current	300 A, 1 cycle

3. Inverter

The inverter is very similar to the PDR in design. Due to the nature of the propulsion system, voltage transients generated on the load side are less severe than on the source side, so only 10 thyristors per leg are required by the inverter in order to share the voltage.

In the drive mode of vehicle operation, the inverter converts the dc link voltage from the inductor into a variable frequency voltage, which is supplied to the SC/LIM load. In the braking mode, the roles of the PDR and inverter are reversed, with power flowing in the opposite direction, from SC/LIM into the wayside power source. Inverter driver logic and capacitors for the transient suppression circuit are mounted atop the inverter.

The thyristor devices in the PDR and inverter incorporate modular packaging. Each thyristor module is common to both units and contains two thyristors with their respective gating circuits, voltage sharing circuits, and water-cooled heat sinks. Figure 1-15 shows the module.

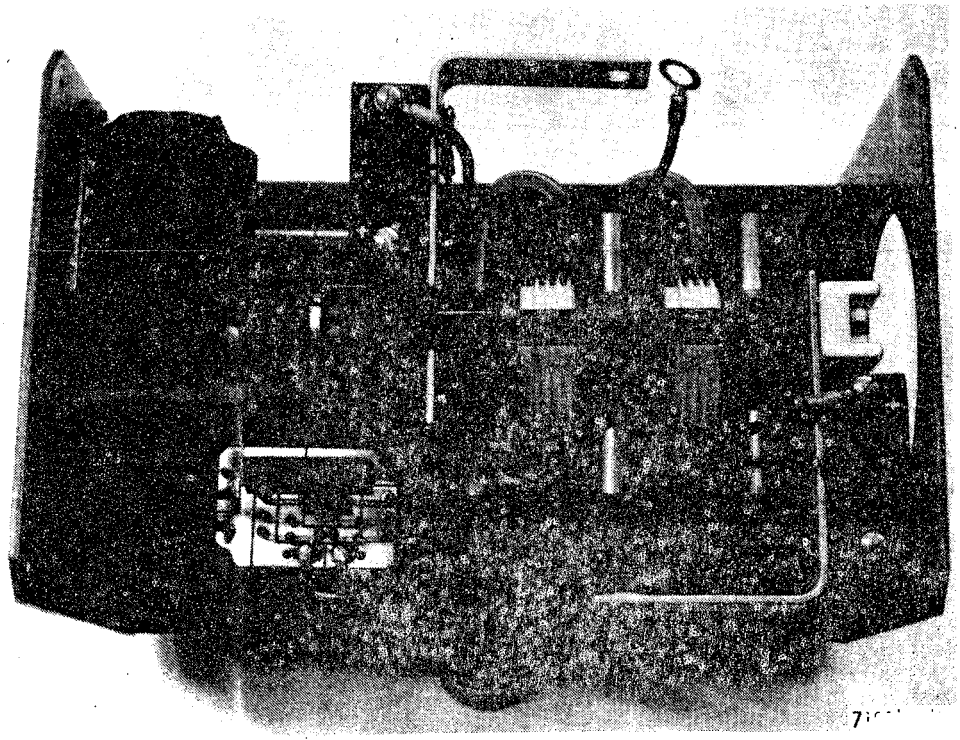

a. FRONT VIEW SHOWING LIQUID-COOLED THYRISTORS AND GATE FIRING CIRCUITRY

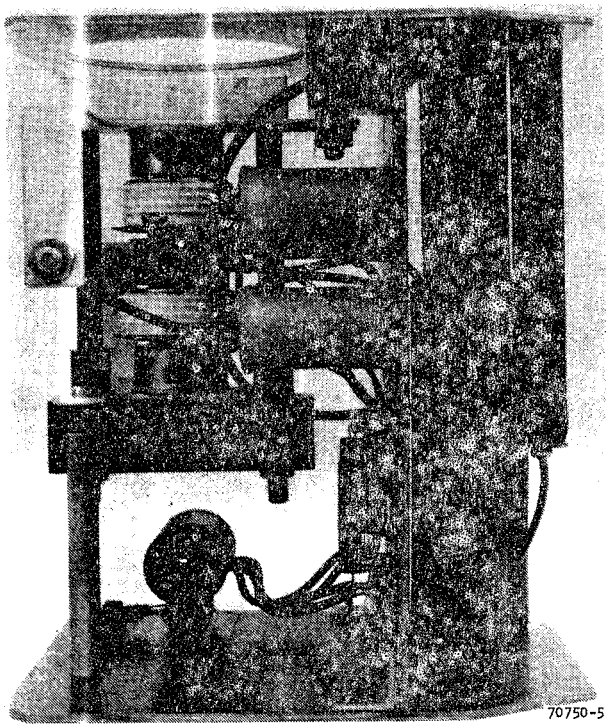

F-21436 -A

b. SIDE VIEW (ALONG RIGHT EDGE) SHOWING VOLTAGE SHARING NETWORK

Figure 1-15. PDR/Inverter Thyristor Module

Figure 1-16 shows the inverter fully assembled, but without the side covers in place. Figure 1-17 locates the inverter as installed in the test mockup.

Load Break Switch

The primary sources of electrical protection for the LIMPS components are the high-voltage load break switches mounted in the load break switch (LBS) enclosure. The three-phase, high-voltage, input power is supplied, through the LBS, to the two LIMPS loads:

Propulsion power components

Auxiliary power transformer

The LBS enclosure houses two switch assemblies, each comprising autonomous three-phase switches, suitably fused. Figure 1-18 shows both propulsion power and auxiliary power switch assemblies, and Figure 1-17 shows the enclosure into which the switches are mounted as installed in the test mockup.

The propulsion power switches, those supplying LIM power, are rated 10 to 12 kV at 630 A. The switch that controls the input to the auxiliary power transformer is rated 10 to 12 kV at 400 A. Both switches will interrupt their rated current at rated voltage without sustaining contact damage. The load break switches are equipped with 24- to 28-Vdc actuators for closing. A spring (trip spring) is preloaded and latched during the closing operation. Application of a 24- to 28-Vdc signal to the latch will open the switch.

The LBS assembly dimensions (H x W x L) are 1.37 x 0.46 x 1.47 m (54 x 18 x 59 in.). It weighs 470 kg (1035 lb).

Auxiliary Power Transformer

The auxiliary power transformer (APT) reduces the high-voltage power supplied from the auxiliary power load break switch to a lower voltage level compatible with the electrical power required by the various subsystems of the propulsion system. Electrical power for the water coolant pumps, ventilating

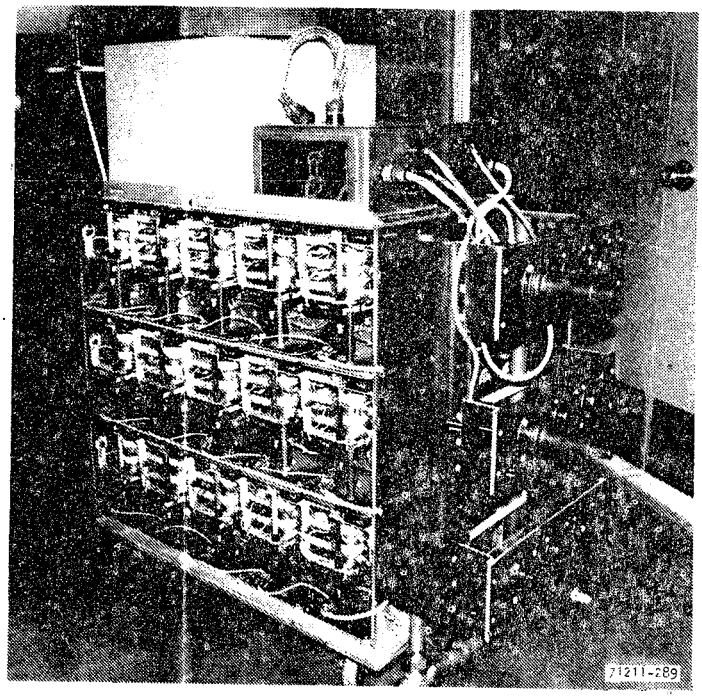

Figure 1-16. Inverter

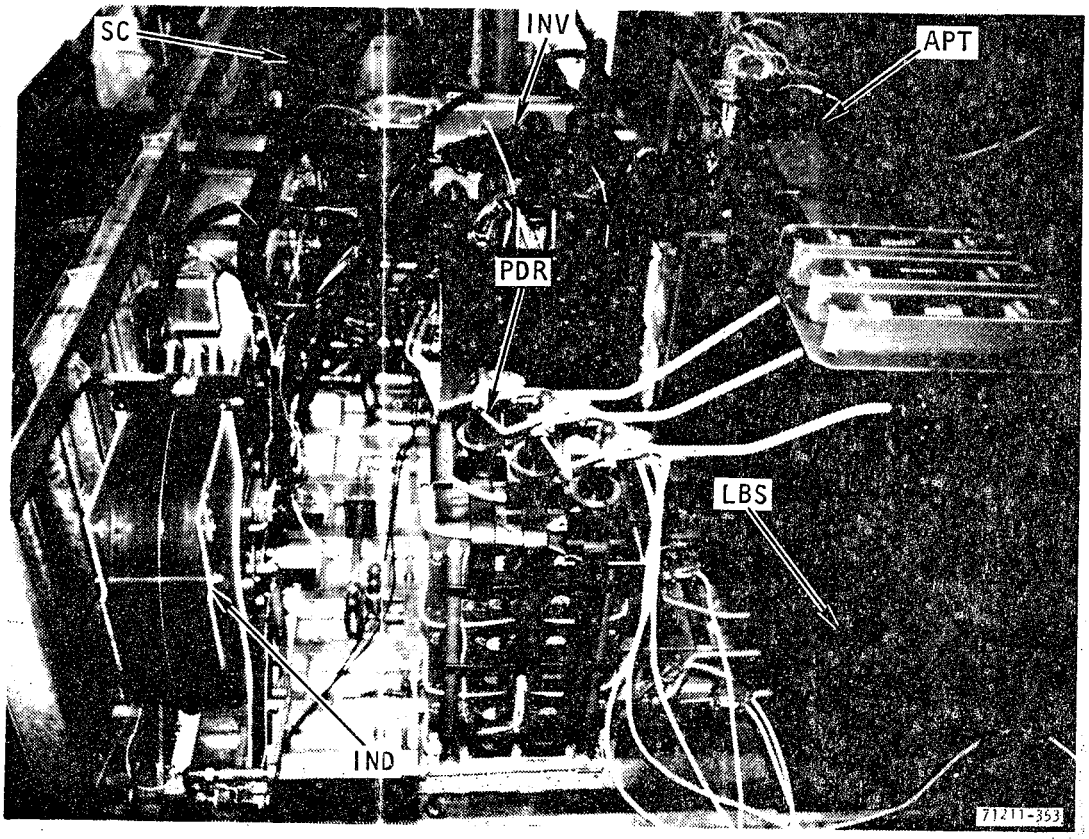

F-21423

Figure 1-17. Static Test Mockup Showing Component Locations

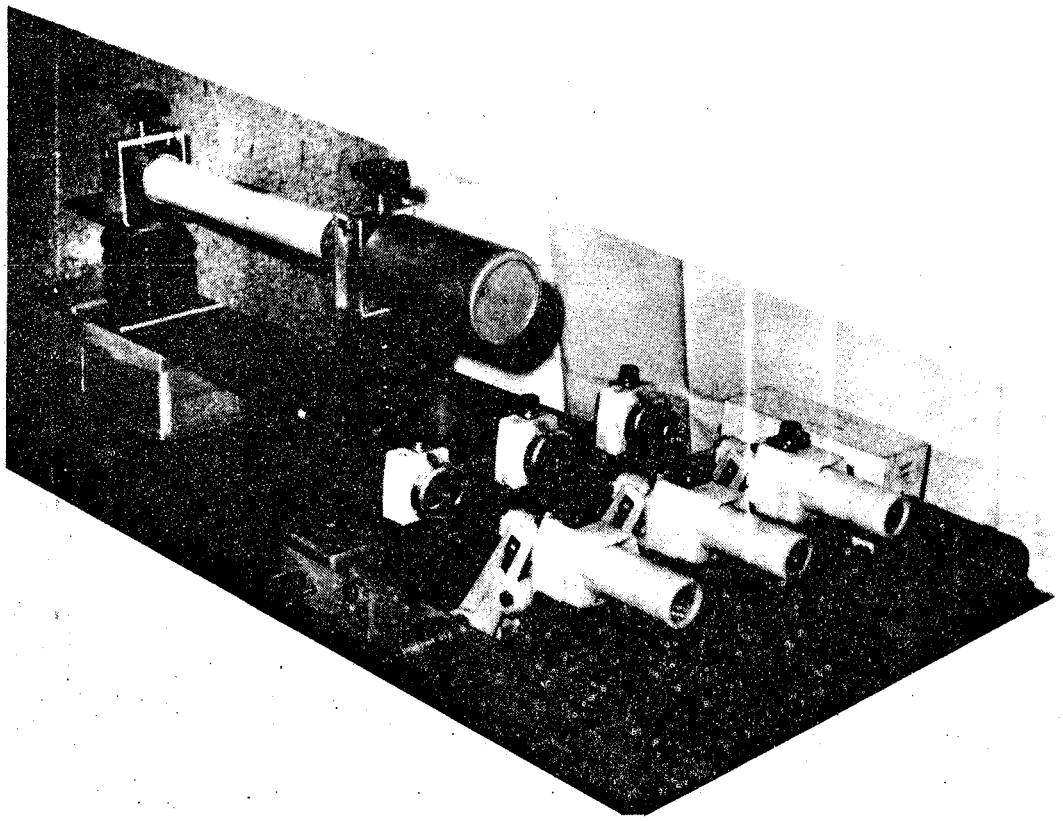

a. PROPULSION POWER SWITCH ASSEMBLY
(SINGLE FUSE SHOWN)

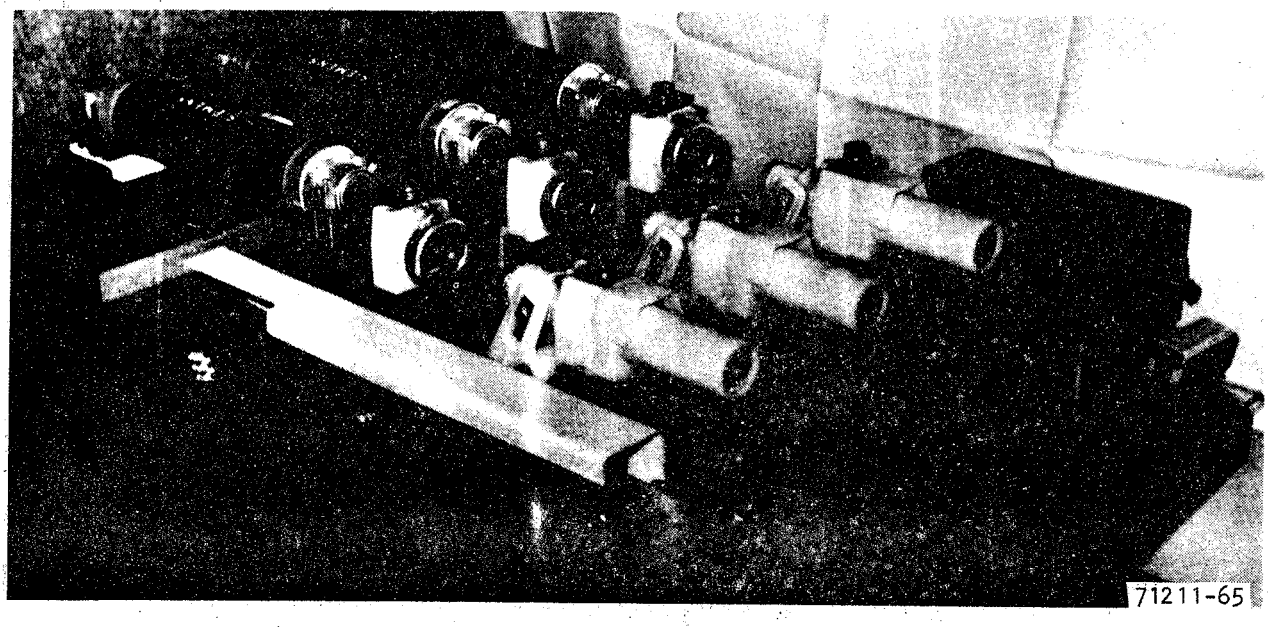

F-21437-A

b. AUXILIARY POWER SWITCH ASSEMBLY

Figure 1-18. Load Break Switches

fans, louver actuator motors, fire protection system, field power supplies, logic circuits, and other incidental electrical loads are supplied from the five secondary windings of the APT.

The APT is extremely light and compact for its high power rating. These characteristics are achieved through the use of direct liquid cooling and vanadium permendur material for the core laminations.

Figure 1-12b shows the APT installed in the test mockup, shrouded by a thermal blanket, and without its enclosure panels. The APT, including its heat blanket, mounting frame, and enclosure, has H x W x L dimensions of: 0.99 x 0.63 x 0.66 m (39 x 25 x 26 in.). It weighs 701 kg (1546 lb). The APT primary winding is rated at 8250 V, 810 kVA (full load), 1210 kVA (overload).

The secondary windings provide outputs of 140 V (delta-connected), 40 V (wye-connected), 208 V (wye-connected), rated, respectively, at 314 kVA (498 kVA overload), 5 kVA, and 100 kVA.

Controls, Displays, and Instrumentation

The system controls and displays are intended not only to allow normal operation of the system, but also to provide functional performance monitoring and protective shutdown. The four major components are:

A control quandrant

A control panel

A display panel

A control cabinet

The control quandrant allows the system operator to select both a predetermined speed limit and the desired system thrust level. The speed limit automatically overrides the thrust command whenever the latter exceeds the value required to maintain the selected speed.

The control panel provides an array of pushbutton switches for starting and shutting down the system, and also provides various performance indicators and fault warning indicators. These switches are used primarily to guide the normal system start sequence, as the buttons are functionally interlocked so that actuation of an out-of-sequence function will have no effect; the next function cannot be actuated until the prior function has signalled its readiness.

The display panel contains four meters and four corresponding rotary switches for selecting various parameters in the system for display/monitoring purposes. The selectable parameters are mostly nonperformance types (e.g., temperatures and pressures throughout the cooling system).

Figure 1-19 shows the control quadrant and control/display panels installed in the vehicle. The combined weight of these three units is 14.1 kg (31 lb).

The control cabinet accepts command signals from the control quadrant and control panel, compares them with suitable feedback signals from various system components, and provides output signals to the control circuitry of the various system components (e.g., the PDR, inverter, and field power supply). In addition to merely demanding more or less propulsion power for example, the control circuitry performs many logic functions and checks to take the system through its various operating modes (e.g., start, transition, run, and brake modes).

The control cabinet is a standard 4-drawer, 48.3-cm (19-in.) rack, as is the instrumentation cabinet. Figure 1-20 shows the electronics and packaging typical of these two cabinets, whose H x W x L dimensions are: 1.05 x 0.58 x 0.58 m (41 x 23 x 23 in.). The control cabinet weighs 124 kg (274 lb) and the instrumentation cabinet 163 kg (360 lb).

One primary objective of the TLRV program is to gather operating data on the LIMPS. For this reason very extensive instrumentation has been incorporated

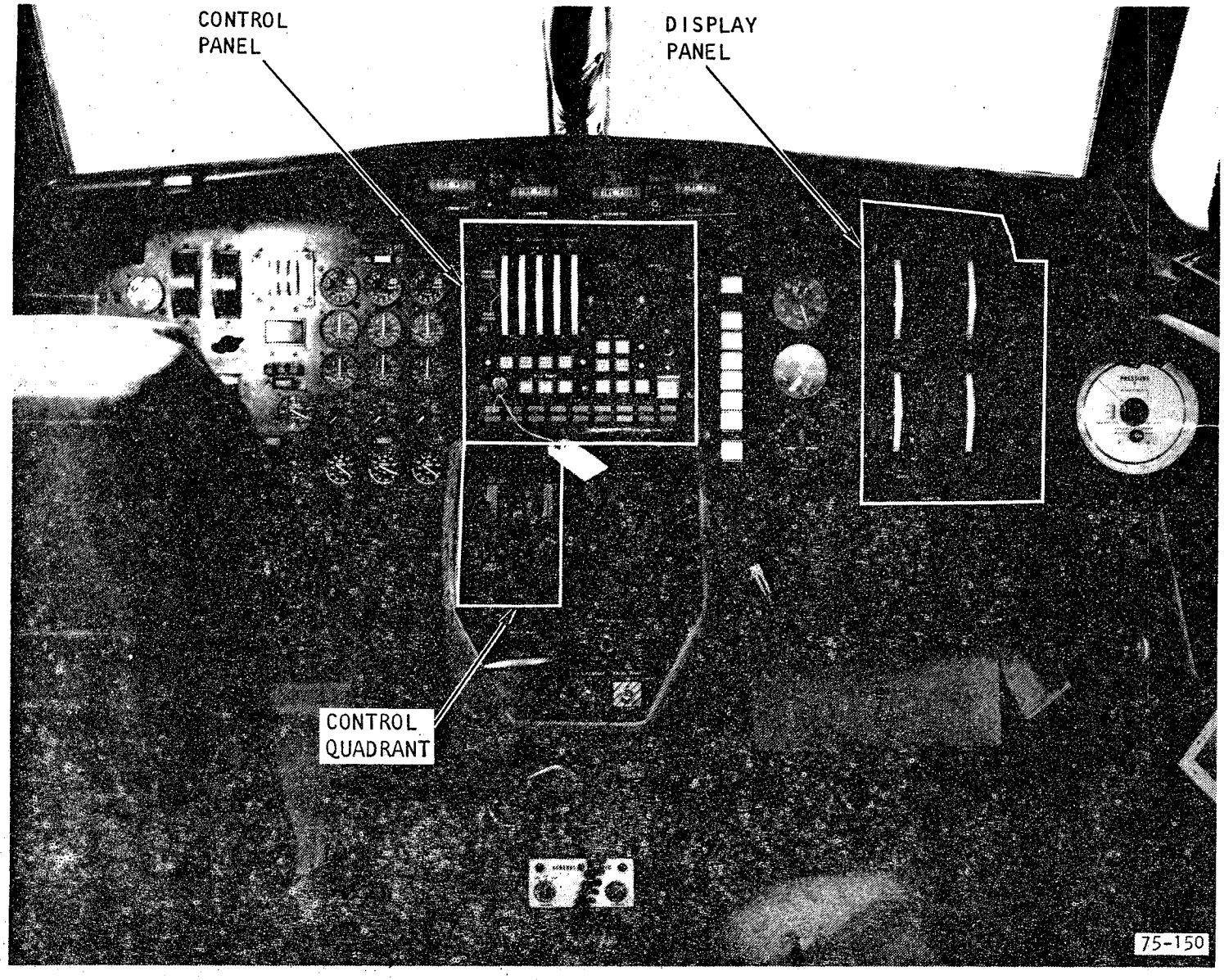

Figure 1-19. TLRV Cockpit Controls/Displays

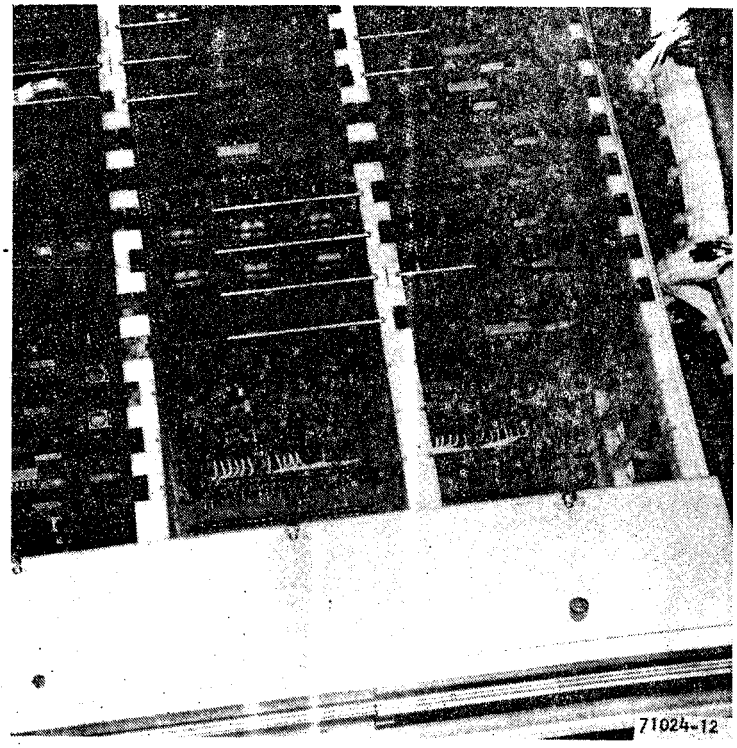

a. CONTROL CABINET DRAWER

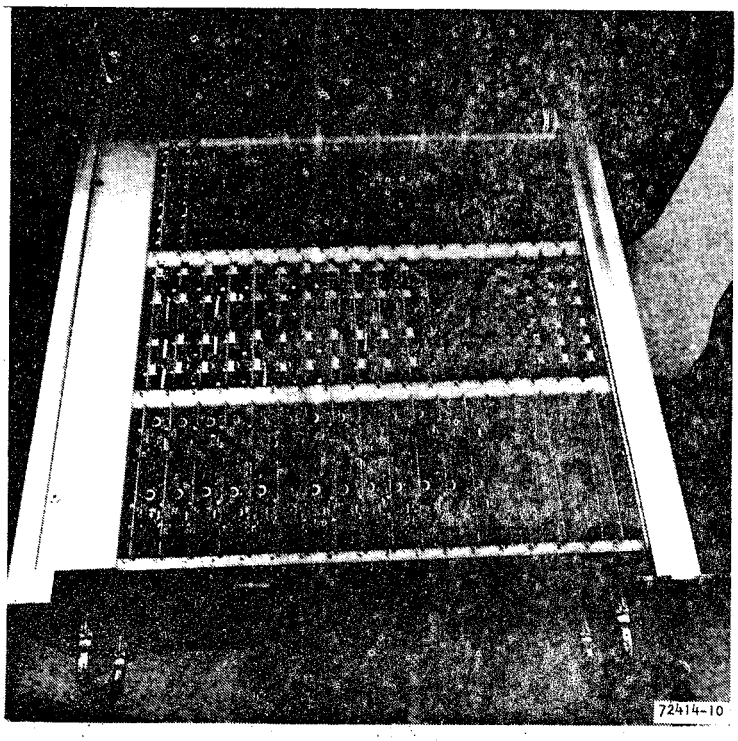

F-21438 -A

b. INSTRUMENTATION CABINET DRAWER

Figure 1-20. Typical Control/Instrumentation Cabinet Drawers

into the LIMPS, much more than would be required for normal control and monitoring. Table 1-9 lists the parameters to be recorded. Both digital and analog signals are generated, which are conditioned as necessary in the instrumentation cabinet in the vehicle equipment bay. Digital data is multiplexed and telemetered to a tape recorder at the ground based data van for subsequent computer processing. Analog data is fed to onboard oscillograph and tape recorder equipment.

Cooling System

Direct liquid cooling is a major, though indirect, contributing factor in the achievement of high power densities for the LIMPS components. The cooling system comprises two liquid cooling loops and a ventilation subsystem. The liquid loops are divided into a high-pressure loop for flow through the hollow conductors of the traditional electrical machinery and a low-pressure loop for flow through the power electronics (thyristors) heat sinks. The high-pressure loop is closed, with heat being removed by a liquid-to-liquid heat exchanger that is fed on the cold side by expendable liquid from the cold low-pressure loop. Figure 1-21 shows the liquid cooling system schematic diagram.

The ventilation system inducts outside air from the forward roof area of the PCU compartment, blows it through the compartment, and exhausts it through floor louvers near the rear of the compartment. It features both inlet and outlet louvers, water separators, and high-capacity blowers.

Figure 1-22 shows some of the cooling system components.

TABLE 1-9

LIM PARAMETERS AVAILABLE FOR RECORDING

AiResearch Measurand	Parameter	Units	Mnemonic	EU Channel (See Note 2)	Format	System Range	Sensor		Notes *
							Manufacturer, Model or PN	Location	
101	INV Aø OUT voltage	kV RMS	INVVA	1	10	0-1.5	Caddock PS 101-1	INV output	(3)
102	INV Bø OUT voltage	kV RMS	INVVB	2	10	0-1.5	Caddock PS 101-1	INV output	(3)
103	INV Cø OUT voltage	kV	INVVC	3	10	0-1.5	Caddock PS 101-1	INV output	(3)
107	LIM Aø IN current	A RMS	LIA	4	10	0-1000	AiResearch 2002508	INV output	(3) (4)
108	LIM Bø IN current	A RMS	LIB	5	10	0-1000	AiResearch 2002508	INV output	(3) (4)
109	LIM Cø IN current	A RMS	LIC	6	10	0-1000	AiResearch 2002508	INV output	(3) (4)
113	LIM avg power	MW RMS	LIMP	7	10	±1000	None	None	(3) (5) (6)
115	LIM electrical freq	Hz	FE	8	10	0-60		Top sync condenser	(3)
116	LIM thrust, uncorrected	kN	THR	9	10	±17.79	Solvere VM19-4A1	LIM linkage	(3)
141	LIM winding temp	^{o}C	LT1	49	13	0-260	Thermal Systems (2002278)	Primary #2 13-14	
142	LIM winding temp	^{o}C	LT2	50	13	0-260	Thermal Systems (2002278)	Primary #2 25-26	

* See page 61.

TABLE 1-9 (Continued)

AiResearch Measurand	Parameter	Units	Mnemonic	EU Channel (See Note 2)	Format	System Range	Sensor		Notes
							Manufacturer, Model or PN	Location	
143	LIM winding temp	°C	LT3	51	13	0-260	Thermal Systems (2002278)	Primary #2 33-34	
144	LIM winding temp	°C	LT4	52	13	0-260	Thermal Systems (2002278)	Primary #2 43-44	
145	LIM winding temp	°C	LT5	53	13	0-260	Thermal Systems (2002278)	Primary #2 53-54	
146	LIM winding temp	°C	LT6	54	13	0-260	Thermal Systems (2002278)	Primary #2 65-66	
147	LIM winding temp	°C	LT7	55	13	0-260	Thermal Systems (2002278)	Primary #1 23-24	
148	LIM winding temp	°C	LT8	56	13	0-260	Thermal Systems (2002278)	Primary #1 33-34	
149	LIM winding temp	°C	LT9	57	13	0-260	Thermal Systems (2002278)	Primary #1 43-44	
150	LIM winding temp	°C	LT10	58	13	0-260	Thermal Systems (2002278)	Primary #1 53-54	
151	LIM winding temp	°C	LT11	59	13	0-260	Thermal Systems (2002278)	Primary #1 63-64	
152	LIM winding temp	°C	LT12	60	13	0-260	Thermal Systems (2002278)	Primary #1 73-74	
153	LIM OUT coolant temp	°C	CLIM	61	12	0-260	Tylan FG 645	LIM OUT line	
154	LIM backiron temp	°C	LBT1	83	13	0-100	Thermal Systems (2002278)	Primary #2 19	

TABLE 1-9 (Continued)

AiResearch Measurand	Parameter	Units	Mnemonic	EU Channel (See Note 2)	Format	System Range	Sensor		Notes
							Manufacturer, Model or PN	Location	
155	LIM backiron temp	°C	LBT2	84	13	0-100	Thermal Systems (2002278)	Primary #2 68	
156	LIM backiron temp	°C	LBT3	85	13	0-100	Thermal Systems (2002278)	Primary #1 19	
157	LIM backiron temp	°C	LBT4	86	13	0-100	Thermal Systems (2002278)	Primary #1 68	
158	Speed limit command	V dc	SLC	33	10	0-5	Spectrol 930-279	Speed quadrant	
159	Thrust command	V dc	THRCOM	34	10	±2.5	Spectrol 930-278	Thrust quadrant	
160	Vehicle land speed	m/s	VEL	35	10	0-25	Nucleus NC-7	Trailing vehicle	
161	LIM acceleration	m/s^2 peak	ACC	36	10	±10			(3)
201	Sync cond Aø current	A RMS	SCIA	10	10	0-1000	None	None	(3)(5)
202	SC Bø current	A RMS	SCIB	11	10	0-1000	None	None	(3)(5)
203	SC Cø current	A RMS	SCIC	12	10	0-1000	None	None	(3)(5)
204	SC 3ø VAR	MVAR RMS	SCQ	13	10	±2	None	None	(5)
205	SC field current	kA dc	SCIF	14	10	0-3	AiResearch 2002506	Field power supply	(3)(4)(7)

TABLE 1-9 (Continued)

AiResearch Measurand	Parameter	Units	Mnemonic	EU Channel (See Note 2)	Format	System Range	Sensor		Notes
							Manufacturer, Model or PN	Location	
206	SC field voltage	V dc	SCVF	15	10	0-150			
207	SC field resistance	Ω	SCRF	16	10	0.02 to 0.06	None	None	(5)
208	SC vibration	g peak	SCVB1	37	11	0 to 5	Endevco 2217E	Upper lateral	(3)
209	SC vibration	g peak	SCVB2	38	11	0 to 5	Endevco 2217E	Upper vertical	(3)
210	SC vibration	g peak	SCVB3	39	11	0 to 5	Endevco 2217E	Upper longitud (approx.)	(3)
211	SC vibration	g peak	SCVB4	40	11	0 to 5	Endevco 2217E	Lower lateral	(3)
213	SC vibration	g peak	SCVB5	41	11	0 to 5	Endevco 2217E	Lower longitud (approx.)	(3)
214	SC temp	°C	SCT1	62	12	0-260	Thermal Systems (2002278)	Upper ball bearing	
215	SC temp	°C	SCT2	63	12	0-260	Thermal Systems (2002278)	Lower ball bearing	
216	SC temp	°C	SCT3	64	12	0-260	Thermal Systems (2002278)	Upper roller bearing	
217	SC temp	°C	SCT4	65	12	0-260	Thermal Systems (2015043)	Inner winding	

TABLE 1-9 (Continued)

AiResearch Measurand	Parameter	Units	Mnemonic	EU Channel (See Note 2)	Format	System Range	Sensor		Notes
							Manufacturer, Model or PN	Location	
218	SC temp	°C	SCT5	66	12	0-260	Thermal Systems (2002278)	Mid winding	
219	SC temp	°C	SCT6	67	12	0-260	Thermal Systems (2002278)	Outer winding	
220	SC temp	°C	SCT7	68	12	0-260	Thermal Systems (2002278)	Stator lamina-tions	
221	SC temp	°C	SCT8	69	12	0-260	Thermal Systems (2002278)	Housing	
222	SC temp	°C	SCT9	70	12	0-260	Thermal Systems (2002278)	Lower dynamic seal	
223	SC temp	°C	SCT10	71	12	0-260	Thermal Systems (2002278)	Brush heat sink	
224	SC temp	°C	SCT11	72	12	0-260	Thermal Systems (2002278)	Internal ambient	
225	SC temp	°C	SCT12	73	12	0-260	Thermal Systems (2002278)	Internal housing	
226	SC coolant temp	°C	CSCS	74	12	0-260	Tylan FG 645	Stator OUT	
227	SC coolant temp	°C	CSCR	75	12	0-260	Tylan FG 645	Rotor OUT	
228	SC brush temp	°C	SCT13	107	14	0-260			
229	SC brush position	mm	SCBP	108	14	0 to 1.27			

TABLE 1-9 (Continued)

AiResearch Measurand	Parameter	Units	Mnemonic	EU Channel (See Note 2)	Format	System Range	Sensor		Notes
							Manufacturer, Model or PN	Location	
301	PDR AØ IN voltage	kV RMS	PVA	17	11	2.0-2.5	Transrex (2000972)	Aux trans	(3)
302	PDR BØ IN voltage	kV RMS	PVB	18	11	2.0-2.5	Transrex (2000972)	Aux trans	(3)
303	PDR CØ IN voltage	kV RMS	PVC	19	11	2.0-2.5	Transrex (2000972)	Aux trans	(3)
304	PDR AØ IN current	A RMS	PIA	20	11	0-1000	AiResearch 2002508	PDR input	(3)(4)
305	PDR BØ IN current	A RMS	PIB	21	11	0-1000	AiResearch 2002508	PDR input	(3)(4)
306	PDR CØ IN current	A RMS	PIC	22	11	0-1000	AiResearch 2002508	PDR input	(3)(4)
307	PDR avg 3Ø power IN	MV RMS	PDRP	23	11	±2	None	None	(5)
308	PDR α command	Vdc	PDRA	24	11		None		(3)(4)
309	PDR OUT air temp	^{o}C	PDRT1	87	13	0-100	Thermal Systems 5001-19A	Lower	
310	PDR OUT air temp	^{o}C	PDRT2	88	13	0-100	Thermal Systems 5001-19A	Lower	
311	PDR OUT air temp	^{o}C	PDRT3	89	13	0-100	Thermal Systems 5001-19A	Upper	
312	PDR OUT air temp	^{o}C	PDRT4	90	13	0-100	Thermal Systems 5001-19A	Upper	
313	PDR OUT air temp	^{o}C	PDRT5	91	13	0-100	Thermal Systems 5001-19A	Logic box	

TABLE 1-9 (Continued)

AiResearch Measurand	Parameter	Units	Mnemonic	EU Channel (See Note 2)	Format	System Range	Sensor		Notes
							Manufacturer, Model or PN	Location	
314	PDR OUT air temp	°C	PDRT6	92	13	0-100	Thermal Systems 5001-19A	Logic box	
401	Inductor coolant temp	°C	CIND	76	12	0-260	Tylan FG 645	OUT line	
501	INV AØ current OUT	A RMS	INIA	25	11	0-1000	AiResearch 2002508	INV output	(3) (4)
502	INV BØ current OUT	A RMS	INIB	26	11	0-1000	AiResearch 2002508	INV output	(3) (4)
503	INV CØ current OUT	A RMS	INIC	27	11	0-1000	AiResearch 2002508	INV output	(3) (4)
504	Dc link voltage	kV dc	DV1	28	11	±2	Caddock PS 504-1	PDR output	(3)
505	Dc link current	A dc	DI1	29	11	0-1000	AiResearch 2002508	PDR output	(3) (4)
506	Link ripple current	A RMS	DIR	30	11	0-300	AiResearch 2002508	PDR output	(4)
507	INV IN air temp	°C	INVT1	93	13	0-100	Thermal Systems 5001-19A	INV input	
508	INV avg power	MW	INVP	31	11	±2	None	None	(5)
509	Mode monitor, start/run	V dc	M	32	0/1		None	INV controls	
601	Primary Pump IN pressure	MPa gage	PPP	48	12	0-2.08	Bourns 2005831901		

TABLE 1-9 (Continued)

AiResearch Measurand	Parameter	Units	Mnemonic	EU Channel (See Note 2)	Format	System Range	Sensor		Notes
							Manufacturer, Model or PN	Location	
602	Primary pump IN temp	°C	TEMIN	94	12	0-100	Tylan FG 645		
603	Input coolant temp: PDR, FS, INV	°C	CI	77	12	0-100	Tylan FG 645		
604	Output coolant temp: PDR, FS, INV	°C	CO	78	12	0-100	Tylan FG 645		
605	Aux trans coolant temp	°C	CIND	76	12	0-260	Tylan FG 645		
607	Closed loop resistivity	MΩ cm	RCC	95	10	0-8	Balsbaugh 900M/900-.01T		
608	Open loop resistivity	MΩ cm	RCO	96	10	0-8	Balsbaugh 900M/900-.01T		
609	Boiler IN coolant temp	°C	CBI	80	12	0-260	Tylan FG 645		
613	#1 pressure switch	V ac	S1	42	12	208/160 psig	Custom Components 8G		
614	#2 pressure switch	V dc	S2	43	12	282/238 psig	Custom Components 8G		
616	#4 pressure switch	V dc	S4	4	12	30/psig	Custom Components 8G		
801	Collector arm vert position	rad	CAVP	45	11	-0.157 to 0.262	Cal Best 805080	Junction box	

TABLE 1-9 (Continued)

AiResearch Measurand	Parameter	Units	Mnemonic	EU Channel (See Note 2)	Format	System Range	Sensor		Notes
							Manufacturer, Model or PN	Location	
802	Collector arm extension	cm	CAE	46	11	0-30	Research 7101-12	Top of arm	
803	Collector arm drag force	N	CAD	47	11			Arm joint	
G68	Thrust deflector position	rad	GTDP	99	14	0-1.69			(1)
G79	Air duct pressure	kPa gage	GADP	100	14				(1)
G166	Crew REF signal	V	GCRS	101	14	0/1		Cockpit	(1)

TABLE 1-9 NOTES

1. Installed on vehicle by AiResearch.
2. Additional channels:

103	IRIG-B hours
104	IRIG-B minutes
105	IRIG-B seconds
106	frame count

3. These measurands are connected also for analog recording of instantaneous values.
4. Hall-effect device.
5. Calculated in the signal conditioner from other measurands.
6. Analog signal is unfiltered.
7. The current pickup is located between the power supply and the free-wheeling diode. The peak supply current value is approximately equal to the constant current in the synchronous condenser field coil.

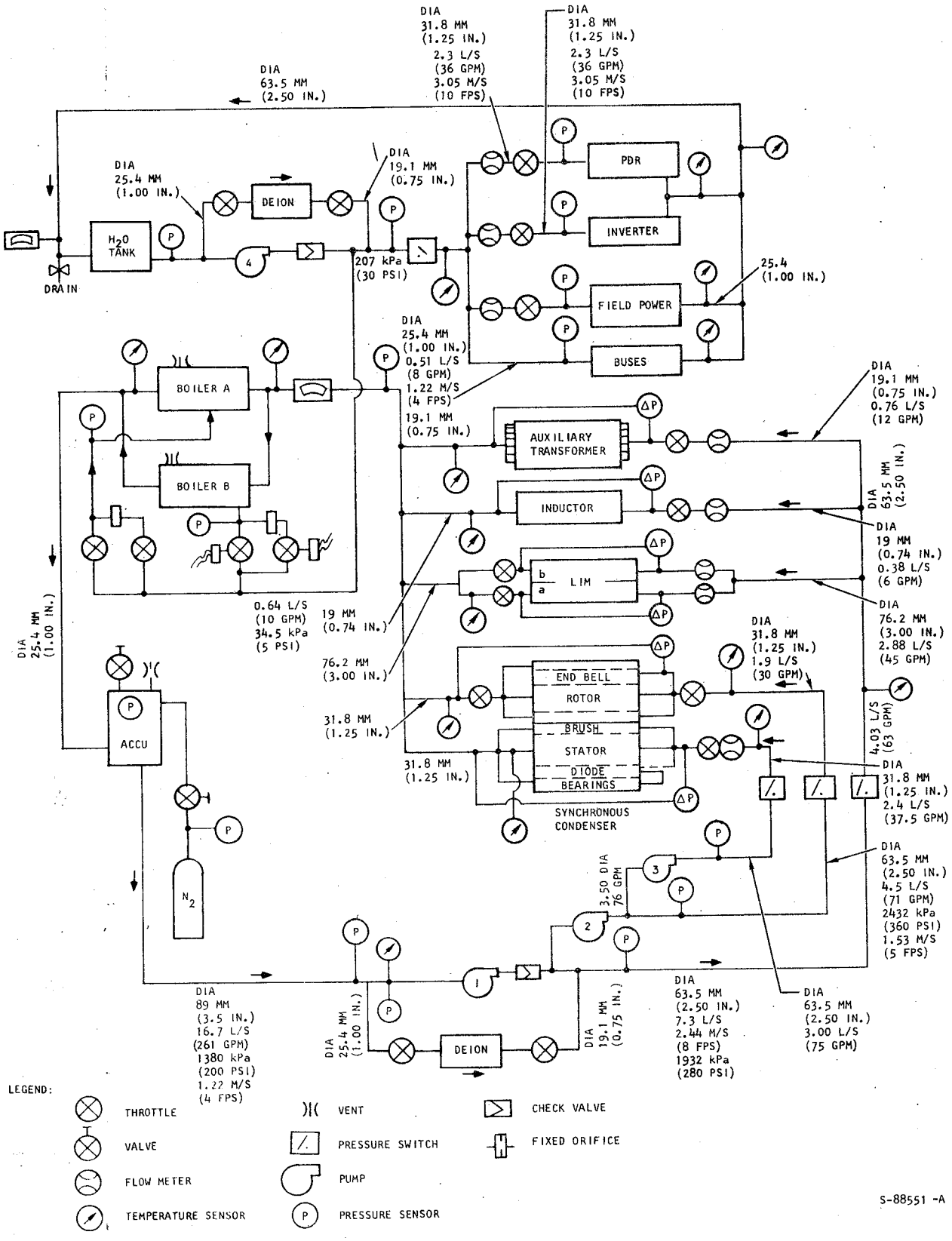

Figure 1-21. LIMPS Liquid Cooling System Schematic

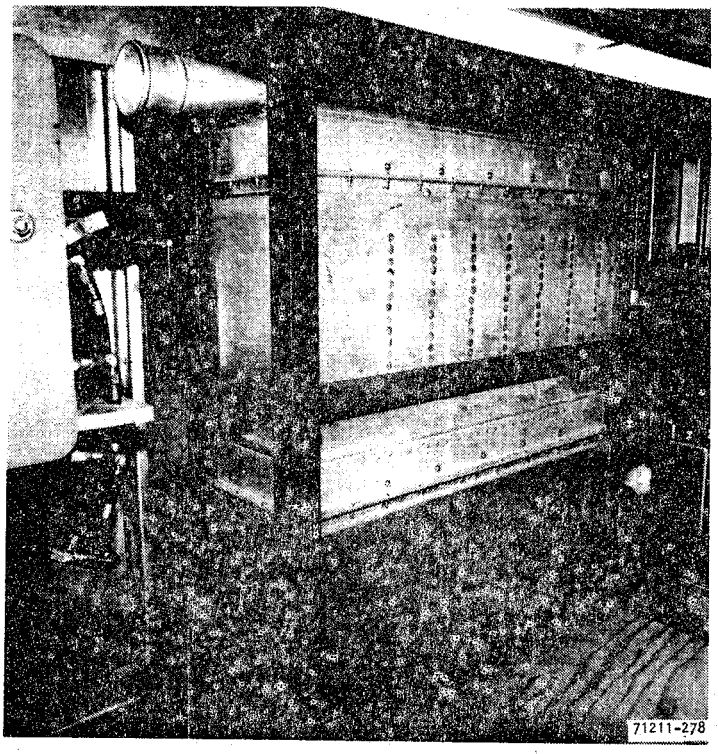

a. HEAT EXCHANGERS

F-21439

b. PUMPS--TWO OF FOUR SHOWN

Figure 1-22. Cooling System Components

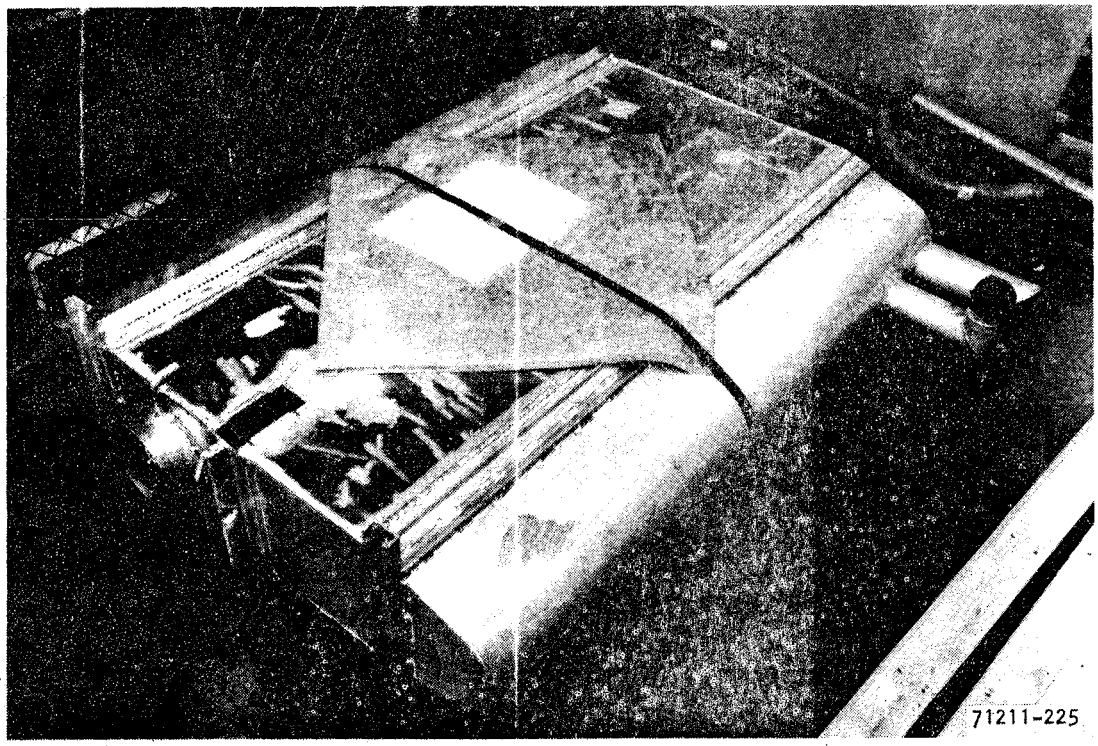

c. COOLANT STORAGE TANK

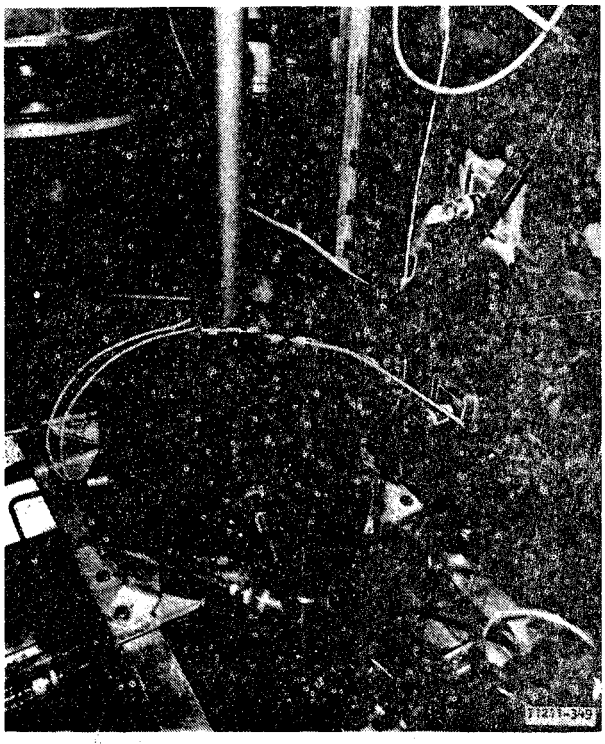

F-21440

d. HIGH PRESSURE ACCUMULATOR

Figure 1-22. (Continued)

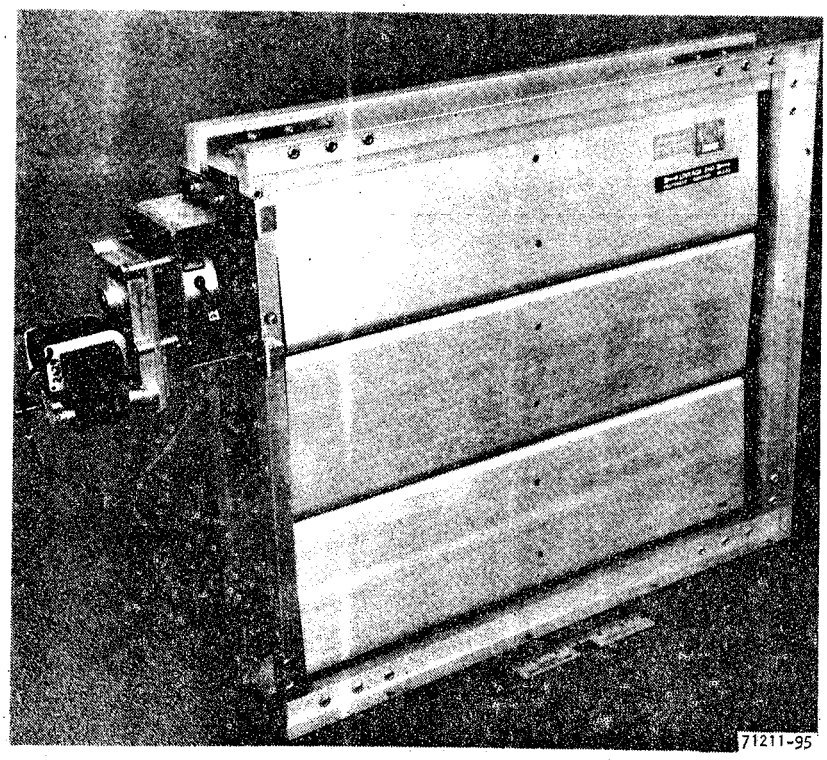

e. INLET LOWER ASSEMBLY--ONE OF TWO SHOWN

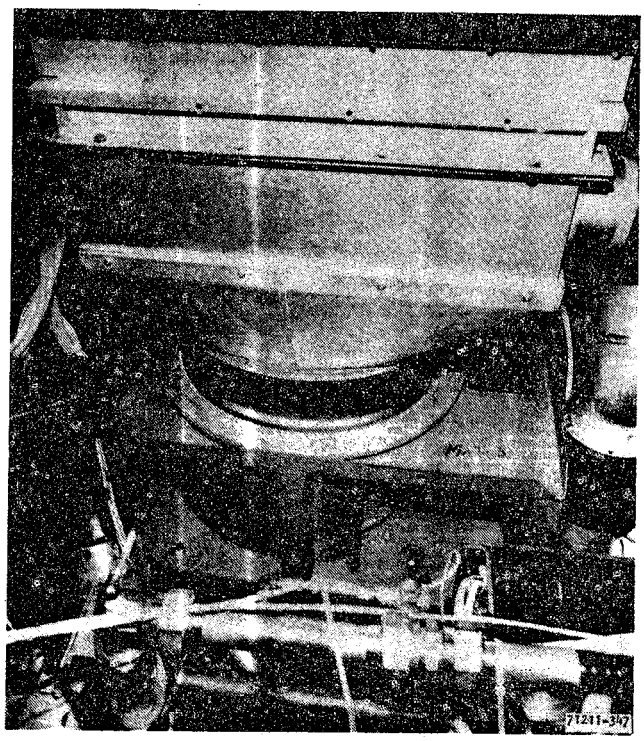

F-21444

f. VENTILATION BLOWER ASSEMBLY--ONE OF TWO SHOWN

Figure 1-22. (Continued)

SECTION 2

MOCKUP ASSEMBLY

The geographical areas of primary importance in the TLRV program included Bethpage, New York, where the vehicle was built; Torrance, California, where the LIMPS and wayside power system (WPS) were built; and Pueblo, Colorado, where the Transportation Test Center is located. Considerable distances were involved between the LIMPS site and the vehicle site, both during its manufacture and during LIMPS installation/field testing. Further, the vehicle development preceded the LIMPS development by nearly one year. Based on these circumstances, along with the diversity and complexity of the LIMPS components, it was decided early in the program to reconstruct the portion of the vehicle that would serve as the compartment for the LIMPS power conditioning unit hardware. This structure came to be referred to as the mockup and was intended to:

Act as a shipping container when the LIMPS was transferred from Torrance, California, to Pueblo, Colorado.

Simulate the vehicle dimensionally in size and shape to help minimize interface problems.

Provide a test enclosure for assembly of the system for component and system checkout tests.

This approach proved to be extremely beneficial; several interface difficulties were revealed and rectified during development phases when corrective actions were relatively easily accomplished. Considerable design time for the cooling system plumbing was saved by observing the equipment assemblage in its installation rather than having to visualize it from dozens of drawings. Determination of the acceptability of various electromagnetic fields was possible. Static tests were expedited through ease of access and the whole

shipping cycle was shortened by AiResearch being able merely to button up the mockup and load it on a commercial truck bed. At the Transportation Test Center (TTC) reinstallation of the system components into the actual vehicle (the TLRV) was also considerably simplified.

Figures 2-1 and 2-2 show, respectively, the mockup (1) near the finish of its fabrication, and (2) installed on an adjustable, movable stand, buttoned up and ready for shipment to the TTC.

Figures 2-3 and 2-4 show, respectively, the cooling system plumbing layout, and the mockup on its stand with its roof panels removed, undergoing trial fitting of the cooling system plumbing. Various skid-plates, intercostals, the sidewall hat section, mounting brackets, subfloor plumbing holes, and other LIMPS installation provisions can be seen in Figure 2-4.

Figure 2-5 shows the mockup in the test cell being prepared for the static tests with most of the LIMPS components installed.

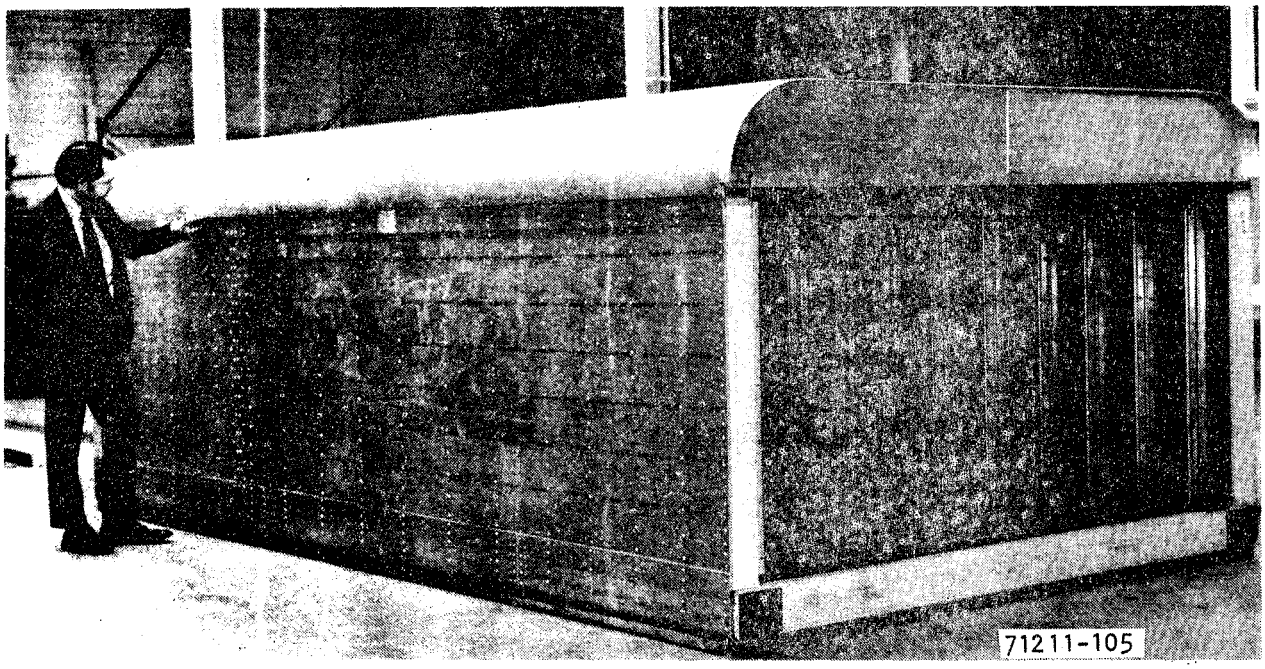

Figure 2-1. PCU Compartment Mockup

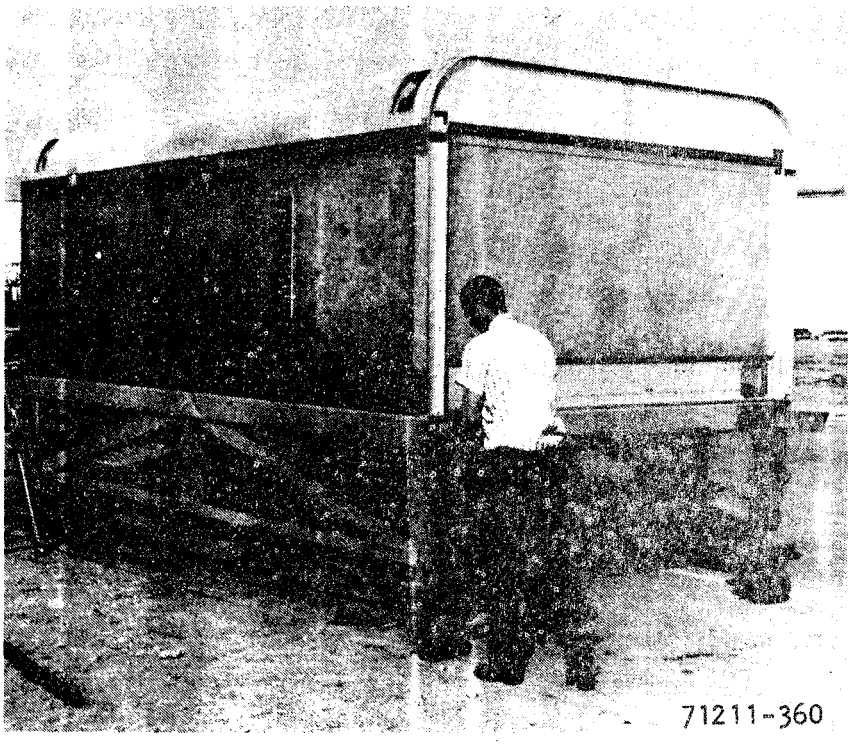

Figure 2-2. PCU Mockup Awaiting Shipment

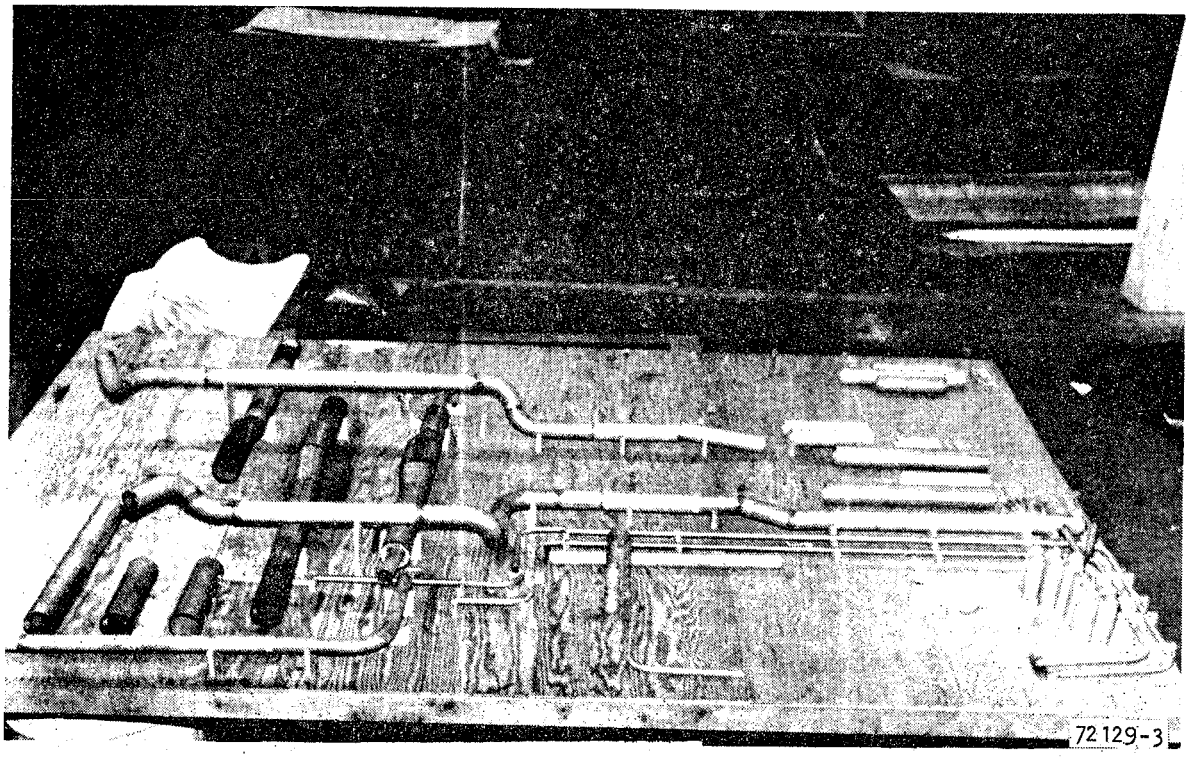

Figure 2-3. Cooling System Plumbing Layout

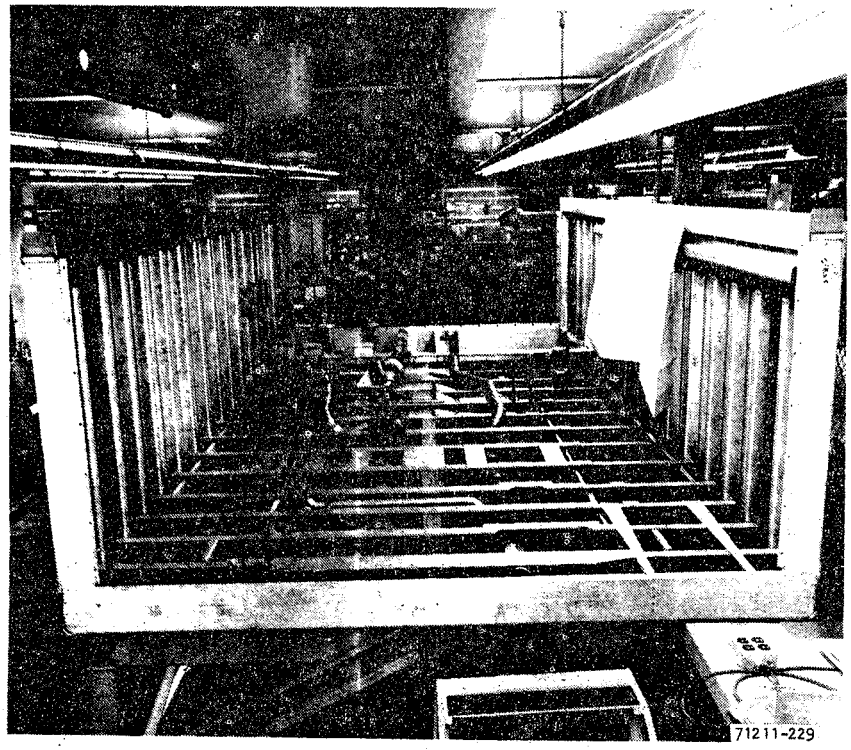

Figure 2-4. PCU Mockup during Trial Fitting of Cooling System Plumbing

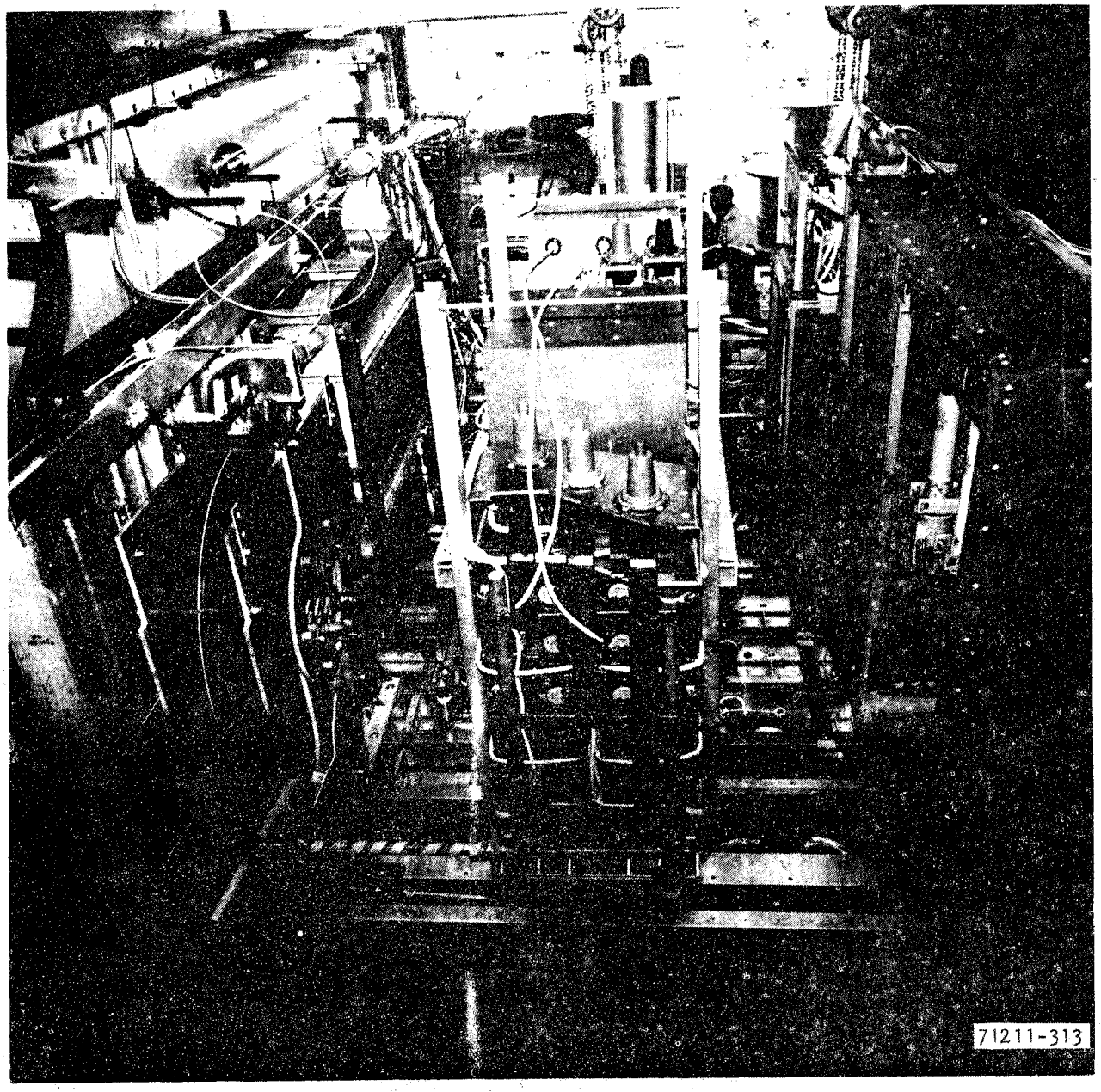

Figure 2-5. PCU Mockup in Test Cell

SECTION 3

STATIC TEST INTRODUCTION

The tests performed on the system as it was assembled in the full-scale mockup of the LIMPS power conditioning unit compartment are termed static solely because no movement of the LIM was allowed. All other components of the system were operated in their normal dynamic manner, as if the whole assembly were being operated on a vehicle moving along its test track. The tests were performed at the high-voltage test cell of the AiResearch Manufacturing Company, Torrance, California.

OBJECTIVE

The primary objective of the tests was to verify the basic performance of the assemblage of components as an integrated, predictable system. This overall goal was approached methodically in broad steps by checking the following characteristics of the system:

- Proper operation of the cooling system
- Proper operation of the protection system
- Ability to withstand rated voltage
- Ability to carry full-load current
- Ability to accept input power and produce thrust
- Ability to start and accelerate the system from zero speed
- Ability to self-limit to a selected speed
- Ability to produce regenerative power during braking
- Deviation of measured system parameters from theoretically predicted values

CONCLUSIONS

Table 3-1 summarizes the pertinent statistics of the test.

TABLE 3-1

LIMPS STATIC TESTS SUMMARY

Run Time	
At: 480 V	2 hr, 42 min, 0 sec
4160 V	3 hr, 11 min, 18 sec
8250 V	1 min, 45 sec
Total	5 hr, 55 min, 3 sec
Maximum Input Voltage	8250 V line-to-line (full rated)
Maximum Input Current	
Dc Link	600 A (129% of rated)
LIM	438 A (84% of rated)
Synchronous Condenser	444 A (79% of rated)
Maximum Synchronous Condenser Speed	488.25 rad/sec (4650 rpm), 94% of rated speed

All aspects of the test objectives were satisfied. The system demonstrated the ability to withstand full voltage, to carry load currents on the order of magnitude of rated current, and to produce thrust. The power conversion system was able to produce variable-voltage, variable-frequency power, and to commutate the inverter in both the start and the run modes. The use of water cooling for major electrical components at high voltage was successful. A problem in starting under locked-rail conditions was discovered, identified, and analyzed. It was concluded that failure to achieve transition from the start to run mode was due to the low LIM impedance associated with a locked secondary, but under conditions where the vehicle is free to move, the system will start and run. A problem in thyristor voltage sharing and operation at full voltage was encountered. Design changes were incorporated in the voltage sharing circuitry and a thyristor matching procedure was instituted to overcome this difficulty.

The ultimate result of the tests was demonstration of system readiness for actual field operational testing.

SECTION 4

TEST FACILITIES

Fabrication and testing of the LIMPS was performed in the laboratory facilities of AiResearch, Torrance. The propulsion system power components were mounted in an aluminum enclosure (refer to Section 2), which was a full-scale mockup of the propulsion system compartment in the TLRV. The aluminum enclosure and the propulsion system were located in a test cell, and the control system was set up in the control room of the cell.

Figure 4-1 shows the test cell with the mockup in place.

Figure 4-2 is the power connection diagram for the lab facility. The electrical power for the 4160-V tests was supplied from a 2500-kVA transformer. The transformer rating would permit operation of the power system at nearly full-load current for a limited time. The 8250-V tests were run with a 750 kVA-transformer, and load currents had to be limited to less than 100 A (about 200 percent of rated transformer current).

DATA ACQUISITION

The LIMPS data acquisition system (DAS) comprised an analog recording system and a computer-controlled digital recording system, together with appropriate sensors and signal conditioning circuitry. Figure 4-3 is a schematic block diagram of the entire system. As indicated, the pertinent system variables were measured by use of an appropriate sensor installed in the propulsion system itself. The output of each sensor, usually a voltage, was conditioned (amplified or attenuated), isolated where needed by operational amplifier buffers, converted to dc if initially ac, and generally operated upon by circuitry to produce an output signal proportional to the input signal

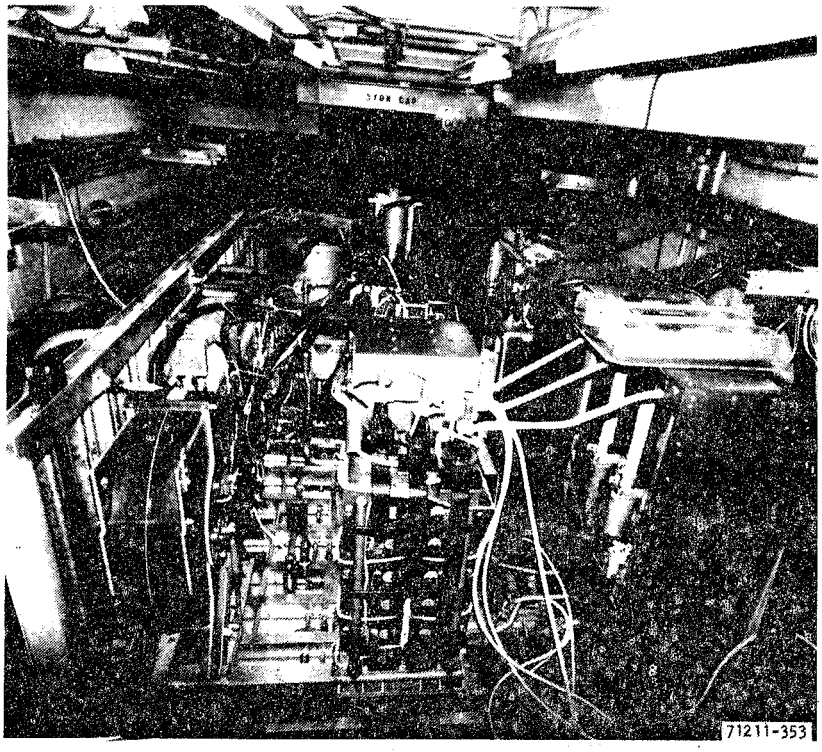

a. FORWARD VIEW, SHOWING (FOREGROUND) LEFT TO RIGHT, INDUCTOR, PDR, AND LOAD BREAK SWITCH ASSEMBLY

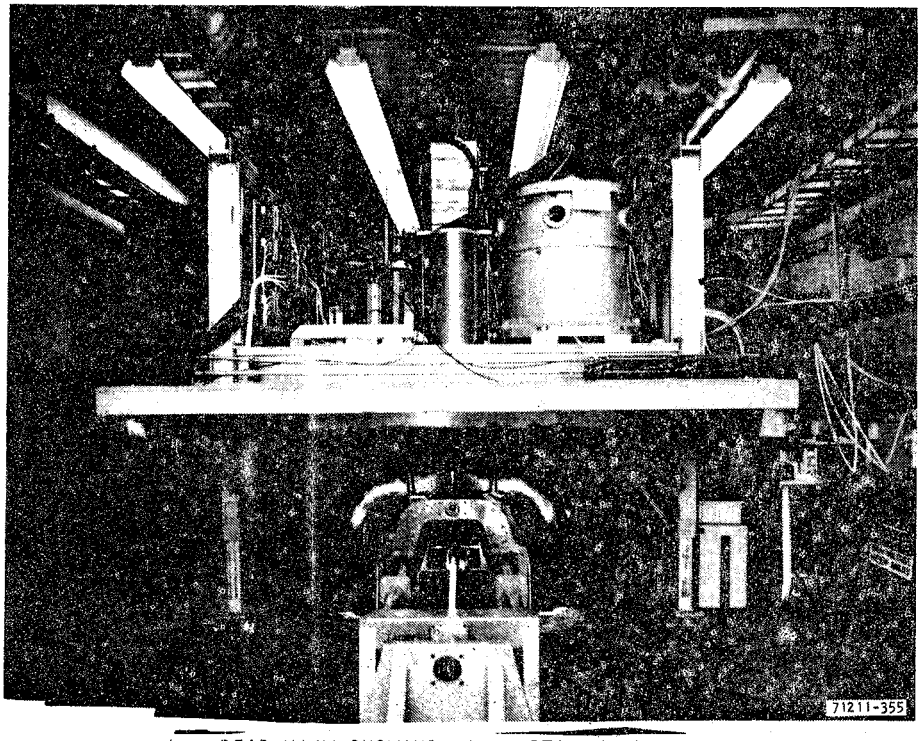

F-21441-A

b. REAR VIEW, SHOWING LIM INSTALLED BENEATH MOCKUP AND SYNCHRONOUS CONDENSER (RIGHT FOREGROUND)

Figure 4-1. Mockup with LIMPS Components Installed in the Test Cell during Static Tests

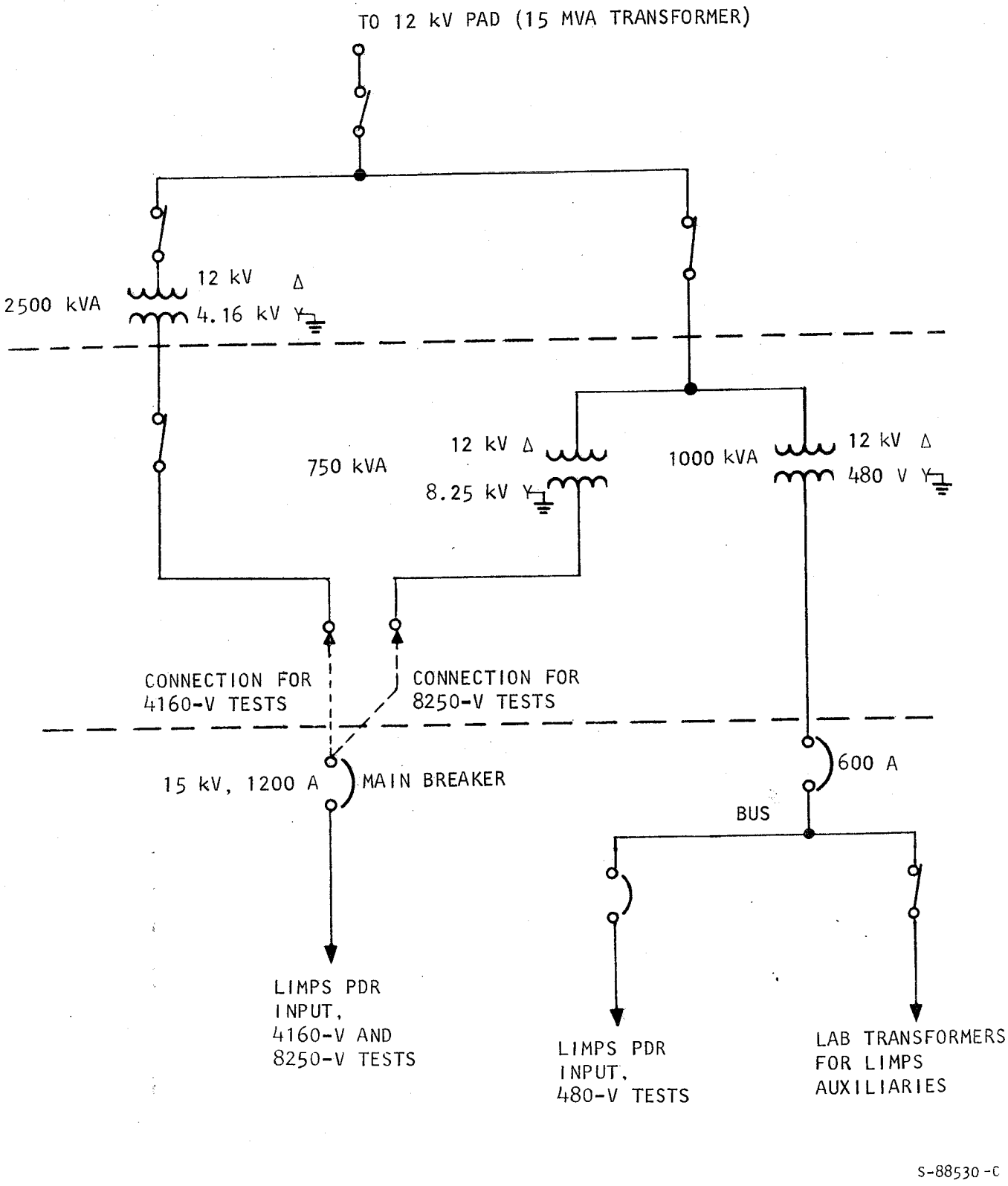

Figure 4-2. Facility Power Distribution

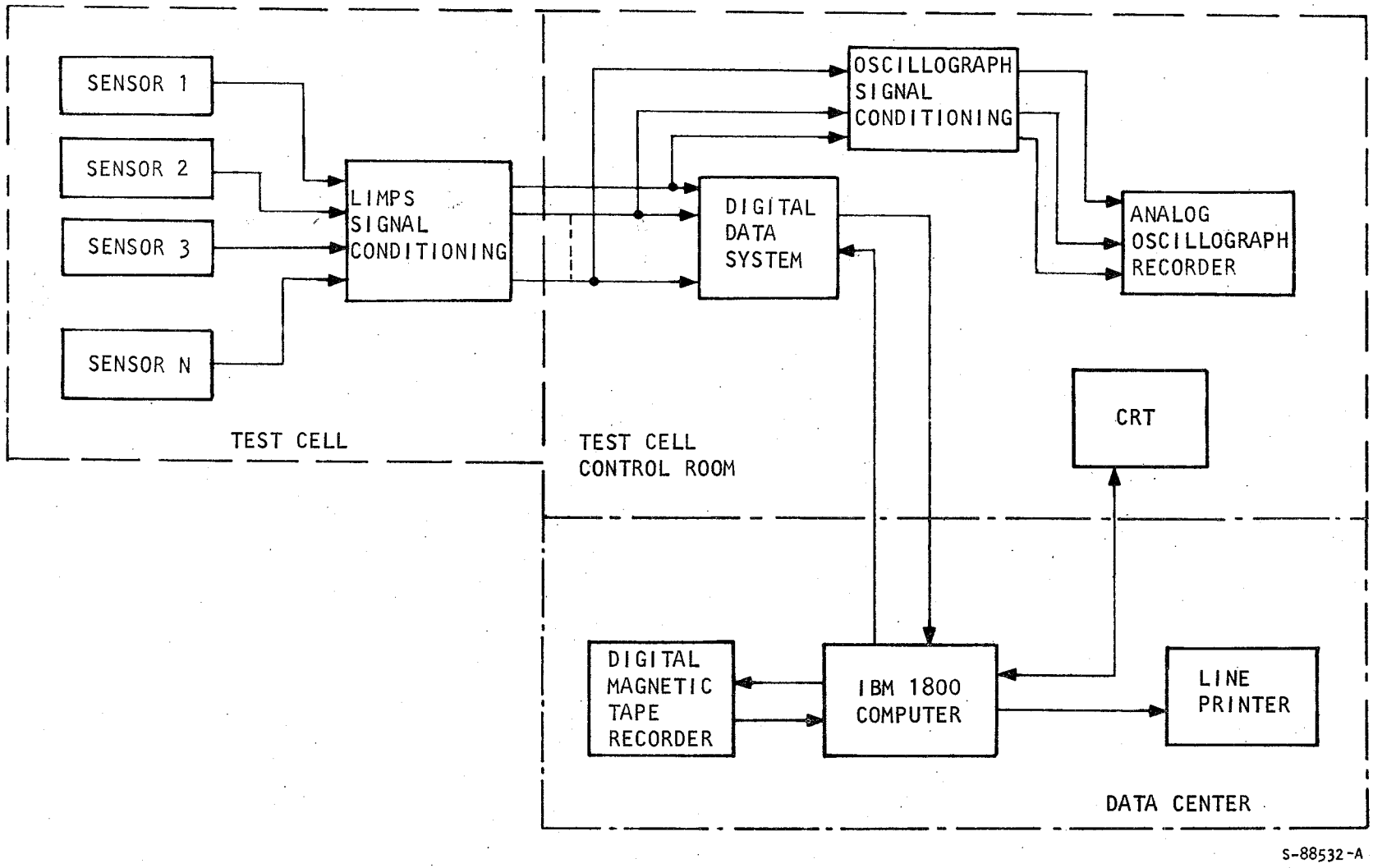

Figure 4-3. LIMPS Data Acquisition System

(sensor output), scaled so that full range of the system variable corresponded to 0 to 5 Vdc or ±2.5 Vdc. The conditioned signals were fed into either the digital or the analog recording system.

The analog system was used primarily for on-line continuous recording of critical parameters where transient information was required. The system consisted of an ultraviolet light beam oscillograph recorder and signal conditioning necessary to drive high-frequency galvanometers. The signals were recorded on 27.9-cm (11-in.) wide, light-sensitive recording paper. The number of channels recorded and their scale factors were selected to provide good readability and resolution.

The computer-controlled digital system was used primarily for recording all parameters during steady-state conditions and providing engineering calculations. The sensor outputs to be recorded were conditioned and then sampled by the data system at a rate of two samples per channel per second. These digital data were then transmitted to the IBM 1800 computer for storage and processing. This data was then transmitted to a cathode ray oscilloscope (CRT) in the test cell ontrol room for use by the test conductor. In addition, data were displayed as the output of a line printer when the test conductor requested a data point. This was accomplished by a keyboard entry on the CRT. The digital data acquisition software was set up on a priority basis: (1) save all data scans and store on magnetic tape, (2) perform engineering calculations, (3) transmit data to CRT, and (4) print out requested data points. This system was adopted to assure the retention of all data for later analysis and reduction. With this setup, the CRT was updated approximately every second. Data printout was normally available within two to three minutes after a data point was requested.

INSTRUMENTATION

Problems in measurement, and techniques used in their solution varied with the type of variable measured.

Voltage

Measurement of PDR input voltage, dc link voltage, and LIM voltage presented a special problem in that all were above 4000 V under rated conditions. Precision resistance dividers were used to reduce the dc link voltage and the LIM voltages to signal levels. For the full-voltage tests, the PDR input voltage was measured by using the output of a low-voltage winding on the auxiliary power transformer, which is proportional to the input voltage. The signals representing these voltages were buffered and conditioned to provide 0 to 5 Vdc or $\pm$2.5 Vdc signals for recording.

Current

All current measurements were made with AiResearch-designed, Hall-effect current sensors. These sensors have no direct connection to the current carrying lines and, therefore, impose a very low burden. All units are magnetically shielded and temperature compensated to achieve stability and reduce noise. Their output was buffered and amplified to provide 5.0 Vdc or $\pm$2.5 Vdc levels for recording.

Flow

Coolant flows were measured with turbine-type flowmeters. The frequency output of these meters was buffered and conditioned to provide a 5.0 Vdc analog signal proportional to flow and suitable for recording.

Thrust

For the locked-rail tests, thrust was measured with a universal strain gage-type load cell mounted between the LIM and a stationary test fixture. The

load cell output signal was amplified and buffered to provide a ±2.5 Vdc signal for recording.

Vibration

Component vibration was measured with piezoelectric accelerometers and charge amplifiers. All charge amplifier output signals were buffered and conditioned to provide ±2.5 Vdc signals for recording.

Temperature

All temperature measurements were made with platinum resistance temperature sensors. The outputs of these sensors were conditioned and filtered to provide an output signal of 5.0 Vdc for their full-scale range.

LIM Frequency

LIM frequency was obtained from one phase of the LIM voltage sensor. This ac signal was conditioned with a frequency-to-dc converter to provide a 0 to 5 Vdc signal proportional to the frequency of the LIM voltage.

Power

Average power was computed by multiplying instantaneous values of voltage and current and obtaining the average value of that product. This signal was then conditioned and buffered to provide a 0 to 5 Vdc signal for recording.

Reactive VA

Three-phase reactive VA was measured by multiplying each line current by the (line-to-line) voltage between the other two lines on an instantaneous basis and averaging the result. The output signal was conditioned to give a 0 to 5 Vdc full-range signal.

DATA DISPLAY/PRESENTATION

Both analog and digital methods were used to acquire and display data. Analog data was recorded on an ultraviolet light beam oscillograph recorder. The signals to be recorded were conditioned and amplified to provide ±2.5 Vdc

or 5.0 Vdc signal levels. The oscillograph recorder was run at a chart speed of 2.54 or 25.4 cm/s (1 or 10 ips), depending on the nature of the test. The high paper speed was useful in recording transient conditions and in providing resolution of traces during steady-state conditions. The resulting oscillograph charts were used for preliminary analysis during testing before proceeding to other test conditions. Charts were also retained for more detailed reduction and analysis later in the program.

The computer-processed digital data were displayed in the test cell control room on a CRT and were also printed out on a line printer in the data center. The CRT display provided real-time data feedback to the test conductor. Several different displays, called page options, were available for the CRT. Changes in displays were initiated by the test conductor through the CRT keyboard. Page options consisted of displays of overall system performance, heat balances, coolant system conditions, and major component performance. All sensor outputs were converted to engineering values, calculations were made, and these sensor values and calculations were printed out on a line printer. The data were displayed in the form of tabulations and flow charts that schematically represented the TLRV system. During testing, printouts were made for all test conductor flagged points. These printouts were available for review before proceeding to new test conditions. The sampling rate of the digital system was such that a data record was obtained every second. These data records were stored on digital tape for posttest retrieval and subsequent engineering calculations.

The printout pages of the digital data corresponded in format to the CRT displays. One printout page lists values of all the measurands in tabular form. A second page is a power flow diagram and shows voltages, currents, thrust, frequency, and real and reactive power values at pertinent system points. The third page is a heat balance diagram that lists and compares

calculated values of the losses with values of heat carried away from the major components by the cooling water. An example of the power flow printout sheet is shown in Figure 4-4.

Problems

Several problems were encountered with the instrumentation and signal conditioning, generally in the following categories:

- Manufacturing
- Concept/Design
- Scaling
- Noise

Most of the problems associated with manufacturing were readily found and corrected: improper wiring, missing wiring, and loose connections. Some of these problems, however, required considerable troubleshooting and consumed time due to system complexity. Most of the concept/design-related problems involved grounding and the effective matching of impedances. Scaling errors were the kind typically associated with the measurement of ac quantities. Some channels were scaled in RMS units, others in peak units, and still others in average units; thus the resolution of scaling problems was relatively complex.

Noise on signals is always a serious problem with a system like LIMPS, due to the existence of high voltage levels and large transient currents. Problems were encountered due to incorrect grounding of signal conditioning circuitry, improper impedance matching, and inadequate common mode rejection. Many of these problems were corrected, but the design objective for the signal-to-noise ratio was never achieved.

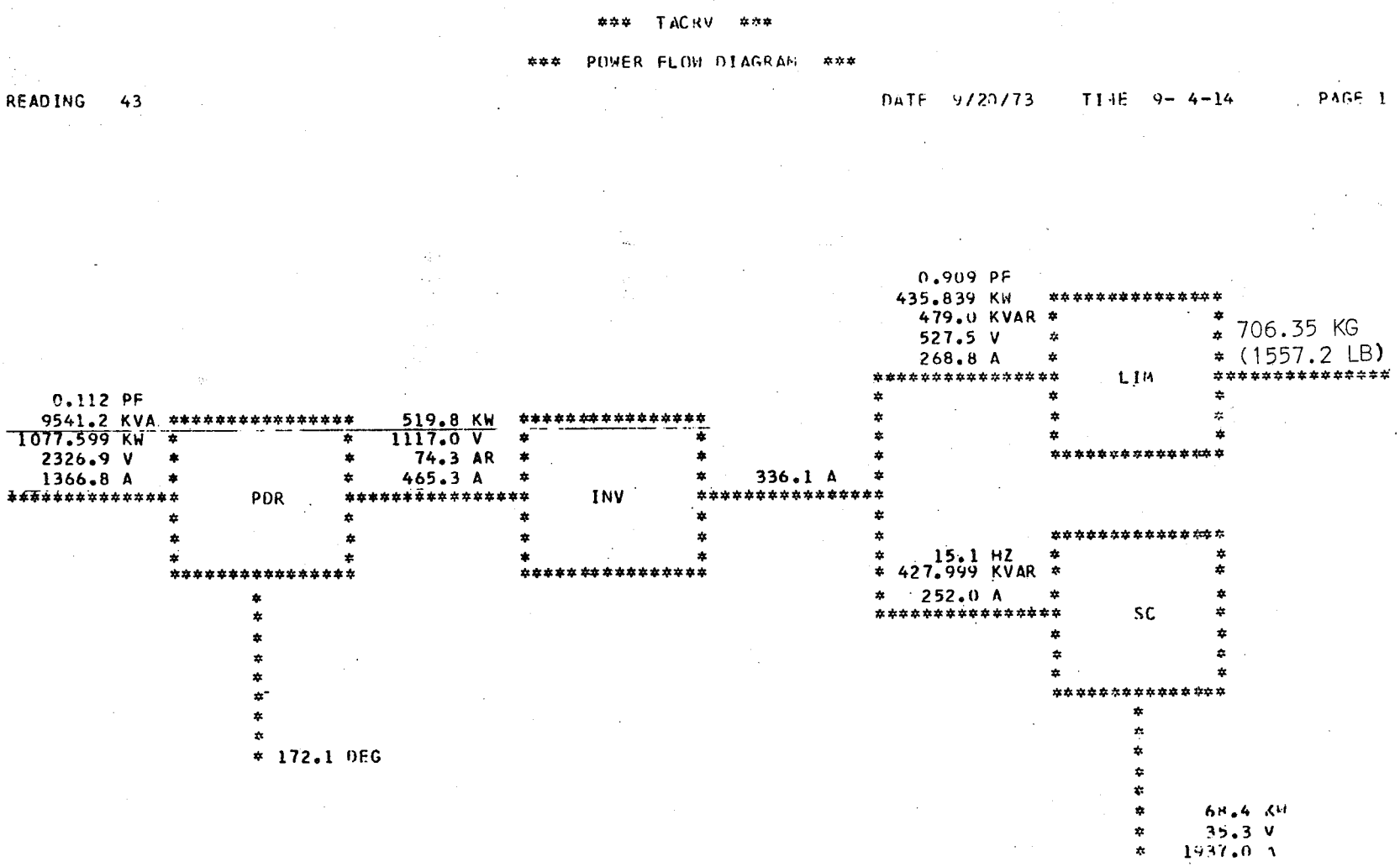

Figure 4-4. Typical Computer Program Printout of Power Flow Diagramm

SECTION 5

TESTS PERFORMED

PRELIMINARY SUBSYSTEM TESTS

Cooling System

The cooling system, which uses deionized water as the coolant for major system components, was earlier shown schematically in Figure 1-17. The system used to deionize the water is shown in Figure 5-1. This system was operated prior to any electrical system tests to assure adequate dielectric characteristics of the cooling water. Initial cooling system tests involved pump operation to verify plumbing integrity and to set and verify the desired pressure levels and flow rates at various points in the cooling loops. This was accomplished with water actually flowing through the power conversion components, but with no propulsive energy applied to the power conversion system. In adjusting the pressures and flow rates, it was found that for the half-system built, two (rather than three) pumps in the high-pressure loop were sufficient to provide the desired flows. Accordingly, the third pump was not energized during the static test program. It was left in place, however, to avoid a redesign of the plumbing layout.

After initial difficulties with plumbing integrity were overcome, the cooling system performed well, though not without incident. One motor failure was experienced near the end of the program; the cause was not fully determined. A possibility was that contamination of the cooling water caused blockage of the water line providing lubrication for the motor upper bearing. The motor was replaced with a new unit. Another problem was the occurrence of repeated water leaks at Tygon tubing joints between the PDR and inverter thyristor modules and the thyristor heat sinks. Nonelastic deformation, which apparently is a

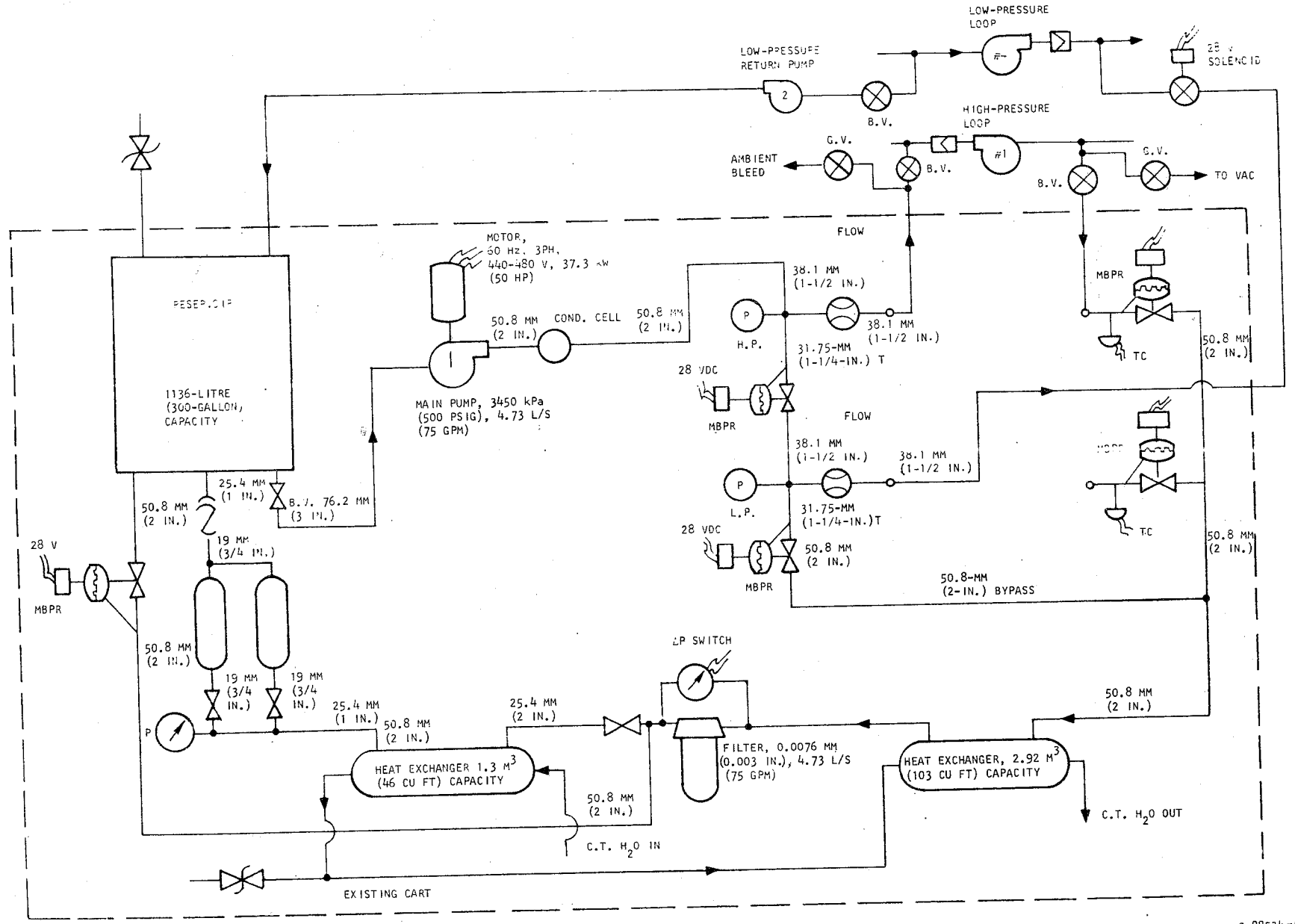

Figure 5-2. Facility Deionization System

s-88534-A

property of this tubing, could cause leakage in the low-pressure cooling loop if the system remains inoperative for long periods of time.

Instrumentation and Control System

Those portions of the control and instrumentation system required to regulate the startup and shutdown sequences were tested with the power conversion system deenergized. The manual startup and shutdown sequence was checked by operation of the pushbutton controls and simulation of the appropriate feedbacks during simulated startup and shutdown. Automatic shutdown was checked by simulating malfunctions and observing the resulting signal that opened the high-voltage switches. Instrumentation channels were calibrated prior to actual system operation.

PCU Control and Protection System

The PCU control and protection system was tested prior to actually energizing the power conversion system. Again, the appropriate responses on the part of the control system to simulated requests for thrust and braking were noted, on a signal level. Likewise, appropriate responses to simulated failure modes were observed, again on a signal level. After correction of some initial difficulties the system performed well. During the later system tests, the response of the protection system to actual malfunctions, such as inverter commutation failures, was fast and effective.

In addition to the subsystem tests, a dielectric test was performed on the high-voltage elements of the system prior to energizing them.

SYSTEM TESTS AT 480 V

Basic No-Load Testing

Initial system testing was conducted at 480 V to insure the lowest possibility of dielectric failure. Figure 5-2 shows the test setup. Field power for

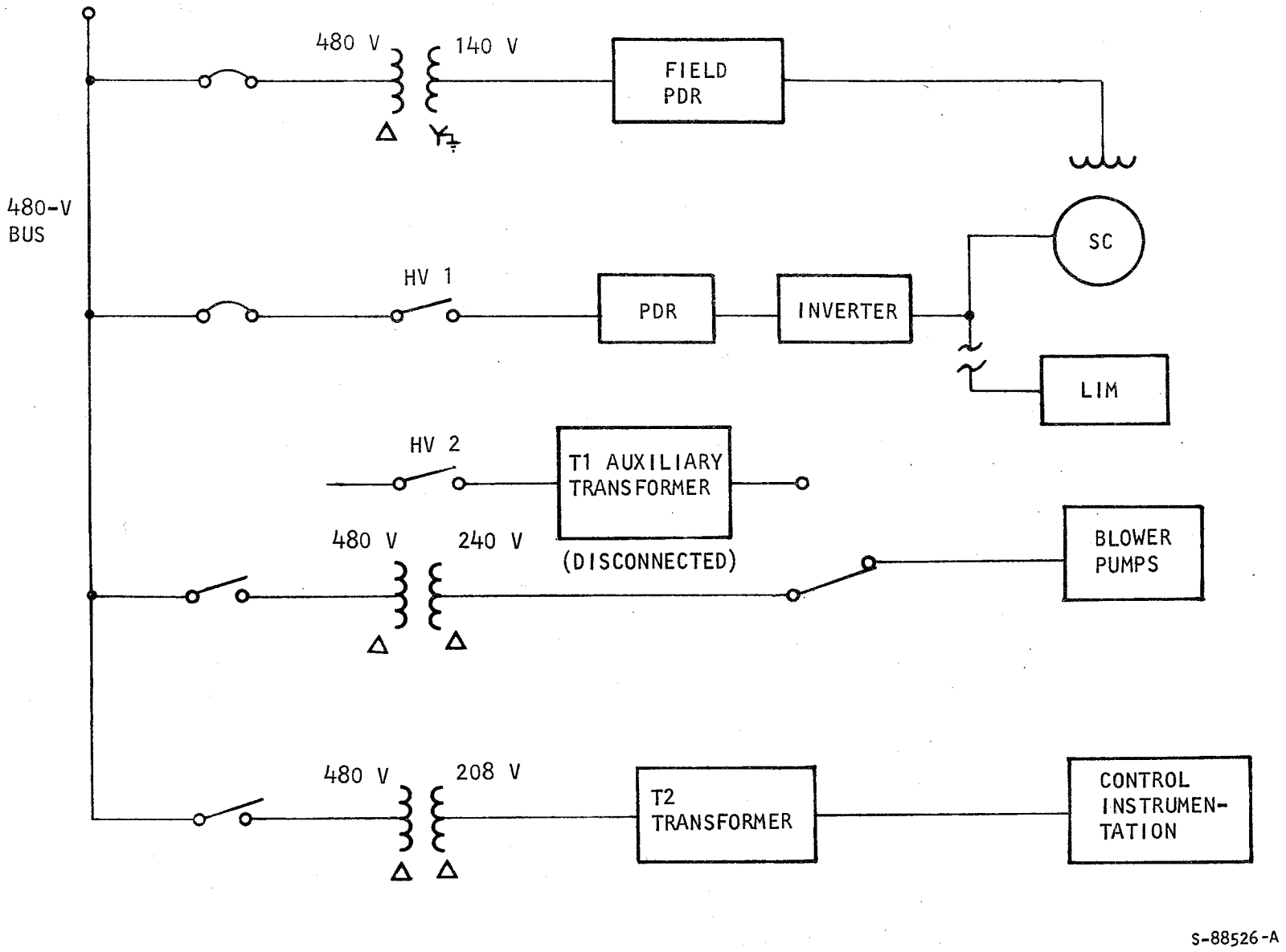

Figure 5-2. System 480-V Test Setup

the synchronous condenser was supplied by the facility; the pumps were fed from a facility source; the auxiliary transformer was not energized; and the PDR itself was fed from the 480 V bus in the test cell. During these tests, the system started, made the transition from the start mode to the run mode, and operated satisfactorily. Figure 5-3 shows oscillograms of the line-to-neutral and line-to-line voltages during this test. Figure 5-4 shows an oscillogram of SC basic variables during operation at about 18 Hz. These voltages are at the output terminals of the inverter with the SC connected, but the LIM not connected.

Operation in Brake Mode

Figures 5-5 and 5-6 show system operation in coast and brake modes. Figure 5-5 shows the system initially in the run mode as indicated by the positive value of the dc link voltage. Figure 5-5 also shows the dc link voltage decreasing to approximately zero, which occurred when the thrust command lever was set to zero position. Figure 5-6 shows the transition into the brake mode when the thrust command lever was set into the braking quadrant. The dc link voltage becomes negative at this transition, indicating the transfer of power from the SC back into the power system. This would, in actual vehicle operation, decelerate the TLRV.

Deceleration Testing

In addition to running and braking tests, deceleration testing was conducted at 480 V. Figure 5-7 depicts the results. The two curves are graphs of speed vs time, one with no field current, the other with a field current of about 300 A. The difference between the two curves represents the decelerating torque due to the iron loss corresponding to these test conditions. It is interesting to note that the slopes of the curves are relatively constant, indicating that the decelerating torques are approximately constant rather than

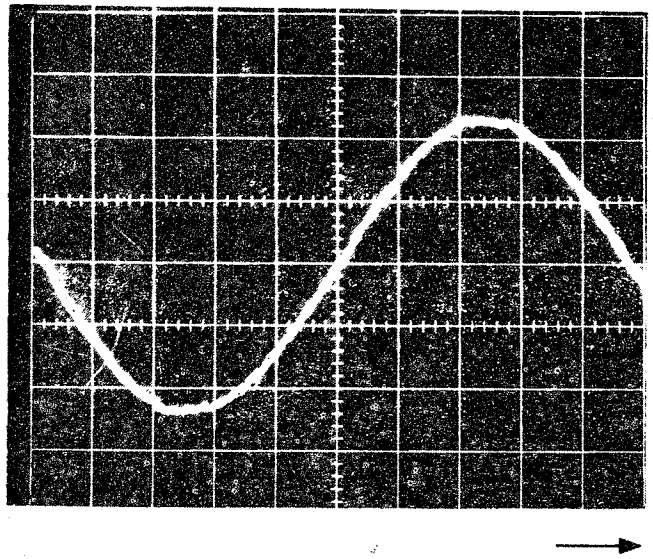

VOLTAGE LINE-TO-NEUTRAL, 328 VRMS
200 V/CM
10 mS/CM

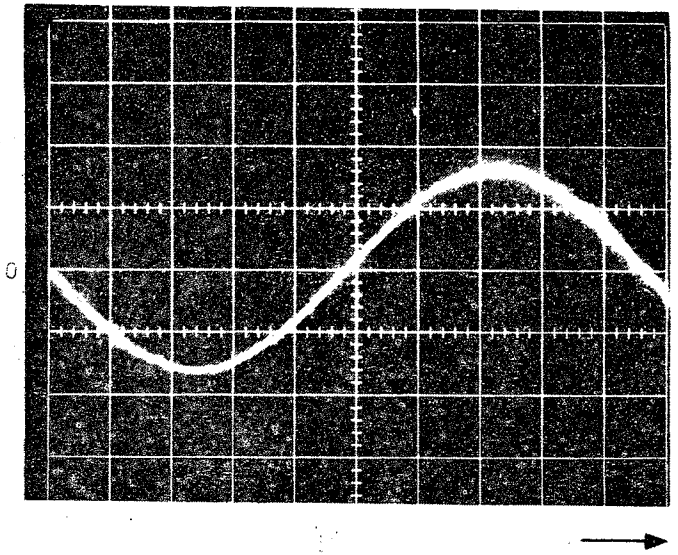

VOLTAGE LINE-TO-LINE, 570 VRMS
500 V/CM
10 mS/CM

Figure 5-3. Inverter Output Voltage (Frequency = 10.4 Hz)

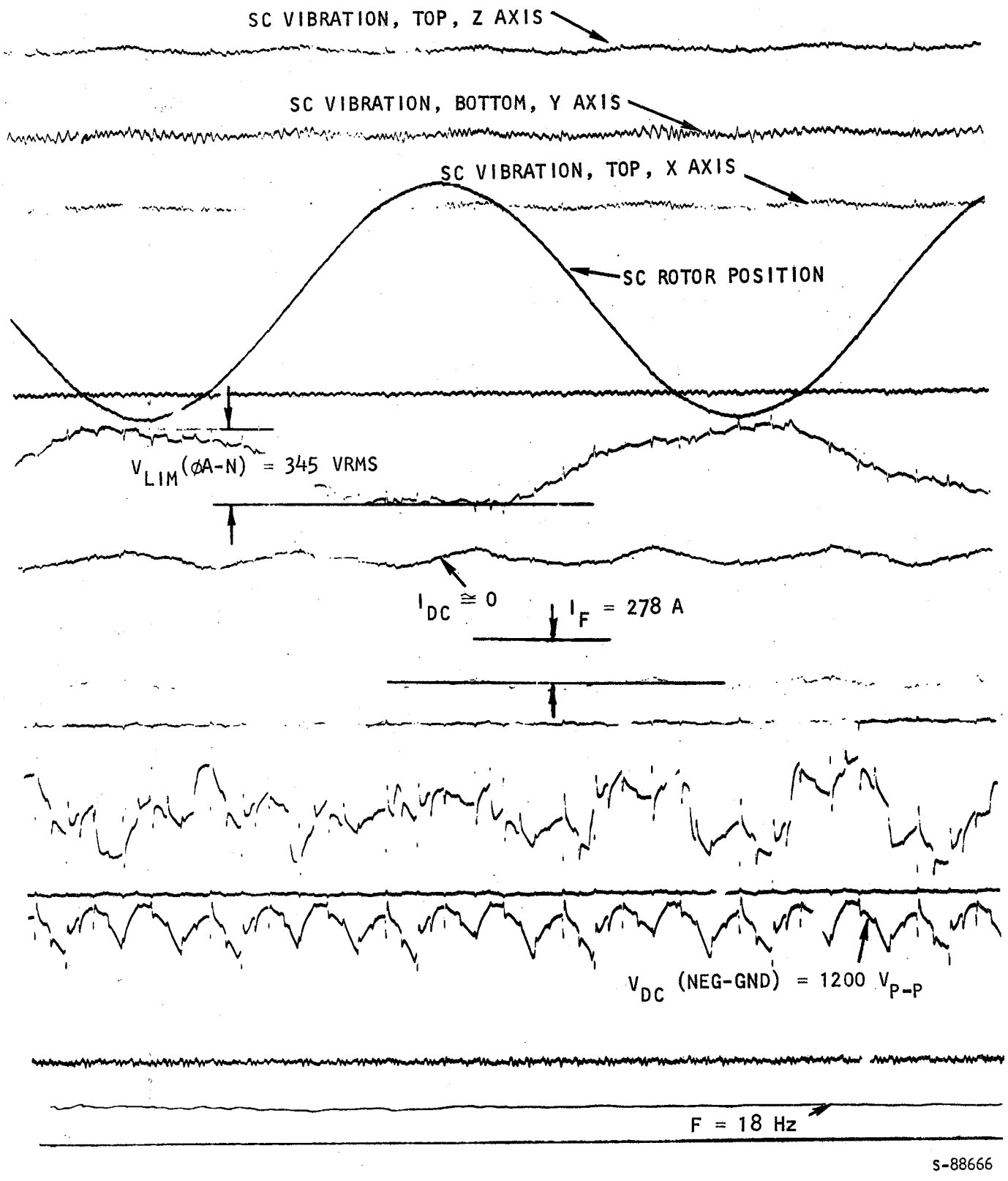

Figure 5-4. SC Performance, 480-V No-Load (No Rail) Test

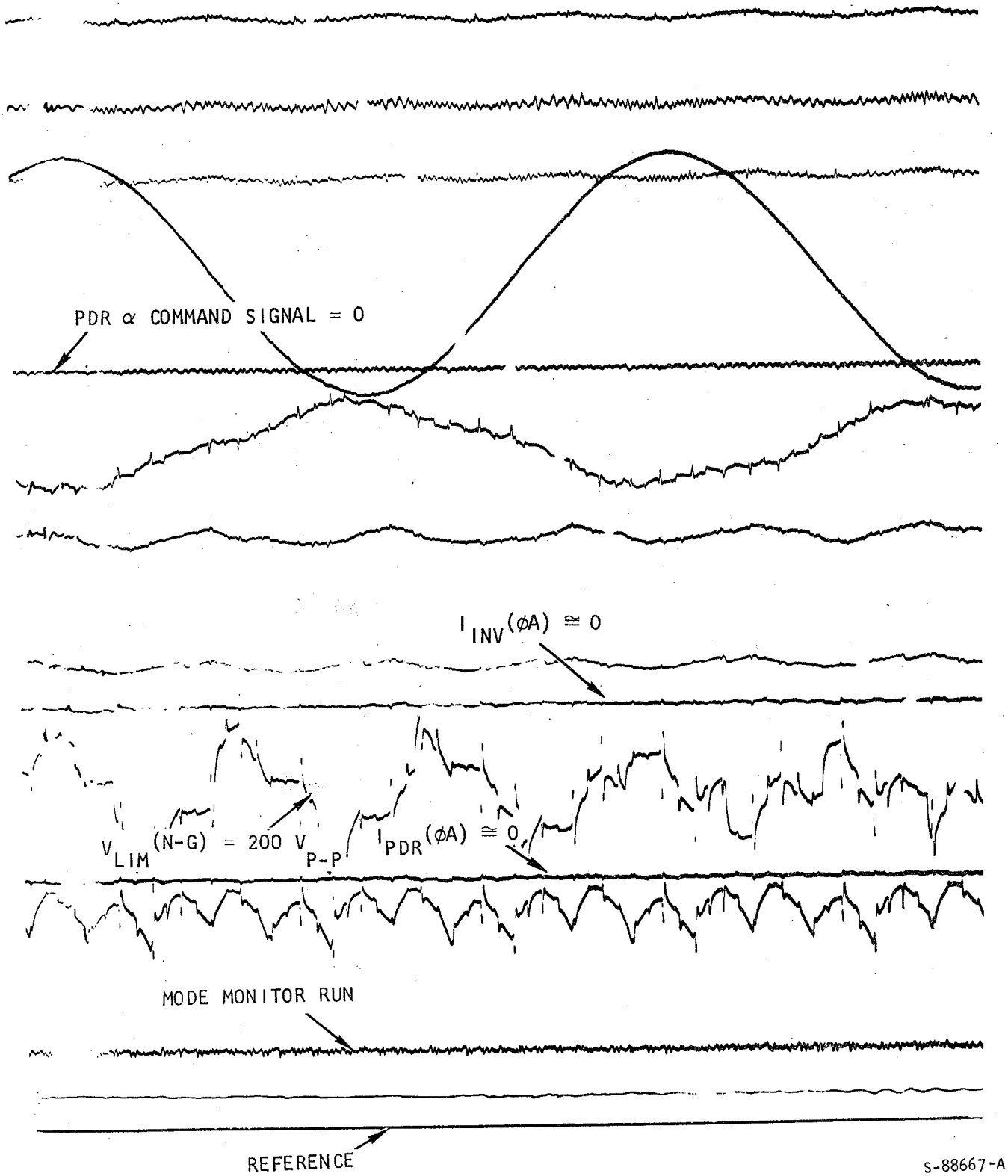

Figure 5-4. (Continued)

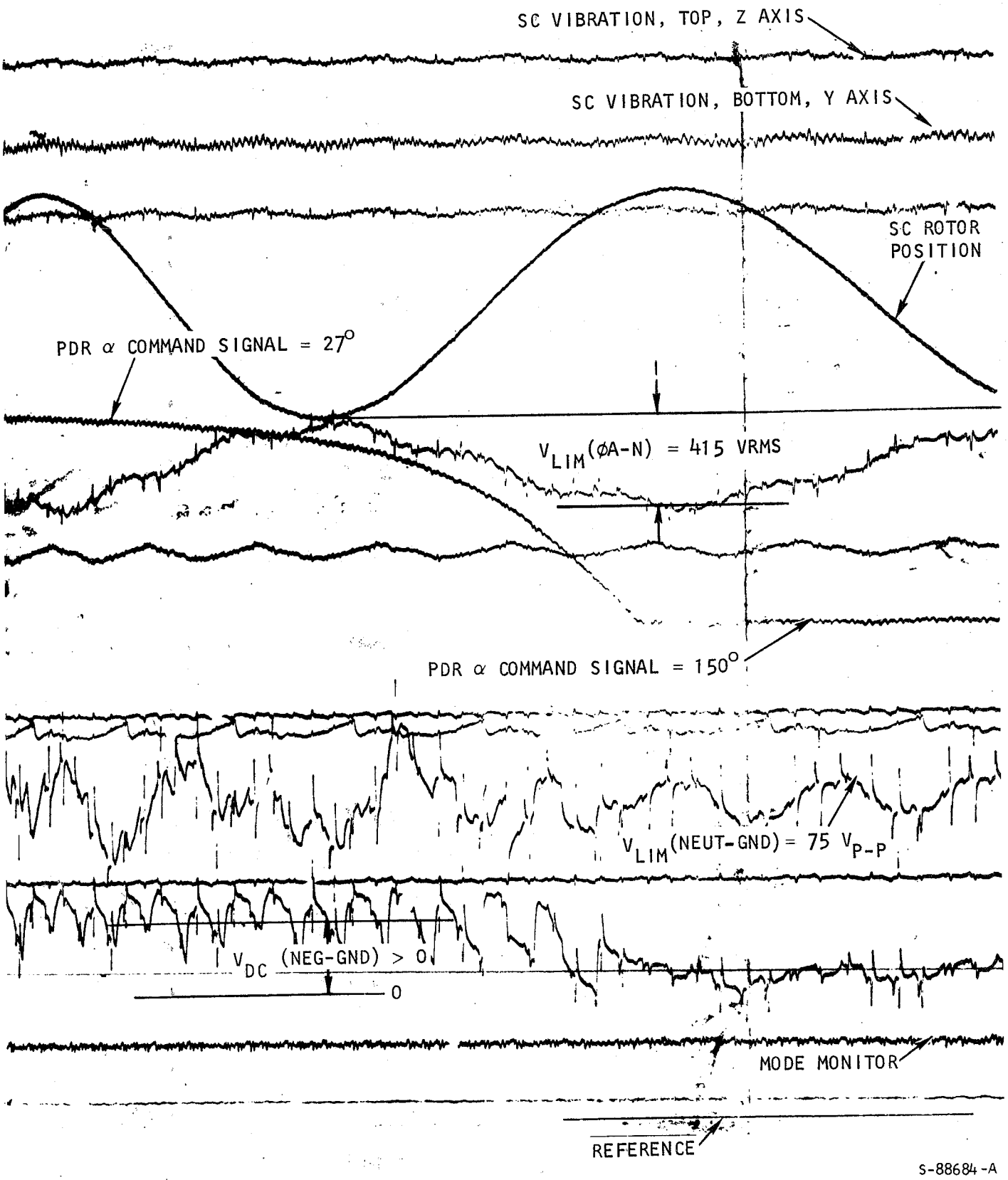

Figure 5-5. Coast Mode Test at 480 V

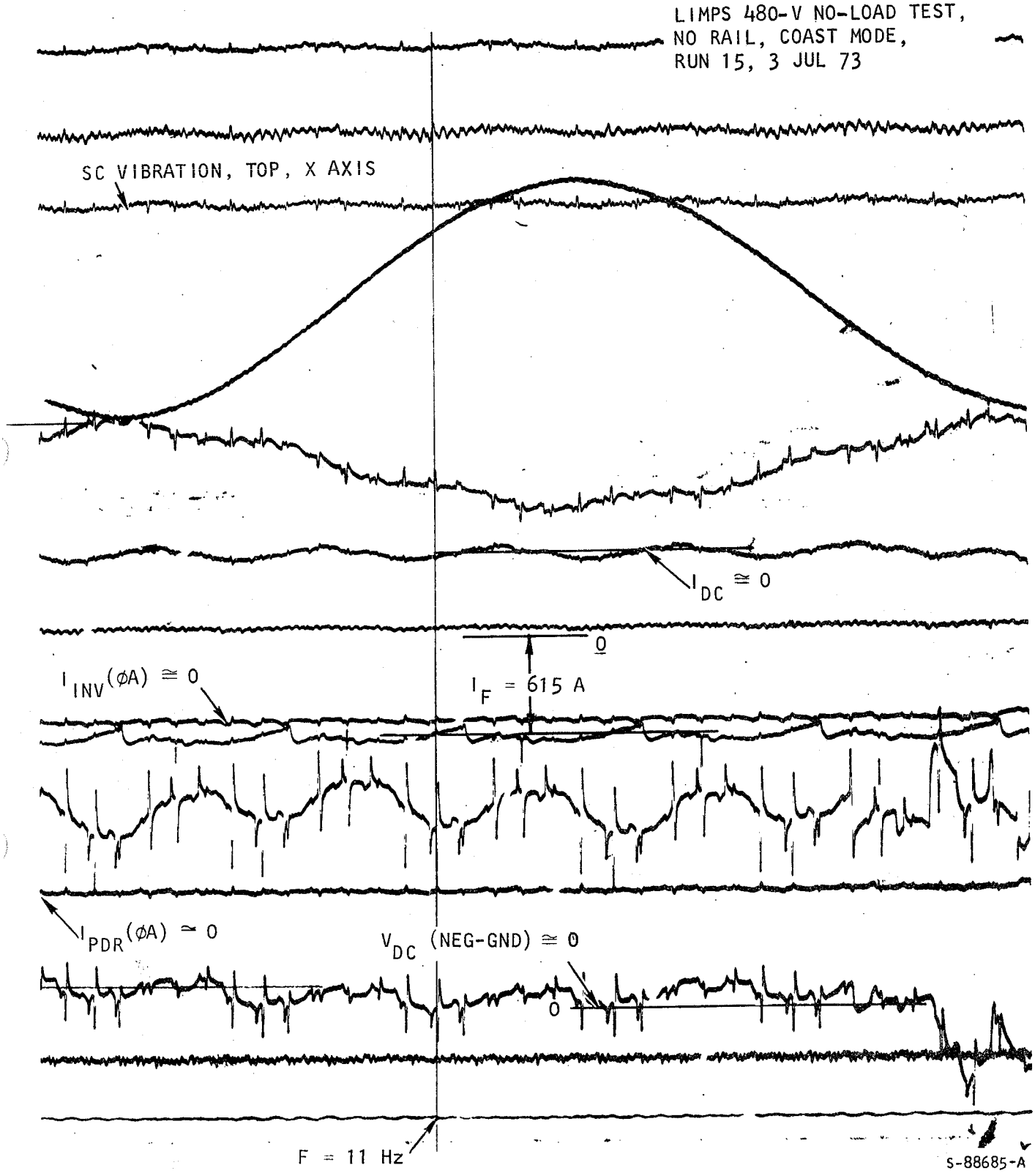

Figure 5-5. (Continued)

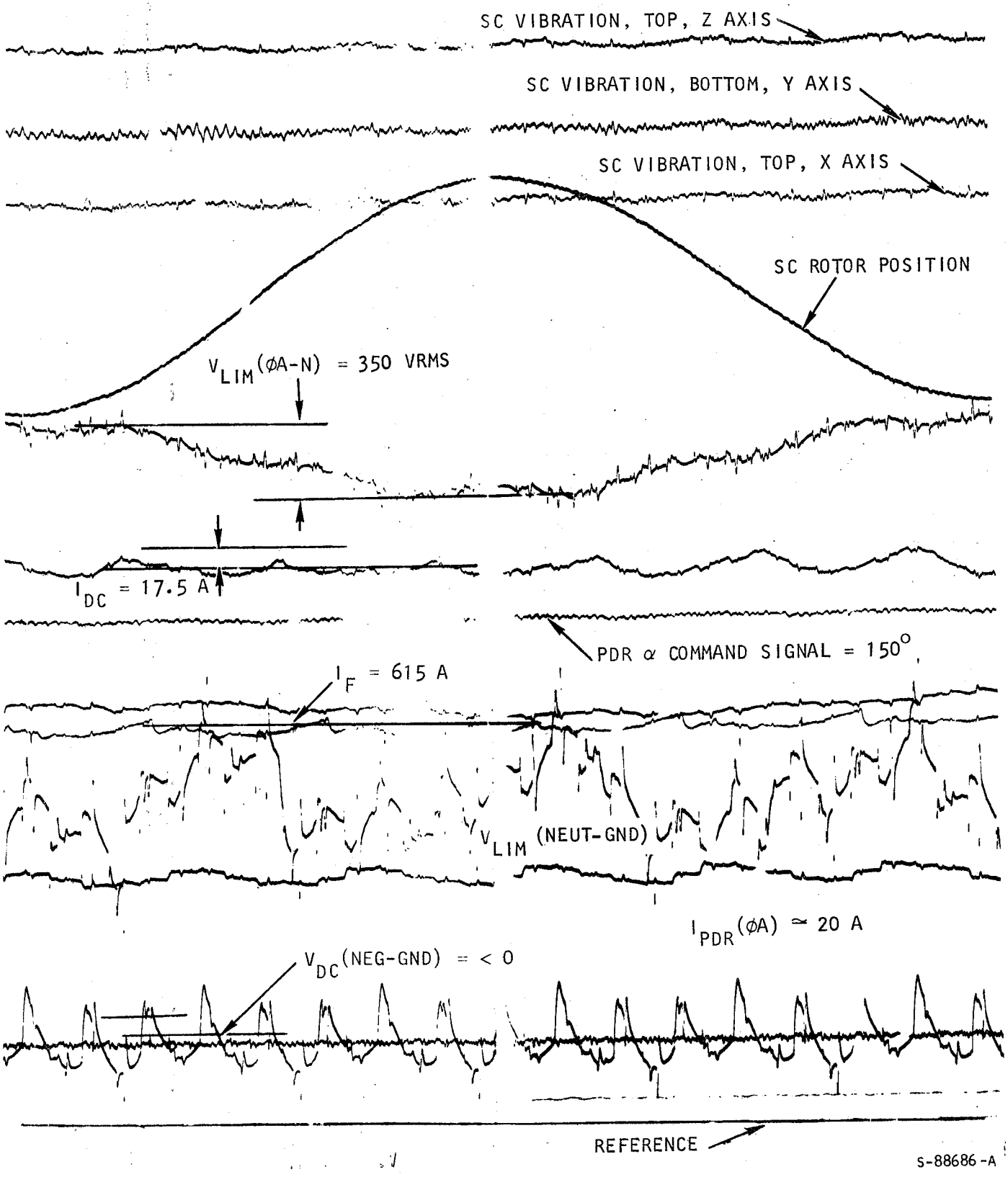

Figure 5-6. Brake Mode Test at 480 V

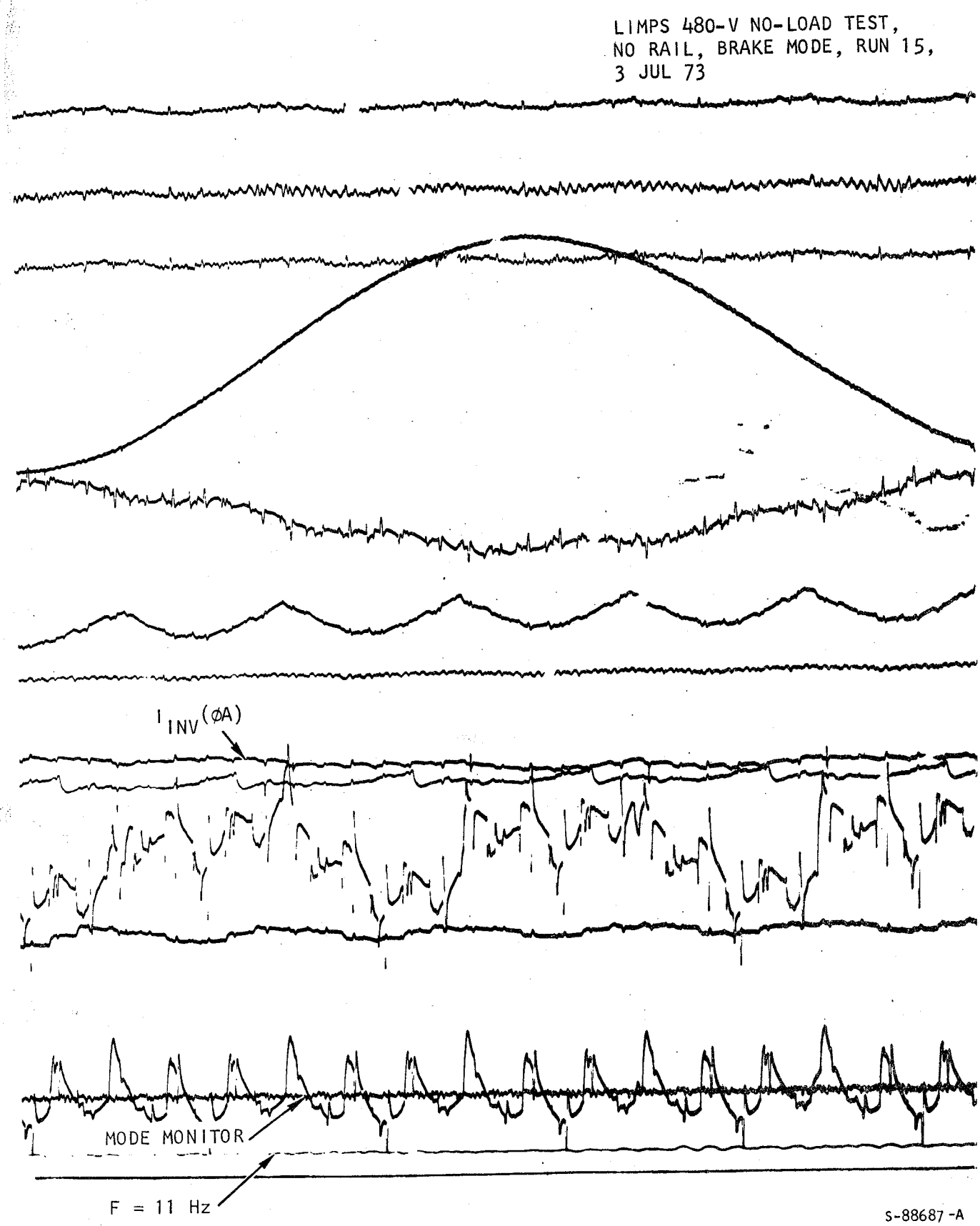

Figure 5-6. (Continued)

CURVES REPRESENT COASTDOWN WITH
NO ARMATURE POWER APPLIED

DATA RECORDED 3 JUL 73

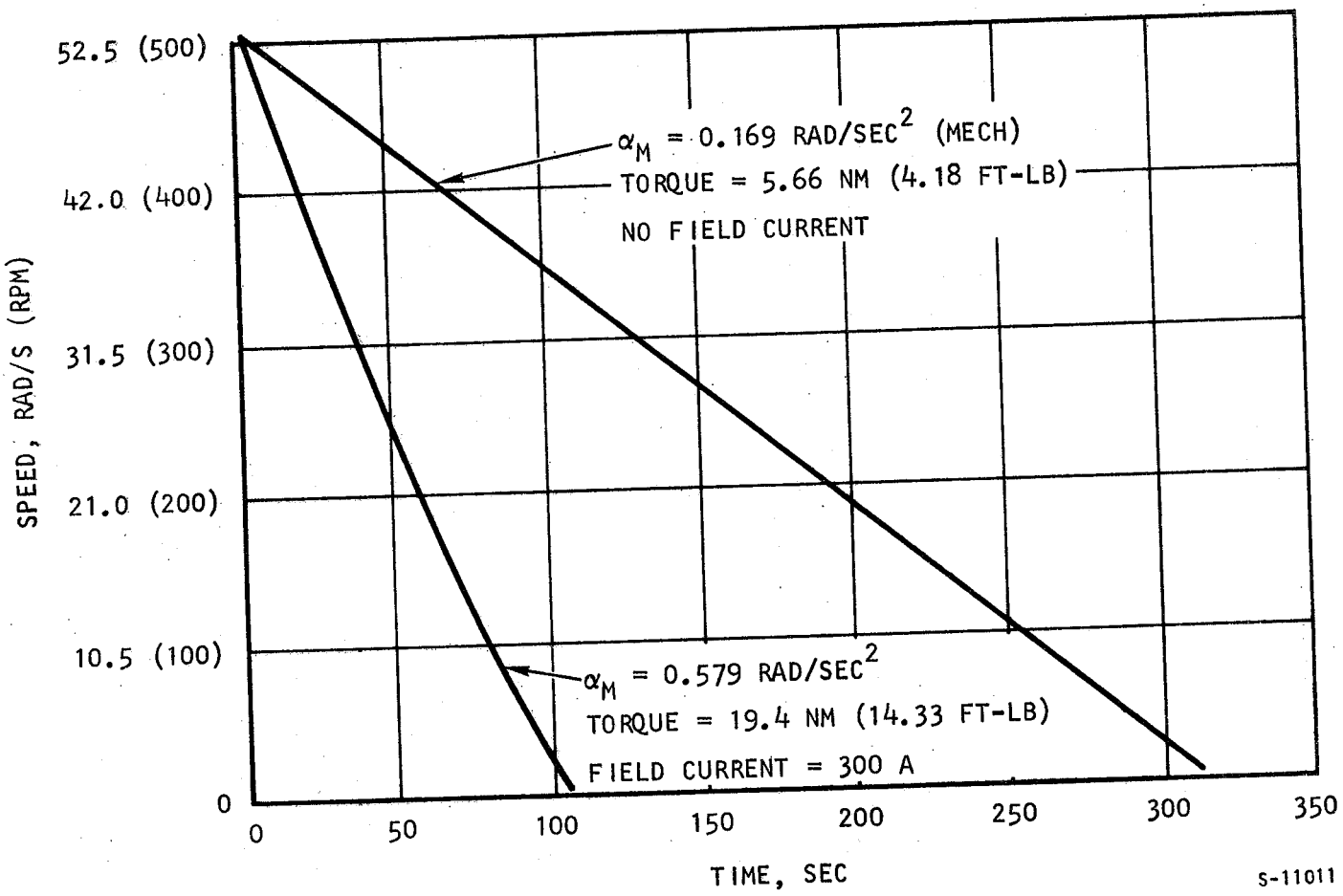

Figure 5-7. Synchronous Condenser Deceleration

varying with the square or the cube of the speed. This would suggest that the major part of no-load losses under these conditions is due to friction rather than windage.

SYSTEM TESTS AT 4160 V

The 4160-V system test setup (Figure 5-8) was similar to that for the 480 V tests. The power for the SC field was supplied by a facility source; the power for the pumps was supplied by a facility source; the auxiliary power transformer was deenergized; and the main PDR was energized from the 4160-V facility source. For some of the tests, the LIM was disconnected, for some it was connected but had no rail installed, and for some it was connected with a locked (stationary) rail.

Tests with LIM Disconnected

1. No-Load, High-Speed Testing

The initial 4160-V tests were intended to determine whether the SC and power conversion elements could operate at approximately rated speed. These tests were run with the LIM disconnected and were conducted incrementally, that is, the machine was run up to a given speed and the vibration levels carefully monitored; speed was then increased, and the vibration levels again monitored. The effects of any critical speeds were thus investigated with assurance that the SC vibration levels were not sufficient to cause serious damage. The specimen was operated in this fashion at speeds up to 94 percent of rated synchronous machine speed. The vibration levels were relatively low, less than 1 g peak in the frequency range of interest, as shown in Figure 5-9.

Table 5-1 summarizes some of the 4160-V, no-load tests.

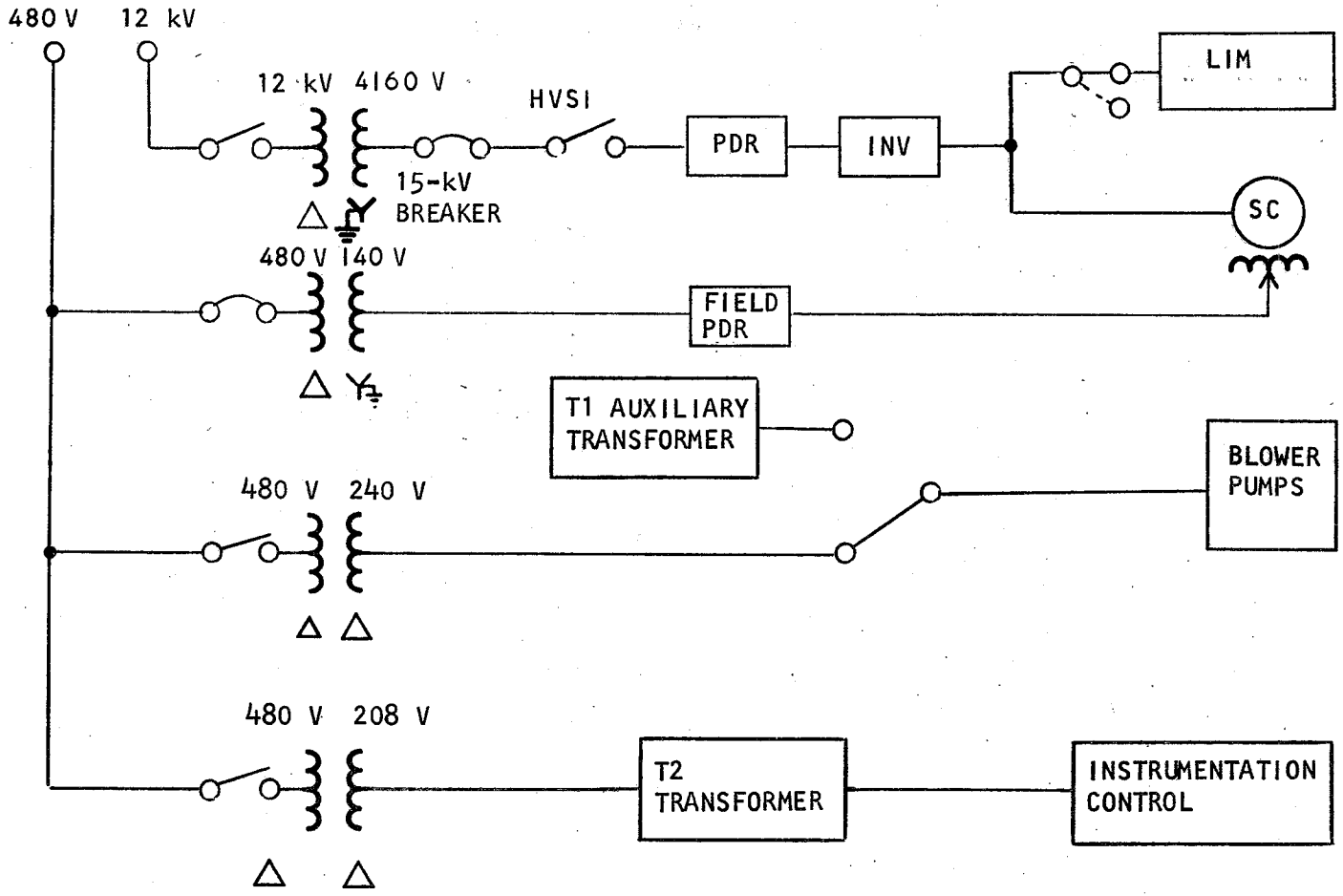

Figure 5-8. System 4160-V Test Setup

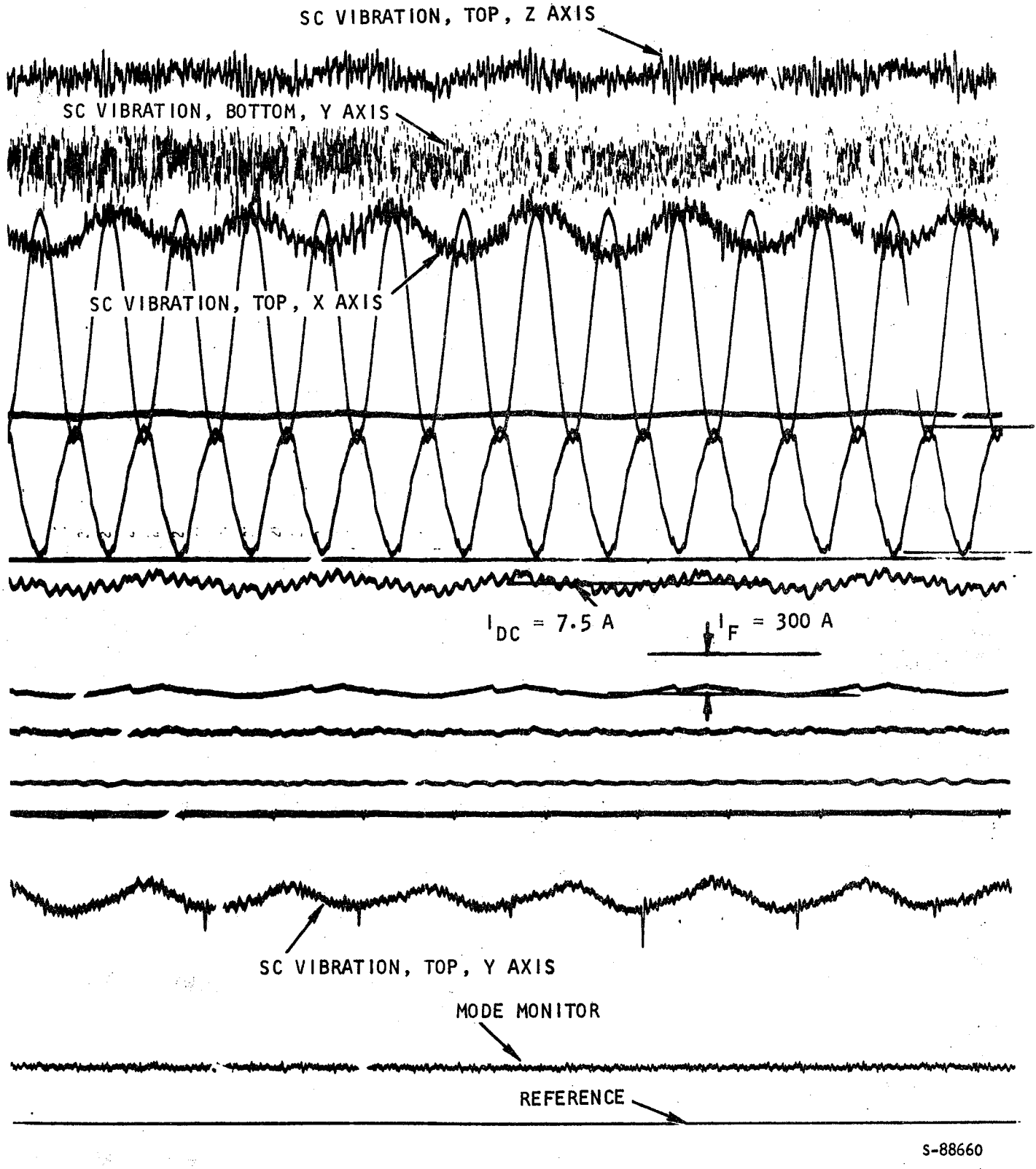

Figure 5-9. Ninety-Four Percent Synchronous Speed Test

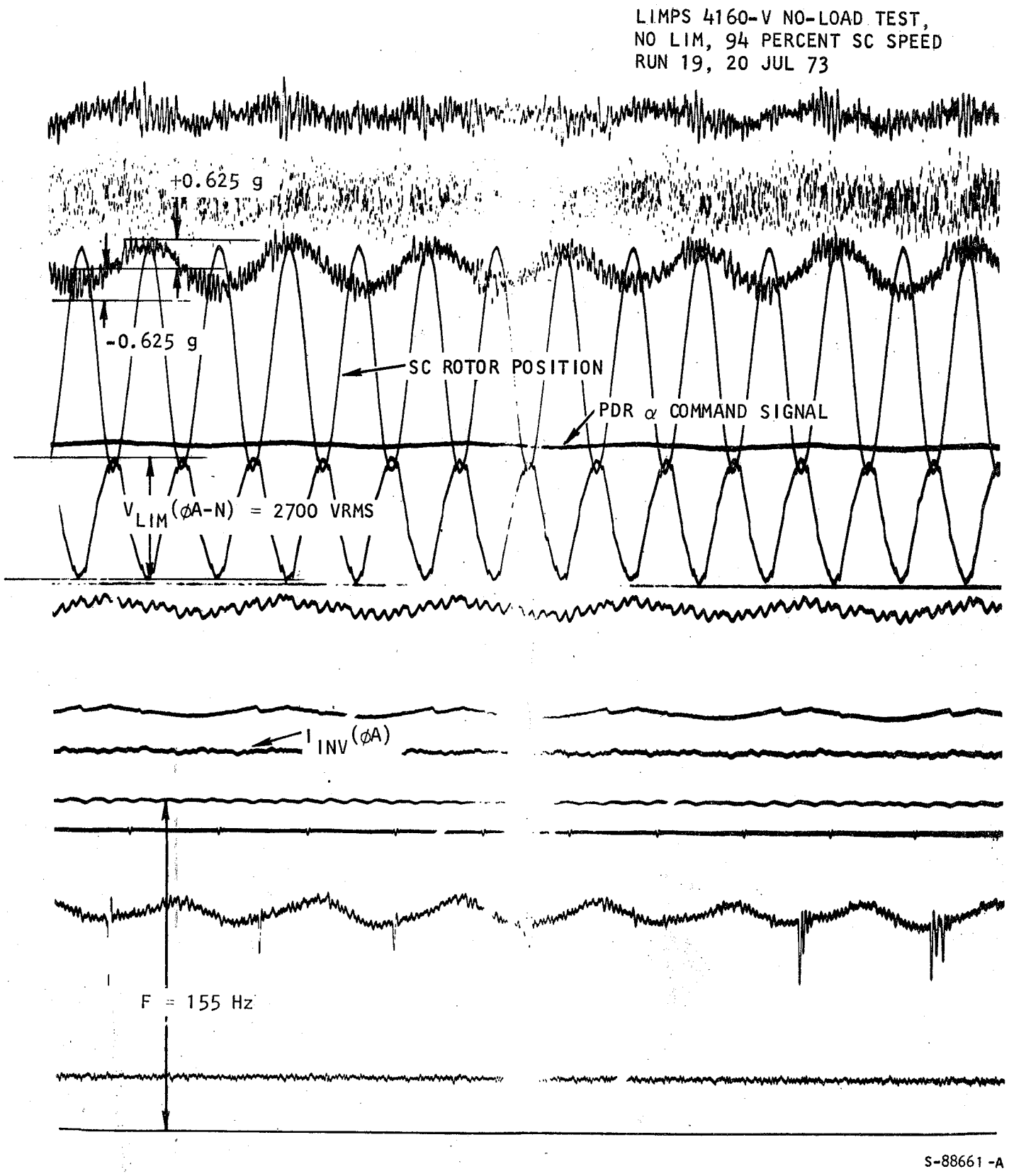

Figure 5-9. (Continued)

TABLE 5-1

PARTIAL SUMMARY OF 4160-V, NO-LOAD SYSTEM TESTS

Date	Run	I_f, A	I_{dc}, A	$f_{max.}$, Hz	f_o, Hz	f_r, Hz	Mode Transition	Result	Remarks
LIM Disconnected									
13 Jul 73	-	1250	150	5.0	2	5	Yes	C, ran	
8 Aug 73	4	1950	240	7.0	7	7	Yes	C, ran	
16 Aug 73	1	1275	75	24.1	-	-	Yes	C, ran	Speed limit
	2	900	270	14.8	-	-	Yes	CF (QSD)	
	3	1613	60	24.1	-	-	Yes	C, ran	Speed limit
LIM Connected, No Rail									
13 Jul 73	1	1250	150	5.0	2	5	Yes	C, ran	38.1-mm (1.50-in.) airgap

LEGEND: I_f = SC field current

I_{dc} = Dc link current

$f_{max.}$ = Maximum frequency

f_o = Field transition frequency

f_r = Mode transition frequency

C = System commutated in run mode

CF = Inverter commutation failure

QSD = Quick shutdown

This testing also provided data for evaluation of the operation of the SC and the inverter as a dc motor. In theory, the combination should exhibit a speed vs field current curve that is roughly hyperbolic at constant input voltage. Figure 5-10 shows such a plot based on test results.

2. Speed Limit Mode Testing

In addition, the speed limiting feature of the LIMPS control system was demonstrated. In the speed limit mode, the SC speed increases to the setting of the speed limit lever. At this point, the dc link current drops to essentially zero, and the system coasts down to the lower end of the speed band inherent in the speed limit circuitry. Then the dc current increases to the value corresponding to the thrust command lever setting, and this current is maintained until the speed increases to the speed setting. The dc link current again decreases to zero and an intentional limit cycle results. One such cycle is shown in Figure 5-11; the operation is smooth and in accordance with design.

3. Locked-Rail Testing

Probably the most relevant aspect of the locked-rail testing was the discovery and definition of the starting problem, specifically, the difficulty experienced in achieving transition frequency and in commutating the inverter current at the transition from the start made to the run mode. After a description of test procedure and results obtained the implications of the results are discussed and the nature of the starting problem itself is pinpointed. The solution of this problem is subsequently described in subparagraph 4.

The locked-rail test setup was similar to that shown in Figure 5-8, except that the LIM was connected, with a reaction rail section installed in its air-gap and bolted to the test bed. This rail section was designed for the LIMRV

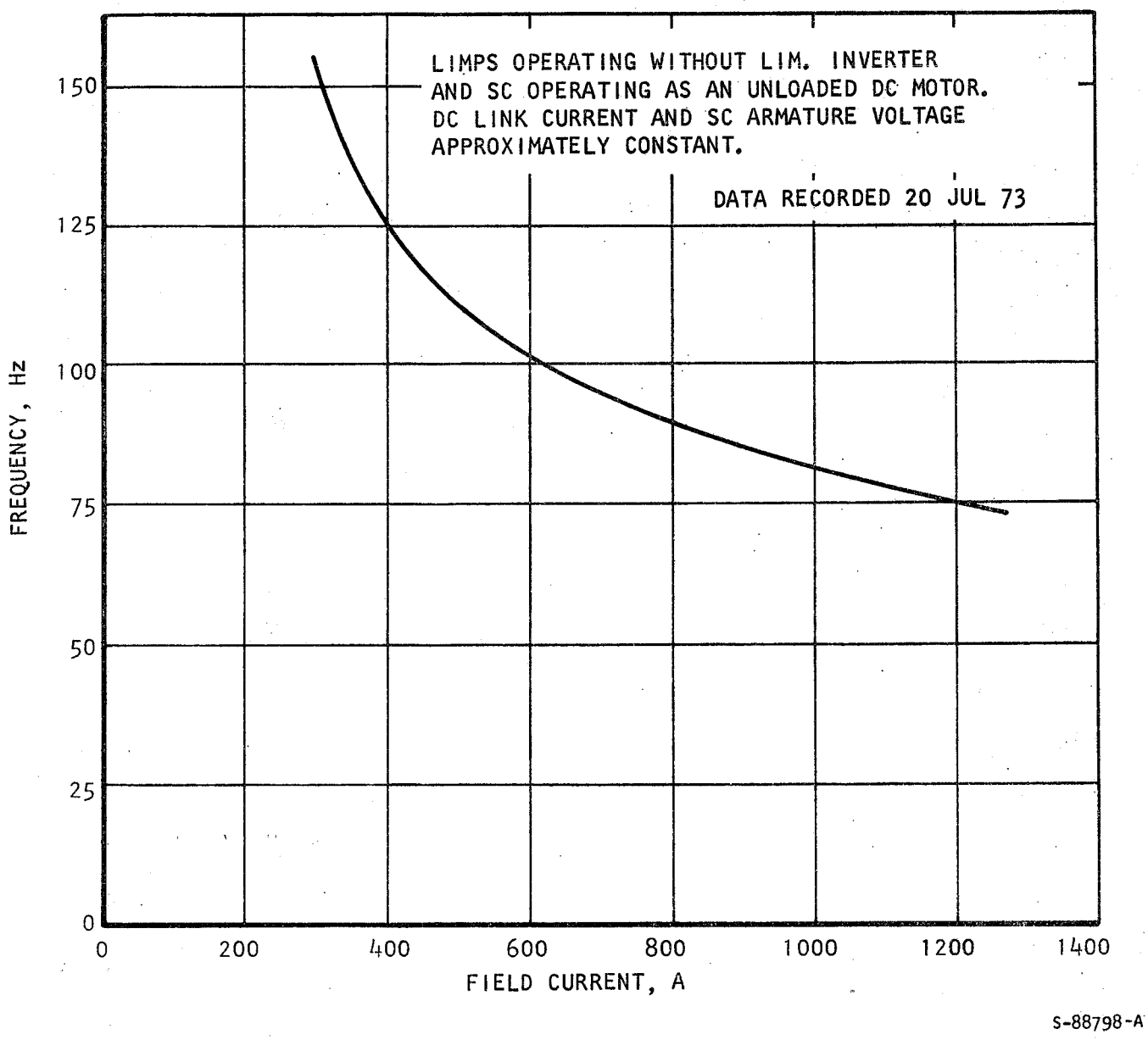

Figure 5-10. Synchronous Condenser Frequency vs Field Current

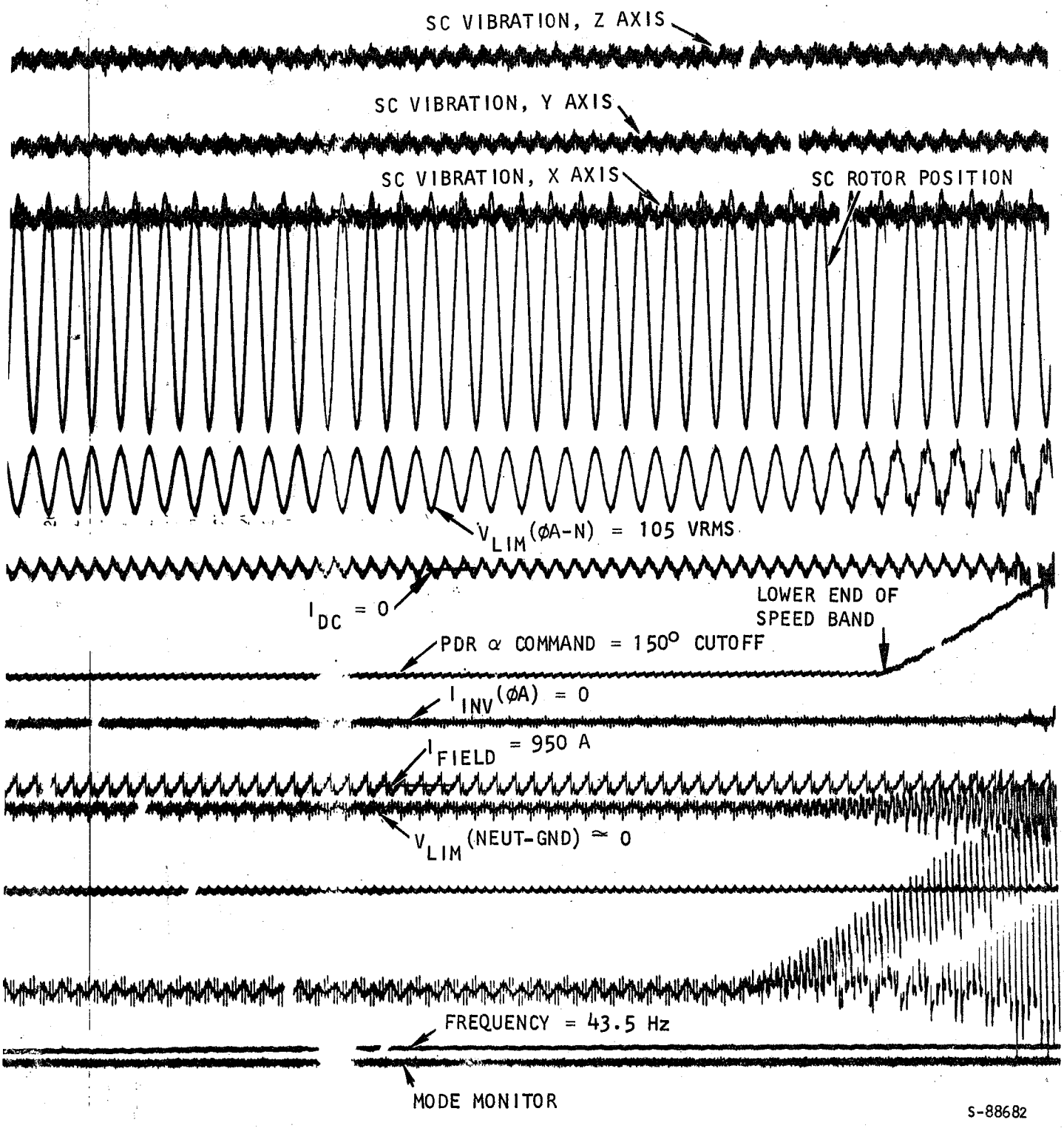

Figure 5-11. Speed Limit Mode Test, No Load

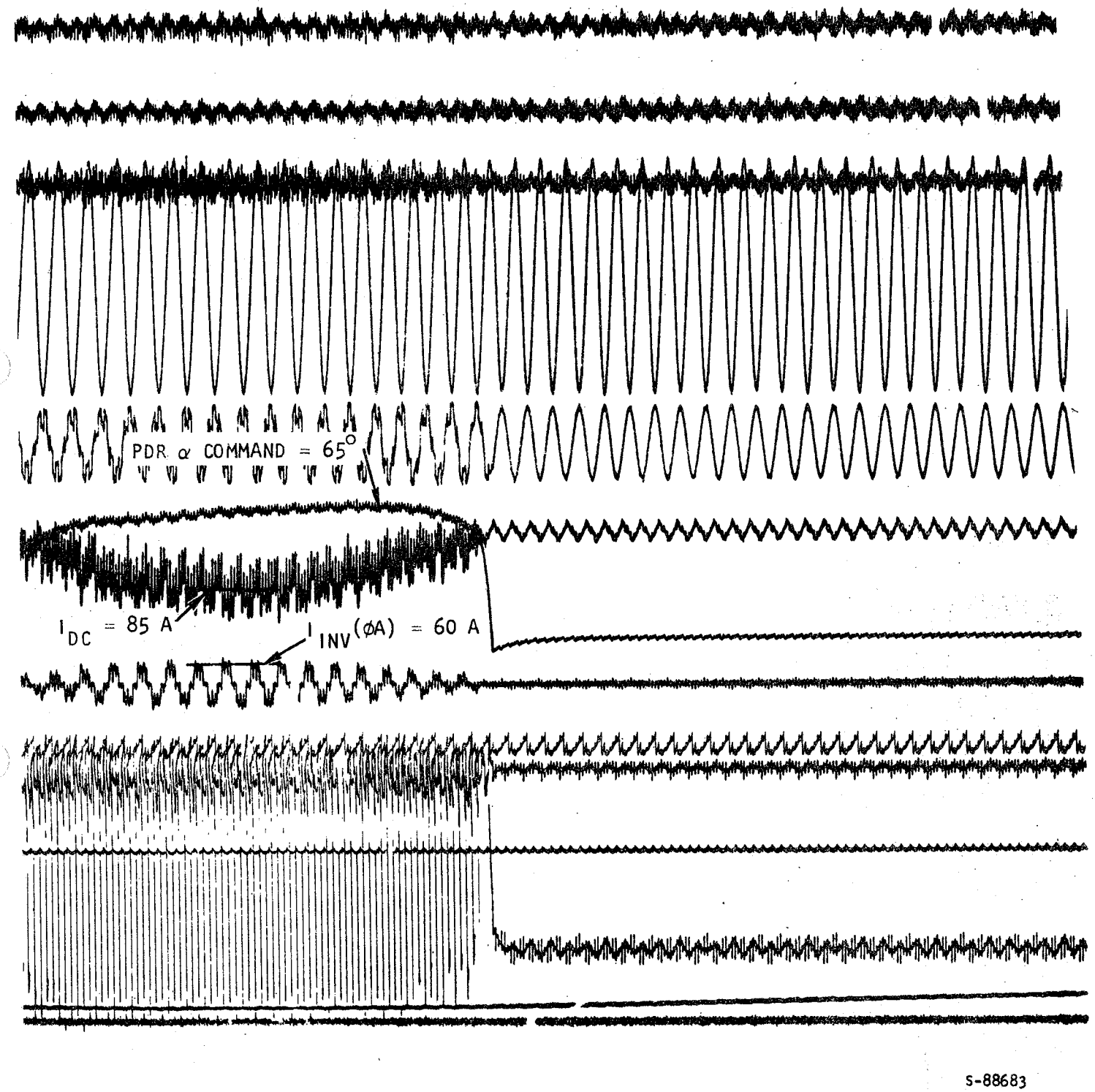

Figure 5-11. (Continued)

program, but differs only slightly from that designed for the TLRV LIM in electrical characteristics. It does, however, have provision for water cooling, as shown in Figure 5-12, which made it possible to run the locked-rail tests without overheating the rail.

For the initial locked-rail tests, the control system was connected so that as soon as the thrust command lever was moved from zero position the field current automatically increased from zero to about 375 A. Then, when an SC frequency of about 2 Hz was attained (field transition frequency), the field current automatically increased to a value determined by a potentiometer setting controlled by the test operator. The mode transition frequency at which the mode automatically changed from start to run was set at about 5 Hz. Under these conditions, the locked-rail tests were initiated 24 July 1973. At a dc link current of 185 A, the maximum frequency attained was about 0.8 Hz. Mode transition was not achieved.

On 25 July the testing sequence was as follows:

a. Run No. 1

With field current of 375 A and dc link current of 250 A, the SC frequency increased to about 2 Hz (field transition frequency), at which point the field current increased to 1500 A. Thereupon the SC frequency decreased to less than 1 Hz. When the thrust command lever setting was increased to obtain a dc link current of about 440 A, the SC frequency increased to about 1.6 Hz, which was approximately the maximum attained. A transition from start to run was not made.

b. Run No. 2

At a dc link current of about 250 A, the SC accelerated to the field transition frequency, about 2 Hz. At this point, the field current increased automatically to 1500 A, and the SC decelerated. When the dc link current was

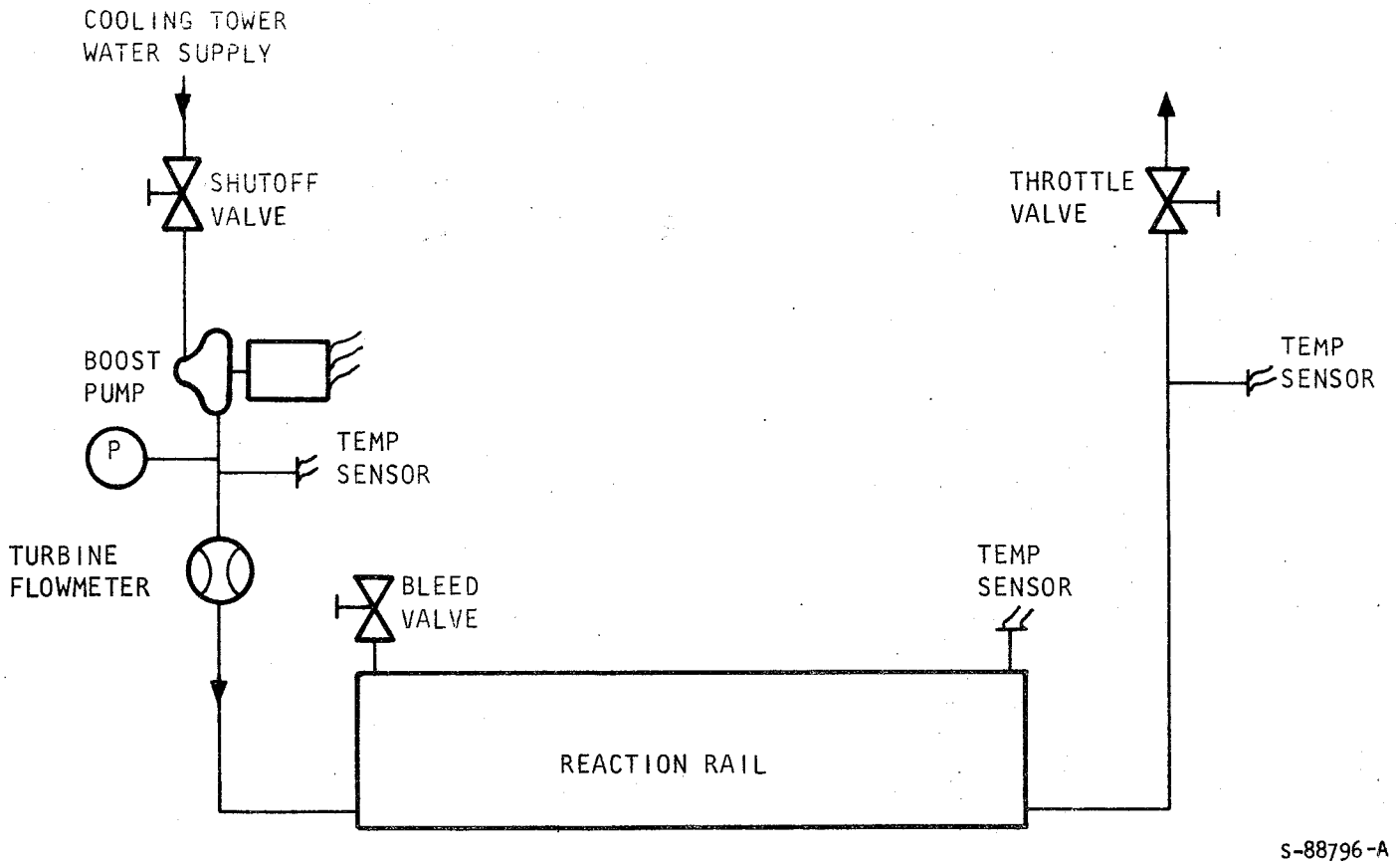

Figure 5-12. Reaction Rail Cooling System Flow Diagram

increased to 400 A, the SC frequency increased to slightly more than 2 Hz, and when the dc link current was increased to about 625 A and the field current decreased to 825 A, an SC speed corresponding to a frequency of 4.2 Hz was attained. Mode transition was not achieved.

c. Run No. 3

For this run the mode transition frequency was set at 3.5 Hz. With a dc link current of about 275 A, the SC accelerated to the field transition frequency of about 2 Hz, at which point the field current increased to 900 A, corresponding to the control setting for this run. The SC decelerated, but accelerated again when the dc link current was increased to 625 A. With 625-A dc current and 940-A field current, the mode transition frequency of 3.5 Hz was attained and the mode transition was achieved. A quick shutdown initiated by an inverter commutation failure followed immediately.

d. Run No. 4

The control for the post-transition field current was set at 1270 A. With a field current of 1270 A and a dc link current of 625 A, the SC frequency increased to 3.1 Hz and mode transition occurred. A quick shutdown again followed immediately, the inverter again having failed to commutate.

In commenting on these results, it should be observed that to start the system, two basic requirements exist:

1. The SC must accelerate to the transition frequency, and
2. The SC voltage at the time of transition must be sufficient to commutate whatever dc link current exists at the time of transition to the run mode.

Test results clearly indicate that to satisfy the first requirement (accelerating to the transition frequency), a high dc link current and a low

field current are needed. This is reasonable, since a high SC armature current (corresponding to a high dc link current) generates a high core loss, which acts to decelerate the SC. Conversely, to meet the second requirement (adequate SC voltage to commutate at the mode transition), a high field current and a low dc link current are needed. These tests indicate (with the 3-Hz transition frequency adopted thus far) that the conditions just described overlap in a negative sense. That is, with a sufficient dc link current and a field current low enough to accelerate to the transition frequency, there is not a high enough field current nor a low enough dc link current to effect commutation after the transition. Validating these contentions by reference to the test data just reported (and also summarized in Table 5-2) in Run 2 at a field current of 1500 A (which is less than rated value), we note that the machine decelerates with a dc link current of 300 A. On the other hand, in Run 4, we find that making the transition at about 3.1 Hz with 625-A dc link current and 1270-A field current results in a commutation failure, that is, the SC voltage is insufficient to commutate the inverter.

Subsequent efforts to find a combination of the variables that allow starting and transition into the run mode with adequate commutation may be described as follows:

The efficacy of a higher field current was investigated by setting the field transition frequency very close to the mode transition frequency (about 5 Hz, Run 7, 3 Aug 73). That is, the machine was operated in the start mode at a low field current until it reached the transition frequency, at which point the field current increased to 2100 A and mode transition occurred. A commutation failure followed immediately. On that run, the peak LIM voltage was about 140 V. For that run and subsequent runs the LIM airgap width was decreased

TABLE 5-2

PARTIAL SUMMARY OF 4160-V, LOCKED-RAIL SYSTEM TESTS

Date	Run*	I_f, A	I_{dc}, A	$f_{max.}$, Hz	f_o, Hz	f_r, Hz	Mode Transition	Result	LIM Airgap, mm (in.)
24 Jul 73	1	375	185	0.8	2	5	No		38.1 (1.50)
25 Jul 73	1	1500	437	1.6	2	5	No		38.1 (1.50)
	2	825	625	4.2	2	5	No		38.1 (1.50)
	3	940	625	3.5	2	3	Yes	CF	38.1 (1.50)
	4	1270	625	3.1	2	3	Yes	CF	38.1 (1.50)
26 Jul 73	1	1800	675	2.7	2	3	No		38.1 (1.50)
	2	1800	650	2.6	1.6	2.6	No		38.1 (1.50)
	3	1800	587	3.3	1.6	3.3	Yes	CF	38.1 (1.50)
27 Jul 73	1	1912	506	2.5	1.6	4	No		38.1 (1.50)
	2	1425	534	3.0	1.6	4	No		38.1 (1.50)
	3	285	506	6.7			No		38.1 (1.50)
3 Aug 73	7	2100	410	5.0	5	5	Yes	CF	31.7 (1.25)
13 Aug 73	1	225	540	7.5	7.6	7.6	No		31.7 (1.25)
	3	-	555	6.5	8	8	No		31.7 (1.25)

TABLE 5-2 (Continued)

Date	Run*	I_f, A	I_{dc}, A	$f_{max.}$, Hz	f_o, Hz	f_r, Hz	Mode Transition	Result	LIM Airgap, mm (in.)
13 Aug 73	4	750	264	5.7	6	6	Yes	Decel	31.7 (1.25)
	6	225	165	2.6	8	8	No		31.7 (1.25)
	7	225	630	7.6	8	8	No		31.7 (1.25)
	8	825	360	7.5	8	8	Yes	CF	31.7 (1.25)
14 Aug 73	1	225	300	8.8	12	12	No		31.7 (1.25)
	2	863	225	10.2	12	12	Yes	Decel	31.7 (1.25)
	3	263	705	12.0	12	12	No	Speed Limit	31.7 (1.25)
	4	825	240	11.8	12	12	Yes	Decel	31.7 (1.25)
14 Aug 73	5	863	390	11.8	12	12	Yes	Decel	31.7 (1.25)
	6	855	405	12.0	12	12	Yes	Decel	31.7 (1.25)
	7	863	450	11.8	12	12	Yes	CF	31.7 (1.25)
	8	863	300	11.8	12	12	Yes	Decel	31.7 (1.25)
	9	1050	390	11.8	12	12	Yes	Decel	31.7 (1.25)
	10	1200	420	11.8	12	12	Yes	Decel	31.7 (1.25)
	11	1425	450	11.8	12	12	Yes	Decel	31.7 (1.25)

TABLE 5-2 (Continued)

Date	Run*	I_f, A	I_{dc}, A	$f_{max.}$, hz	f_o, Hz	f_r, Hz	Mode Transition	Result	LIM Airgap, mm (in.)
15 Aug 73	1	1275	600	11.8	12	12	Yes	CF	31.7 (1.25)
	2	1650	450	11.8	12	12	Yes	Decel	31.7 (1.25)
	3	1575	540	12.0	12	12	Yes	Decel	31.7 (1.25)
	4	1612	615	12.0	12	12	Yes	CF	31.7 (1.25)
	5	1875	570	12.0	12	12	Yes	Decel	31.7 (1.25)
	6	2175	720	12.0	12	12	Yes	CF	31.7 (1.25)
	7	1950	-	11.8	12	12	Yes	CF	31.7 (1.25)
	8	1725	540	11.8	12	12	Yes	CF	31.7 (1.25)
	9	1650	465	11.8	12	12	Yes	CF	31.7 (1.25)

* = LIM connected directly to inverter terminals

LEGEND: I_f = SC field current

I_{dc} = Dc link current

$f_{max.}$ = Maximum frequency

f_o = Field transition frequency

f_r = Mode transistion frequency

Decel = System commutated but SC decelerated, usually resulting in a reversion to start mode and quick shutdown.

CF = Inverter commutation failure

from 38.1 to 31.7 mm (1.5 in. to 1.25 in.). The rationale for this change was that increasing the magnetizing reactance of the LIM would force more current into the SC and consequently less into the LIM, thus increasing the accelerating torque for a given inverter current.

Another factor that could abet commutation in the run mode is a higher mode transition frequency. For a given field current, the higher the transition frequency, the higher the SC voltage available to commutate the inverter immediately after transition into the run mode. Therefore, to investigate how much this could help, the mode transition circuitry was defeated and the system was run in the start mode with as low a field current deemed feasible (225 A) and as high a dc link current considered safe (750 A). The maximum SC speed attained corresponded to a frequency of about 12 Hz. Accordingly, the field transition frequency and the mode transition frequency were set at about 12 Hz, and the system was operated again, with the 31.7-mm (1.25-in.) LIM airgap. The results are shown in Table 5-2 (see entries with 31.7-mm (1.25-in.) airgap). The conclusive runs are 5 and 6, 15 Aug 73. On Run 5, at a dc link current of 570 A and a field current of 1875 A after transition, the SC decelerated after transition to the run mode, causing the system to revert to the start mode and thus initiating a quick shutdown. On Run 6, at a dc link current of 720 A and a field current of 2175 A, a mode transition followed immediately but a commutation failure occurred. Oscillographic records of Runs 5 and 6 are reproduced in Figures 5-13 and 5-14, respectively.

These results led to the conclusion that it was not practical to start and run this system under locked-rail conditions at this facility.

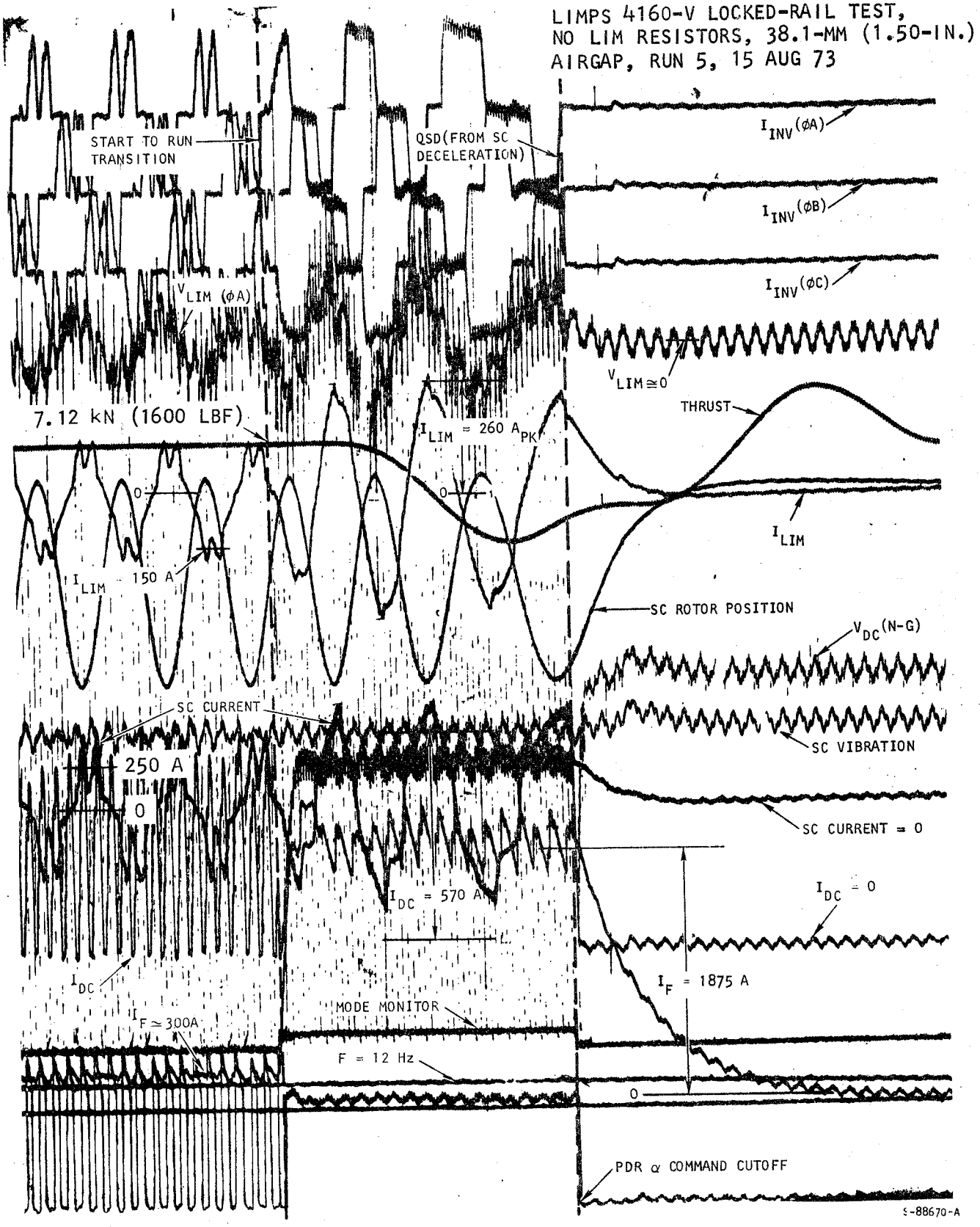

Figure 5-13. Quick Shutdown Immediately Following Transition

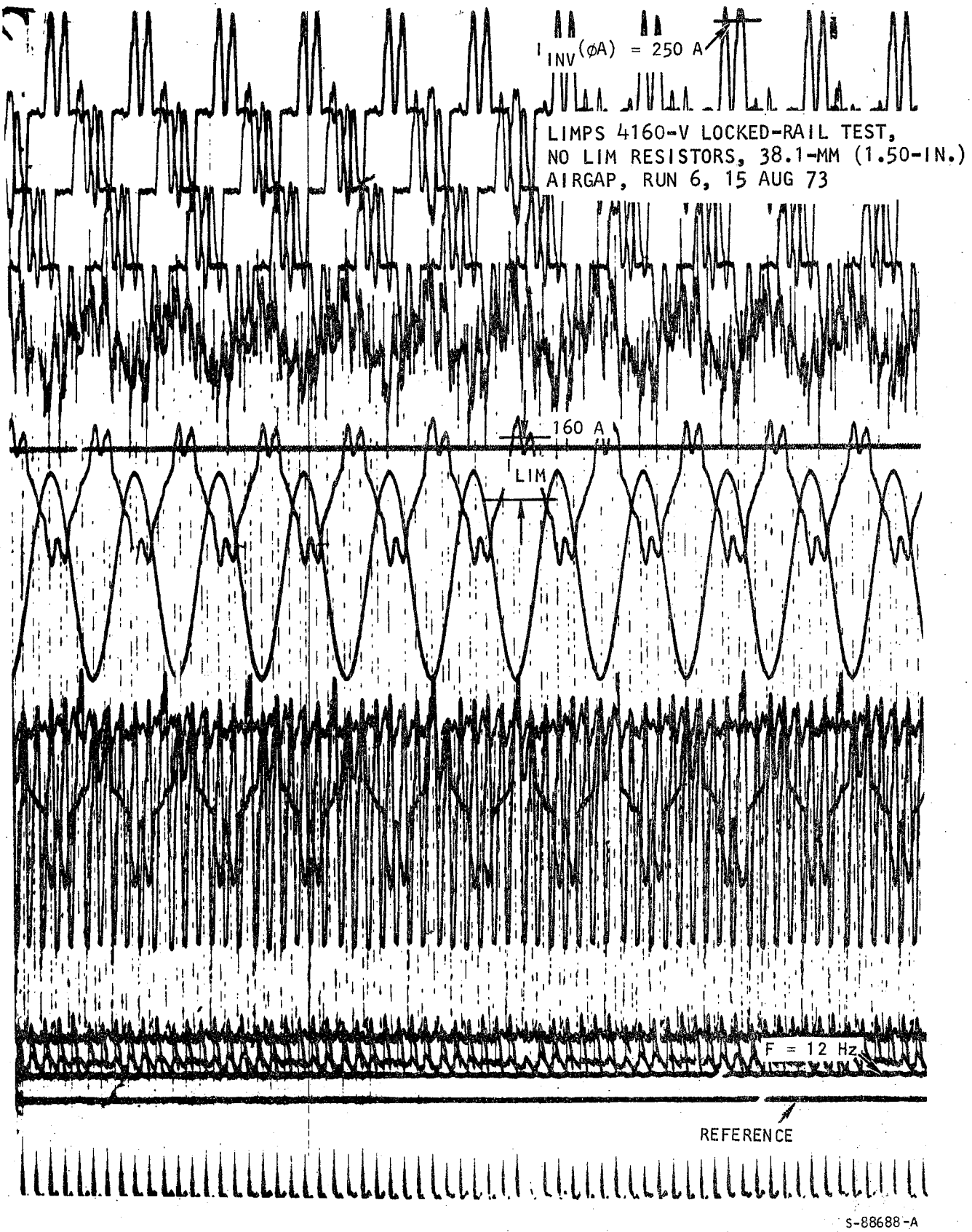

Figure 5-14. Transition Mode Oscillogram Showing Quick Shutdown

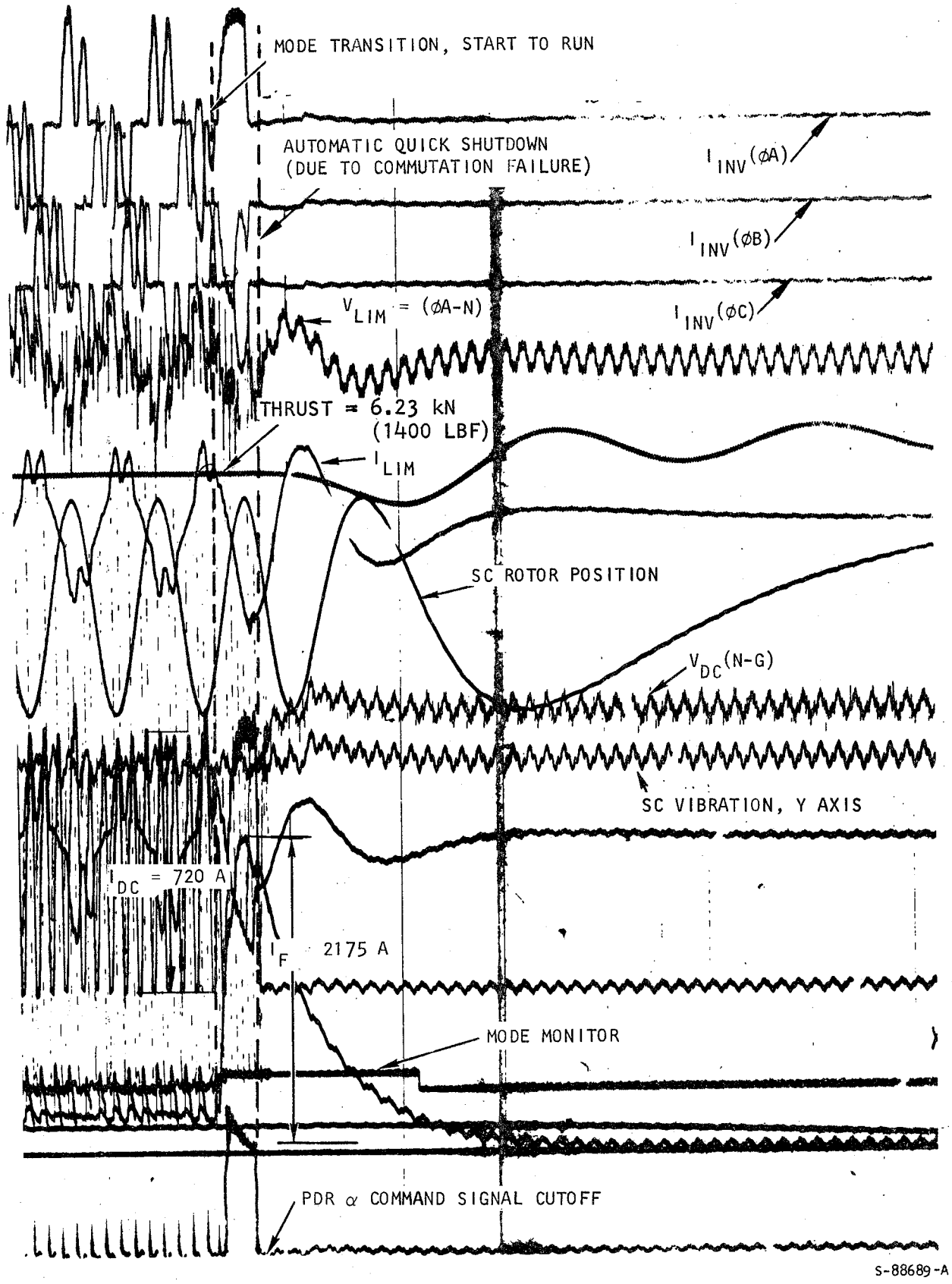

Figure 5-14. (Continued)

4. Locked-Rail Tests with External Resistors in Series with the LIM

The solution to the starting problem described in subparagraph 3, which was implemented for the static testing at Torrance, was the addition of external resistors in series with the LIM. There are two reasons for using these resistors in the lines between the inverter and the LIM. One relates to the ability to predict the starting characteristics of the system on the test track; the other is a practical one with respect to running the static locked-rail tests at Torrance. Analyzing the test results previously described, it is noted that the inverter current divides between the SC and the LIM. The SC may be considered a passive impedance in series with a back emf; the LIM is simply a passive impedance under starting conditions. Thus, the higher the LIM impedance the more current flows in the SC for a given inverter current and a given back emf and frequency. Therefore, adding series resistors to the LIM circuit would enable it to divert more inverter current into the SC armature winding and increase its accelerating torque without increasing the dc link current, which must be commutated in the inverter. Thus, adding these series resistors represents a pragmatic approach to making a successful transition in the terms previously described. That is, adding series resistors should increase the ability to attain the transition frequency and also to commutate the inverter current after transition to the run mode. For these reasons, then, the next sequence of tests was run with external resistors connected in series with the LIM.

The results are summarized in Table 5-3. As indicated, with an external resistance value of 1.2 ohms per phase, the system did start satisfactorily. The transition frequency was attained, the transition from start to run was achieved, and commutation in the run mode was adequate.

TABLE 5-3

PARTIAL SUMMARY OF 4160-V, LOCKED-RAIL SYSTEM TESTS WITH EXTERNAL RESISTORS IN SERIES WITH LIM

Date	Run	r_e, ohm	I_f, A	I_{dc}, A	I_{LIM}, A	I_{sc}, A	V_{LIM}, A	Thrust, kN (lbf)	Freq, Hz	LIM Airgap, mm (in.)
17 Sep 73	2	1.2	2550	378	256	216	430	5.34 (1200)	12.0	31.7 (1.25)
	3	1.2	1838	360	293	248	495	5.34 (1200)	11.6	31.7 (1.25)
	5	1.2	338	225	191	159	318	1.34 (300)	12.2	31.7 (1.25)
	6	1.2	2100	399	308	255	407	6.68 (1500)	11.6	31.7 (1.25)
	7	1.2	1125	450	300	272	583	6.14 (1380)	12.9	31.7 (1.25)
	8	0.6	1875	600	446	403	495	13.8 (3100)	13.4	31.7 (1.25)
19 Sep 73	1	0.6	1875	555	439	446	504	10.7 (2400)	10.8	31.7 (1.25)
	2	0.6	1913	570	451	382	539	12.46 (2800)	12.2	31.7 (1.25)
	3	0.6	1875	525	413	356	454	12.32 (2770)	11.3	31.7 (1.25)
	4	1.2	1913	405	320	265	594	6.14 (1380)	12.5	31.7 (1.25)
	5	1.2	**	540	399	329	698	8.01 (1800)	16.5	31.7 (1.25)
	6	1.2	**	456	337	338	590	6.58 (1480)	13.2	31.7 (1.25)
20 Sep 73	1	1.2	**	384	308	245	494	6.40 (1440)	12.0	38.1 (1.50)
	2	1.2	**	420	318	273	512	6.85 (1540)	12.8	38.1 (1.50)
	3	0.6	**	486	375	314	642	7.83 (1760)	15.5	38.1 (1.50)
	4	0.6	**	361	439	371	486	12.64 (2840)	11.9	38.1 (1.50)
	5	0.6	**	456	509	338	562	12.81 (2880)	15.3	38.1 (1.50)
	*6	0	**	600	276	191	265	5.34 (1200)	11.9	38.1 (1.50)

* = Quick shutdown

** = No oscillograms recorded

Once it was determined that the system would start and commutate in the run mode with a resistance of 1.2 ohms per phase in series with the LIM, an additional question of interest arose: How small can these series resistors be and still permit adequate starting? The experimental search for an answer to this question was carried to the point of ascertaining that the system would start and commutate adequately with 0.6 ohm per phase in series with the LIM. Additional testing to determine what smaller resistance might be effective was deferred in the interest of collecting load data on the system.

Achieving the mode transition enabled the demonstration of system ability to operate at load currents on the order of magnitude of rated currents. For example, in Run 8, 17 Sep 73, the dc link current was 129 percent of its rated value, the LIM current was 84 percent of its rated value, and the SC rated current was 71 percent of its rated value. These do not represent full-voltage, full-current tests; however, they do demonstrate that the system is capable of operating at load currents on the order of magnitude for which it was designed. Figure 5-15 reproduces an oscillogram of mode transition during a locked-rail test with an external resistance of 1.2 ohms per phase. Figure 5-16 is an oscillographic record of steady-state operation in the run mode with an LIM airgap of 31.7 mm (1.25 in.) and an external resistance of 1.2 ohms per phase. Figure 5-17 is a similar oscillogram with a LIM airgap of 38.1 mm (1.5 in.) and an external resistance of 0.6 ohm per phase.

SYSTEM TESTS AT 8250 V

Figure 5-18 shows the 8250-V (rated voltage) test setup, which differed from the 4160-V setup in that the auxiliary transformer was energized from the facility 8250-V transformer. The pumps for the cooling system were supplied by the auxiliary power transformer, but the field PDR supplying the SC field

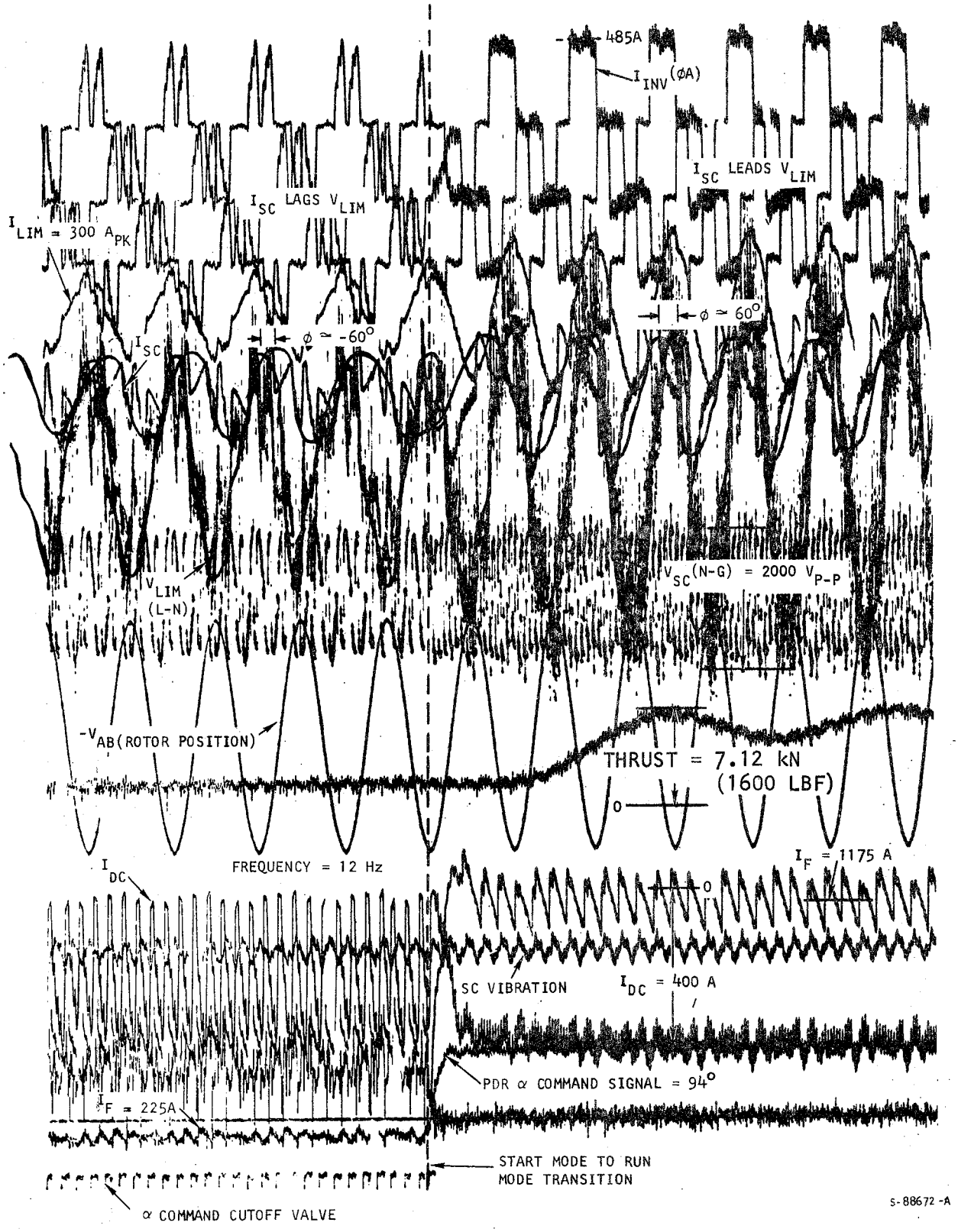

Figure 5-15. Successful Transition From Start Mode to Run Mode, 1.2-Ohm External Resistors

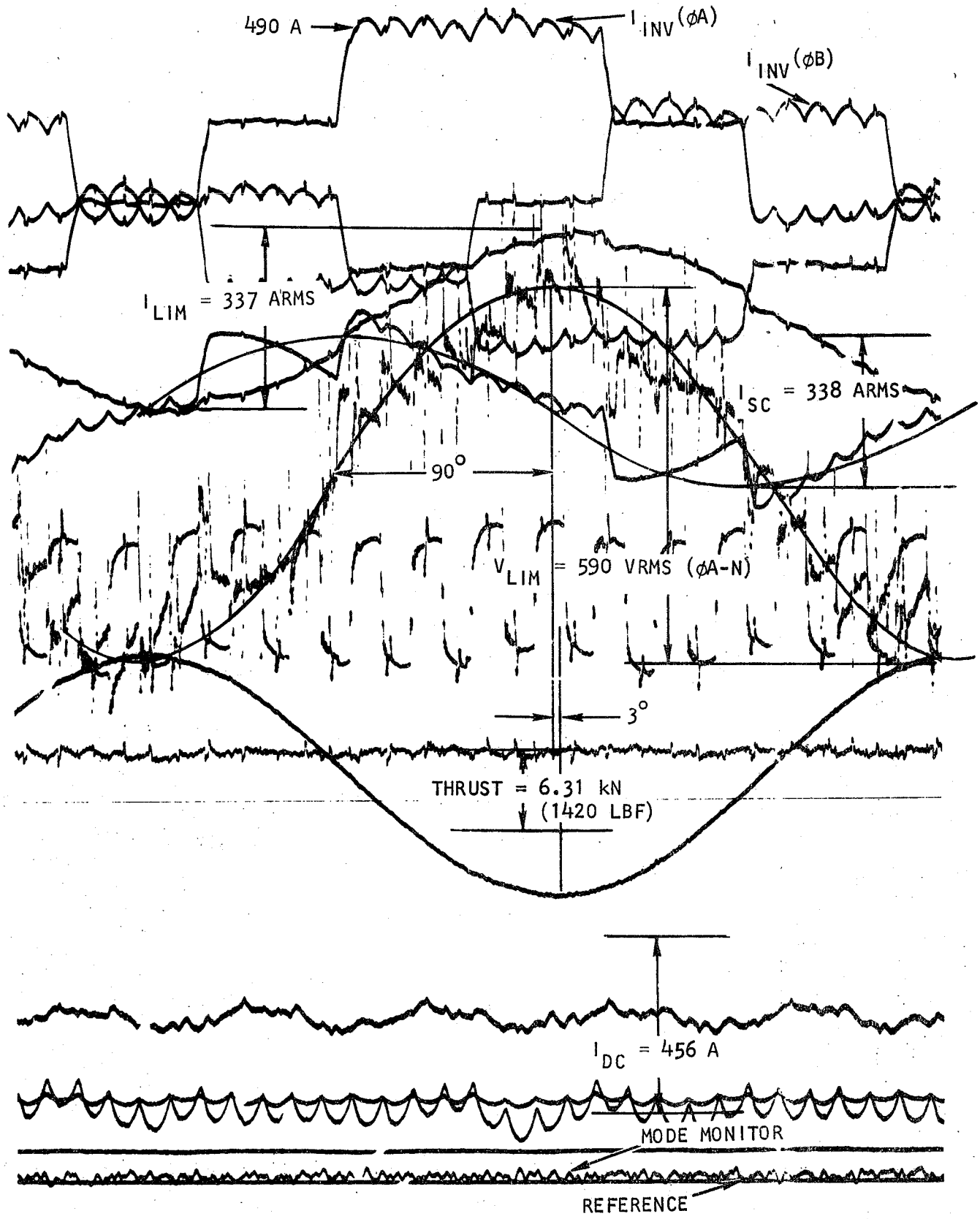

S-88662-A

Figure 5-16. Run Mode, 31.7-mm (1.25-in.) Airgap, 1.2-Ohm External Resistors

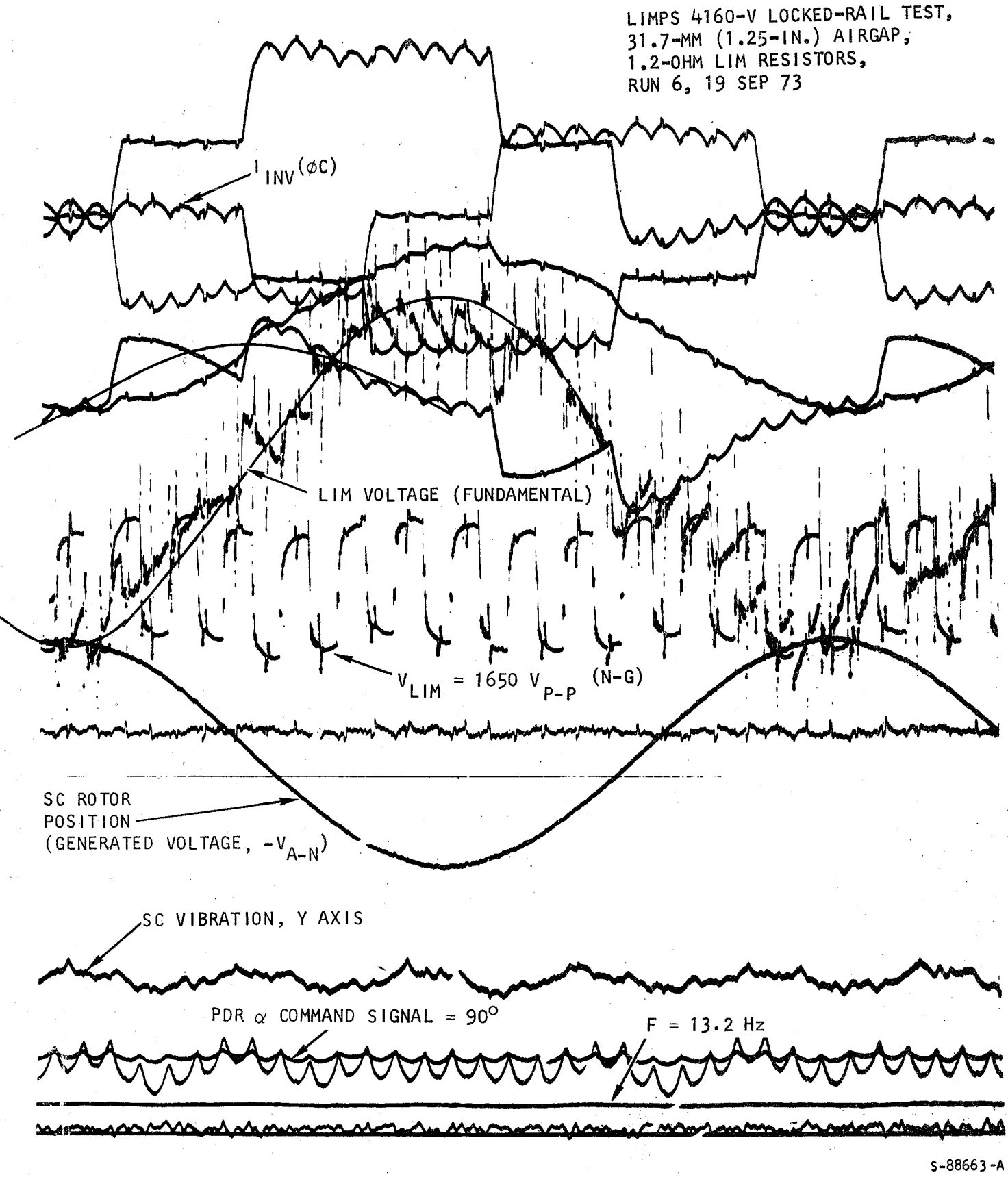

Figure 5-16. (Continued)

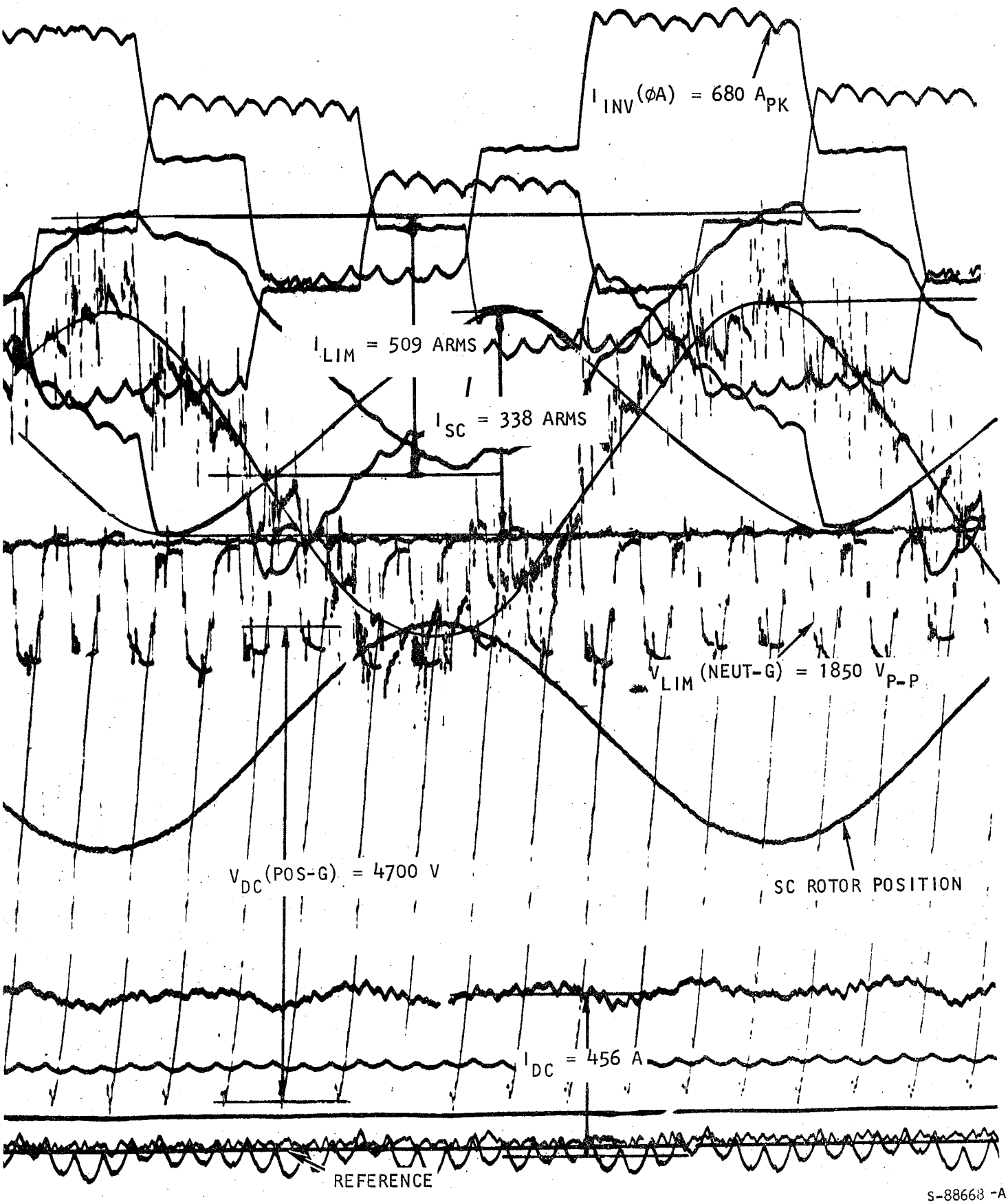

Figure 5-17. Run Mode, 38.1-mm (1.5-in.) Airgap, 0.6-Ohm External Resistors

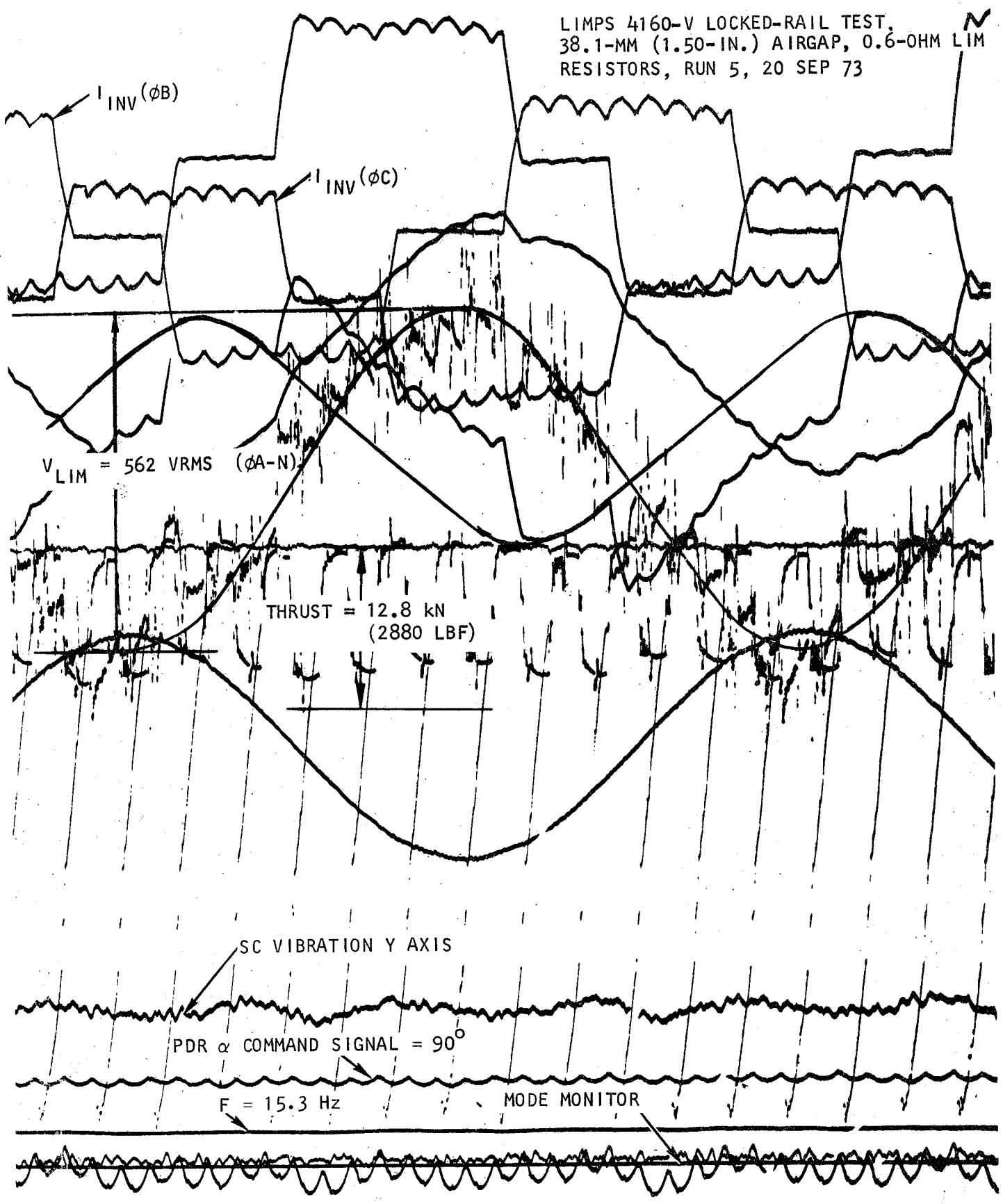

Figure 5-17. (Continued)

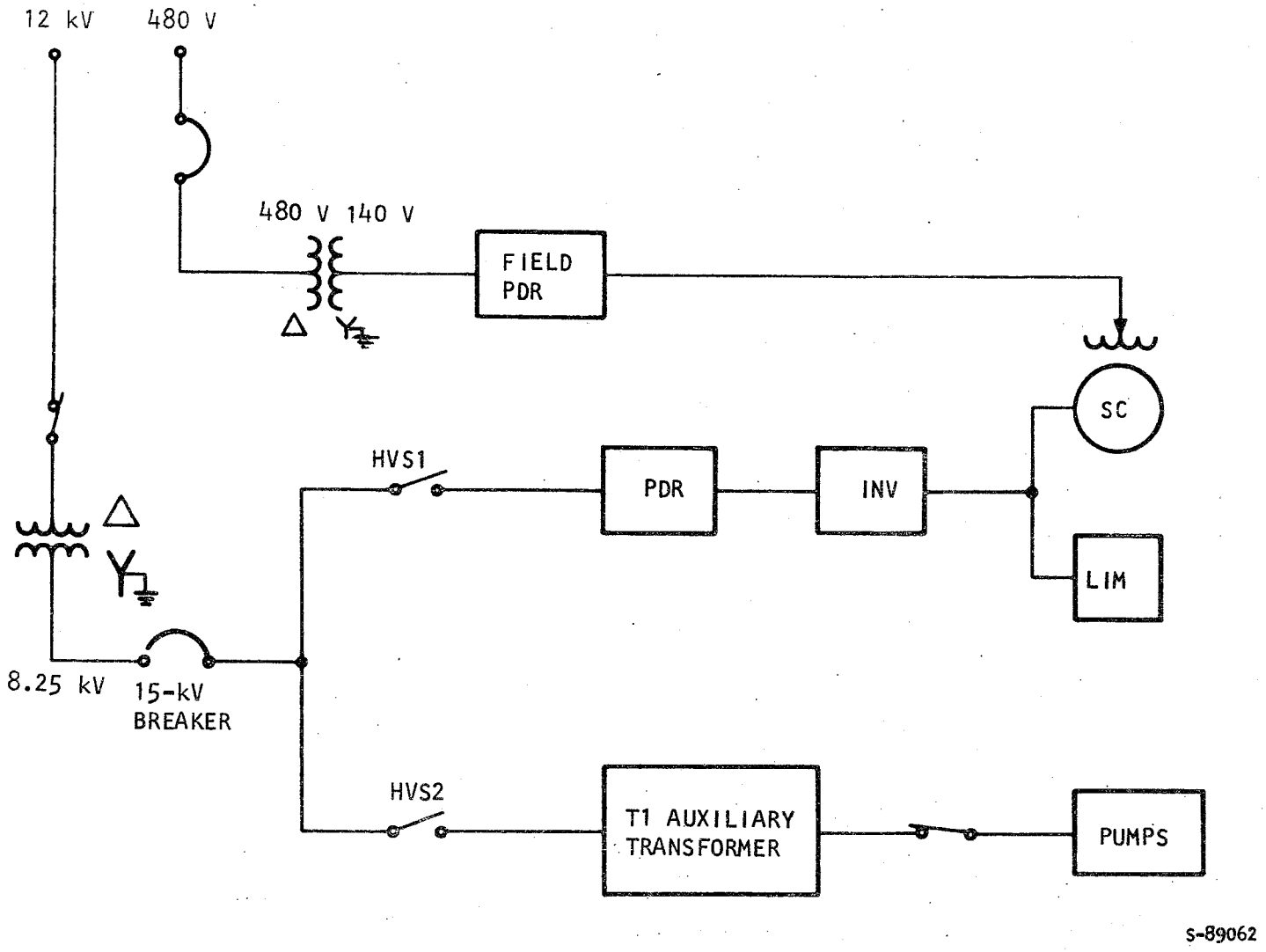

Figure 5-18. System 8250-V Test Setup

current was fed from the facility power source previously used in the 4160-V test series because of the limited capacity of the 8250-V source. The main PDR was supplied from the 8250-V source. The LIM was connected with no rail.

Initially, the system was subjected to full voltage for 5 min, with no gate signals applied to the PDR. The purpose was to ascertain system capability to withstand full voltage without dielectric breakdown, it being well known that failures sometimes occur after the initial moment of full-voltage application. Results were satisfactory; no failures or difficulties were encountered.

The system was then operated at full voltage with no load. Figure 5-19 shows test results oscillographically, indicating that with a dc link current of 180 A, a field current of 1800 A, and a mode transition frequency of about 12 Hz, the system started and commutated satisfactorily in the run mode. It achieved a maximum frequency of about 13 Hz on this run. Under these test conditions, the system met design operating specifications.

These results essentially reflect achievement of the major objectives of the high-voltage, no-load tests. It was demonstrated that the LIMPS could operate at full voltage and that the power conditioning unit control system was functioning properly. In an effort to operate the system at rated speed, testing was continued on 2 and 3 Oct 73. Some difficulties with noise on the instrumentation channels and associated quick shutdown initiation circuitry were encountered. However, at the end of Run 2 (2 Oct 73), which ended in a commutation failure shutdown, examination of the applicable oscillogram (Figure 5-20) showed clear evidence that a commutation failure had occurred. Investigation revealed that 12 thyristors in the PDR and 11 in the inverter had failed. The failures in the PDR were diagnosed as being associated with repeated di/dt "hammering" during turnon. The snubber circuits were changed

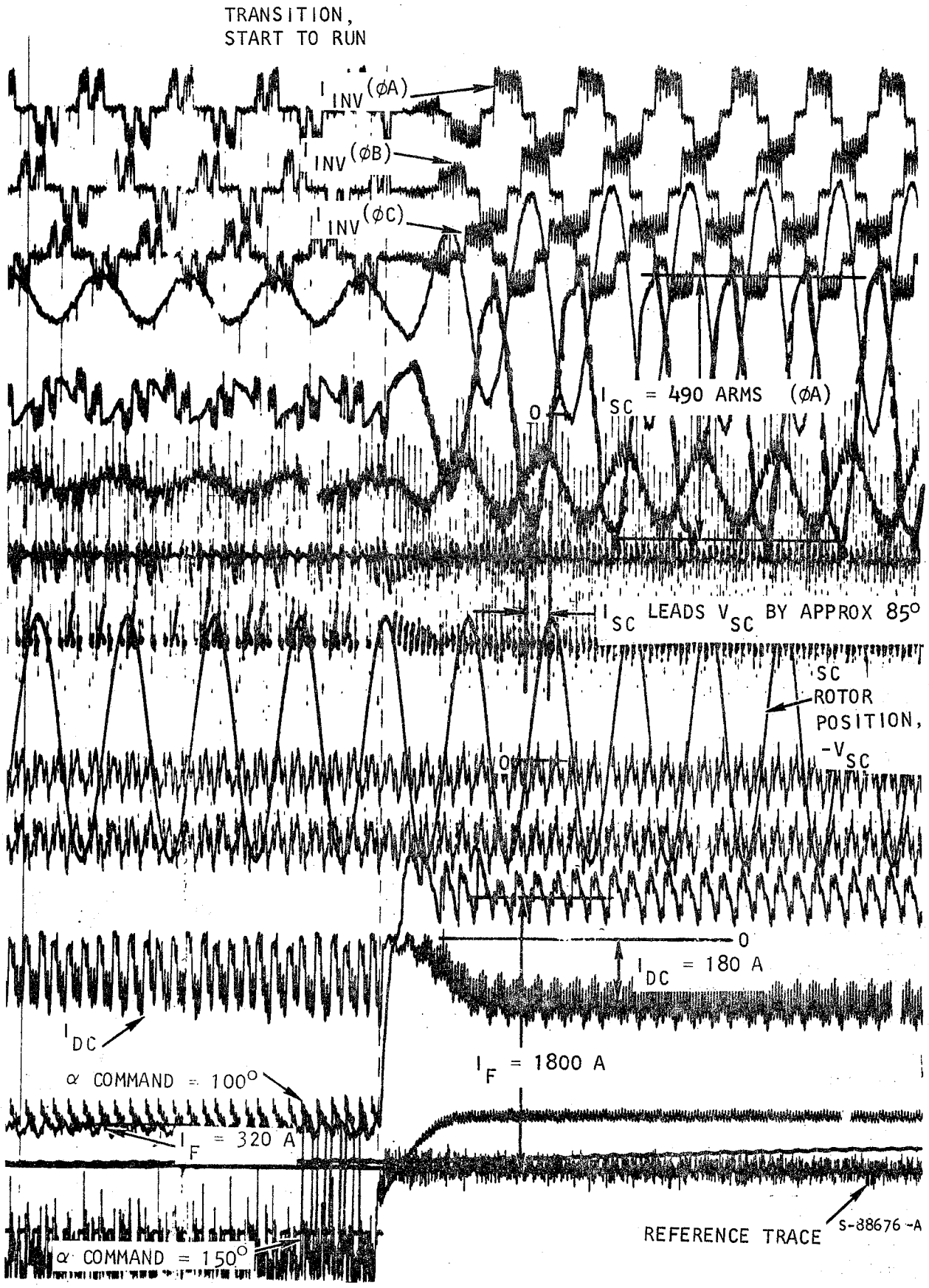

Figure 5-19. Successful Test Run at 8250 V without External Resistors

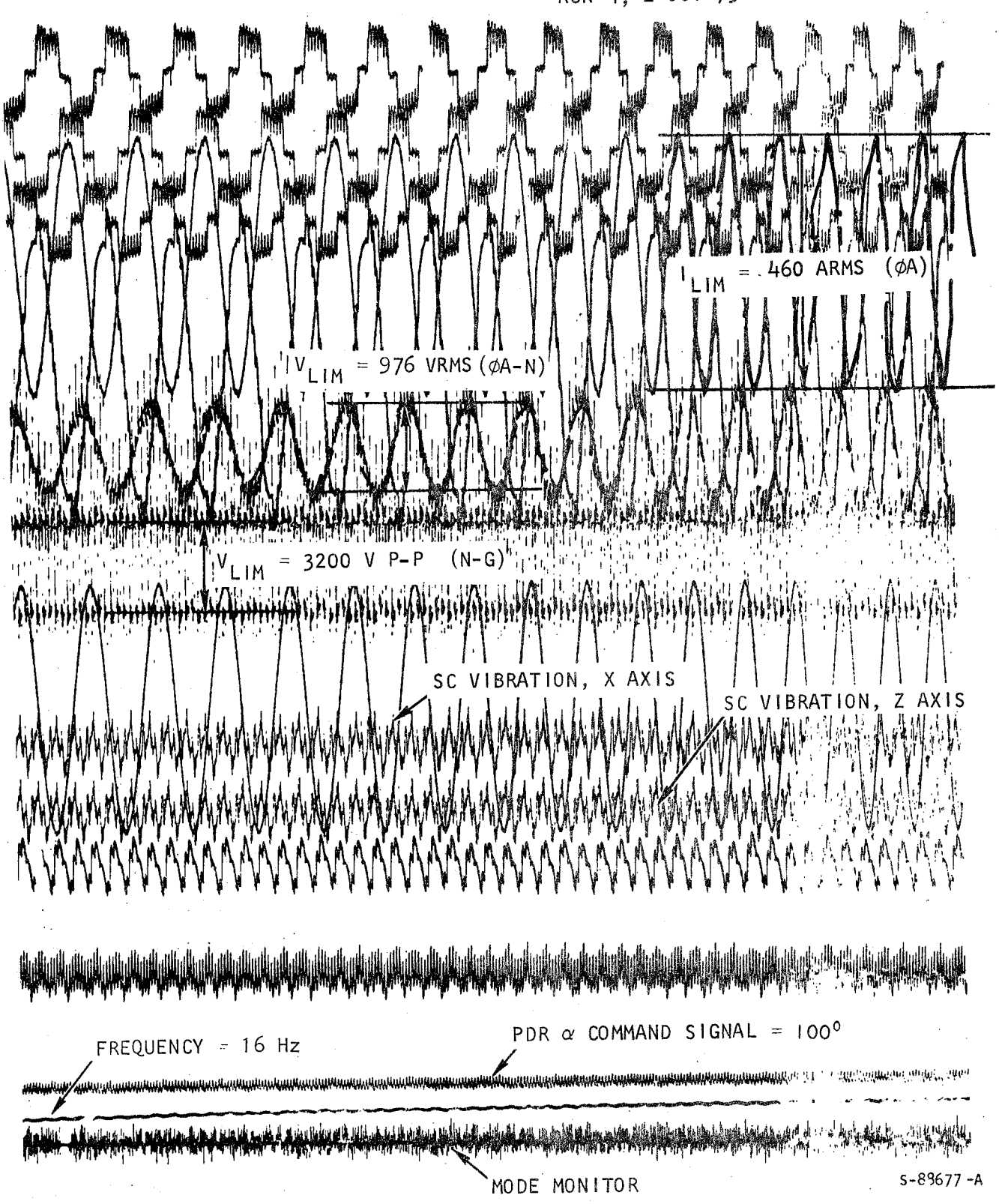

Figure 5-19. (Continued)

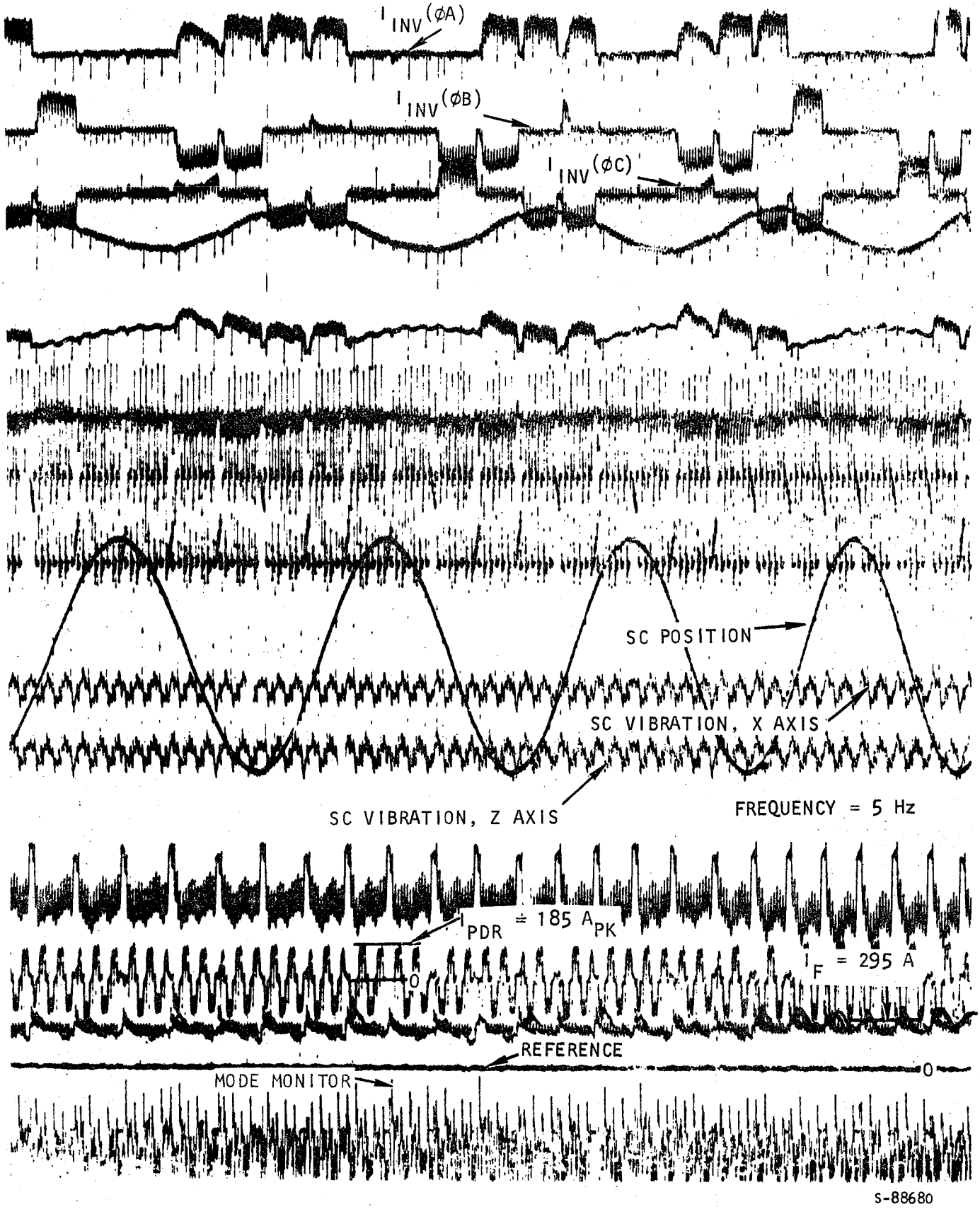

Figure 5-20. System 8250-V Test, Commutation Failure

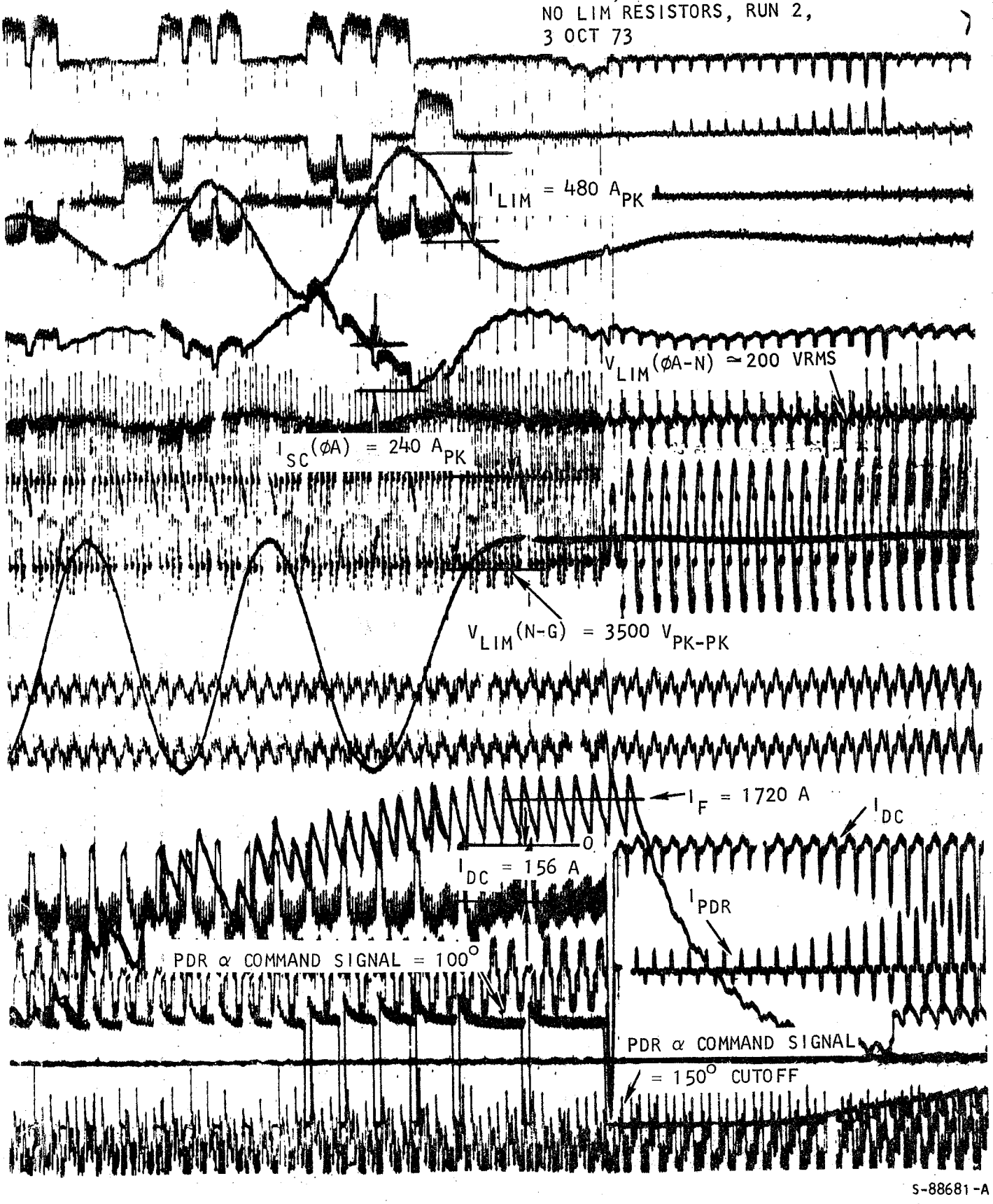

Figure 5-20. (Continued)

and turnon delay times and storage charge characteristics of the thyristors were matched to correct this problem. The failures in the inverter were apparently caused by voltage failures of two signal power level diodes in the carrier generator circuit, resulting in the loss of gate signals to one phase. Higher voltage-rating diodes have been substituted.

TEST STATISTICS

Table 5-4 lists pertinent data for the static test series.

TABLE 5-4

STATIC TEST STATISTICS

Maximum Input Voltage	8250 V, line-to-line (rated voltage)
Input Voltage Test Levels	Running Time
480 V	2 hr, 42 min, 0 sec
4160 V	3 hr, 11 min, 18 sec
8250 V	1 min, 45 sec
	*Total 5 hr, 55 min, 3 sec
Maximum SC Speed	488 rad/s (4650 rpm), 94 percent of rated speed
Percent of Rated Load Currents	
Dc link	129
LIM	84
SC	79

*Total running time does not include component testing.

SECTION 6

FIELD TEST INTRODUCTION

Section 6 is the first of four that comprise Part 3, the field test portion of this report. Section 6 provides brief introductory, background, and summary material on the field test program. Subsequent sections describe the test facilities, data acquisition and processing, and data analyses in that order.

The LIMPS field tests were conducted in early 1976 and included about 100 vehicle runs, 63 of which produced LIMPS data. The LIMPS data runs are summarized in Table 6-1.

TABLE 6-1

DATA RUNS SUMMARY

Run No.	Test Objectives per Test Log	Data Analysis Reference*
183	Initial speed and transition tests	189-190
194-197	LIM drag and LIMPS familiarization	133
200-211	Speed limit control and LIM drag tests	
212-220	Speed upgrading and braking tests	222-223
221-224	LIMPS performance test	173-176, 180-187, 191, 204-217
237-239	Inverter voltage and PDR power test	221
240-242, 245	Inverter voltage checkout	221, 204-217
246-259	Reaction rail temperature test	193, 226-234
264-275	Reaction rail temperature test, transition checkout	175-177, 192, 196-222

*Specifies applicable page number.

TEST PROGRESSION

The initial field test activity was preparatory in nature and included checkout and preliminary testing of all the facilities/equipment to be used during the testing. The major areas of preparatory effort were the LIMPS, the wayside power system, the TLRV electrical substation, the TLRV, and the supporting ground equipment and crews. Upon completion of these tasks, the performance portion of the field tests was begun and conducted approximately in the following sequence.

Pulsed Mode Tests

The LIMPS was operated at very low speeds, below the point at which the transition from start mode to run mode occurred. This not only provided valuable initial experience in operating the propulsion system and handling the vehicle while it was propelled by the LIM, but produced data in the areas of:

Control system response under start mode logic

Operational constraints

Real and reactive power distribution

Filtering effectiveness of the synchronous condenser

Pulsed mode LIMPS operation

Start/Run Transition Tests

The TLRV was then permitted to accelerate to speeds that would permit the start-mode to run-mode transition. This was an area of considerable concern, since during static testing of the LIMPS external resistors in the LIM circuit had been required to achieve transition. However, as predicted, with the vehicle free to move, transition occurred readily.

Transition performance was so good, in fact, that it was not necessary to perform some of the planned testing to map out the limiting conditions for transition, in view of the reduced scope of the test program.

Data was obtained, however, during these and other tests, which demonstrates that transition can be attained over a wide operating range.

Performance Tests

A series of tests was conducted to thoroughly explore acceleration-cruise-deceleration performance of the LIMPS. The vehicle was accelerated under successively higher thrust commands. The highest vehicle speed attained over the 500-m electrified guideway was 20 m/s. Electrical performance data was acquired during acceleration, cruise, and regeneration braking.

BACKGROUND

The decision to deemphasize high-speed air cushion vehicle research (as described in the preface to this report) had two effects on LIMPS field testing. The obvious first effect was diversion of both interest and resources from the TLRV as a test bed vehicle for air cushion research. The second effect was an indirect compromise of the scope of LIMPS testing by diluting the available LIMPS funds. The net result was a shortening of the originally contemplated 35,000-m (22-mile) long electrified guideway to a mere 500-m (1500 ft). This guideway length limitation, in turn, constrained the LIMPS test regime to a relatively low-speed and low-power operating envelope, both much lower than the LIMPS capabilities. Since interest in the LIMPS concept remained high, due to its applicability to more conventional traction systems, the LIMPS test program was continued in spite of these inherent test facility limitations. Thus, the LIMPS test program functioned to obtain data, though limited in scope, to investigate the following overall characteristics of the system:

- LIMPS steady-state characteristics
- LIMPS performance during the following operating modes:

  Start

Transition

Run

Coast

Regenerative braking

- LIMPS vehicular control characteristics
- LIMPS influence on the wayside power system
- LIMPS thermal characteristics

OBJECTIVES

To satisfy the specified data requirements, the following general test objectives were defined.

System Performance during Start Mode

The objectives under this classification were to obtain steady-state data on performance of the system and its components in the pulsed-commutation mode, investigate operating techniques at very low speeds, and approach the mode transition speed systematically. Attainment of these objectives was sought through tests addressed to:

(a) Investigate the control system response under start-mode logic, in terms of:

1. Magnitude and duration of the dc link current pulses
2. Inverter current phasing with respect to the synchronous condenser rotor position
3. Inverter current as a function of thyristor gating at the command of the zero crossover detector

(b) Determine the operational constraints in the pulsed mode manifested by:

1. Rate of current rise limiting by the control system

2. Built-in time delay between application of current pulses

3. Maximum attainable synchronous condenser speed as limited by the real power transfer through the dc link, at given current command and field current

(c) Identify the real and reactive power distribution throughout the LIMPS during pulsed-mode operation at specified dc link current and inverter frequency values.

(d) Demonstrate the filtering effectiveness of the synchronous condenser vs the LIM relative to the disposition of the current harmonics as a function of the dc link current command and inverter frequency.

(e) Measure the generated current harmonics reflected back into the wayside electric system dc link current as an indication of potential source of interference with communication and signal equipment.

(f) Define qualitatively the pulsed-mode operation through phasor diagrams, or through the loci of such diagrams, based on the fundamental frequency components of the electrical quantities on the inverter side.

(g) Generate pulsed-mode LIMPS performance data

System Performance during Start-to-Run Transition

The objectives under this classification were to demonstrate that start-to-run mode transition will take place properly, without external resistors in the LIM circuit, when the vehicle is free to move (see Section 9) and identify the parameter limits within which mode transition will occur. Attainment of these objectives was sought through tests designed to:

(a) Establish the minimum synchronous condenser speed at which inverter line commutation can be sustained following a start-run transition, as a function of:

1. Thrust command
2. Synchronous condenser field current setting

(b) Determine, if necessary, the go/no-go regions of successful start-to-run transition, for given dc link current, field current, and transition frequency values, by indicating whether the start mode terminated in:

1. Successful transition
2. Insufficient synchronous condenser speed, below transition frequency
3. Transition attempt resulting in commutation failure and QSD

(c) Using test data (dc link voltage and current, LIM voltage, and frequency) taken just after start-to-run transition, compare the inverter regulation with that based on normalized converter charts.

Low-Speed Run-Mode Performance

The objectives under this classification were to demonstrate satisfactory operation of the propulsion system within the speed regime permitted, obtain performance data on acceleration and cruise, and demonstrate operation at the maximum speeds possible with the 500-m electrified guideway. Attainment of these objectives was sought through tests addressed to:

(a) Determine the real and reactive power flow throughout the propulsion system, at specified LIM thrust and vehicle speed.

(b) Establish the voltage stress level at, and the adequacy of, the damping resistor connected to the synchronous condenser floating

neutral, as a function of LIM thrust and vehicle speed, by extrapolating low-speed test results to the higher speed regime.

(c) Define qualitatively the run-mode operation through the phasor diagrams (or through the loci of such diagrams) of the fundamental frequency components of the electrical quantities on the inverter side.

(d) Prepare vehicle performance curves, subject to data limitations at low vehicle speed, time from start, and distance from start with such electrical propulsion system parameters as:

1. Real power
2. Reactive power
3. Dc link voltage
4. Dc link current
5. Thrust command
6. Thrust
7. Electrical frequency

(e) Generate run-mode LIMPS performance data such as:

1. Thrust developed vs slip frequency, normalized to the dc link current
2. Harmonic content
3. Real and reactive power flow
4. Efficiency vs power level
5. Current unbalance at several current and slip frequency values, in terms of symmetrical components of the fundamental frequency terms

Low-Speed Braking Characteristics

The objectives under this classification were to obtain performance data on regenerative braking, and investigate the influence of the wayside power system on braking capability. All previously low-speed run-mode test objectives are again applicable; the following additional tasks cover only those objectives that pertain solely to the braking mode:

(a) Determine as a function of the braking effort the minimum vehicle speed at which the propulsion system reverts to the start mode.

(b) Establish an envelope of electrical brake fading, assuming that (1) the wayside power system is receptive to regeneration, and (2) regeneration is unacceptable due to a nonreceptive wayside power system.

Influence of Vehicle Operation on Wayside Power System

The objectives under this classification were to ascertain the influence of vehicle operation on the wayside power system, and determine the harmonic content, phase balance, symmetry, and power factor of the wayside power system. Attainment of these objectives was sought through tests addressed to:

(a) Determine the harmonic content of the line current. These harmonics are generated by the PDR and reflected back to the substation, appearing as current distortion in the line. As the input current to the PDR is the only major load on the wayside power system, measuring it allows determination of the following:

1. Conducted EMI (low-frequency range of EMI spectrum) through the power rails back to the substation
2. Correlation with radiated EMI data measured at a specified distance from the power rail, with background noise as a reference level

3. Potential interference with communication lines and equipment in terms of calculated telephone interference factor
4. Additional copper and iron losses in the power rail and substation transformer
5. Possible modifications in power system protection (relaying and instrumentation) because of the harmonic components

Temperatures and Cooling System Performance

The objectives under this classification were to investigate the duration and characteristics of the cooling load and equipment performance, and measure reaction rail temperature during both stationary tests and in the start mode. Attainment of these objectives was sought through tests addressed to:

(a) Determine major component heat loads at several current levels, calculate copper losses, which predominate at low speeds; and measure heat rejected into cooling medium.

(b) Measure heat rejected through the boiler system in thermal steady-state condition and compare with sum of component heat losses from (a).

(c) Investigate reaction rail temperature rise during the vehicle stationary test as a function of LIM current and slip frequency. Compare readings of temperature sensors located under the stack with those mounted on rail overhang.

CONCLUSIONS

As a result of the field testing and subsequent data analyses (see Section 9) the following major conclusions may be drawn concerning the LIMPS characteristics and operation:

(a) The LIM propulsion system performed according to predictions in terms of:

1. Developing up to rated (22,000 N) propulsive thrust
2. Converting 4160 V, 3-phase, 60-Hz, constant-voltage/constant frequency power to variable-voltage/variable-frequency power, in the 0 to 35 Hz frequency range delivered
3. Effecting smooth vehicle control by appropriate thrust, speed, and regenerative braking commands
4. Delivering nearly 850 kW real power (14.1 percent of rated) through the dc link at 19.3 m/s (14.4 percent of rated)
5. Overall efficiency consistent with the power achieved

(b) During the start mode the current or real power that can be delivered through the dc link is limited only by the current control loop response.

(c) The synchronous condenser can effectively filter the inverter current by absorbing over 95 percent of the current harmonics in both the pulsed and run modes, as a result of which the LIM current consists of the fundamental component.

(d) The LIMPS can achieve the transition from start mode to run mode consistently and reliably at an electrical frequency of 6 Hz or higher, with a thrust command of 60 percent or higher.

(e) The LIM and synchronous condenser are parallel connected at the inverter terminals and jointly influence the line commuation process.

(f) The potential at the synchronous condenser neutral, which is grounded through a 10-kilohm resistor, rises as the synchronous condenser frequency. The ground insulation of both machines (LIM and synchronous condenser) withstands this elevated potential at maximum generated frequency.

(g) The current harmonic content of the wayside power system is characteristic of a 6-pulse converter operation.

(h) The radiated emission in the vicinity of the electrified guideway, in general, does not exceed recommended values.

(i) The reaction rail temperature rise associated with rated LIM thrust at starting is negligible due to the low frequency power supplied by the LIMPS.

(j) The steady-state relationship between thrust command and dc link response is linear over the entire control range. Typical settling time is 1.6 s maximum.

(k) The (nominal) 30-deg phase-back of the inverter, generally, provides adequate commutation margin throughout the tested load range.

(l) Inverter thyristor gating with respect to the synchronous condenser rotor position rather than the terminal voltage reduces the commutative margin in the low-speed region.

(m) Additional filtering is not required since no interference was reported with test site communication or power relaying equipment.

SECTION 7

TEST FACILITIES

The LIMPS tests were conducted within the ambit of facilities especially provided for overall testing of vehicle dynamics, wayside power characteristics, and LIMPS propulsion, at the Transportation Test Center in Pueblo, Colorado. This section very briefly describes the major components of the facilities provided, as they affected the LIMPS tests.

VEHICLE FACILITIES

As noted earlier, the primary impetus in development of the TLRV as a vehicle was DOT interest in a high-speed test bed for vehicle air cushion/suspension and ride quality testing. The TLRV was developed for this purpose as was the guideway in which it was intended to be operated. The TLRV vehicle program led, in time, the LIMPS program. After considerable vehicle development effort, a decision was made to develop and utilize the LIMPS to provide motive thrust for the high-speed tests planned for the TLRV. In effect, the vehicle was to have served as a test bed for both the vehicle air cushion/suspension system and the LIMPS.

Three jet engines were provided on the vehicle to produce the airflow necessary to support and guide the vehicle and the LIM via their respective air cushion systems. The air supply characteristics available to the LIM are shown in Figure 7-1. The nominal weight of the vehicle, including normal fuel, instrumentation, cooling water, and LIMPS components was about 24,000 kg (over 52,000 lb).

The guideway for the vehicle was provided as a U-shaped trough approximately 5 km (3.1 miles) in length. The LIM reaction rail was secured to the center of the floor of the guideway extending about 500 m (1500 ft) in length, and upward about 60 cm (23.5 in.).

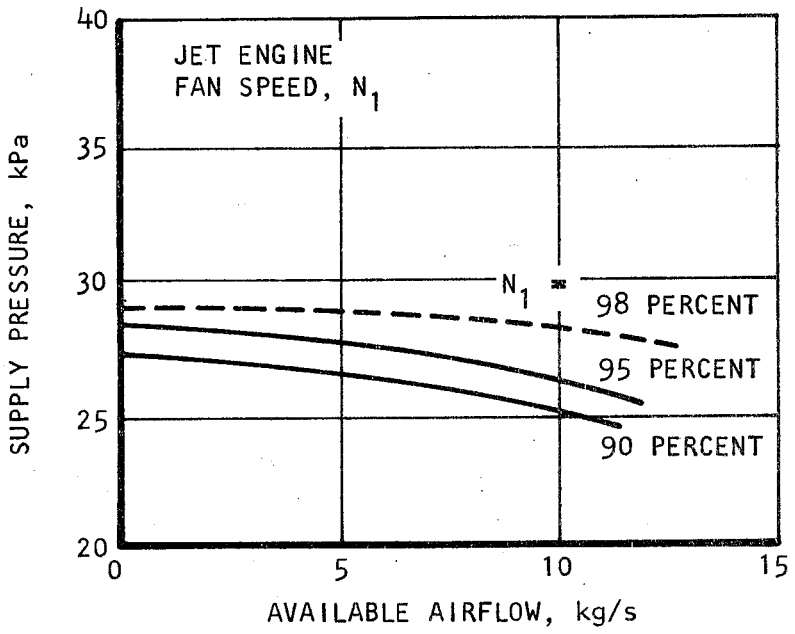

Figure 7-1. LIM Air Supply Characteristics

WAYSIDE ELECTRIC POWER SYSTEM FACILITIES

Power for the LIMPS was obtained from an on-site 12-MVA substation operated by the Department of Transportation. For this test program, the voltage along the electrified guideway was 4160 V, 3-phase, 60-Hz, and was regulated by equipment at the substation. This regulated voltage was distributed through appropriate switchgear and protective devices to three horizontal power rails. Figure 7-2 shows the electrical schematic of the LIMPS and its supply. The power rails are mounted along the top of one side of the guideway. The LIMPS receives its power from the power rails by means of a vehicle-mounted collector arm, which slides the collector head within the rails*. Figure 7-3 shows the collector head, engaged within the rails, with the collector arm extending to the vehicle. Approximately 500 m (1500 ft) of power rails were installed along the guideway, coincident with the LIM reaction rail.

* See Reference (6), page iv.

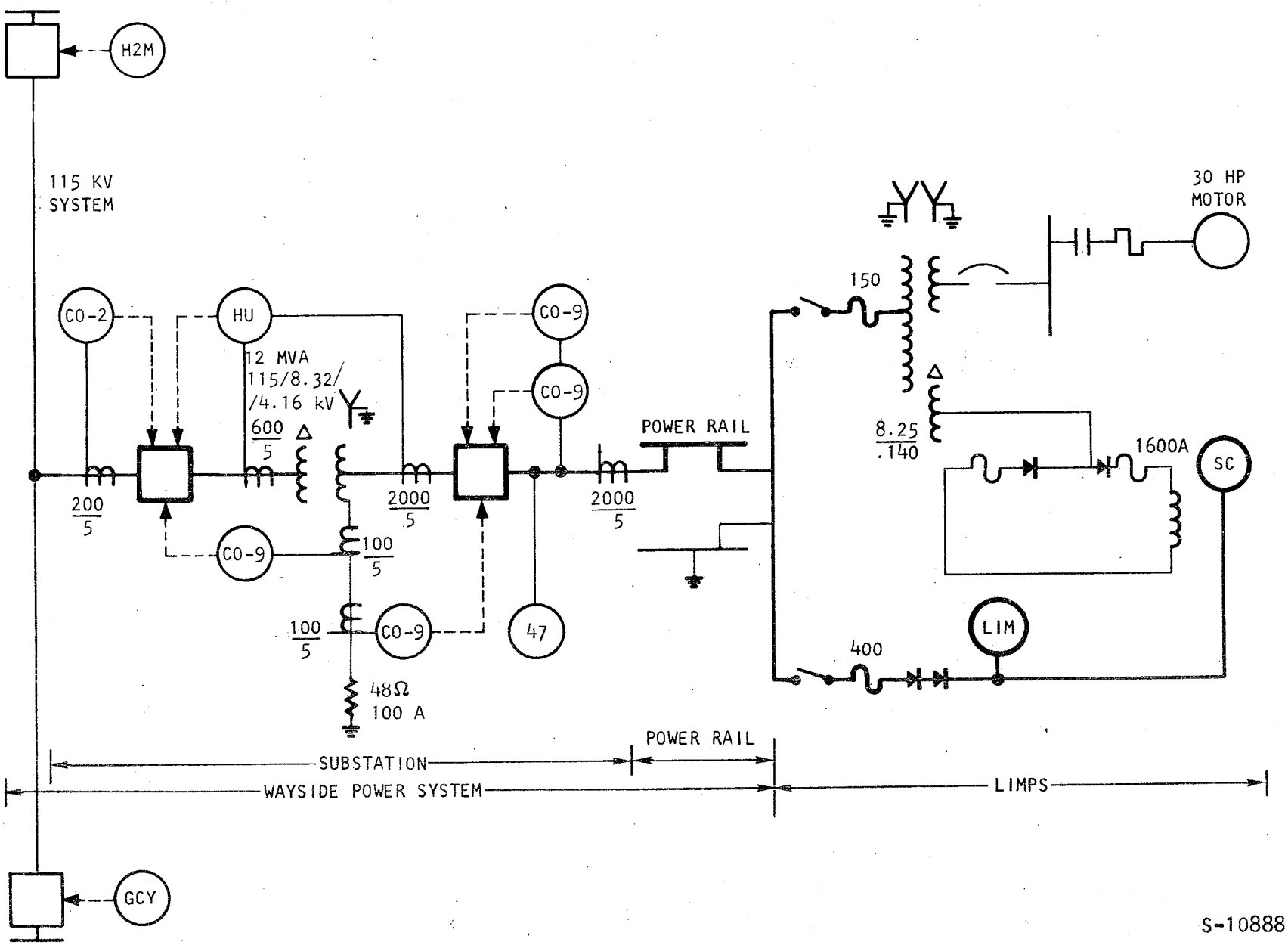

Figure 7-2. Overall LIMPS-Supply Electrical Schematic

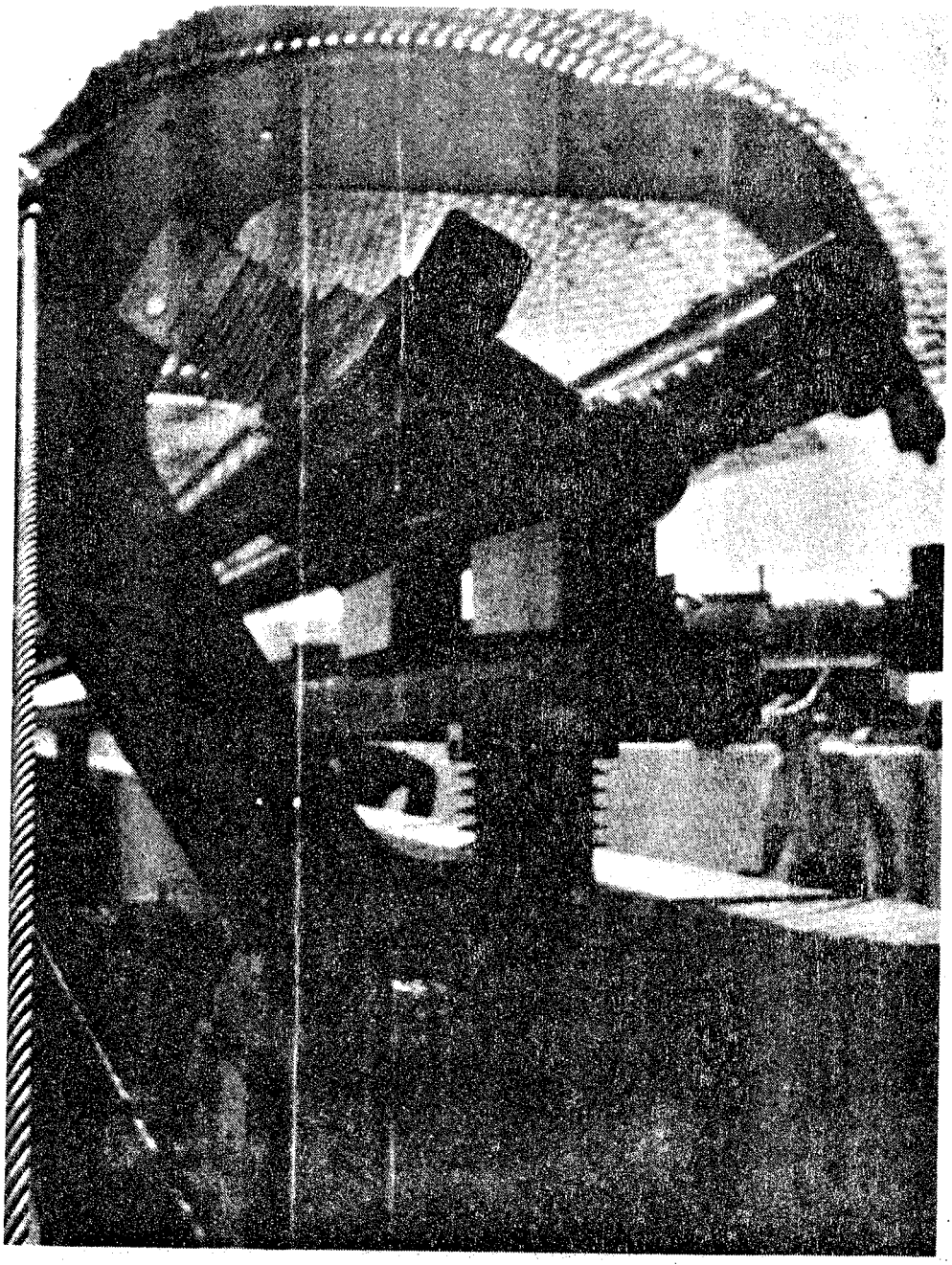

F-24544

Figure 7-3. Wayside Power Collector Engaged In the Wayside Power Rails

SECTION 8

DATA ACQUISITION AND PROCESSING

An onboard digital data acquisition system (DAS) sampled a total of 125 electrical and mechanical operating parameters. Selected analog parameters were also recorded onboard on a oscillograph and a tape recorder. The DAS parameters were simultaneously transmitted via PCM/FM telemetry to the data van. Equipment in the data van received the telemetered data for storage, real-time display of selected parameters, and preliminary processing. All data was sent to the AiResearch facility in Torrance, California, for final processing and analysis. This section discusses significant aspects of the data collection and processing activities.

INSTRUMENTATION

The LIMPS was instrumented to provide, for digital recording, the parameters listed in Table 8-1. Parameters available for analog recording are listed in Table 8-2.

DATA ACQUISITION

The data acquisition process involved, generally, two distinct sets of hardware. The onboard set comprised the sensors, signal conditioning, sampling, digitizing, and telemetry transmitter. The fixed station (data van) set comprised the telemetry receiver, decoders, displays, printers, processors, and tape recorders.

A 14-channel tape recorder and a 9-channel light beam oscillograph (ultraviolet) were installed for analog recording and for quick-look information for the test personnel. Both direct and FM recording were possible with the tape recorder. A slow code was produced by an autonomous time code generator for both of these recorders, enabling correlation among the two recorders and the

TABLE 8-1

DIGITAL INSTRUMENTATION

AiResearch Measurand No.	Parameter	Unit	Mnemonic	System Range	Sensor	
					Manufacturer, Model or PN	Location
101	INV AØ Voltage	kV RMS	INVVA	0-1.5	Caddock PS 101-1	INV Output
102	INV BØ Voltage	kV RMS	INVVB	0-1.5	Caddock PS 101-1	INV Output
103	INV CØ Voltage	kV RMS	INVVC	0-1.5	Caddock PS 101-1	INV Output
107	LIM AØ Current	A RMS	LIA	0-1000	AiResearch 2002508	INV Output
108	LIM BØ Current	A RMS	LIB	0-1000	AiResearch 2002508	INV Output
109	LIM CØ Current	A RMS	LIC	0-1000	AiResearch 2002508	INV Output
113	LIM Avg 3Ø Power	MW RMS	LIMP	±1	None (Onboard Calc)	None
115	Electrical Freq	Hz	FE	0-60	Kearfott CR41093005	Top Sync Condenser
116	LIM Thrust Uncorrected	kN	THR	±17.79	Solvere VM19-4A1	LIM Linkage
141	LIM Winding Temp	°C	LT1	0-260	Thermal Systems (2002278)	Primary #2 13-14
142	LIM Winding Temp	°C	LT2	0-260	Thermal Systems (2002278)	Primary #2 26-26
143	LIM Winding Temp	°C	LT3	0-260	Thermal Systems (2002278)	Primary #2 33-34
144	LIM Winding Temp	°C	LT4	0-260	Thermal Systems (2002278)	Primary #2 43-44
145	LIM Winding Temp	°C	LT5	0-260	Thermal Systems (2002278)	Primary #2 53-54

TABLE 8-1 (Continued)

AiResearch Measurand No.	Parameter	Unit	Mnemonic	System Range	Sensor	
					Manufacturer, Model or PN	Location
146	LIM Winding Temp	°C	LT6	0-260	Thermal Systems (2002278)	Primary #2 65-66
147	LIM Winding Temp	°C	LT7	0-260	Thermal Systems (2002278)	Primary #1 23-24
148	LIM Winding Temp	°C	LT8	0-260	Thermal Systems (2002278)	Primary #1 33-34
149	LIM Winding Temp	°C	LT9	0-260	Thermal Systems (2002278)	Primary #1 43-44
150	LIM Winding Temp	°C	LT10	0-260	Thermal Systems (2002278)	Primary #1 53-54
151	LIM Winding Temp	°C	LT11	0-260	Thermal Systems (2002278)	Primary #1 63-64
152	LIM Winding Temp	°C	LT12	0-260	Thermal Systems (2002278)	Primary #1 73-74
153	LIM OUT Coolant Temp	°C	CLIM	0-260	Tylan FG 645	LIM OUT Line
154	LIM Back-iron Temp	°C	LBT1	0-100	Thermal Systems (2002278)	Primary #2 19
155	LIM Back-iron Temp	°C	LBT2	0-100	Thermal Systems (2002278)	Primary #2 68
156	LIM Back-iron Temp	°C	LBT3	0-100	Thermal Systems (2002278)	Primary #1 19
157	LIM Back-iron Temp	°C	LBT4	0-100	Thermal Systems (2002278)	Primary #1 68

TABLE 8-1 (Continued)

AiResearch Measurand No.	Parameter	Unit	Mnemonic	System Range	Sensor	
					Manufacturer, Model or PN	Location
158	Speed Limit Command	V dc	SLC	0-5	Spectrol 930-279	Speed Quadrant
159	Thrust Command	V dc	THRCOM	±2.5	Spectrol 930-278	Thrust Quadrant
160	Vehicle Land Speed	m/s	VEL	0-25	Nucleus NC-7	Trailing Vehicle
161	LIM Acceler-ation	m/s^2 Peak	ACC	±10	Schaevitz LSDC 89-1	Top of LIM
201	SC Aϕ Current	A RMS	SCIA	0-1000	None (Onboard Calc)	None
202	SC Bϕ Current	A RMS	SCIB	0-1000	None (Onboard Calc)	None
203	SC Cϕ Current	A RMS	SCIB	0-1000	None (Onboard Calc)	None
204	SC 3ϕ VAR	MVAR RMS	SCQ	±2	None (Onboard Calc)	None
205	SC Field Current	kA dc	SCIF	0-3	AiResearch 2002506	Field Power Supply
206	SC Field Voltage	V dc	SCVF	0-150	None (Direct Meas)	None
207	SC Field Resistance	Ω	SCRF	0.02 to 0.06	None (Onboard Calc)	None
208	SC Vibra-tion	g Peak	SCVB1	0 to 5	Endevco 2217E	Upper Lateral
209	SC Vibra-tion	g Peak	SCVB2	0 to 5	Endevco 2217E	Upper Vertical
210	SC Vibra-tion	g Peak	SCVB3	0 to 5	Endevco 2217E	Upper Longitud (approx)
211	SC Vibra-tion	g Peak	SCVB4	0 to 5	Endevco 2217E	Lower Lateral

TABLE 8-1 (Continued)

AiResearch Measurand No.	Parameter	Unit	Mnemonic	System Range	Sensor	
					Manufacturer, Model or PN	Location
213	SC Vibration	g Peak	SCVB5	0 to 5	Endevco 2217E	Lower Longitud (approx)
214	SC Temp	°C	SCT1	0-260	Thermal Systems (2002278)	Upper Ball Bearing
215	SC Temp	°C	SCT2	0-260	Thermal Systems (2002278)	Lower Ball Bearing
216	SC Temp	°C	SCT3	0-260	Thermal Systems (2002278)	Upper Roller Bearing
217	SC Temp	°C	SCT4	0-260	Thermal Systems (2015043)	Inner Winding
218	SC Temp	°C	SCT5	0-260	Thermal Systems (2002278)	Mid Winding
219	SC Temp	°C	SCT6	0-260	Thermal Systems (2002278)	Outer Winding
220	SC Temp	°C	SCT7	0-260	Thermal Systems (2002278)	Stator Laminations
221	SC Temp	°C	SCT8	0-260	Thermal Systems (2002278)	Housing
222	SC Temp	°C	SCT9	0-260	Thermal Systems (2002278)	Lower Dynamic Seal
223	SC Temp	°C	SCT10	0-260	Thermal Systems (2002278)	Brush Heat Sink
224	SC Temp	°C	SCT11	0-260	Thermal Systems (2002278)	Internal Ambient
225	SC Temp	°C	SCT12	0-260	Thermal Systems (2002278)	Internal Housing
226	SC Coolant Temp	°C	CSCS	0-260	Tylan FG 645	Stator OUT
227	SC Coolant Temp	°C	CSCR	0-260	Tylan FG 645	Rotor OUT
228	SC Brush Temp	°C	SCT13	0-260	Thermal Systems (2002278)	Brush Holder

TABLE 8-1 (Continued)

AiResearch Measurand No.	Parameter	Unit	Mnemonic	System Range	Sensor	
					Manufacturer, Model or PN	Location
229	SC Brush Position	mm	SCBP	0 to 1.27	AiResearch LSK 31368	Back of Brush
301	PDR Aϕ Voltage	kV RMS	PVA	2.0-2.5	Transrex (2000972)	Aux Trans
302	PDR Bϕ Voltage	kV RMS	PVB	2.0-2.5	Transrex (2000972)	Aux Trans
303	PDR Cϕ Voltage	KV RMS	PVC	2.0-2.5	Transrex (2000972)	Aux Trans
304	PDR Aϕ Current	A RMS	PIA	0-1000	AiResearch 2002508	PDR Input
305	PDR Bϕ Current	A RMS	PIB	0-1000	AiResearch 2002508	PDR Input
306	PDR Cϕ Current	A RMS	PIC	0-1000	AiResearch 2002508	PDR Input
307	PDR Avg 3ϕ Power	MW RMS	PDRP	± 2	None (Onboard Calc)	None
308	PDR α Command	V dc	PDRA	-6 to 0	None (Feedback)	None
309	PDR OUT Air Temp	°C	PDRT1	0-100	Thermal Systems 5001-19A	Lower
310	PDR OUT Air Temp	°C	PDRT2	0-100	Thermal Systems 5001-19A	Lower
311	PDR OUT Air Temp	°C	PDRT3	0-100	Thermal Systems 5001-19A	Upper
312	PDR OUT Air Temp	°C	PDRT4	0-100	Thermal Systems 5001-19A	Upper
313	PDR OUT Air Temp	°C	PDRT5	0-100	Thermal Systems 5001-19A	Logic Box
314	PDR OUT Air Temp	°C	PDRT6	0-100	Thermal Systems 5001-19A	Logic Box
401	Inductor Coolant Temp	°C	CIND	0-260	Tylan FG 645	OUT Line

TABLE 8-1 (Continued)

AiResearch Measurand No.	Parameter	Unit	Mnemonic	System Range	Sensor	
					Manufacturer, Model or PN	Location
501	INV Aϕ Current	A RMS	INIA	0-1000	AiResearch 2002508	INV Output
502	INV Bϕ Current	A RMS	INIB	0-1000	AiResearch 2002508	INV Output
503	INV Cϕ Current	A RMS	INIC	0-1000	AiResearch 2002508	INV Output
504	Dc Link Voltage	kV dc	DV1	$\pm$2	Caddock PS 504-1	PDR Output
505	Dc Link Current	A dc	DI1	0-1000	AiResearch 2002508	PDR Output
506	Link Ripple Current	A RMS	DIR	0-300	AiResearch 2002508	PDR Output
507	INV IN Air Temp	°C	INVT1	0-100	Thermal Systems 5001-19A	INV Input
508	INV Avg Power	MW RMS	INVP	$\pm$2	None (Onboard Calc)	None
509	Mode Monitor Start/ Run	V dc	M	0/1	None (Feedback)	INV Controls
601	Primary Pump IN Pressure	MPa Gage	PPP	0-2.08	Bourns 2005831901	Pump Intake
602	Primary Pump IN Temp	°C	TEMIN	0-100	Tylan FG 645	Pump Intake
603	PDR, FS, INV IN Coolant Temp	°C	CI	0-100	Tylan FG 645	Pump Outlet
604	PDR, FS, INV OUT Coolant Temp	°C	CO	0-100	Tylan FG 645	OUT Buss
605	Aux Trans Coolant Temp	°C	CAT	0-260	Tylan FG 645	Aux Trans OUT

TABLE 8-1 (Continued)

AiResearch Measurand No.	Parameter	Unit	Mnemonic	System Range	Sensor	
					Manufacturer, Model or PN	Location
607	Closed Loop Resistivity	Mn cm	RCC	0-8	Balsbaugh 900M/900-.01T	Boiler IN
608	Open Loop Resistivity	Mn cm	RCO	0-8	Balsbaugh 900M/900-.01T	Water Tank Return Line
609	Boiler IN Coolant Temp	°C	CBI	0-260	Tylan FG 645	Boiler IN
613	#1 Pressure Switch	V dc	S1	208/160 psig	Custom Components 8G	LIM, IND, AT IN Line
614	#2 Pressure Switch	V dc	S2	282/238 psig	Custom Components 8G	SC IN Line
616	#4 Pressure Switch	V dc	S4	30/24 psig	Custom Components 8G	PDR, INV, FPS IN Line
801	Collector Arm Vert Position	rad	CAVP	-0.157 to +0.262	Cal Best 805080	Junction Box
802	Collector Arm Extension	cm	CAE	0-30	AiResearch 7101-12	Top of Arm
803	Collector Arm Drag Force	N	CAD	0-9	AiResearch 7101-12	Arm Joint

TABLE 8-2

PARAMETERS AVAILABLE FOR ANALOG RECORDING

Parameter	AiResearch Measurand No.	Unit	Range
LIM tooth flux density	117	T	0 to 2
LIM tooth flux density	118	T	0 to 2
LIM tooth flux density	119	T	0 to 2
LIM tooth flux density	120	T	0 to 2
LIM tooth flux density	121	T	0 to 2
LIM tooth flux density	122	T	0 to 2
LIM tooth flux density	123	T	0 to 2
LIM tooth flux density	124	T	0 to 2
LIM tooth flux density	125	T	0 to 2
LIM tooth flux density	126	T	0 to 2
LIM tooth flux density	127	T	0 to 2
LIM tooth flux density	128	T	0 to 2
LIM tooth flux density	129	T	0 to 2
LIM tooth flux density	130	T	0 to 2
LIM tooth flux density	131	T	0 to 2
LIM tooth flux density	132	T	0 to 2
LIM tooth flux density	133	T	0 to 2
LIM tooth flux density	134	T	0 to 2
Tooth flux density distr	135	T	0 to 2
Tooth flux density distr	136	T	0 to 2
Tooth flux density distr	137	T	0 to 2
Tooth flux density distr	138	T	0 to 2

TABLE 8-2 (Continued)

Parameter	AiResearch Measurand No.	Unit	Range
Slot flux density	139	T	0 to 0.8
Slot flux density	140	T	0 to 0.8
SC voltage (neutral)	None	kV peak	0 to 5
LIM ϕ voltage	101-103	kVRMS	0 to 1.5
LIM ϕ current	107-109	ARMS	0 to 1000
LIM frequency	115	Hz	0 to 60
LIM thrust	116	kN	$\pm$17.79
SC ϕ current	201-203	ARMS	0 to 1000
SC field current	205	kAdc	0 to 3
SC vibration	208-212	g peak	$\pm$5
PDR input ϕ voltage	301-303	kVRMS	2 to 2.5
PDR input ϕ current	304-306	ARMS	0 to 1000
INV output ϕ current	501-503	ARMS	0 to 1000
Dc link voltage (+ to gnd)	None	V peak	$\pm$4000
Dc link voltage (- to gnd)	None	V peak	$\pm$4000
Dc link current	505	Adc	0 to 1000
Dc link voltage	504	kVdc	$\pm$2
SC rotor position	None	Vdc	0 to 5
Mode monitor	509	Vdc	0 to 5
INV α command	None	rad	0 to 2.62
PDR α command	308	rad	0 to 2.62
LIM longitudinal acceleration	161	g	$\pm$1

digital data. The tape recorder could be played back into the oscillograph at the end of a vehicle test run, to provide onsite visualization of the recorded data.

For the digitally recorded data, sensor outputs were conditioned onboard to lie within the ranges of ±2.5 or 0 to 5 vdc. Subsequent signal conditioning typically included filtering to eliminate noise and suppress transients, the derivation of RMS values, and the performance of analog computations, and amplification, attenuation, and/or rectification.

A total of 238 analog input signals were sampled at a rate of 31.25 samples per second (sps), and 84 were sampled at 250 sps. Sixteen digital input channels were sampled at 31.25 sps, and eight were sampled at 250 sps. Three of the 250-sps digital channels were reversed for BCD data from an onboard time coad generator (modified IRIG-B). A fourth channel was used as a frame counter, resetting every second.

A 1-MHz clock in the time code generator is the timing base used to format data into a PCM data field consisting of 8 bits per word, 128 words per frame, and 8 frames per data field.

The outputs of the signal conditioners are connected via patchpanels to an encoder (for telemetry) and/or the analog recorders. The encoder provides serial digital multiplexed data, which is transmitted via PCM/FM at a rate of 32,000 8-bit words per second, on a frequency of 217.0 MHz, with a power of 20 W.

Data Van Equipment

The fixed station, commonly referred to as the data van, received the telemetered data from the vehicle and recorded it on magnetic tapes. By the use of a minicomputer and calibration data stored in a disk memory, this raw

data was re-recorded in modified BCD format on engineering units (EU) tapes. The EU tapes were subsequently transferred to the AiResearch Torrance facility for further processing and analysis.

A 36-channel oscillograph was available to permit real-time analog recording (and display monitoring) of selected parameters in the digital data stream during a test run. Additional interfacing equipment included a teletypewriter, an alphanumeric printer, a paper tape system, and a digital plotter.

DATA ACQUIRED

The combination of onboard oscillograph and tape recorder produced the oscillograms listed in Table 8-3. All of the measurands listed in Table 8-1 were routinely digitally recorded.

TABLE 8-3

OSCILLOGRAMS ACQUIRED

Run Nos. 183, 194-197

Trace No.	Measurand
1	101
2	501
3	Rotor position
4	201
5	505
6	308
7	205
8	509
9	Time code

Run 183

Trace No.	Measurand
1	509
2	159
3	Rotor Position
4	308
5	501
6	502
7	503
8	505
9	Time code

Run 183

Trace No.	Measurand
1	509
2	159
3	Rotor position
4	308
5	INV
6	305
7	306
8	504
9	Time code

Run Nos. 198-211, 221-224, 240-242, 245

Trace No.	Measurand
1	101
2	501
3	Rotor position
4	201
5	107
6	505
7	308
8	205
9	Time code

Run Nos. 201-224, 237-242, 245

Trace No.	Measurand
1	159
2	504
3	-
4	SC neutral volts
5	102
6	502
7	103
8	503
9	Time code

Run Nos. 212-220

Trace No.	Measurand
1	101
2	501
3	Rotor position
4	201
5	107
6	505
7	160
8	205
9	Time code

Run Nos. 212-224, 237-242 245-259, 264, 266, 268, 270-276

Trace No.	Measurand
1	301
2	302
3	-
4	303
5	304
6	305
7	306
8	-
9	Time code

Run Nos. 246, 259, 264, 266 268, 270-276

Trace No.	Measurand
1	101
2	501
3	116
4	201
5	107
6	505
7	308
8	205
9	Time code

DATA PROCESSING

Data (engineering units) tapes were processed by a Digital Scientific META 4/1800 computer at the AiResearch Torrance facility to print out original and computed data. Three different print out formats were available:

Data Dump--The data from the EU tape, without computation, is printed out with parameter columns and constant time rows at 0.128-sec intervals.

Time Based Computations--Computed data (e.g., thrust corrected for acceleration and drag) is printed out with parameter rows and constant time columns at 5.120-sec intervals.

Velocity-Based Computations--Similar data is printed out with parameter rows and constant velocity columns at 2-m/s intervals.

Computer-aided manual techniques were used in analyzing the oscillograms.

INSTRUMENTATION ACCURACY

Instrumentation Description

The LIMPS is a variable-frequency, variable-voltage power system utilizing fundamental frequencies from dc to 165 Hz, with harmonics above ground. The maximum load current, not including faults, is 1000 A. Figure 8-1 shows a simplified schematic of the LIMPS and the principle voltage and current instrumentation.

1. Current Measurements

In order to sense LIMPS currents over the entire frequency range and to obtain isolation between the high LIMPS voltage and sensor output signals, special Hall-effect current sensors were developed. These sensors comprise a C-core magnetic iron structure with a fixed gap in which a Hall-effect generator was placed and on which signal conditioning electronics circuitry was mounted. The entire assembly was potted and encapsulated, but with provisions to electronically trim the gain and to null out offsets.

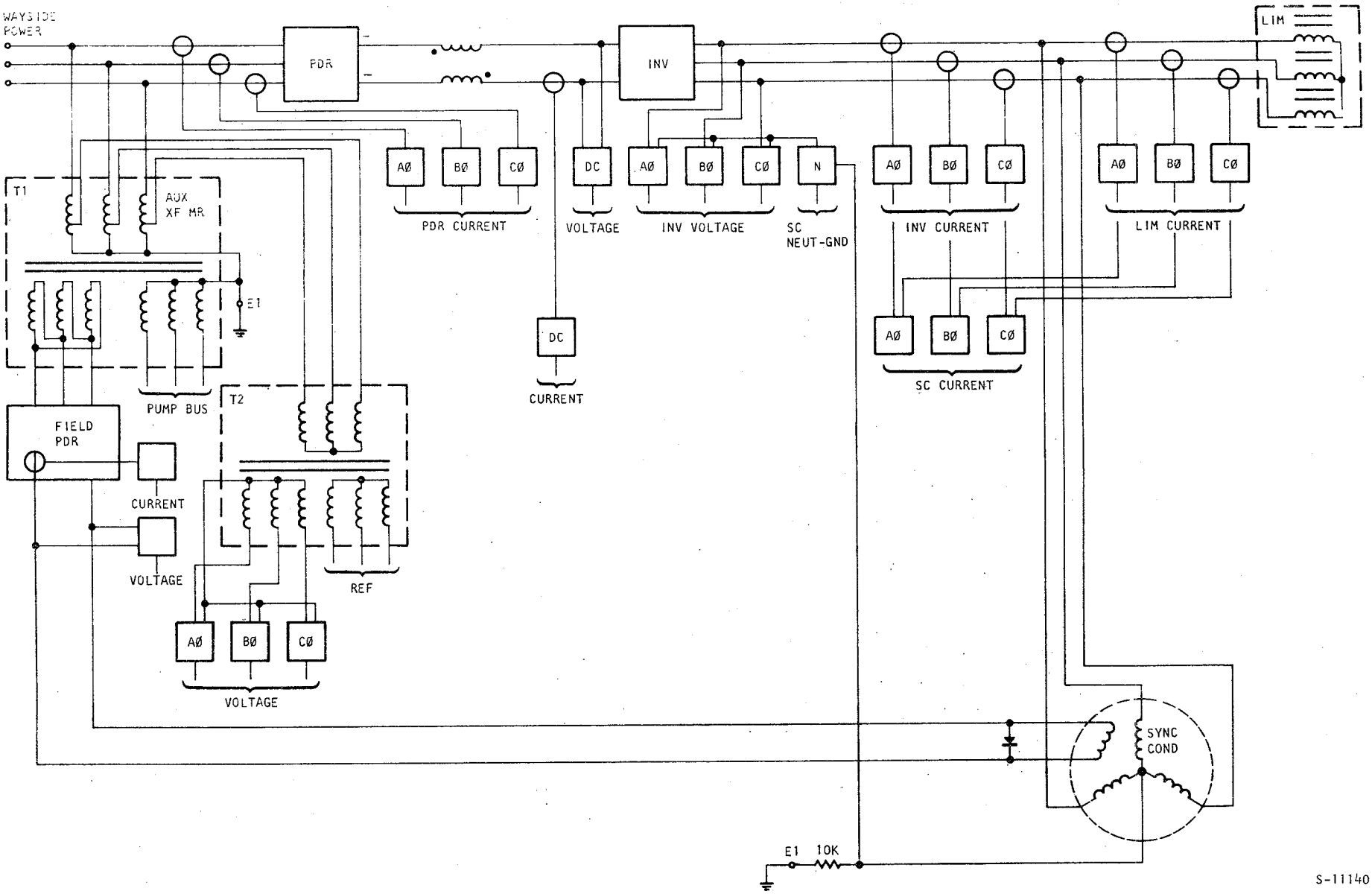

Figure 8-1. Simplified Schematic of LIMPS, Showing Key Elements and Instrumentation

Synchronous condenser field current is also measured by a Hall-effect current sensor. The field current is supplied by an ungrounded 2700-A phase delay rectifier fed from a 140-V delta-connected winding on the auxiliary power transformer. Because the field winding is protected by a freewheeling shunt diode mounted directly on the synchronous condenser, and the field current sensor was mounted within the phase delay rectifier, the sensed signal did not truly represent the field current. To account for this, special signal conditioning, comprising a half-wave rectifier and resistor/capacitor network, was added to the sensor output to simulate the field resistive/inductive delay when current was flowing through the freewheeling diode.

2. Voltage Measurements

Voltage sensing in the dc link and inverter sections was accomplished by using resistive voltage dividers. Since the only defined vehicle ground of the power system was that obtained by grounding the synchronous condenser neutral to the vehicle through a 10-kilohm resistor it was necessary to obtain these voltages by differential measurement.

For the PDR input voltages, which were fixed-frequency, 60-Hz potentials, the auxiliary power transformer primary was tapped to scale the input voltage, the wayside power voltage, by a factor of approximately 40. The tap voltages were fed to a second, wye-wye, transformer with a nominal 1:1 ratio and with the primary side ungrounded. The measured secondary voltges thus represent the approximate phase voltages for the wayside power. When the LIMPS was connected to operate on 4 kV the sensing ratio was nominally 1/20.

3. LIM Thrust Parameters

To determine the LIM performance, the mechanical output of the LIM was also measured. This set of measurements consisted of sensing (1) the speed of

the vehicle with a "fifth" wheel identical to that used for accurately measuring test automobile speed, (2) the thrust transmitted to the vehicle from the LIM, and (3) the longitudinal acceleration of the LIM.

4. Temperature Measurements

In addition to the key electrical and mechanical parameters required for performance testing, numerous subsidiary parameters were required to obtain thermal information. The sensors used for this purpose were resistive temperature detectors. These devices provide for larger signal levels than thermocouples and avoid the extreme shielding and filtering that are normally required when signals are amplified at low signal-to-noise ratios.

5. Vibration Measurements

Critical synchronous condenser vibration was monitored by triaxial accelerometers located near the top bearing housing. This instrumentation, similar to that in the LIM, comprised standard charge-amplifier type accelerometers.

Current Measurement Accuracy

The Hall-effect current sensors were calibrated with standard instruments, an RMS digital voltmeter and a wide-frequency-band, current viewing resistor of 0.00013 ohm $\pm$0.2 percent. The voltmeter accuracy for the 0 to 100 mV range was $\pm$0.6 mV $\pm$0.2 percent of the reading. Thus, for 500-A current, the instruments used as a calibration standard possessed a peak measurement error of 6.6 A.

Because the LIMPS current flow in circuits that are above ground potential, the digital voltmeter has to operate with high common-mode voltages. The meter used for this calibration had the capability of operating with potentials up to 500 Vdc above ground, but could not tolerate time varying common-mode voltages over 50 V. Thus, for phase delay angles large enough to cause discontinuous

currents, common-mode voltages exceeded the meter capability. This occurs at about 175 A, so calibration data below 175 A could not be achieved. In order to calibrate over the full range of the system, one calibration point was taken with the LIMPS power turned off. Four other points were then taken at current levels of 200 to 510 Adc. A line of best fit was then made for the current and standard deviations were calculated for these calibration curves.

The PDR currents were measured using a 2000:5 current transformer, a wide band 0.049 ohm ±0.2 percent current viewing resistor and a true RMS digital voltmeter. The voltmeter accuracy was ±0.6 mV ±0.2 percent of reading. The combined calibration instruments peak error was ±6.6 A. By using current transformers for isolation between the instruments and the supply voltage, the problem of reading small voltages across current viewing resistors at high common-mode voltages was avoided.

Table 8-4 summarizes the various current parameters RSS (root-sum-square), 3-sigma errors.

Voltage Measurement Accuracy

The inverter and dc link voltages were measured by using high-voltage resistive voltage dividers. The measured voltage division ratio of these dividers, calibrated at the Pueblo Army Depot, is 2000 to 1, ±2.5 percent, when tested at 12,000 Vdc. It should be noted that this calibration was performed on a direct current basis. In use the divider was actually exposed to ac voltages with a fundamental frequency up to 165 Hz and harmonics even higher. Under these circumstances the stray distributed capacitances associated with the cables, connectors, circuit boards, and containers of the dividers combine to produce a frequency-sensitive sensor with an equivalent circuit shown in Figure 8-2, where

TABLE 8-4

CURRENT PARAMETERS ACCURACY

Parameter		Measurand	Tolerance	Percent Full Scale
LIM	Phase A	107	±48.13	±4.8
LIM	Phase B	108	±73.23	±7.32
LIM	Phase C	109	±29.26	±2.93
INV	Phase A	501	±21.28	±2.13
INV	Phase B	502	±20.01	±2.01
INV	Phase C	503	±24.94	±2.50
SC	Phase A	201	±57.98	±5.8
SC	Phase B	202	±27.68	±2.7
SC	Phase C	203	±53.78	±5.4
PDR	Phase A	304	±14.90	±1.49
PDR	Phase B	305	±15.01	±1.50
PDR	Phase C	306	±14.84	±1.50
Dc link current		505	±13.97	±1.39
Field current		205	±35.60	±1.39

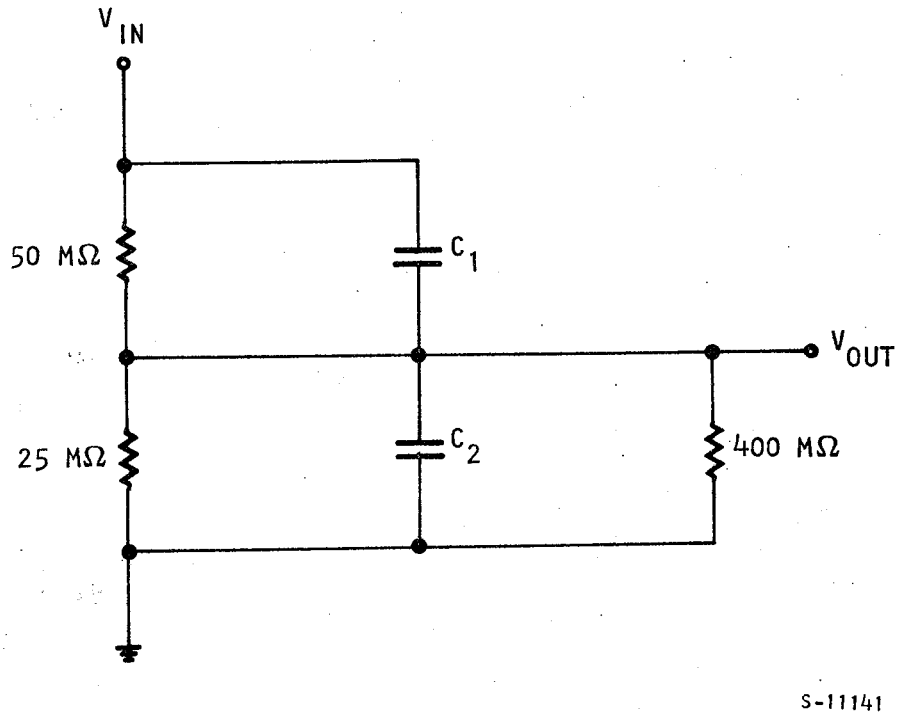

Figure 8-2. Resistive Voltage Divider Equivalent Circuit

C_1 and C_2 represent the net equivalent distributed capacitances. It was not possible to measure these capacitances but estimates of 5 pF for C_1 and 960 pF for C_2 appear reasonable.

Over the frequency range consistent with the relatively low vehicle speeds obtained during the field tests, up to nearly 20 m/s (45 mph) (24.75 Hz), the change in the sensor gain is small, less than 0.1 percent for the fundamental, and gradually increases by about 20 percent for the 17th harmonic.

The PDR voltages are pseudo-phase voltages obtained by establishing a neutral with a wye-wye transformer, as shown in Figure 8-1. The neutral reference point for the 3-phase PDR voltage does not have to be at any specific point, and the only physical requirement is that the phase voltages be reasonably balanced to avoid exceeding design limits of the signal conditioning electronics. Thus the neutral is determined by the balance of loads on the auxiliary power transformer (T1) and instrumentation (T2) transformer. To certify the transformer ratios and phase shifts, it is necessary to test each transformer winding separately. However, in calibrating the system only the overall voltage measurements were taken to establish the voltage ratios. This ratio was found to be 20.03 $\pm$0.25 percent for unloaded transformers. With the transformers loaded, the individual phase voltage ratios deviated by as much as 2 percent. However, the average ratio of all phases for loaded and unloaded transformers varied only $\pm$0.1 percent. Therefore, even though the individual phase ratios are load dependent, the mean ratio of all phases is nearly constant. This accounting compensates for small unbalances in loads because an increase in ratio in one phase is offset by a ratio decrease in the others. Table 8-5 lists the measured data.

TABLE 8-5

PDR NET TRANSFORMER VOLTAGE RATIO MEASUREMENTS

Phase	Unloaded Ratio	Loaded Ratio
A	20.00	19.63
B	20.10	20.41
C	20.05	20.00
Average	20.05	20.01
Deviation	±0.2 percent	±1.98 percent

Oscilloscope measurements did not reveal any measurable phase shift between the phase voltage of the auxiliary power transformer and the secondary voltage of T2 for the case where both transformers were unloaded. Thus the actual phase shift error was not established for the system, but it is discernibly negligible. Oscillographic comparisons of the phase voltage waveforms indicated that a small amount of waveform distortion did exist. No attempt was made to determine the magnitude or harmonic content of the waveforms.

The associated signal conditioning was calibrated by injecting voltage signals equivalent to potentials from the dividers that would correspond to actual potentials of 0 to 1500 Vdc. Injection calibrations were also conducted at 100 Hz over the equivalent range of 0 to 500 V and variable-frequency calibration data was obtained at an equivalent voltage of 500 V over the frequency range of 0 to 10 kHz. From a line of best fit it was found that the 3-sigma deviation was within ±0.76 V for the worst case inverter voltage, ±13.0 V for the PDR voltage, and ±13.8 V for the dc link voltage.

Table 8-6 lists the overall accuracy, including the data system, for each voltage measured.

TABLE 8-6

VOLTAGE PARAMETERS ACCURACY

Parameter		Measurand	Tolerance, V	Percent Full Scale
Inverter	A	101	±18.07	±1.20
Inverter	B	102	±16.80	±1.12
Inverter	C	103	±17.54	±1.17
PDR	A	301	±6.76	±0.45
PDR	B	301	±6.34	±0.42
PDR	C	303	±8.41	±0.56
Dc link current		504	±21.09	±1.41

THRUST MEASUREMENT ACCURACY

The thrust transmitted between the LIM and the vehicle is measured by sensing the twist developed in an interconnecting torque tube. To calibrate the system, the LIM was levitated on its own air cushions while being mechanically loaded by a hydraulic ram, longitudinally, to simulate forces transmitted to the vehicle. The calibration standard is a tension compression load cell placed between the double acting hydraulic ram and the LIM.

For comparison purposes the LIM thrust was also calibrated with the LIM supported on shop-type air bearings. The line of best fit for both calibrations was made and compared for similarity. The deviations from the line of best fit and the independent linearity are given in Table 8-7. The overall accuracy of the measured thrust, including the independent linearity, the signal conditioning and the data acquisition system is ±1475 N (332 lbf).

TABLE 8-7

THREE-SIGMA DEVIATION FROM LINE OF BEST FIT FOR LIM THRUST CALIBRATION

Calibration	Thrust, N (lbf)	
	LIM Levitated by Vehicle Air	LIM Supported by Air Bearings
Positive thrust	±866 (194)	±1086 (244)
Negative thrust	±1274 (286)	±1237 (278)

Temperature Measurement Accuracy

All temperatures were measured with the same type of resistive temperature devices as sensors. Two temperature ranges, however, were employed, 0 to 100°C and 0 to 260°C, by appropriately scaling the signal conditioning circuitry. The accuracy of the instrumentation is given in Table 8-8.

TABLE 8-8

TEMPERATURE MEASUREMENT ACCURACY

Range, °C	Tolerance, °C	Percent Full Scale
0 to 100	±3	±3
0 to 260	±7.8	±3

Power and Reactive Power Measurement Accuracy

The power measurements are obtained by direct multiplication of the instantaneous phase voltages with their respective currents, summing the three phase powers and filtering to obtain the total power input to the PDR, inverter, and LIM. The synchronous condenser power is obtained by instantaneously multiplying the line-to-line voltage with the opposite phase current to obtain the individual phase reactive powers. The powers are then summed and filtered to obtain the total reactive power. Table 8-9 lists the accuracies of the power instrumentation.

TABLE 8-9

ACCURACY OF POWER AND REACTIVE POWER MEASUREMENTS

Parameter	Measurand	Percent Full Scale
PDR power	307	±3.16
INV power	508	±2.85
LIM power	113	±3.35
SC reactive power	204	±3.83

SECTION 9

DATA ANALYSES

This section presents the results of the analysis performed with data obtained during the LIMPS field tests. The analysis is supported by 50 tables and figures. Many of the latter include combinations of graphs, oscillograms, bar charts, phasor diagrams, and block diagrams, to provide the complementary results concisely on a single page for reader convenience. The major topics in this section are pulsed-mode tests, start-to-run-mode transition tests, low speed braking tests, reaction rail temperature rise tests, and LIMPS influence on the wayside power system. In many cases, measured performance results are compared with calculated (theoretical or predicted) results.

PULSED-MODE TESTS

Because the inverter can not be line commutated from the synchronous condenser until sufficient back-emf is available, a special start mode is necessary to bring the synchronous machine up to a minimum operating speed. This is accomplished by selectively pulsing sets of machine windings through the inverter, which causes the machine to accelerate until a speed is reached where the generated voltage will permit line commutation. During start mode, inverter commutation is achieved through current quenching by the phase delay rectifier.

This starting operation is accomplished automatically by logic and shaft position sensors. In Figure 9-1 the affected blocks are marked to indicate the control sequence.

Inverter Commutation

During commutation the inverter current is diverted from one phase to the next phase in a cyclical, three-phase order. The logic that accomplishes

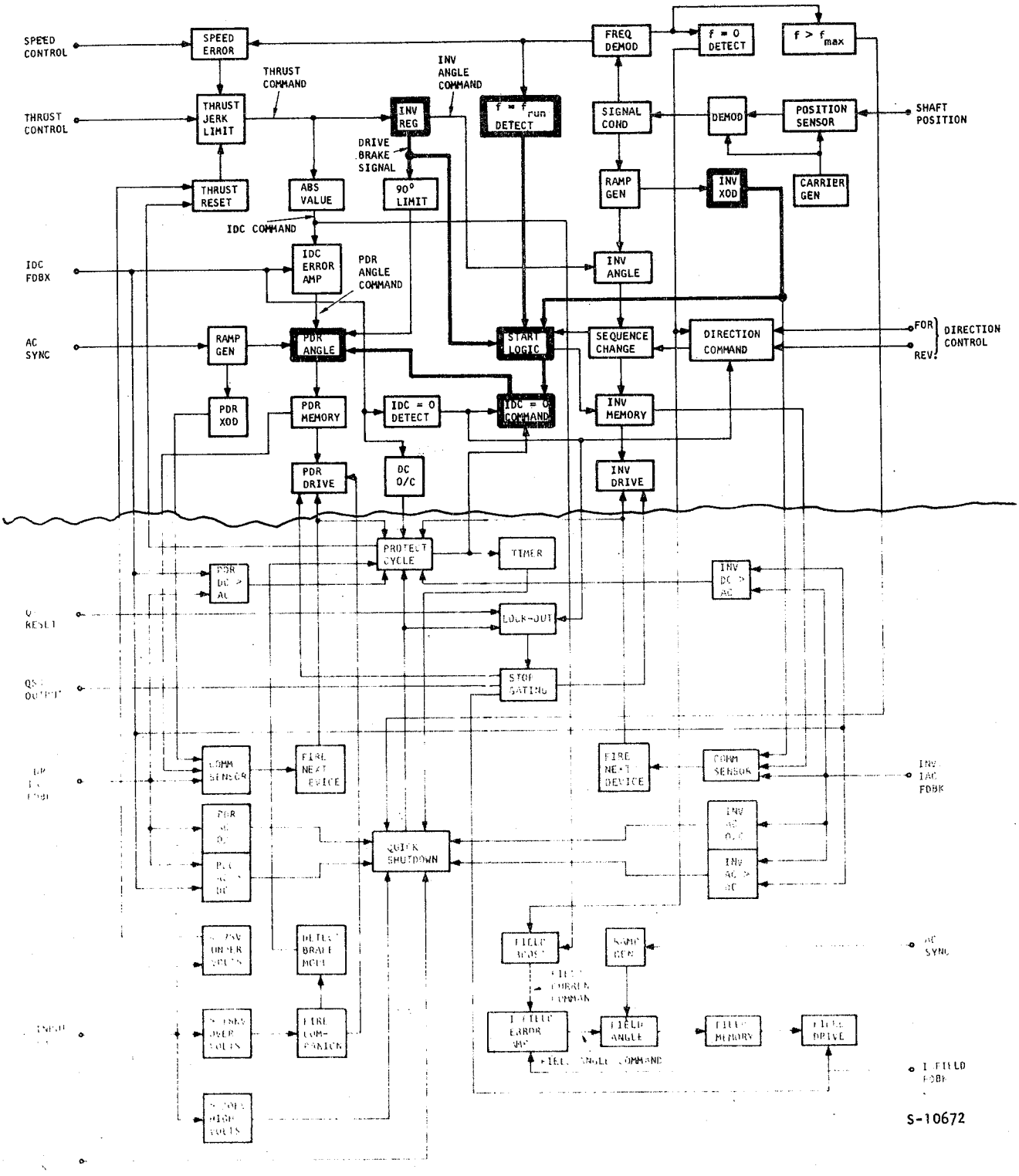

Figure 9-1. Start Mode Control Logic Block Diagram

this receives its input from the synchronous condenser rotor position sensor and commands the dc link current to zero level at the end of every 60-deg rotor position interval. In response to this command the PDR firing angle is driven into the fourth quadrant, to force the dc line current to zero as quickly as possible. After about a 5-ms interval, dictated by the control circuit response, the next set of thyristors is turned on, thereby producing 120-deg displaced three-phase symmetrical inverter current waveshapes. Table 9-1 lists the inverter thyristor firing sequence. Figure 9-2 shows how the inverter commutation takes place as well as the relation of the current pulses through the six inverter legs relative to the rotor position.

Since in the start mode the inverter is not line-commutated by the synchronous condenser, no commutation margin is required. Firing of the thyristors can therefore, be initiated in such a way that the voltage and current at the inverter terminals are 180 deg out of phase and the corresponding displacement factor is unity (see Figure 9-3). However, since thyristor firing in the

TABLE 9-1

INVERTER FIRING ORDER

Thyristor Turn-on Time*	Positive Inverter Leg	Negative Inverter Leg
T_1	+A	-B
T_2	+A	-C
T_3	+B	-C
T_4	+B	-A
T_5	+C	-A
T_6	+C	-B

*See Figure 9-2.

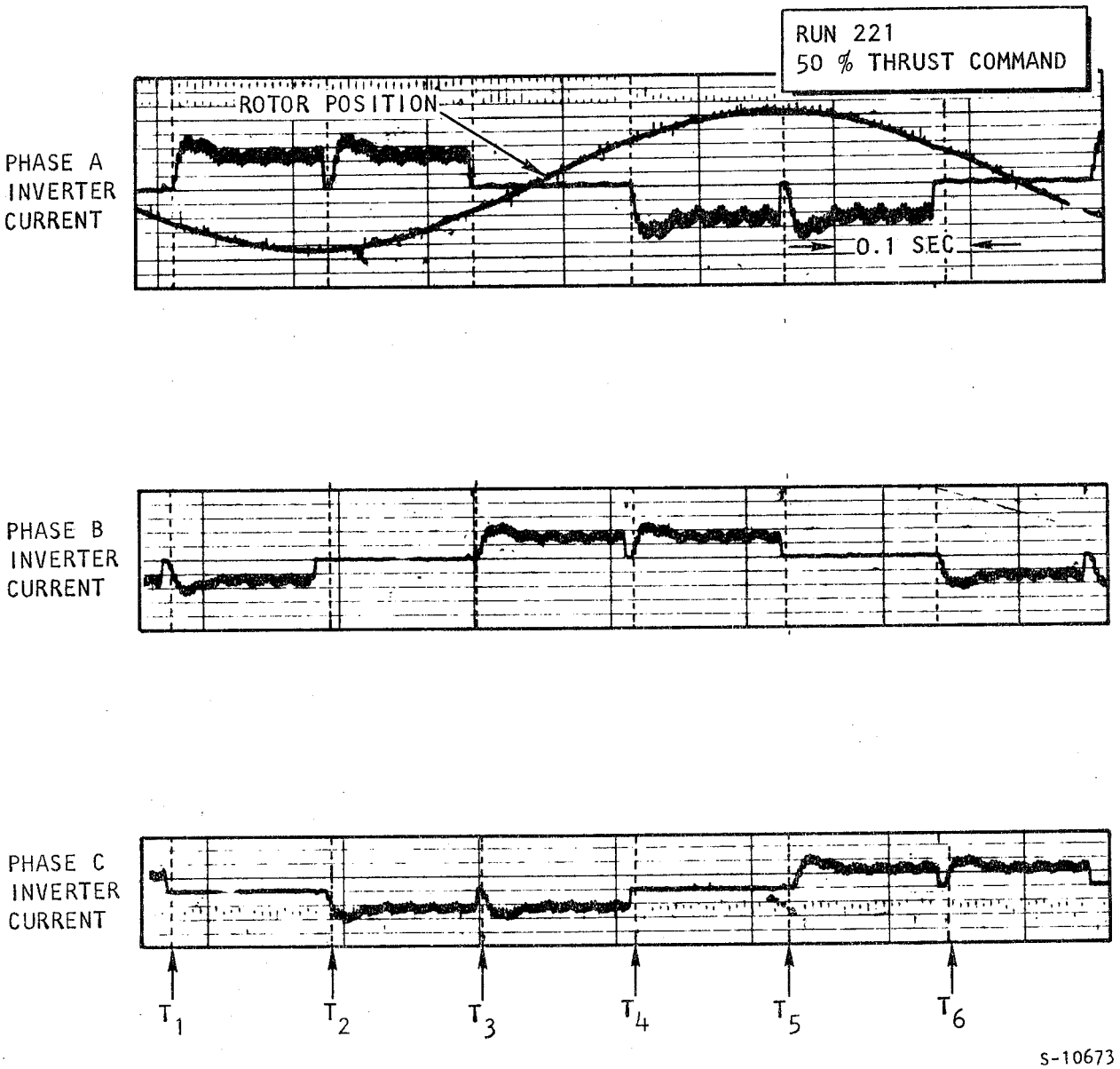

Figure 9-2. Inverter Commutation, Pulsed Mode

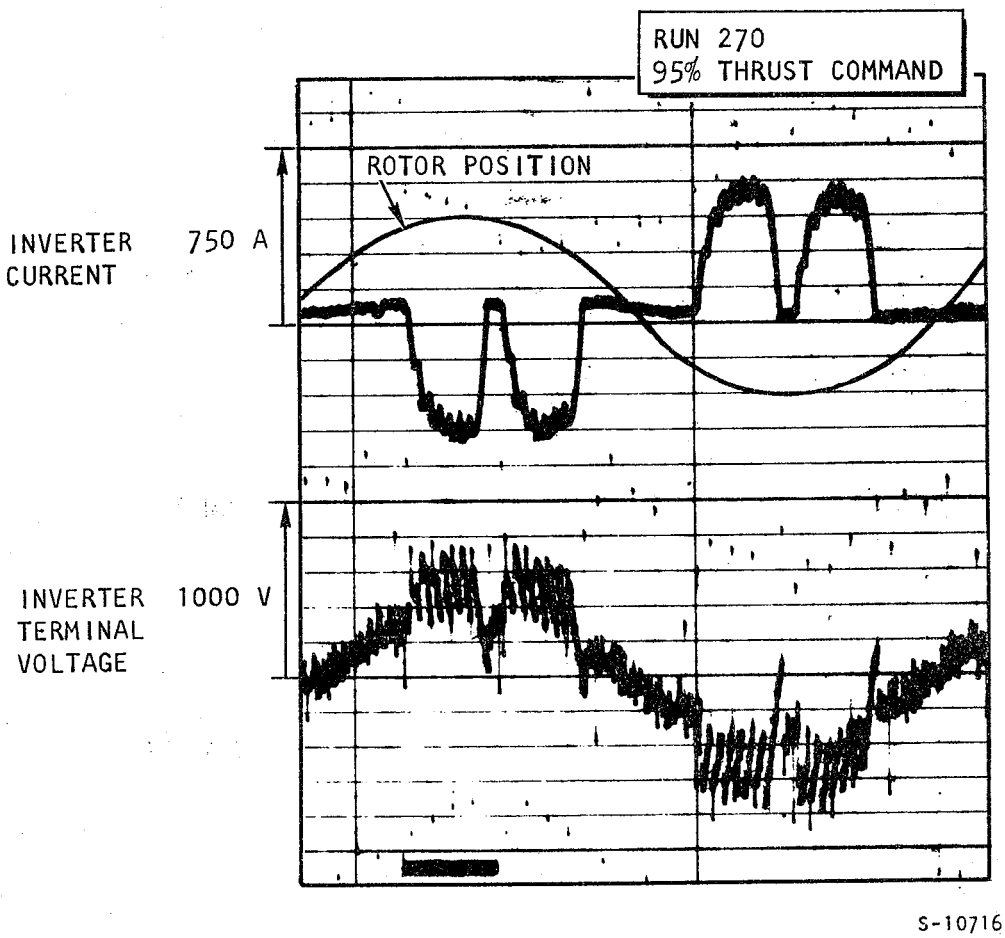

Figure 9-3. Inverter Voltage and Current Phase Relation during Start Mode

LIMPS is referenced with respect to the synchronous condenser rotor position rather than the inverter terminal voltage, and since in the starting mode there is about a 10-deg phase shift between these two quantities, the actual displacement factor is only 0.98, just slightly less than the ideal (unity) value.

For maximum real power transfer through the dc link, the ideal dc current should be constant at a given operating point. However, due to the control loop response time, the actual dc link current waveshape, Figure 9-4, differs markedly from its ideal form. Figure 9-4 shows that for a 470-Adc link current command and at 6.5 Hz, the current rise-time is about 6 ms, the corresponding fall-time is 3 ms, and the dwell-time between commutation is 5 ms. The corresponding average dc link current is only 65 percent of the peak dc link current.

As stated above, the command that corresponds to the conditions illustrated in Figure 9-4 called for a 470-Adc current. The average dc link current, based on evaluation of the actual current waveshape, is 460 A, which indicates that the commanded level was attained. However, in case of a higher current command, which would require the real dc link peak current value to exceed 1100 A, the protection feature of the control system would limit the current at the 1100-A level, thereby preventing attainment of the commanded dc link value. No system performance data was taken in this latter region.

Pulsed-Mode Performance

The pulsed-mode performance of the LIMPS is shown for two typical operating conditions in Figures 9-5 and 9-6, corresponding to 50-percent and 90-percent thrust commands, respectively. In the first case the real power transferred through the dc link is insufficient to accelerate the rotor of the synchronous condenser to a value required for the transition to the run mode. In the second case transition is about to occur.

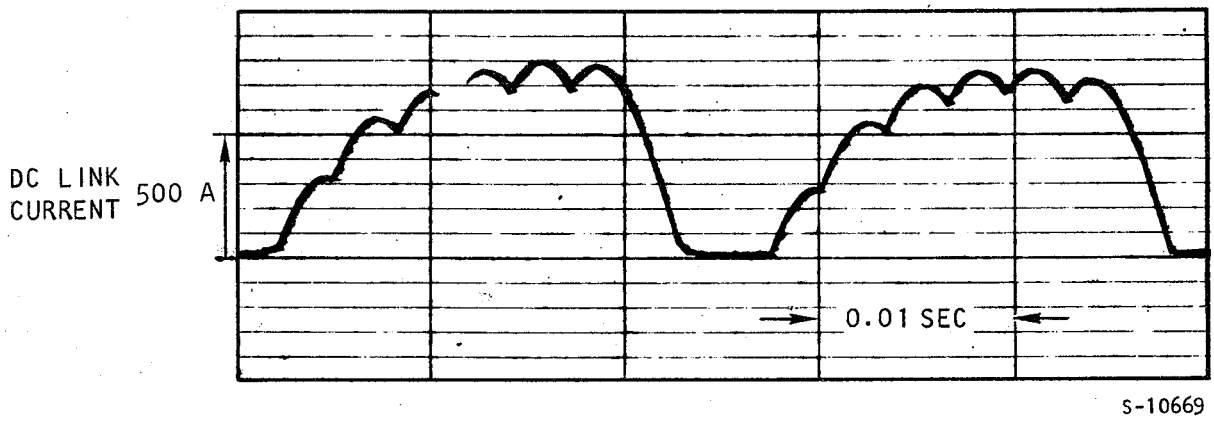

Figure 9-4. Dc Link Current Waveshape, Pulsed Mode

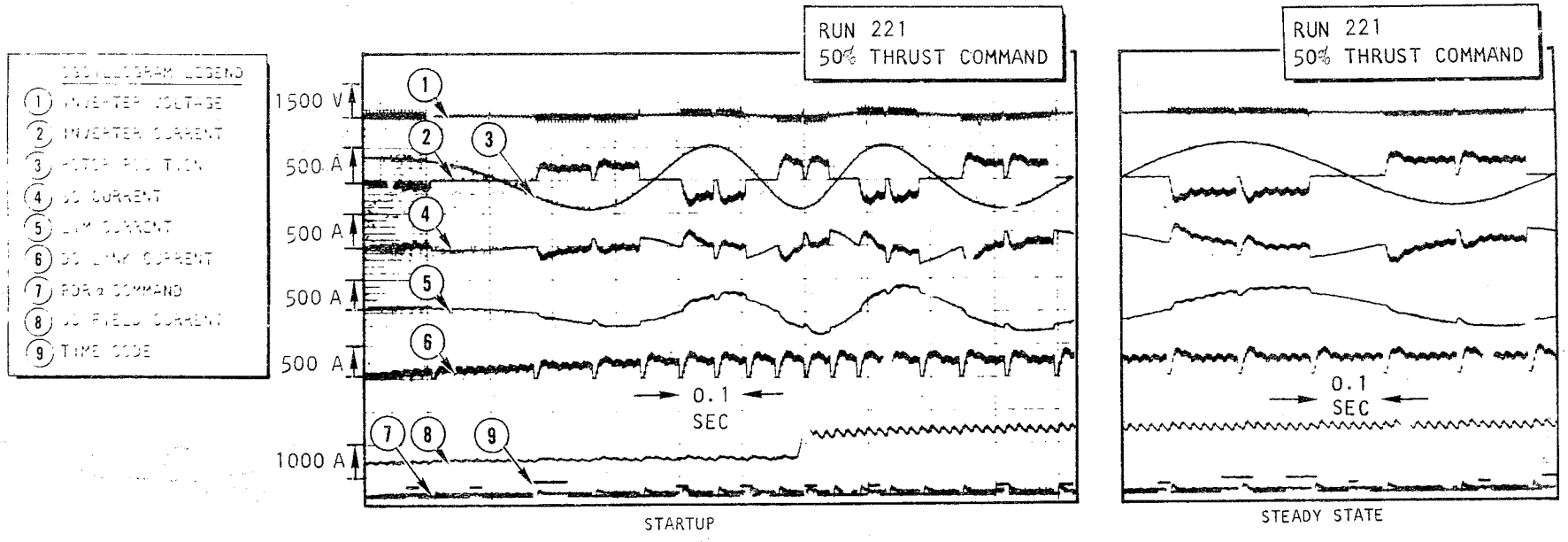

(a) OSCILLOGRAMS

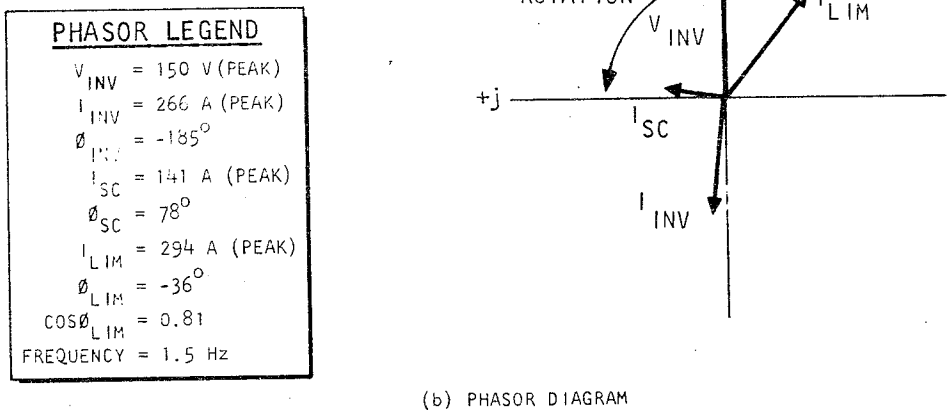

(b) PHASOR DIAGRAM

	INV	SC	LIM
(P) REAL POWER (kW)	59.2	6.3	53.5
(Q) REACTIVE POWER (kVAR)	5.2	30.1	38.9
(S) APPARENT POWER (kVA)	59.8	31.7	66.1

(c) POWER BALANCE TABLE

S-10670

Figure 9-5. Pulsed-Mode Performance Data, 50-Percent Thrust Command

OSCILLOGRAM LEGEND

1. INVERTER VOLTAGE
2. INVERTER CURRENT (X-1)
3. ROTOR POSITION
4. SC CURRENT
5. LIM CURRENT
6. DC LINK CURRENT
7. PDR α COMMAND
8. SC FIELD CURRENT
9. TIME CODE

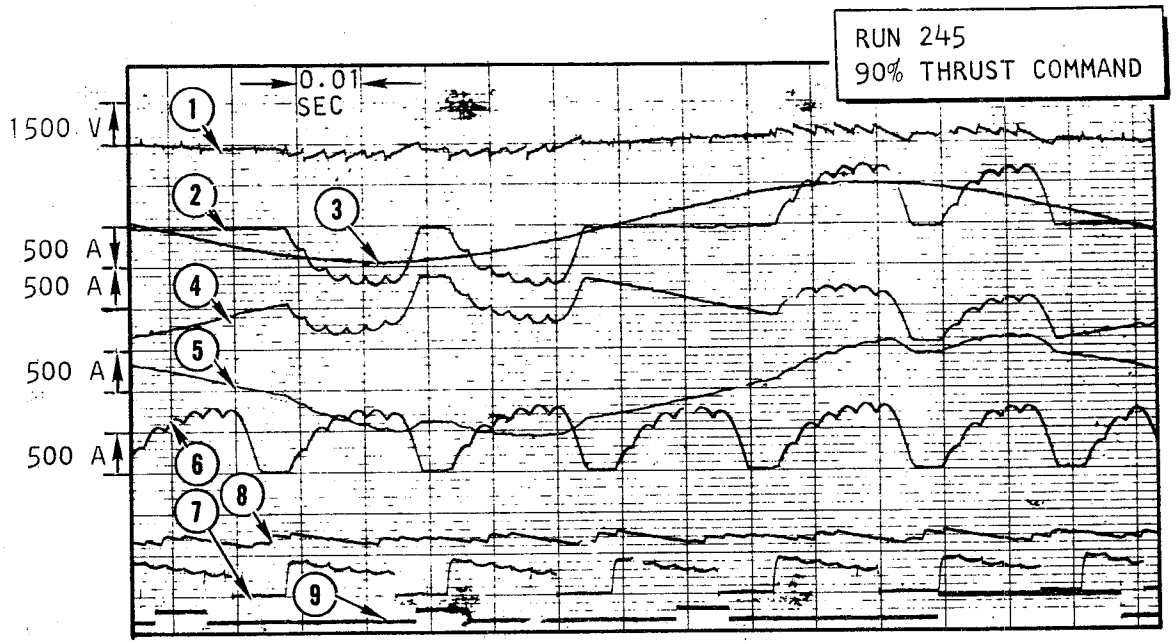

(a) OSCILLOGRAM

PHASOR LEGEND

V_{INV}	= 420 V (PEAK)
I_{INV}	= 464 A (PEAK)
ϕ_{INV}	= -193°
I_{SC}	= 170 A (PEAK)
ϕ_{SC}	= 89°
I_{LIM}	= 542 A (PEAK)
ϕ_{LIM}	= -34°
$\cos\phi_{LIM}$	= 0.83
FREQUENCY	= 6.6 Hz

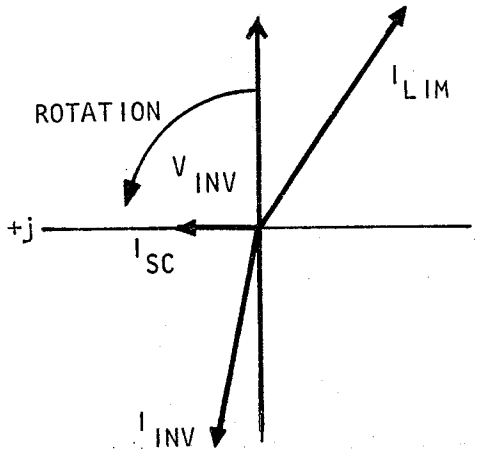

(b) PHASOR DIAGRAM

	LIM	SC	INV
(P) REAL POWER (kW)	283.0	1.9	285.0
(Q) REACTIVE POWER (kVAR)	191.0	107.0	65.8
(S) APPARENT POWER (kVA)	341.0	107.0	292.0

(c) POWER BALANCE TABLE

S-10667

Figure 9-6. Pulsed-Mode Performance Data, 90-Percent Thrust Command

The oscillogram in Figure 9-5(a) was used to generate the phasor diagram shown in Figure 9-5(b), which indicated the voltage and current relationship at the inverter terminal, at a given operating point. The phasor diagram is based on the fundamental components of the voltage and current waveshapes. The real and reactive power flow at the inverter terminals for the corresponding load condition is also given, in Figure 9-5(c). All real power is supplied from the dc link by the inverter, while both the inverter and the synchronous condenser are sources of reactive power. Since the electrical frequency is very low, f = 1.5 Hz, the LIM power factor is relatively high, about 80 percent, because the resistive components still dominate. The real power supplied to the synchronous condenser is required to make up for the copper losses (4.1 kW) and the mechanical losses (2.2 kW). Since the frequency remains constant, no real power is used to change the kinetic energy of the synchronous condenser rotor.

Using the positive reference directions indicated in Figure 9-5, it can be seen that the inverter current is indeed 180 deg out of phase with the rotor position, which in turn slightly lags the terminal voltage.

Similar analysis applies to the case presented in Figure 9-6.

Finally, the power distribution throughout the system can be illustrated with the power flow diagram, given in Figure 9-7. The operating conditions correspond to those of Figure 9-5. It should be pointed out that the electrical frequency under these conditions is less than 1 percent of the rated value for which the LIMPS was designed. Therefore, the overall system efficiency is not indicative of the system capabilities at higher frequencies and power levels. The information presented in Figure 9-7 is also summarized in tabular form in Table 9-2.

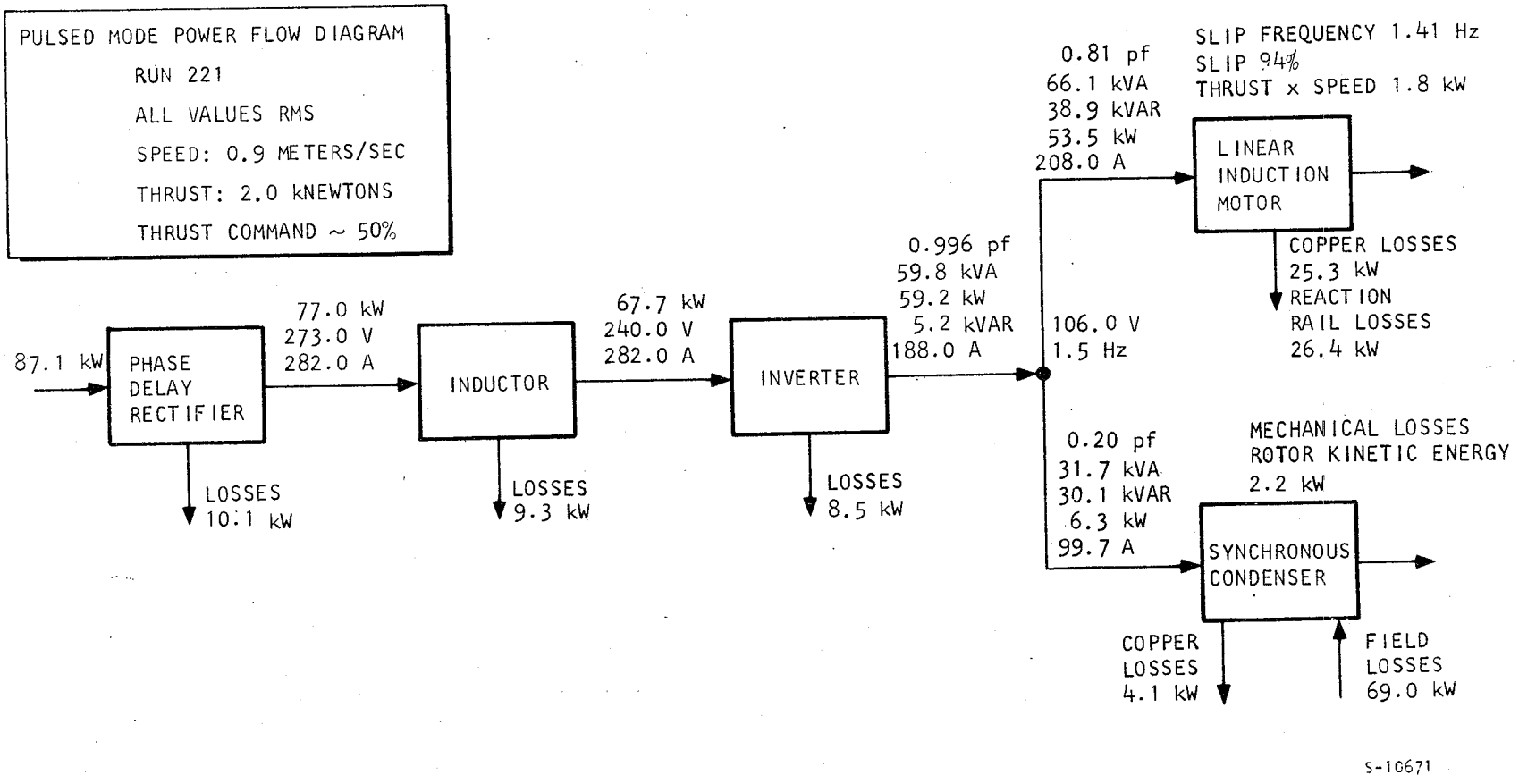

Figure 9-7. LIMPS Power Flow Diagram, Pulsed Mode

TABLE 9-2

POWER ANALYSIS
(RUN 221, THRUST COMMAND 50 PERCENT)

Component or System	Real Input Power, kW	Real Output Power, kW	Losses, kW	Efficiency, Percent	Reactive Power, kVAR
Phase delay rectifier	87.1	77.0	10.1	88.0	X
High-voltage inductor	77.0	67.7	9.3	88.0	X
Inverter	67.7	59.2	8.5	87.0	5.2
Synchronous condenser	6.3	2.2	4.1	35.0	30.1
LIM	53.5	1.8	51.7	3.4	38.9
LIMPS	87.1	1.8	85.3	2.1	X

Synchronous Condenser Filtering Capability

The current harmonics generated by the thyristor switching in the inverter are absorbed primarily by the synchronous condenser. Figure 9-8(a) shows the inverter, LIM, and synchronous condenser current waveshapes under pulsed-mode conditions. Figures 9-8(b), (c), and (d) illustrate the current harmonic content in each component by means of frequency spectrum bar graphs.

The inverter current generates strong $n = kp \pm 1$ order current harmonics, where n is the order of the harmonics, $p = 6$ for the full-wave bridge connected converter, and k is an integer. This relationship applies exactly for the ideal waveshape, and closely approximates the experimental data.

The ideal LIM current is sinusoidal, and the test data establishes that the harmonic content of the LIM current is indeed very small.

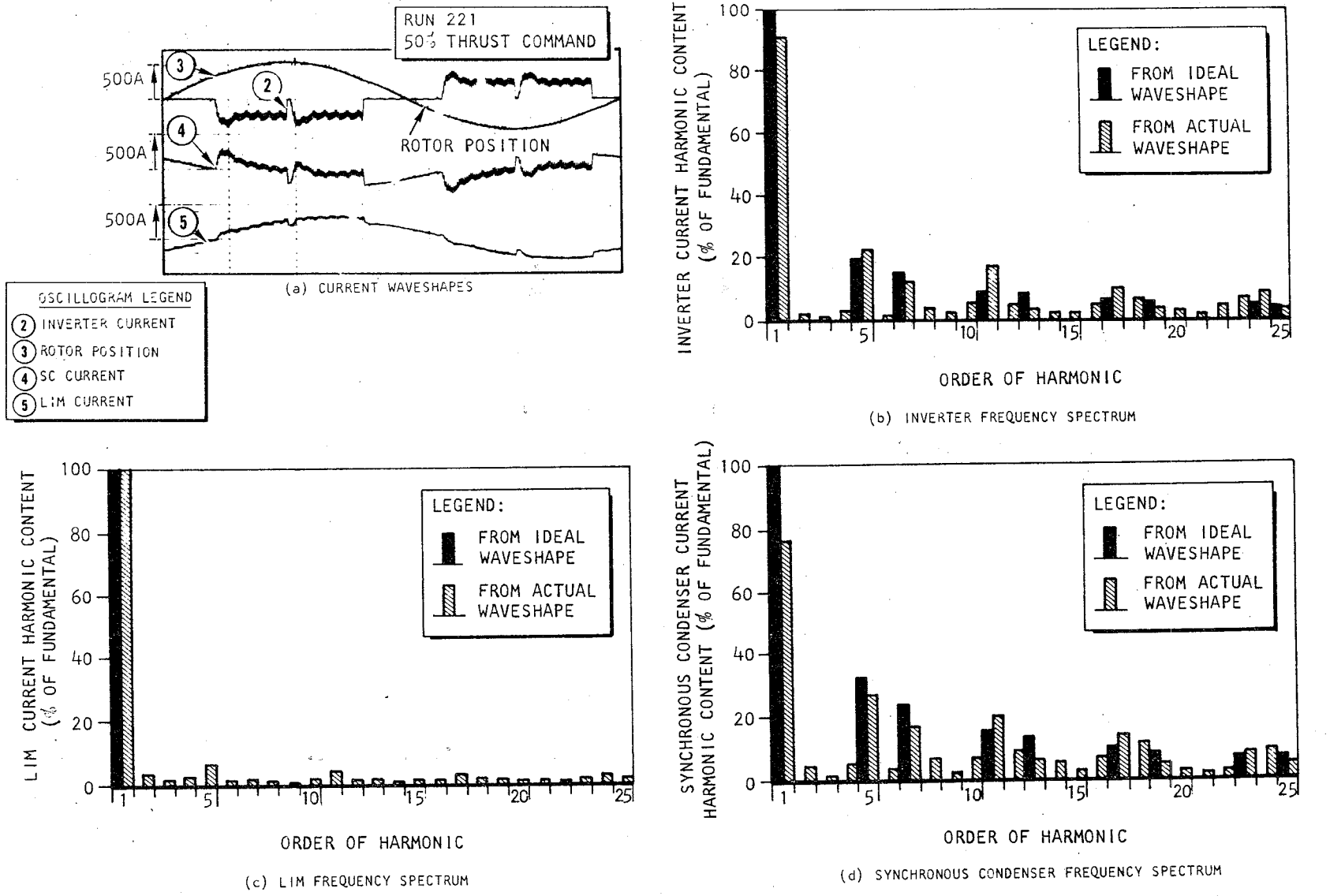

NOTE: ALL HARMONICS ARE EXPRESSED AS % OF FUNDAMENTAL OF IDEAL WAVESHAPE

S-10666

Figure 9-8. Synchronous Condenser Filtering Capability, Pulsed Mode

The major portion of the current harmonics is absorbed by the synchronous condenser because of the low-impedance path provided by the damper winding. Table 9-3 indicates that a substantial portion of a given current harmonic generated by the inverter is absorbed by the synchronous condenser as illustrated by the relatively low harmonic content of the LIM current. The results demonstrate the filtering effectiveness of the synchronous condenser.

Starting Time

Because of the rapid thrust buildup the starting mode does not limit the LIMPS performance. Figure 9-9 indicates that from the time the thrust command is applied until the 90-percent full-thrust level is attained requires about 1.6 s. Also shown is the start mode response of the LIMPS from standstill to the point of transition to the run mode. The rate of dc link current buildup is limited only by the 1.5-s (adjustable) jerk limit designed into the control circuit.

TABLE 9-3

PULSED-MODE HARMONIC CONTENT (RUN 221, THRUST COMMAND 50 PERCENT, FREQUENCY 1.5 Hz)

Order of Harmonic	Inverter Current	LIM Current	Synchronous Condenser Current
1	100.0	100.0	100.0
2	2.8	2.5	5.3
3	1.1	1.0	1.3
4	3.9	2.0	6.6
5	25.3	3.0	34.2
6	2.2	1.0	4.0
7	14.3	1.5	21.0
8	3.3	0.5	7.9
9	2.2	0.3	2.6
10	5.5	1.2	7.9
11	18.7	4.0	25.0
12	5.5	1.3	10.5
13	3.8	1.2	6.6
14	2.7	0.4	6.6
15	2.2	1.0	1.3
16	2.7	1.0	7.9
17	11.0	1.0	17.1
18	7.1	1.2	13.2
19	3.8	1.2	6.6
20	3.3	0.7	2.6
21	1.6	1.0	1.3
22	4.9	0.3	2.6
23	7.1	0.8	10.5
24	9.3	2.5	11.8
25	3.8	1.1	5.3

NOTES: 1. Harmonic content given as percent of actual fundamental specified current.

2. Bold typeface numbers denote harmonics of principal interest.

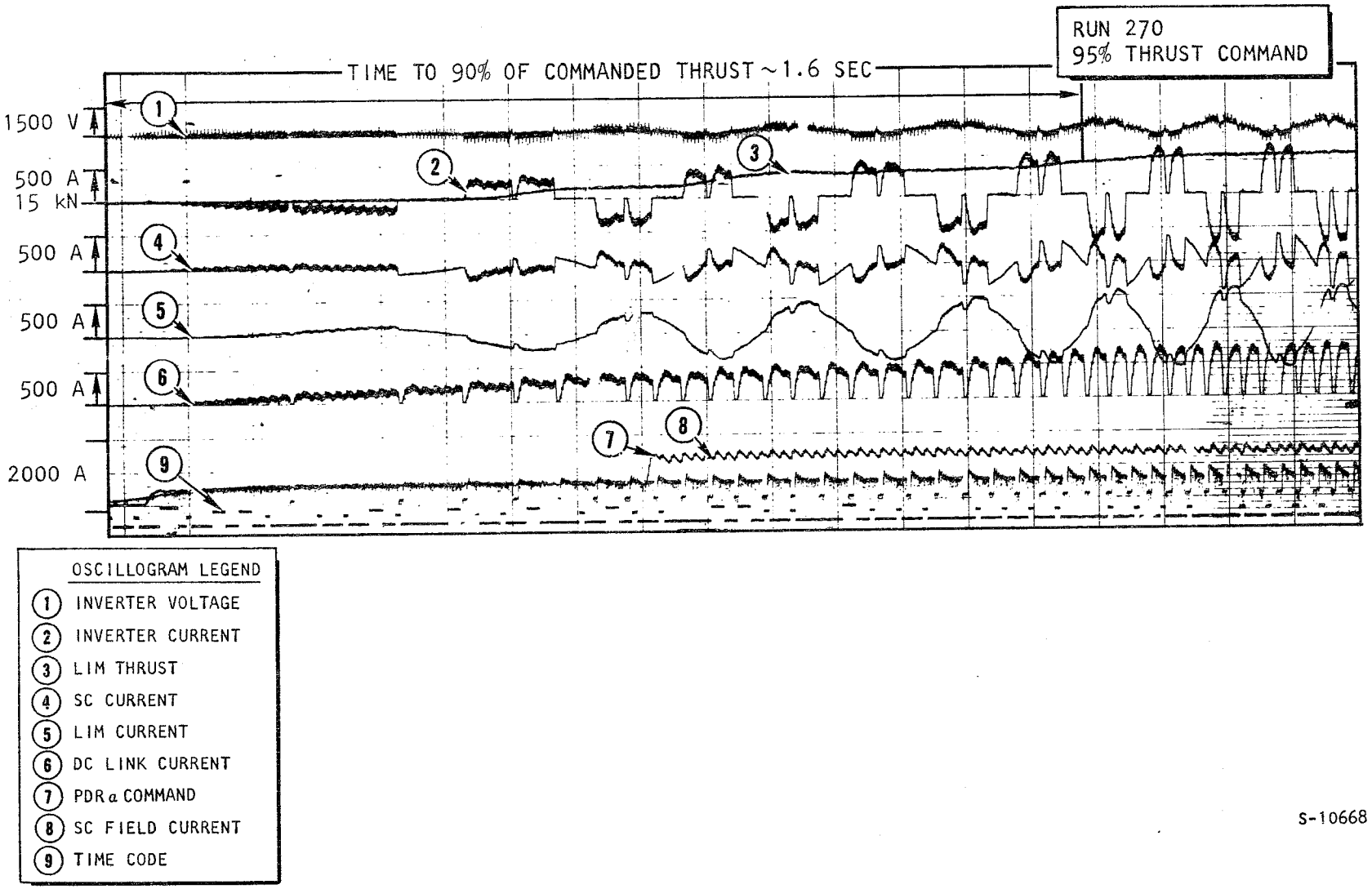

Figure 9-9. LIMPS Dynamic Response During Start Mode

START-TO-RUN-MODE TRANSITION TESTS

As the synchronous condenser frequency attains a preset value, nominally f_T = 6 Hz, the so-called start-to-run-mode transition is initiated by the control system. The transition process includes (1) a final zero dc link current command under the start mode regime (i.e., clearing the dc link by current quenching from the phase delay rectifier end), and (2) the retardation of the firing angle from 180 to 150 deg. As thyristor gating is reapplied the inverter continues to operate, but now in the line-commutated mode.

Successful Transition

Figure 9-10 illustrates how a successful transition takes place. At the instant t_T, indicated also by the abrupt change in the mode-monitor signal trace, the dc link current is commanded for the last time to a zero-current level. As the thyristor gating is reapplied, the firing delay angle is advanced by 30 deg, as shown.

The conditions just after transition can be best examined with reference to the phasor diagram, which represents the fundamental components of the inverter, LIM, and synchronous condenser currents, and the corresponding terminal voltage. The transition frequency is f_T = 6.8 Hz, and the thrust commanded is about 90 percent. The power conditions are also shown. The reactive power requirement is 0.60 kVAR/kW.

The conditions under which run-to-start-mode transition occurred in a consistent, reliable manner are listed in Table 9-4.

Effects Encountered during Transition Tests

The following paragraphs discuse several of the effects observed during transition tests.

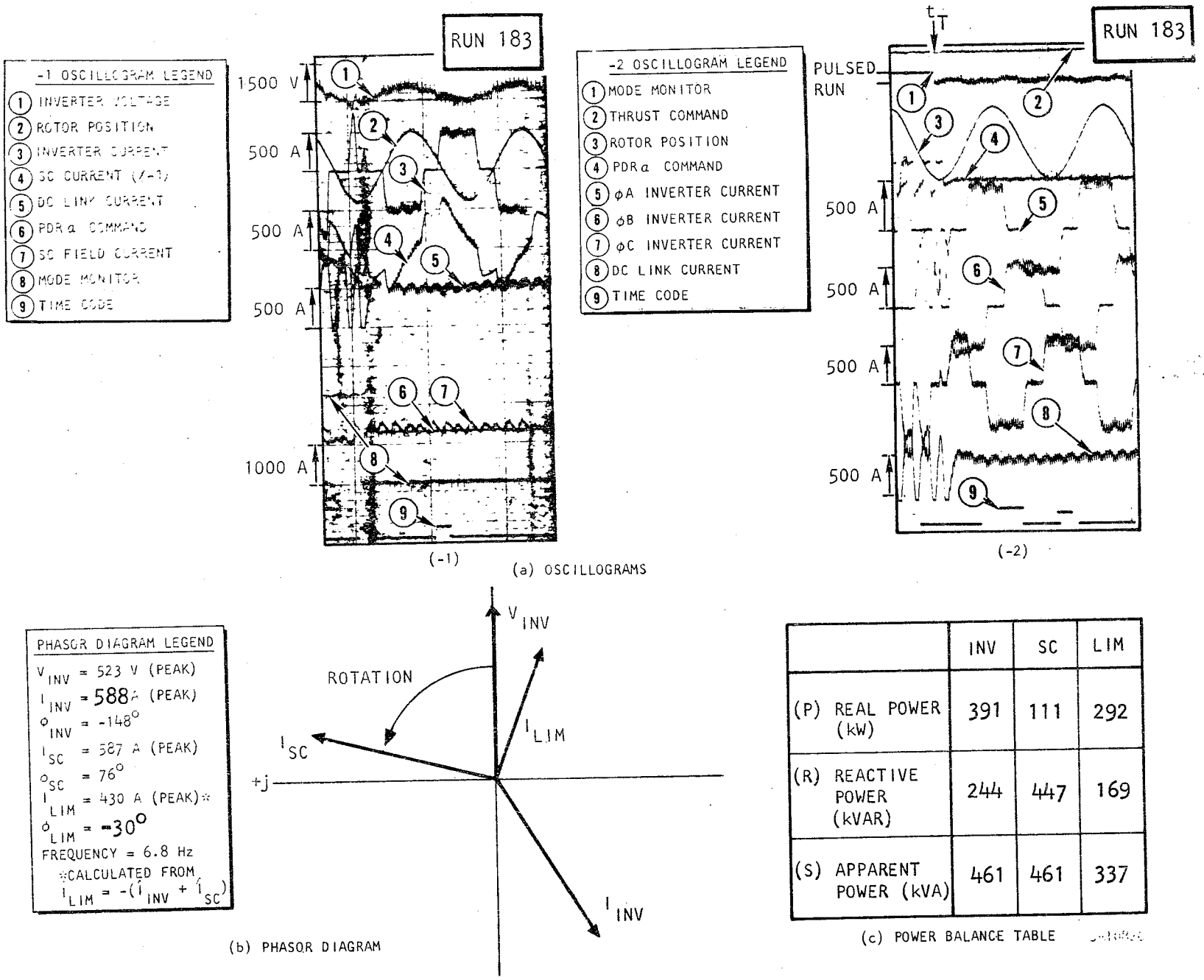

	INV	SC	LIM
(P) REAL POWER (kW)	391	111	292
(R) REACTIVE POWER (kVAR)	244	447	169
(S) APPARENT POWER (kVA)	461	461	337

(c) POWER BALANCE TABLE

Figure 9-10. Start-to-Run-Mode Transition Performance Data

TABLE 9-4

LIMPS RUN-TO-START-MODE TRANSITION CRITERIA

Electrical frequency	≥6.5 Hz
Thrust command	≥60 percent
Synchronous condenser field current	≥1300 A
LIM airgap	≤3.81 cm

1. Insufficient Synchronous Condenser Speed

In Figure 9-5, because the thrust command was only set to a 50-percent value the synchronous condenser did not attain the transition frequency, and therefore transition was not achieved. The vehicle was traveling at a steady 1 m/s speed. The synchronous condenser field current was 1400 A.

2. LIM Propulsion System Reversion to Pulsed Mode

As soon as the electrical frequency falls below f'_T = 4.0 Hz (equivalent to a synchronous condenser speed of 13.1 rad/s (125 rpm)), the LIM propulsion system reverts to the pulsed mode. This normal operating condition is illustrated in Figure 9-11.

3. Transition Followed by Commutation Failure and Quick Shutdown

Figure 9-12 shows an operating run where just after transition a commutation failure occured. The A-leg of the inverter failed to commutate after its first current pulse. As soon as the commutative failure was sensed by the LIM propulsion system control circuit, a quick shutdown was initiated. The synchronous condenser field current was 1400 A, and the thrust commanded was approximately 60 percent. The transition frequency was set to about 6.0 Hz, which is insufficient for line commutation.

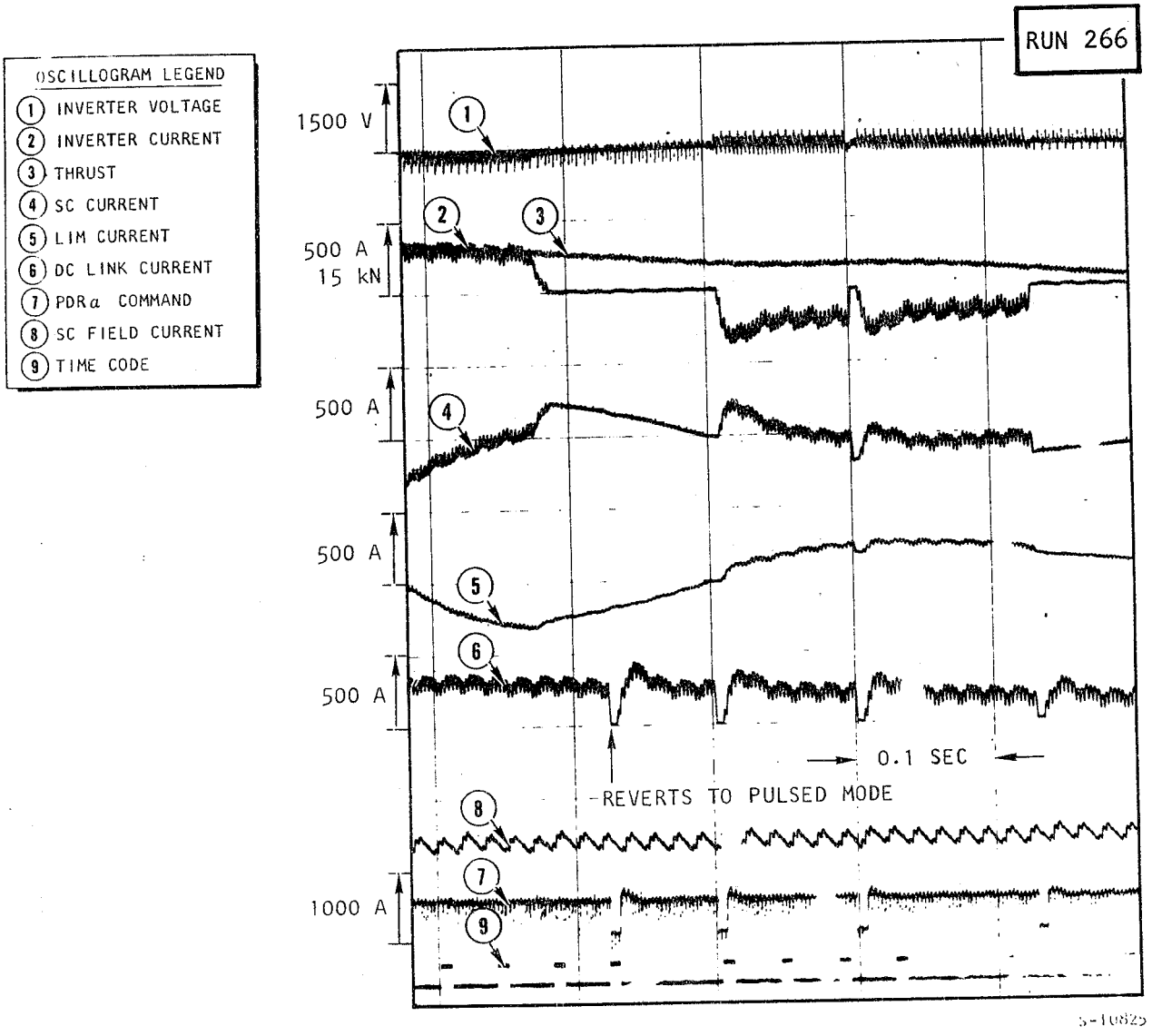

Figure 9-11. Reversion-to-Pulsed-Mode Performance Data

OSCILLOGRAM LEGEND

1. INVERTER VOLTAGE
2. INVERTER CURRENT
3. ROTOR POSITION
4. SC CURRENT
5. LIM CURRENT
6. DC LINK CURRENT
7. PDR a COMMAND
8. SC FIELD CURRENT
9. TIME CODE

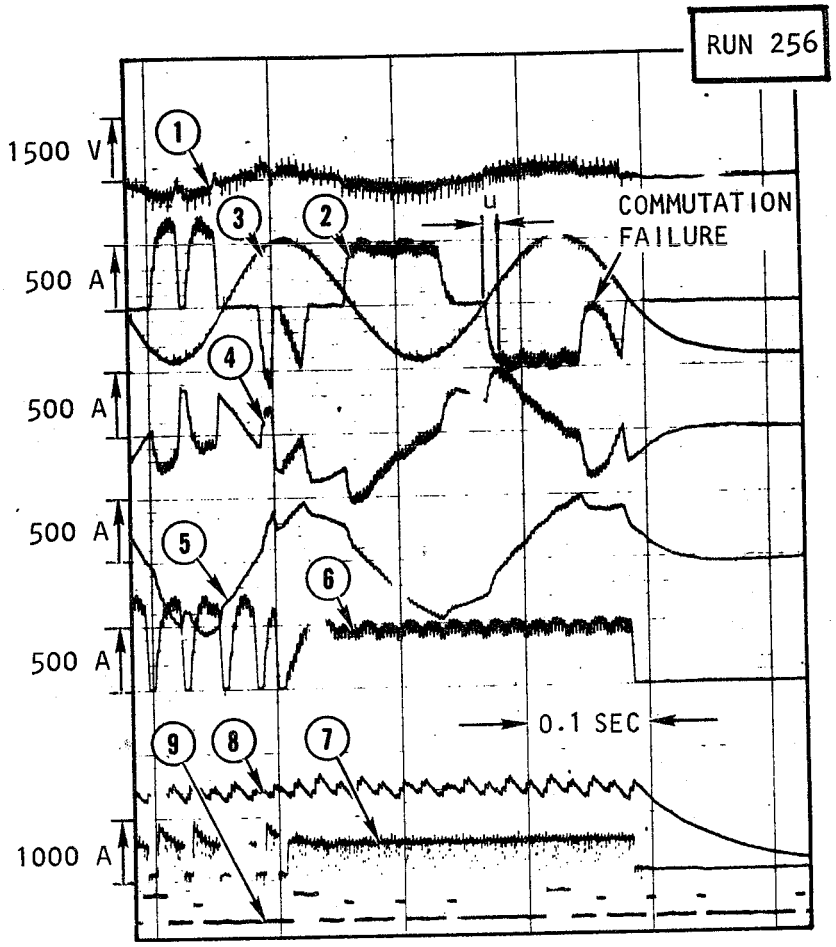

(a) OSCILLOGRAM

PHASOR DIAGRAM LEGEND

V_{INV} = 300 V (PEAK)
I_{INV} = 529 A (PEAK)
ϕ_{INV} = 170°
I_{SC} = 405 A (PEAK)
ϕ_{SC} = 66.4°
I_{LIM} = 450 A (PEAK)
ϕ_{LIM} = - 30°
FREQUENCY = 5.67 Hz
ϕ_{RP} = -14.9°
u = 17.5°

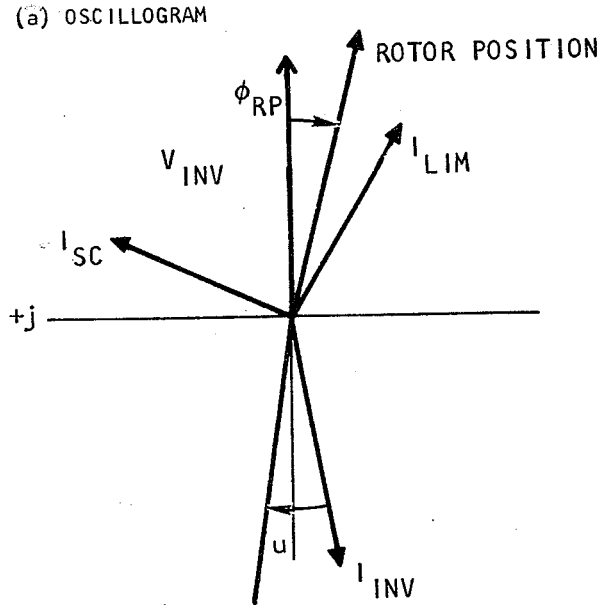

S-10823

(b) PHASOR DIAGRAM

Figure 9-12. Commutation-Failure-after-Transition Performance Data

Figure 9-12 also points out that using the synchronous condenser rotor position as the inverter thyristor gating reference signal may not be fully desirable. The problem is discussed in some detail below, with reference to the phasor diagram in Figure 9-12(b).

4. Inverter Firing with Respect to the Synchronous Condenser Rotor Position

The gate firing signals for the inverter thyristors are derived from the rotor shaft position sensor. The constant-amplitude, sinusoidal output of this sensor represents a signal that is in phase with the no-load emf of the synchronous machine. Thus the thyristor firing delay angle is measured with respect to the no-load voltage. It is shown, below, that the so-called voltage behind the subtransient reactance--rather than the no-load voltage--should be used as a reference signal for firing the inverter thyristors.

During commutation two of the three positive or negative terminals of the inverter are momentarily short circuited. Since commutation occurs at the rate of six times the frequency of the inverter, the LIM and synchronous condenser are constantly in a transient state. Under such repeated transient conditions the main field of the machines cannot collapse, and only the flux associated with the leakage paths can vary. This is in agreement with the well known principle of constant flux linkages.

Since the main flux of the machines is essentially unaffected by such rapidly changing load conditions, the overlap and the dc link voltage of the inverter are governed by the leakage field characteristics of the two ac machines. Therefore, in terms of the customary single-phase representation, reactance X_d'', the subtransient (or commutation) reactance of the machines, and V_d'', which represents the voltage behind the subtransient reactance, govern the line commutation process. The significance of V_d'' is that its

line-to-line value is the voltage that circulates the commutating currents between phases. In a fourth quadrant operation (i.e., in the inverter mode) commutation must be completed before this commutating voltage changes its polarity; otherwise a commutation failure occurs.

Generally, the no-load voltage and the voltage behind the subtransient reactance are not in phase. The relationship between these two voltages is a function of the load. Therefore the shaft position sensor output alone cannot provide information on the phase relationship of the commutating voltage. For example, for the case shown in Figure 9-12(b), the firing of the inverter thyristors is delayed by 150 deg with respect to the no-load voltage. However, in reference to V''_d (the true commutating voltage), the firing delay is actually 10 deg more. Thus, rather than having a 30-deg interval for overlap and device turnoff time, only 20 deg are available for the same functions. This means that the maximum inverter load that can be safely commutated by the synchronous condenser is appreciably reduced.

The problem is particularly noticeable at the two extremes of the operating range:

Low speed--Synchronous condenser copper losses are appreciable compared to the total apparent power, and therefore, the power factor differs from the ideal $\cos\phi = 0$ value for the synchronous condenser. As a result, the inverter load angle (i.e., the phase difference between V''_d and E) appears, which reduces the commutation margin as indicated above.

Very high speed--The thyristor turnoff time, about 200 μs, becomes an appreciable portion of the commutation margin. At 165 Hz rated frequency, this represents 12 electrical degrees.

RUN-MODE TESTS

This subsection presents the data acquired during the run mode tests, which covers the operating regimes when the synchronous condenser frequency exceeds a preset transition frequency, nominally f_T = 6.0 Hz, and the generated emf in the synchronous condenser becomes sufficiently high to assure reliable line commutation.

Because the available electrified guideway was only 500-m long, the test covered only the lower end of the power and speed range for which the propulsion system was designed, as indicated in Table 9-5.

TABLE 9-5

PARAMETERS WITH TEST RANGE LIMITED

Test Parameter	Run No.	Maximum Test Value	
		Actual Units	Percent of Rating
Inverter frequency	268	35.6 Hz	21.6
Dc link power	223	850 kW	14.1
Dc link voltage	223	1520 V	17.1

In terms of current and thrust, however, the propulsion system was tested at near-rated values, as indicated in Table 9-6.

The thrust commanded by the operator controls the dc link current according to the transfer function shown in Figure 9-13. The steady-state values obtained during the individual test runs are also shown.

Steady-State Performance

The steady-state performance of the propulsion system is described here with reference to its phasor diagram, derived from the oscillographic traces of the appropriate electrical quantities. As an illustration, results from

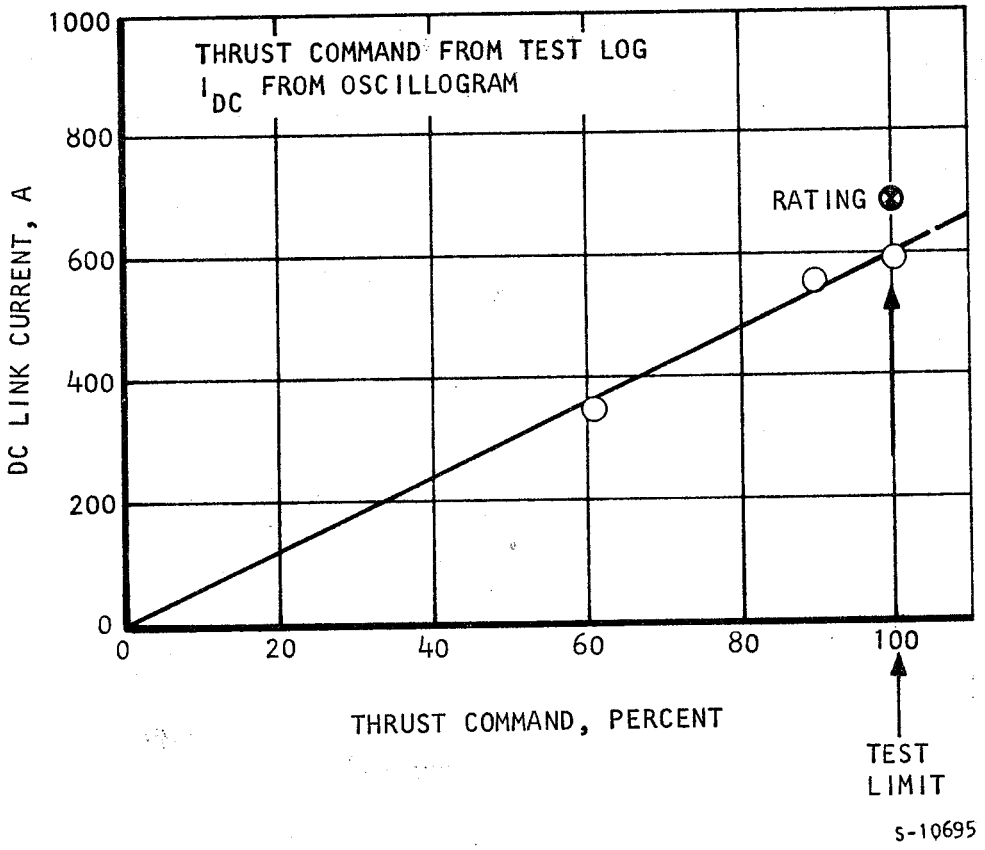

Figure 9-13. Thrust Command Transfer Function

TABLE 9-6

PARAMETERS WITH TEST RANGE NEAR RATED VALUES

Test Parameter	Run No.	Maximum Test Value	
		Actual Units	Percent of Rating
Dc link current	223	580 A	85.3
LIM current	245	424 A	80.0
Synchronous condenser current	245	477 A	84.4
Field current	271	1740 A	96.7
LIM thrust	245	20 kN	90.1

two operating points are shown here, representing the steady-state conditions at a high thrust command (Figure 9-14) and at a low thrust command (Figure 9-15), respectively.

The phasor diagrams also show the major difference between the start and the run mode. In the former mode of operation the inverter is commutated by quenching the dc link current by the PDR; in the latter the inverter is line-commutated by the synchronous condenser. Because of the line commutation process, to prevent commutation failure, sufficient commutation margin is required to allow for commutation overlap and thyristor turn-off time. Therefore, the inverter firing delay angle must be less than 180 deg; in fact during the performance tests the firing delay angle was set at a nominal 150 deg. In the phasor diagram the inverter current lags behind the terminal voltage by approximately 150 deg, since its phase relationship is also dictated by the inverter firing delay. The corresponding displacement factor is about 0.85, indicating that to operate the inverter in a line-commutated mode at a 30-deg commutation margin requires a sizable amount of reactive power. The synchronous condenser functions as such a source of reactive power. The

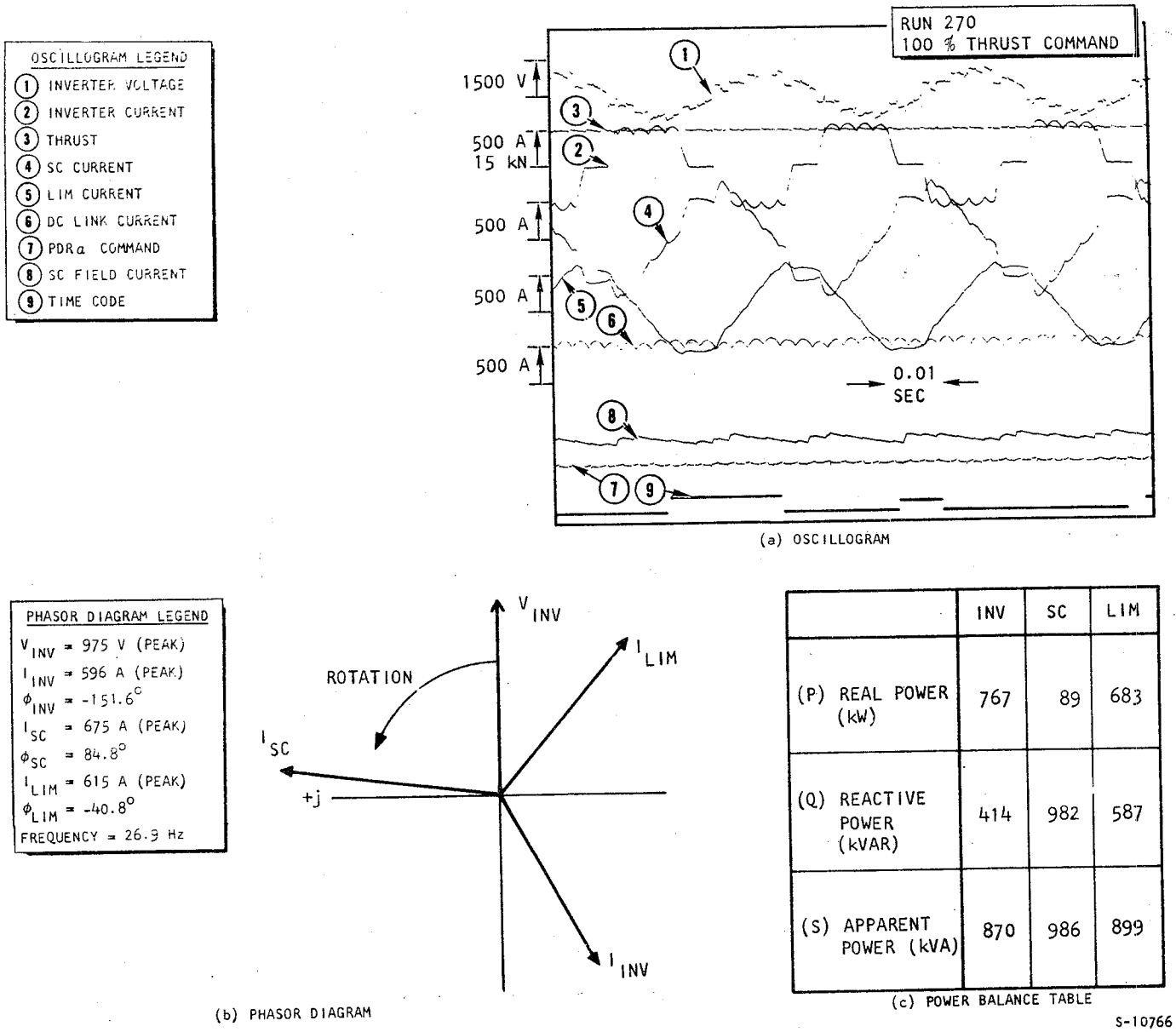

	INV	SC	LIM
(P) REAL POWER (kW)	767	89	683
(Q) REACTIVE POWER (kVAR)	414	982	587
(S) APPARENT POWER (kVA)	870	986	899

Figure 9-14. Run-Mode Steady-State Performance, 100-Percent Thrust Command

OSCILLOGRAM LEGEND

1. INVERTER VOLTAGE
2. INVERTER CURRENT
3. THRUST
4. SC CURRENT
5. LIM CURRENT
6. DC LINK CURRENT
7. PDRα COMMAND
8. SC FIELD CURRENT
9. TIME CODE

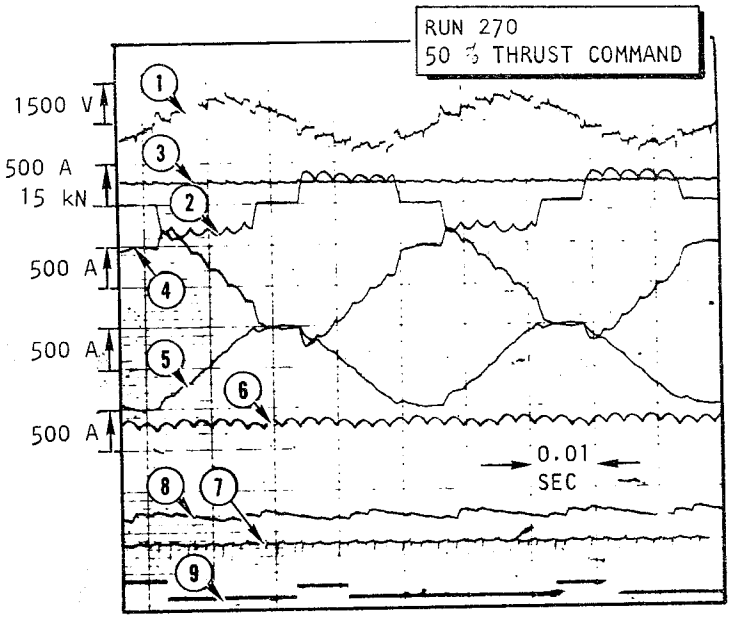

(a) OSCILLOGRAM

PHASOR DIAGRAM LEGEND

V_{INV} = 930 V (PEAK)
I_{INV} = 364 A (PEAK)
ϕ_{INV} = -153.6°
I_{SC} = 600 A (PEAK)
ϕ_{SC} = 82.6°
I_{LIM} = 500 A (PEAK)
ϕ_{LIM} = -59.9°
FREQUENCY = 22.7 Hz

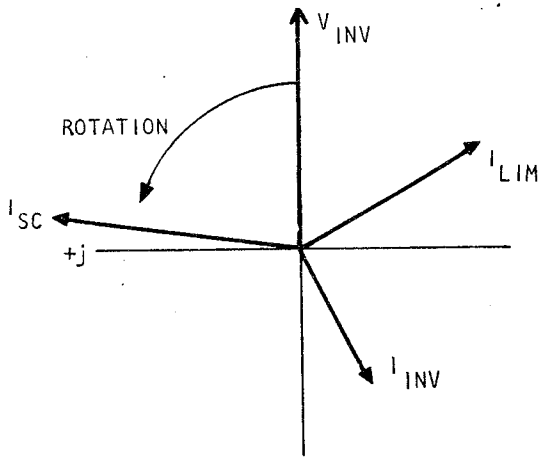

(b) PHASOR DIAGRAM

	LIM	SC	INV
(P) REAL POWER (kW)	350	108	455
(Q) REACTIVE POWER (kVAR)	605	830	225
(S) APPARENT POWER (kVA)	699	837	507

(c) POWER BALANCE TABLE

S-10767

Figure 9-15. Run-Mode Steady-State Performance, 50-Percent Thrust Command

tabulated real and reactive power balances at the inverter terminal, calculated in the two given operating conditions, also confirm the large, approximately 0.5 kVAR/kW, reactive power requirement of the inverter.

Since commutation overlap increases with increasing dc link current, the control circuit adjusted the inverter firing angle as a function of the dc link current, as shown in Figure 9-16.

The relationship between the normalized dc current and the overlap angle is shown in Figure 9-17, indicating good agreement between the calculated and test data.

Since the overlap angle observed during the performance tests with rated dc link current did not exceed 17 deg, the originally selected 30-deg commutation margin is required only at or near rated frequency, where the thyristor turn-off time becomes significant with respect to the overlap angle, as indicated in Table 9-7.

TABLE 9-7

INVERTER COMMUTATION MARGIN REQUIREMENTS

Frequency, Hz	Thyristor Turn-off		Overlap Angle, deg	Required Commutation Margin, deg
	µsec	deg		
15	200	1.08	17	18.08
60	200	4.32	17	21.32
120	200	8.64	17	25.64
165	200	11.88	17	28.88

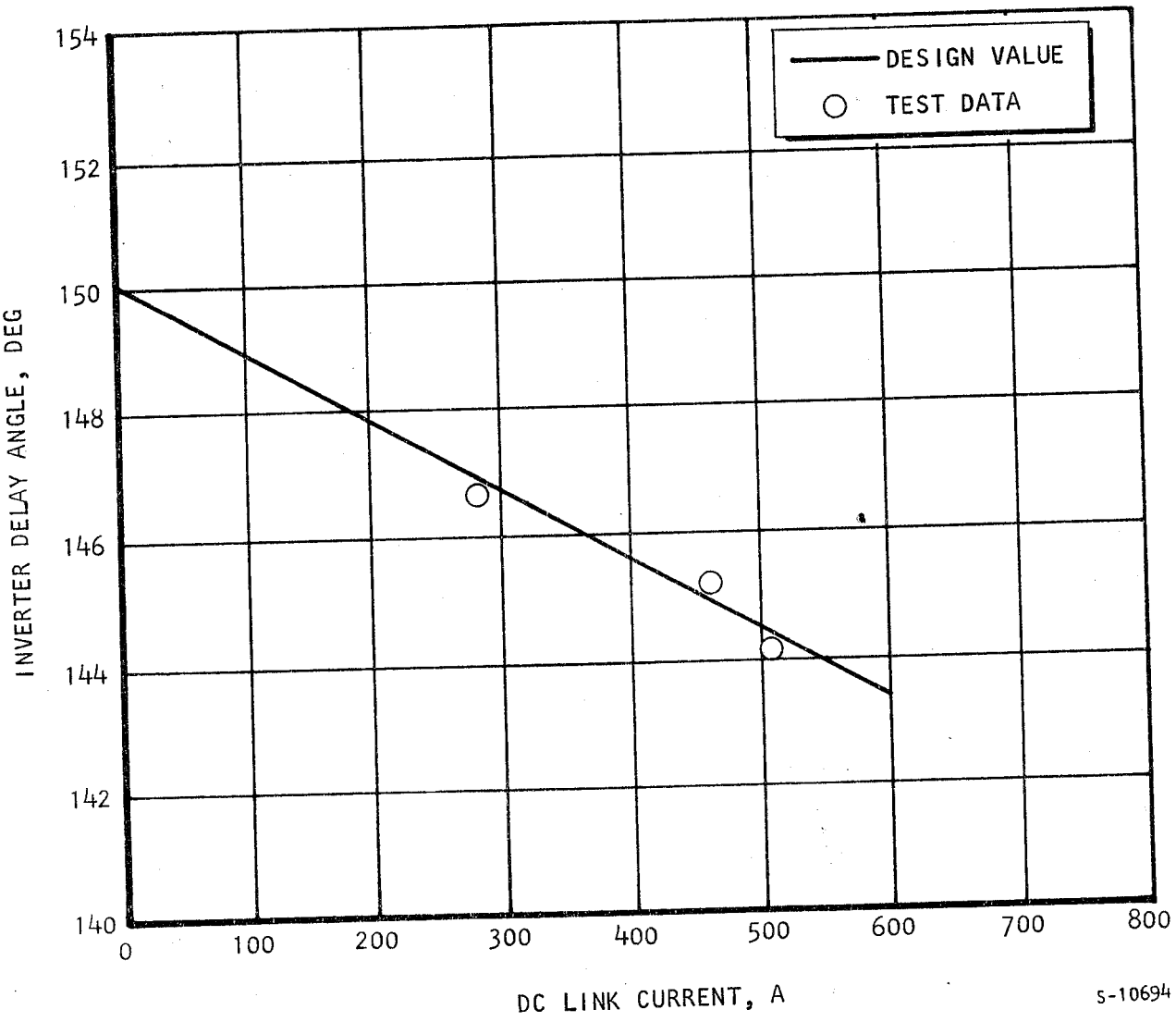

Figure 9-16. Inverter Delay Angle, Dc Link Current Transfer Function

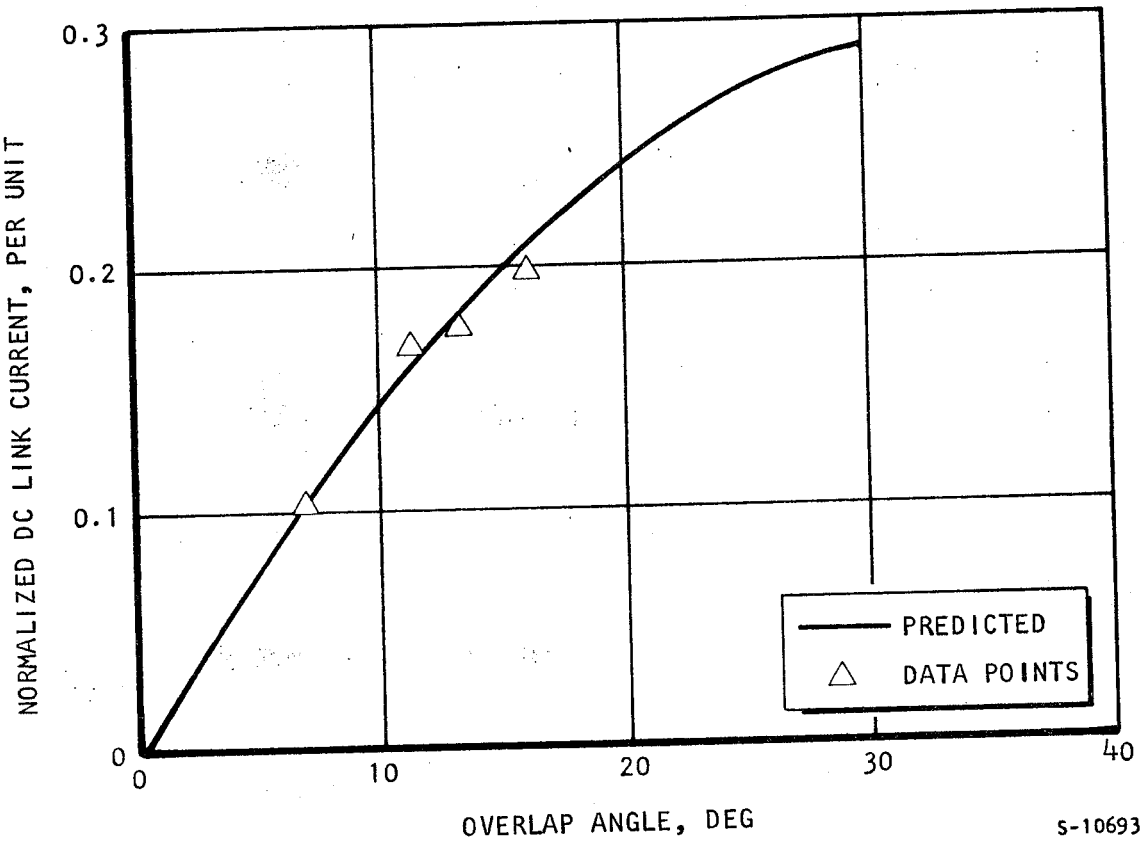

Figure 9-17. Normalized Dc Link Current as a Function of Overlap Angle

The power flow diagrams in Figures 9-18 and 9-19 quantitatively illustrate the LIMPS steady-state performance at 100- and 50-percent thrust command, and points corresponding to Figures 9-14 and 9-15, respectively. To place these results in perspective, the efficiency vs output power of the LIMPS has been plotted over the entire speed range of the system (Figure 9-20), indicating that the system efficiency values derived from the test data at the low-speed and low-power level are consistent with the design data.

Run Profiles

Vehicle and LIMPS performance can best be judged by examining the run profiles of key electrical and mechanical performance parameters during typical performance tests. Within the limitation of the 500-m-long guideway, the propulsion system was able to accelerate the vehicle up to 19.3 m/s, at an average acceleration of 0.57 m/s^2. A summary of the test runs is given in Table 9-8.

TABLE 9-8

TYPICAL ACCELERATION PERFORMANCE SUMMARY

Test Run No.	Thrust Command, Percent	Maximum Thrust, kN	Maximum Velocity, m/s	Average Acceleration, m/s^2
223	100	19.2	19.3	0.57
224	50	12.2	11.4	0.31
245	90	20.0	16.0	0.48

In the run profiles, shown in Figure 9-21 through 9-30, the performance parameters are plotted against distance or time. Again, for perspective, the results are also expressed as a percentage of the rated values.

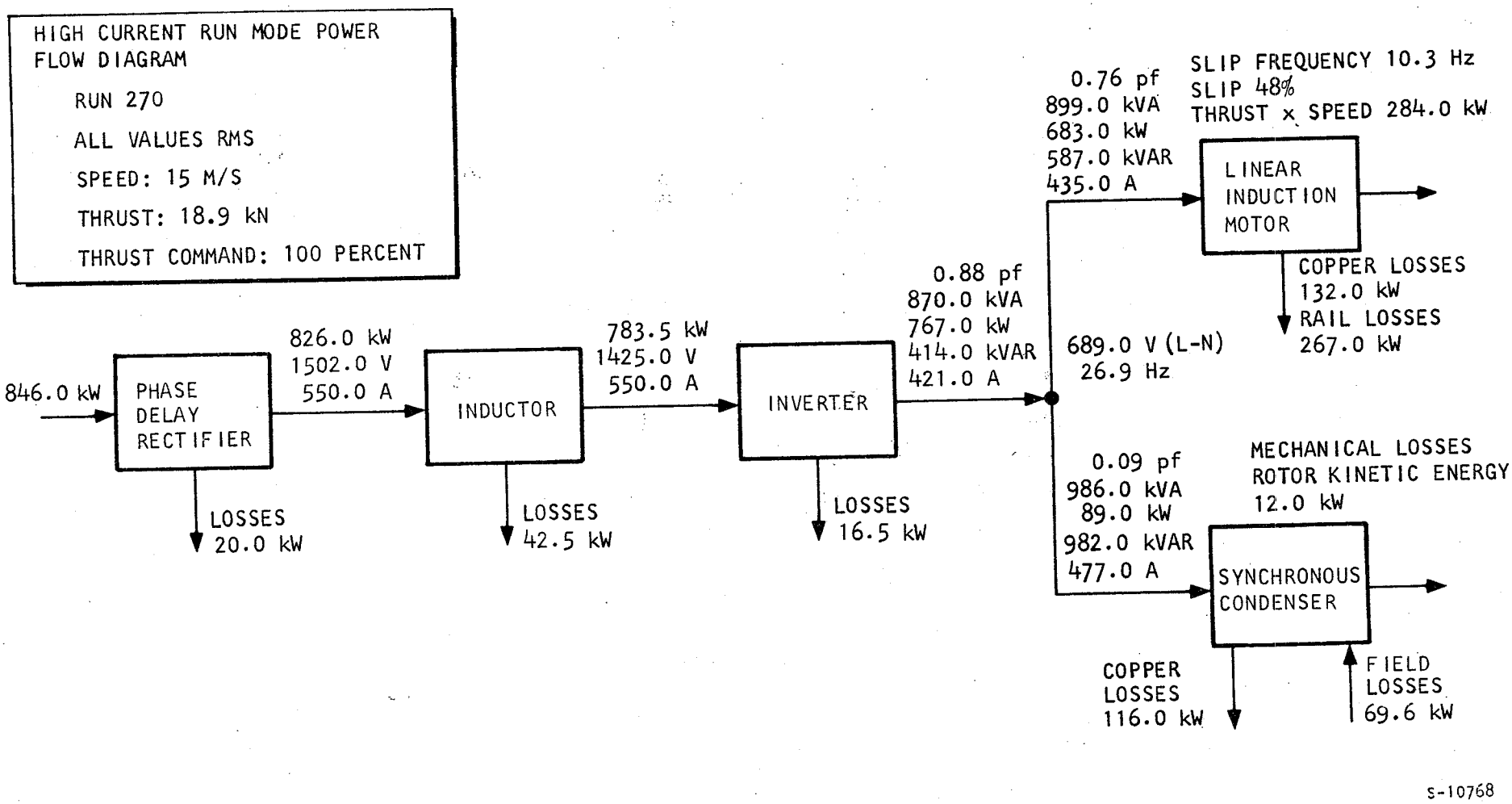

Figure 9-18. LIMPS Power Flow Diagram, 100-Percent Thrust Command

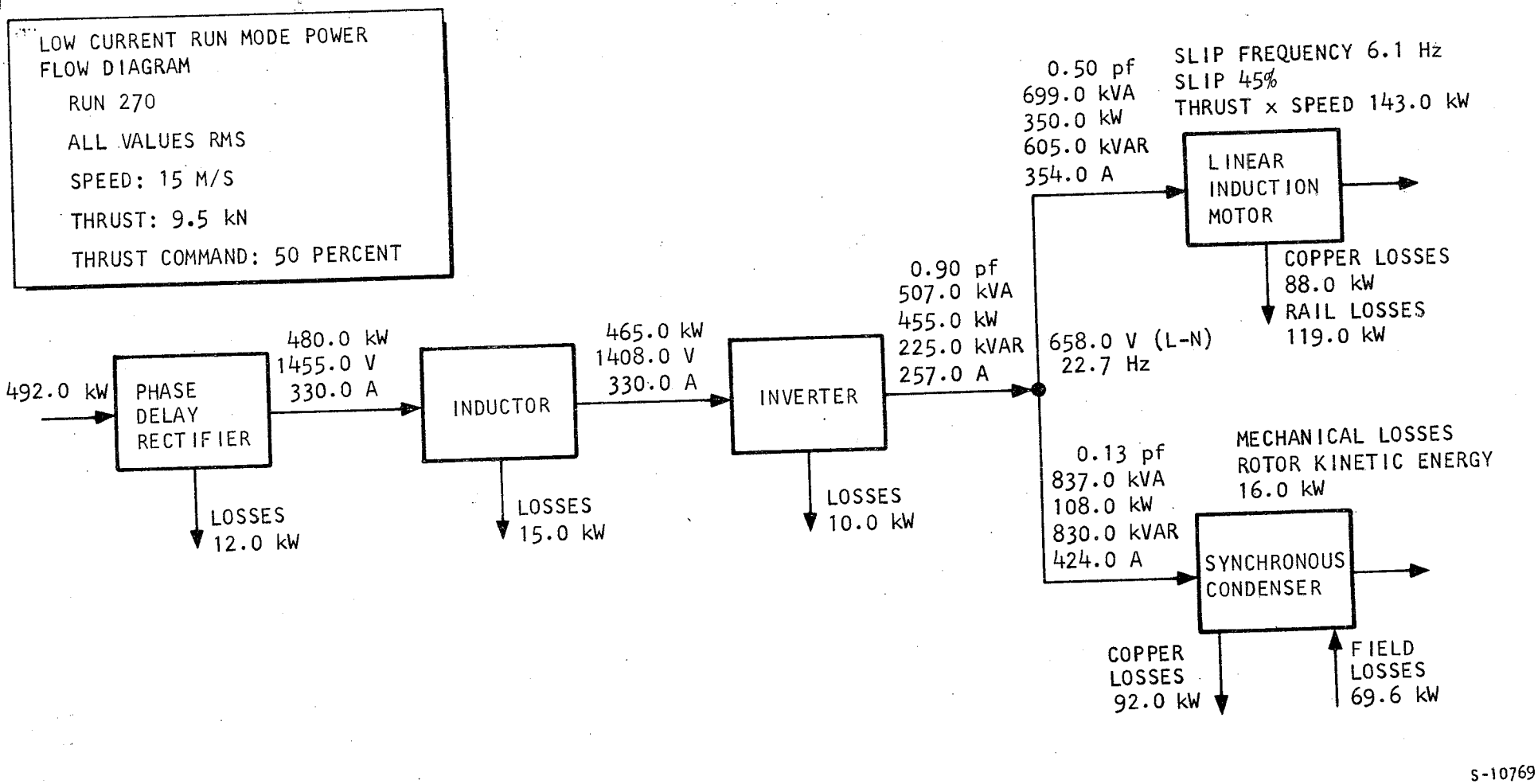

Figure 2-19. LIMPS Power Flow Diagram, 50-Percent Thrust Command

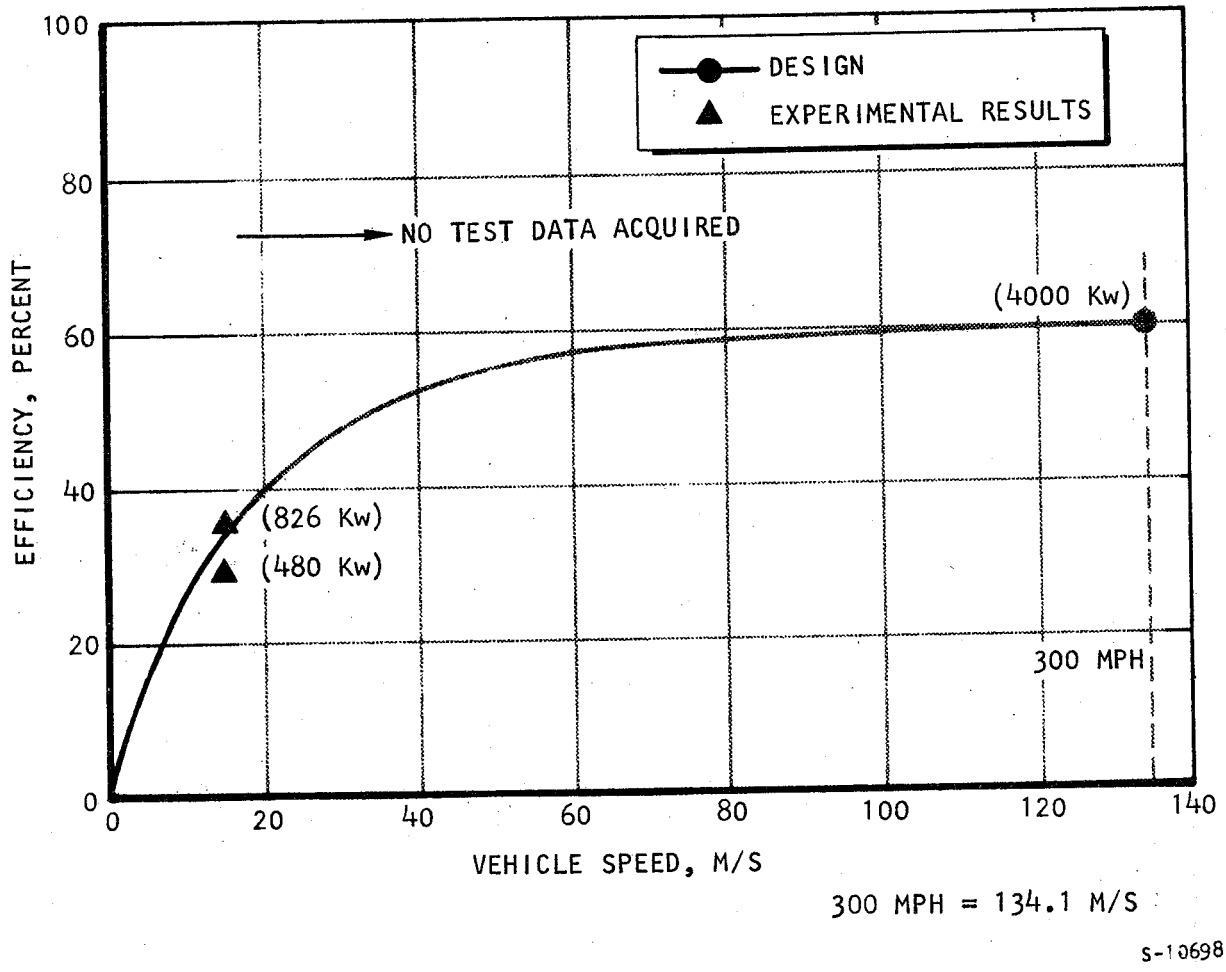

Figure 9-20. LIMPS Efficiency

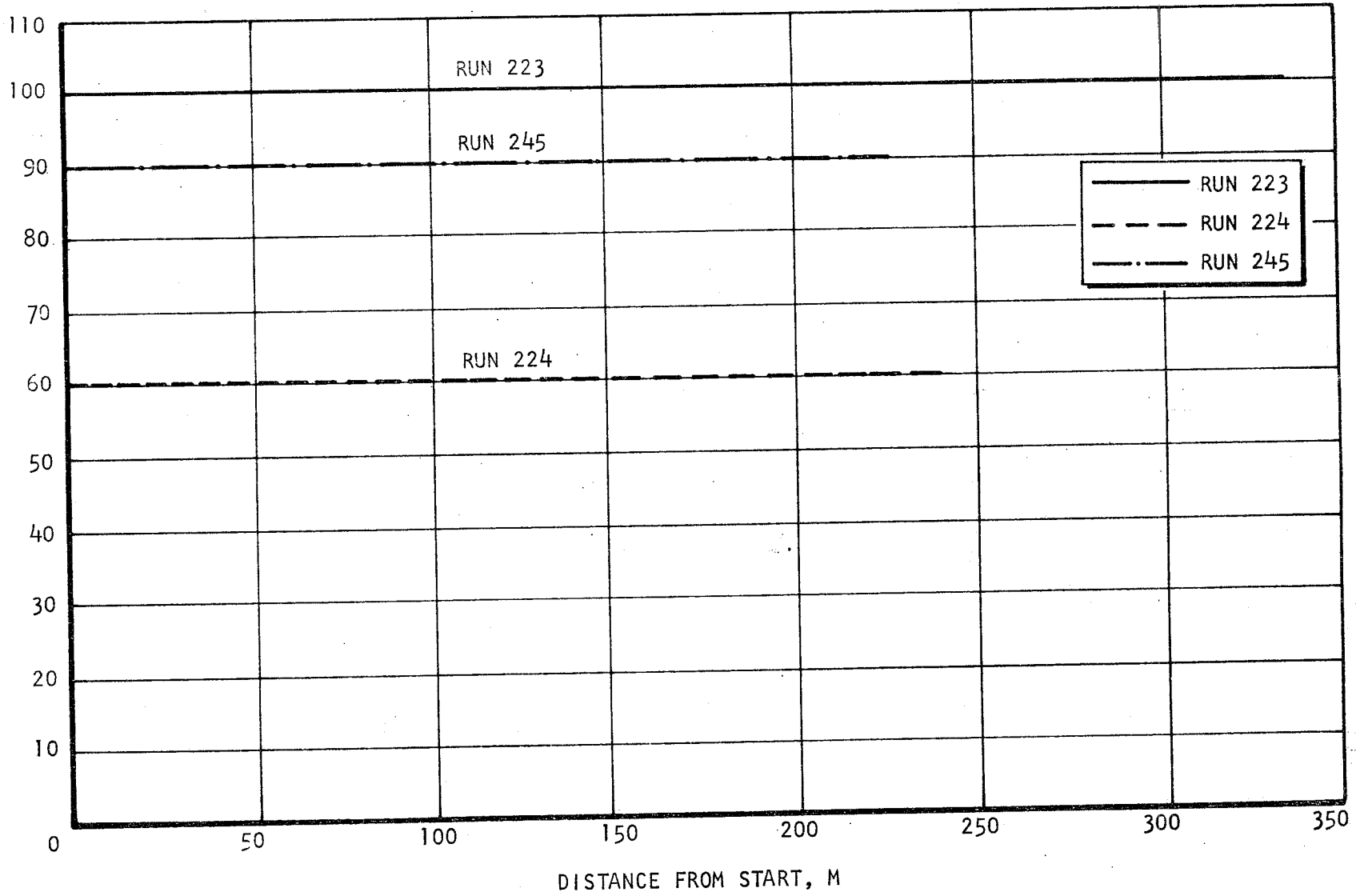

Figure 9-21. Typical Thrust Command Settings

S-1090

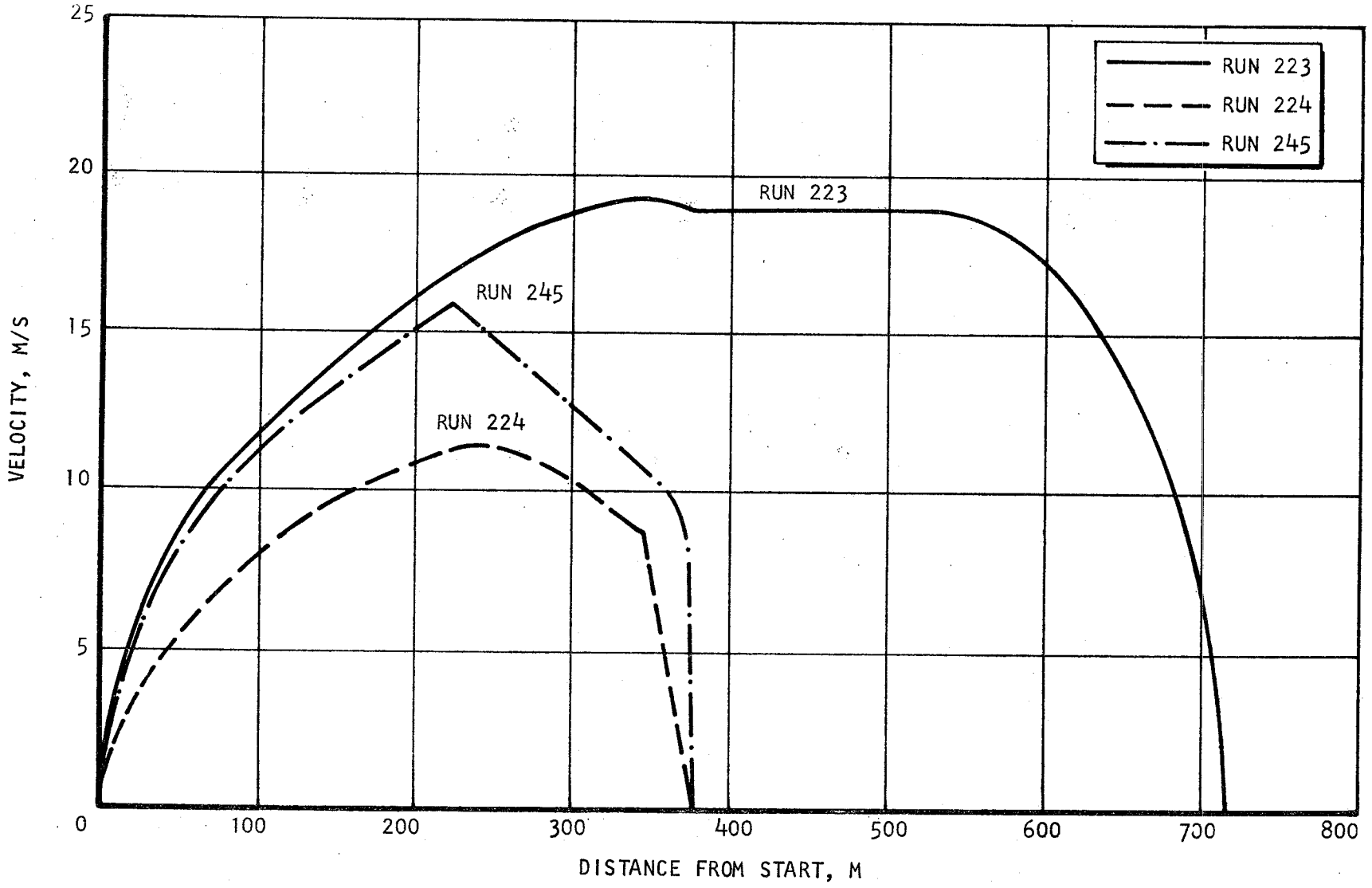

S-1094

Figure 9-22. Typical Speed Profiles

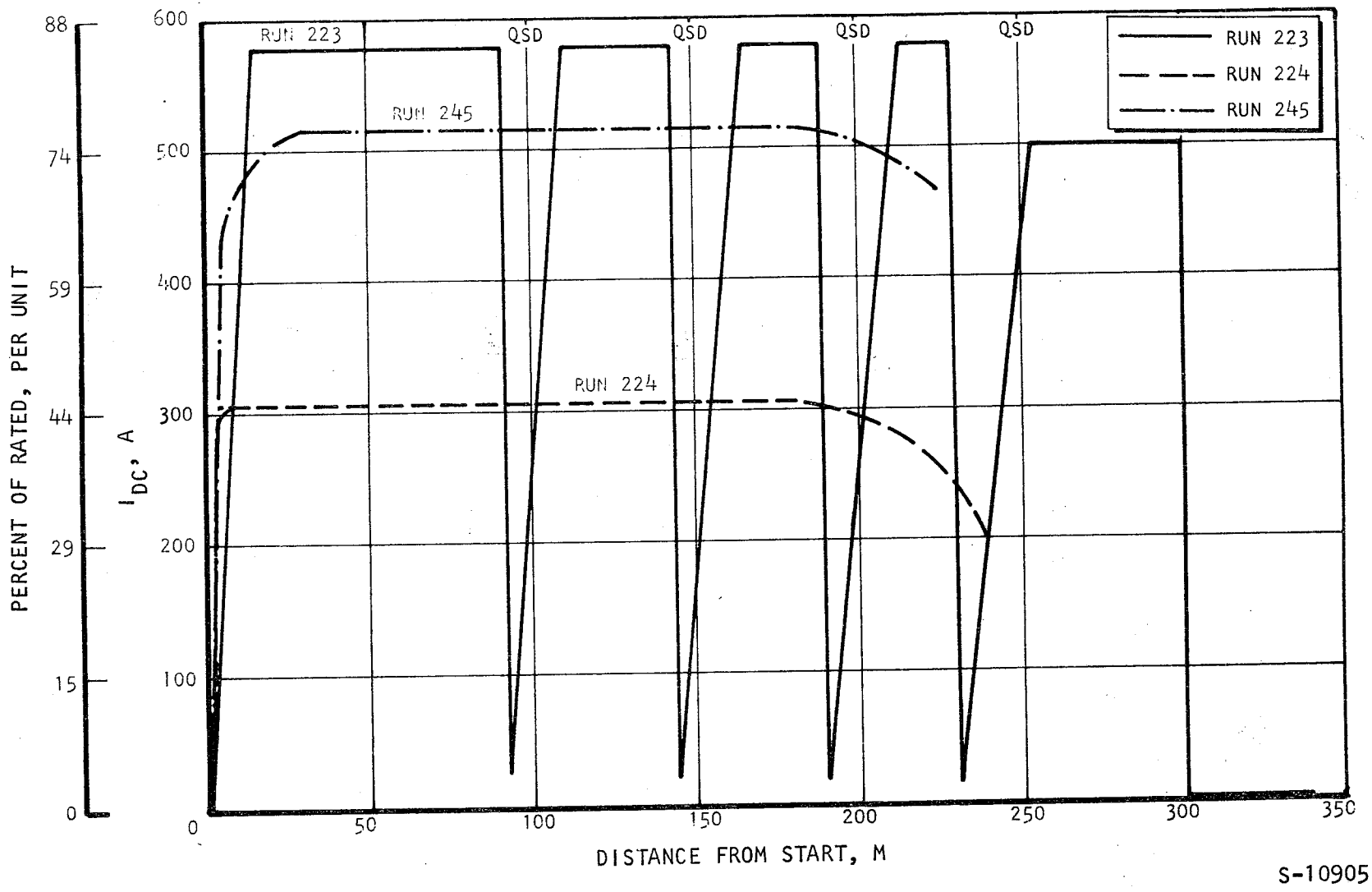

Figure 9-23. Typical Dc Link Current Profiles

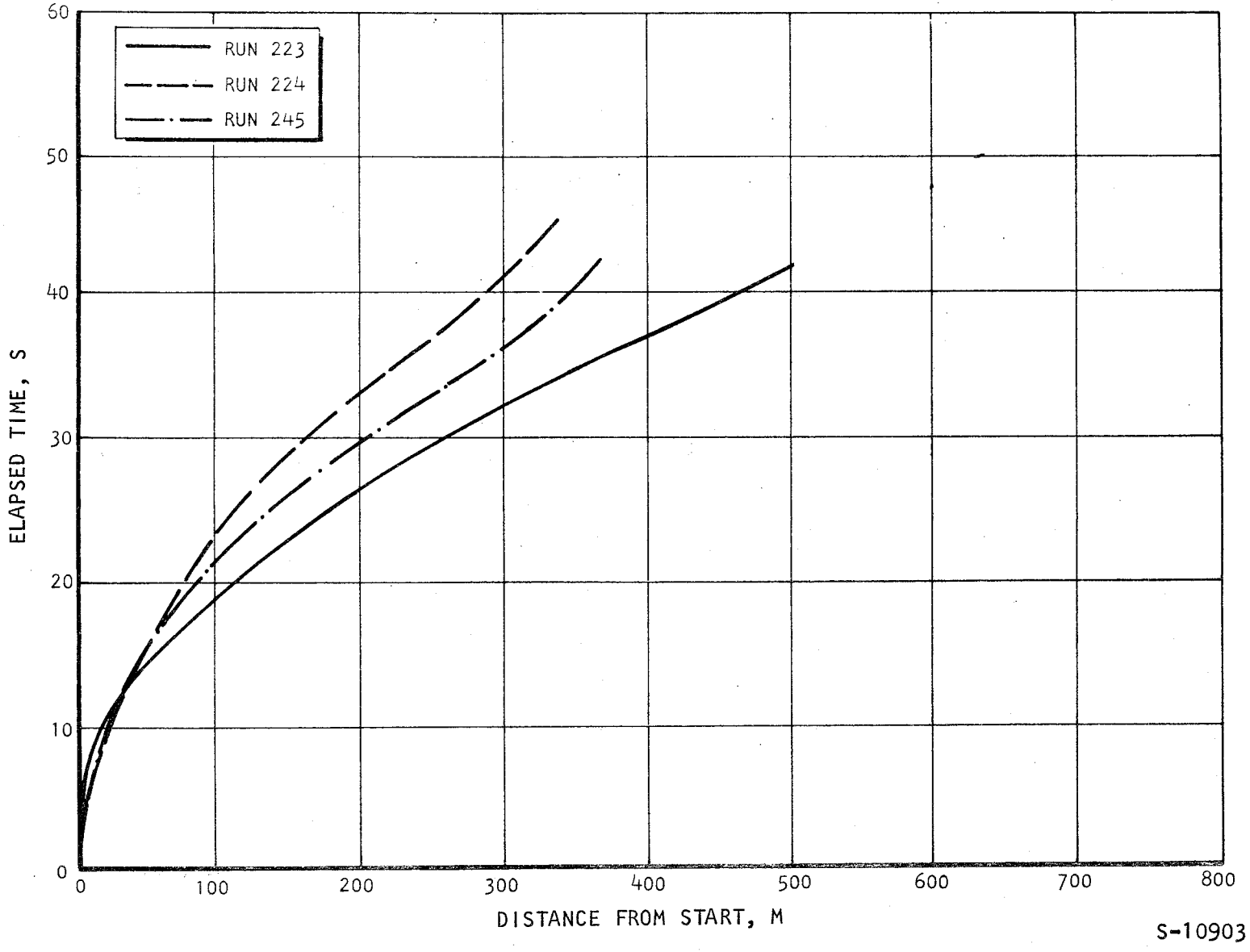

Figure 9-24. Typical Elapsed Time Profiles

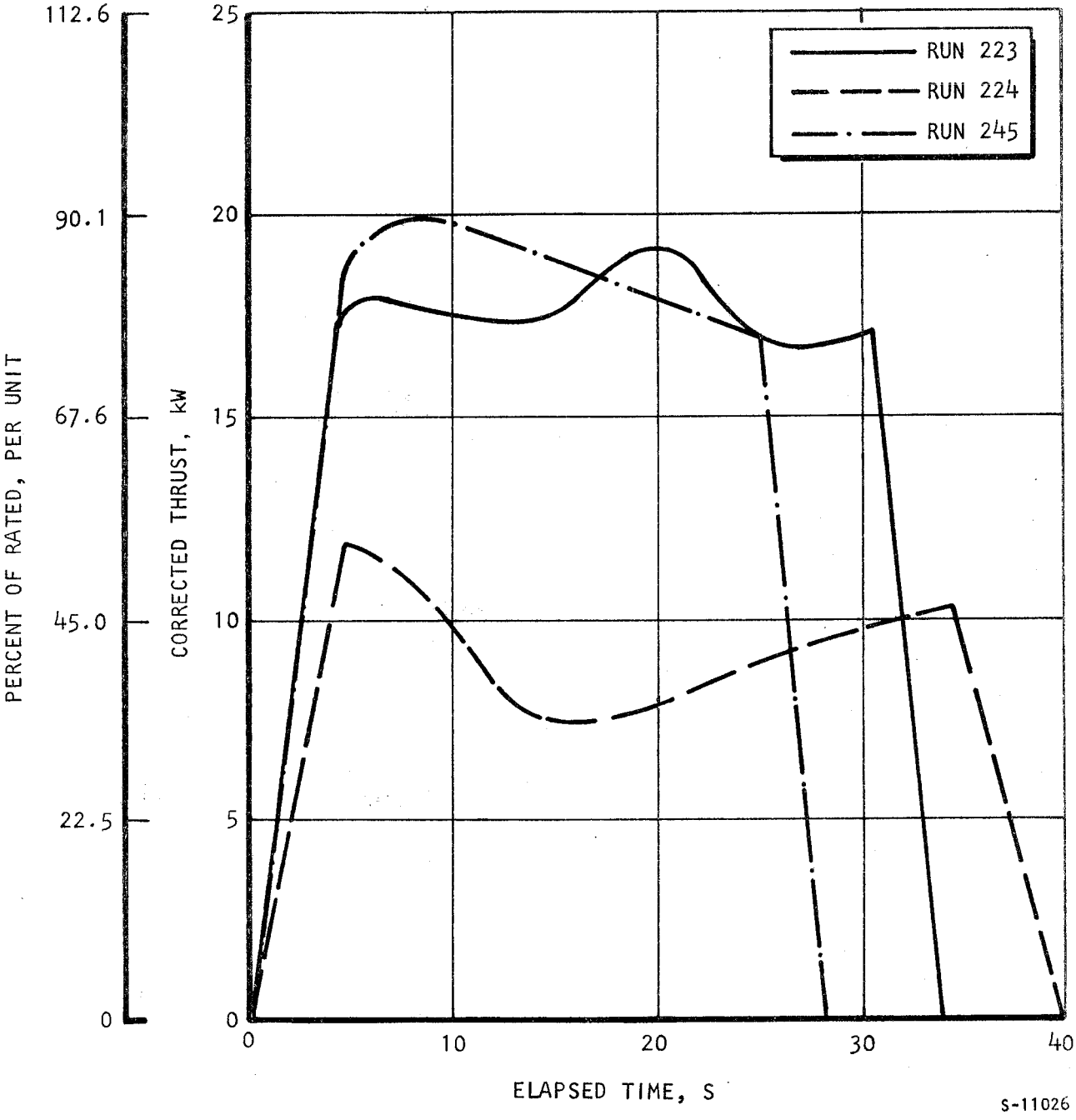

Figure 9-25. Typical Corrected Thrust Profiles

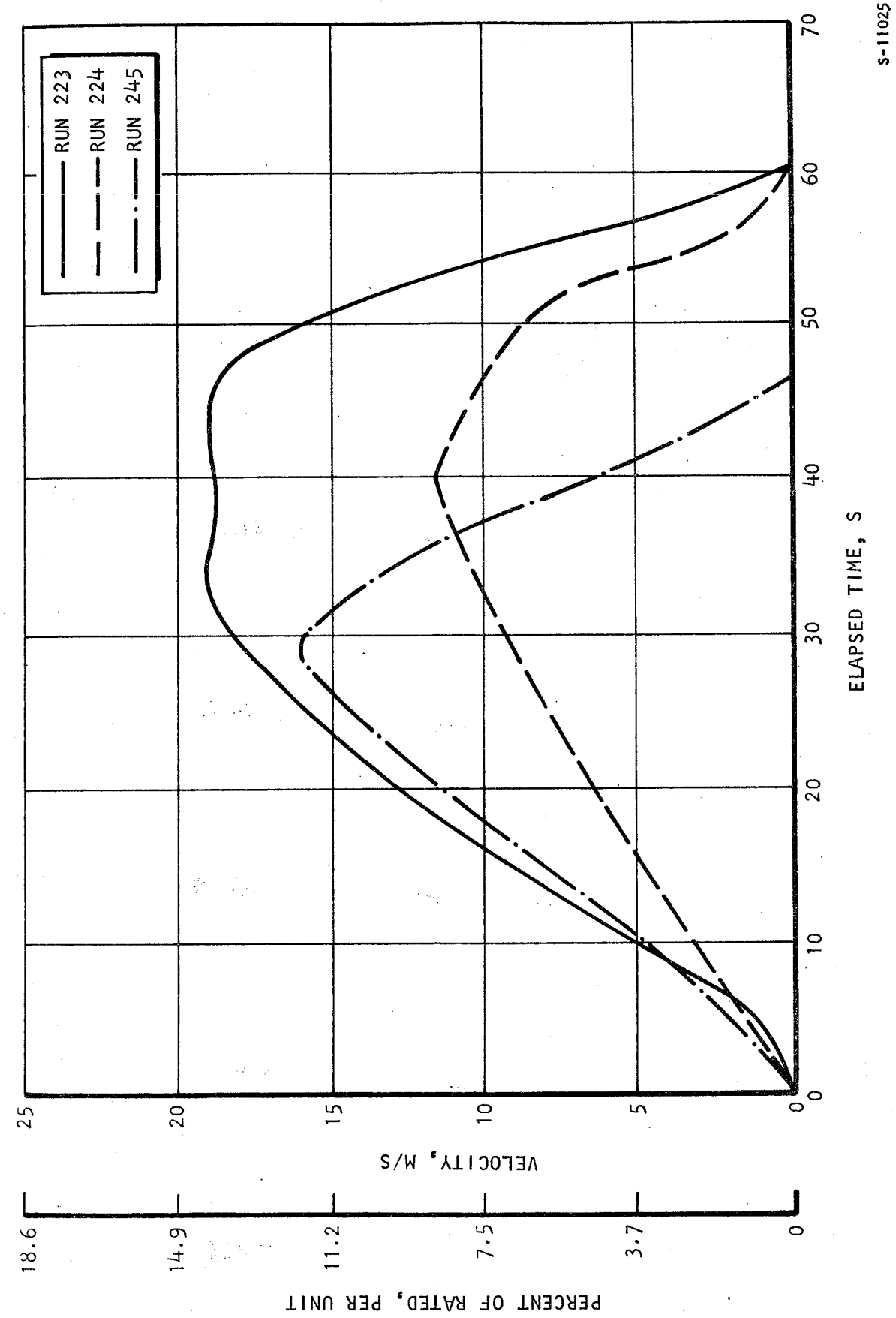

Figure 9-26. Typical Acceleration Profiles

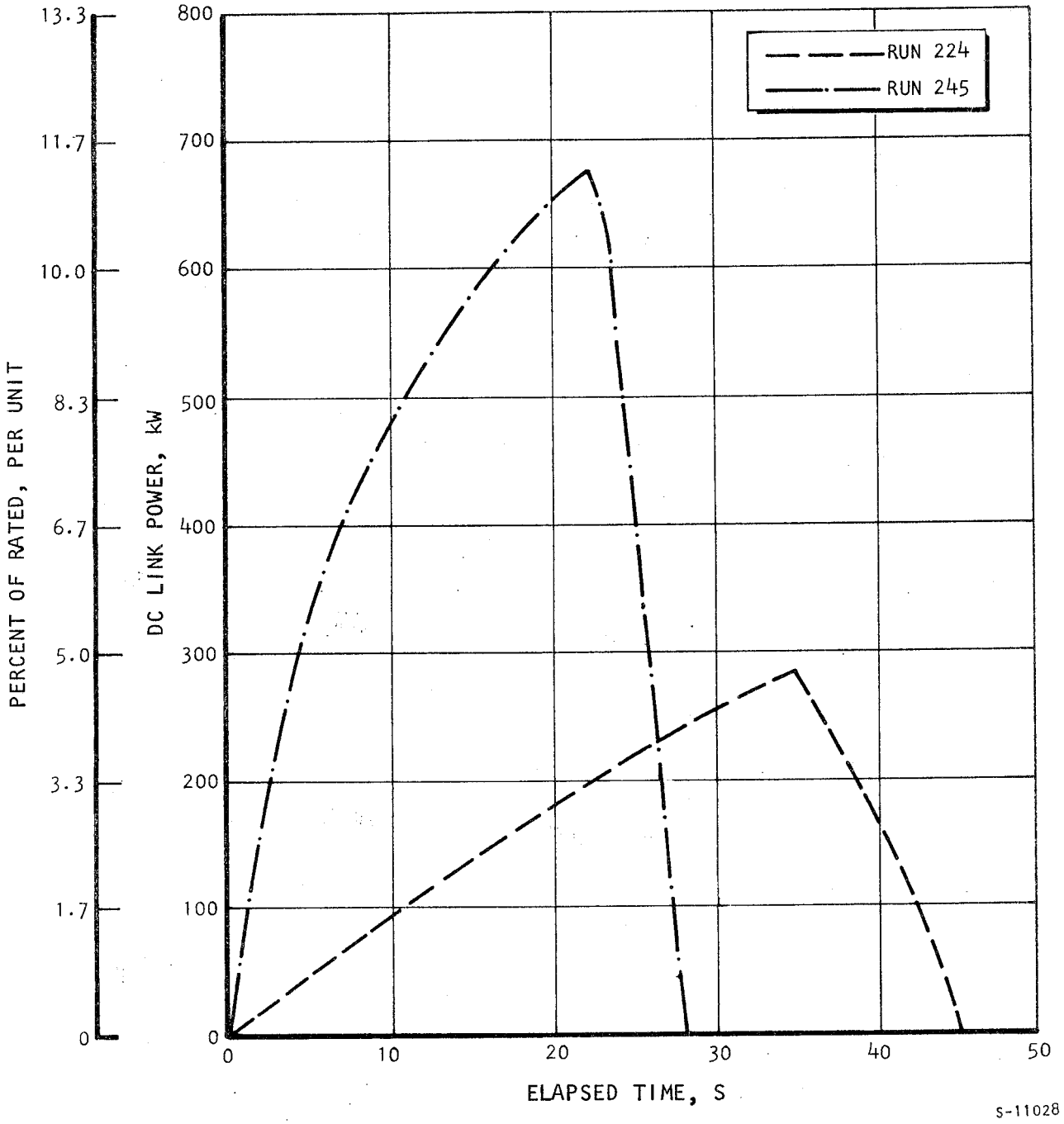

Figure 9-27. Typical Dc Link Power Usage

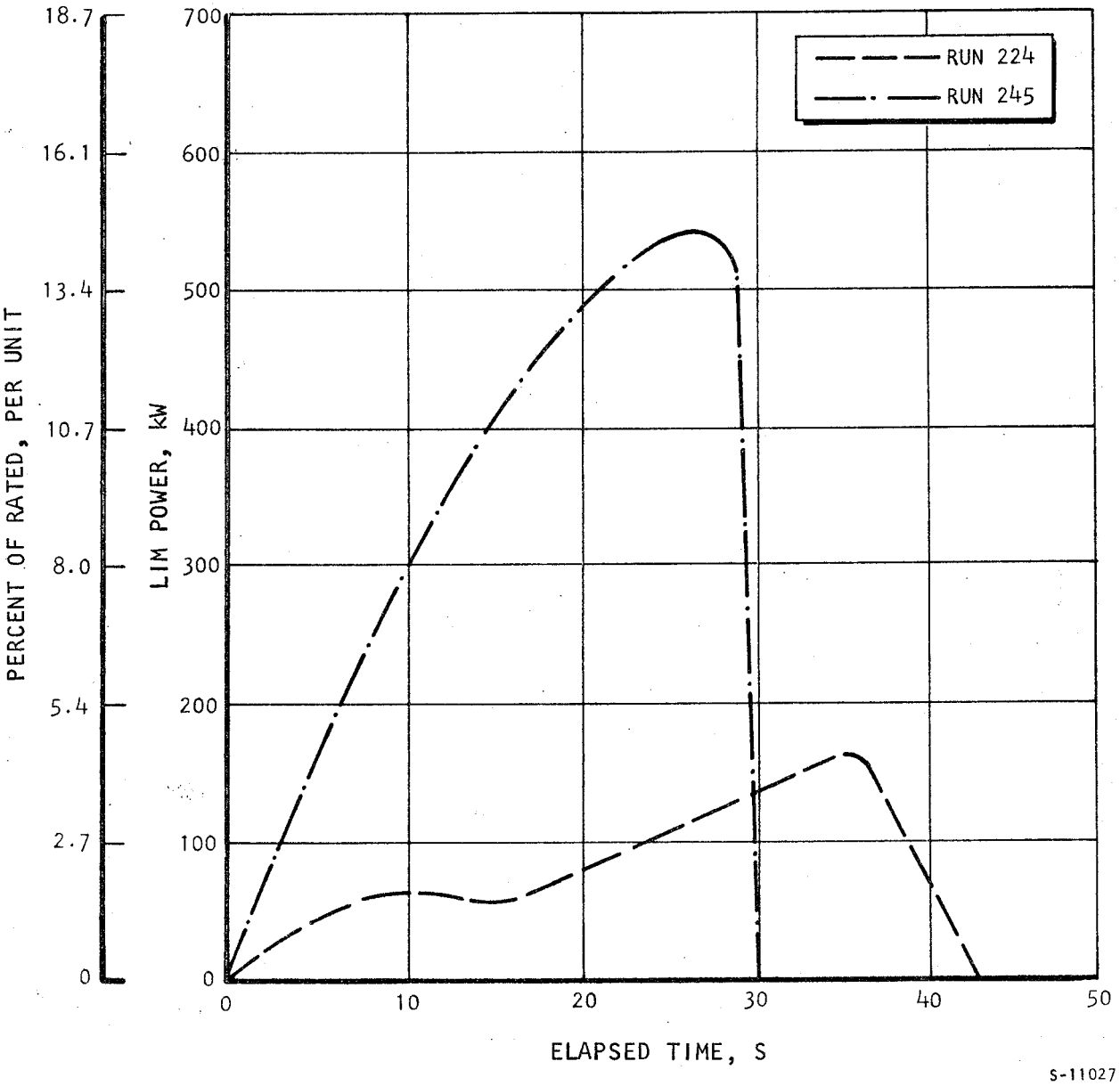

Figure 9-28. Typical LIM Power Usage

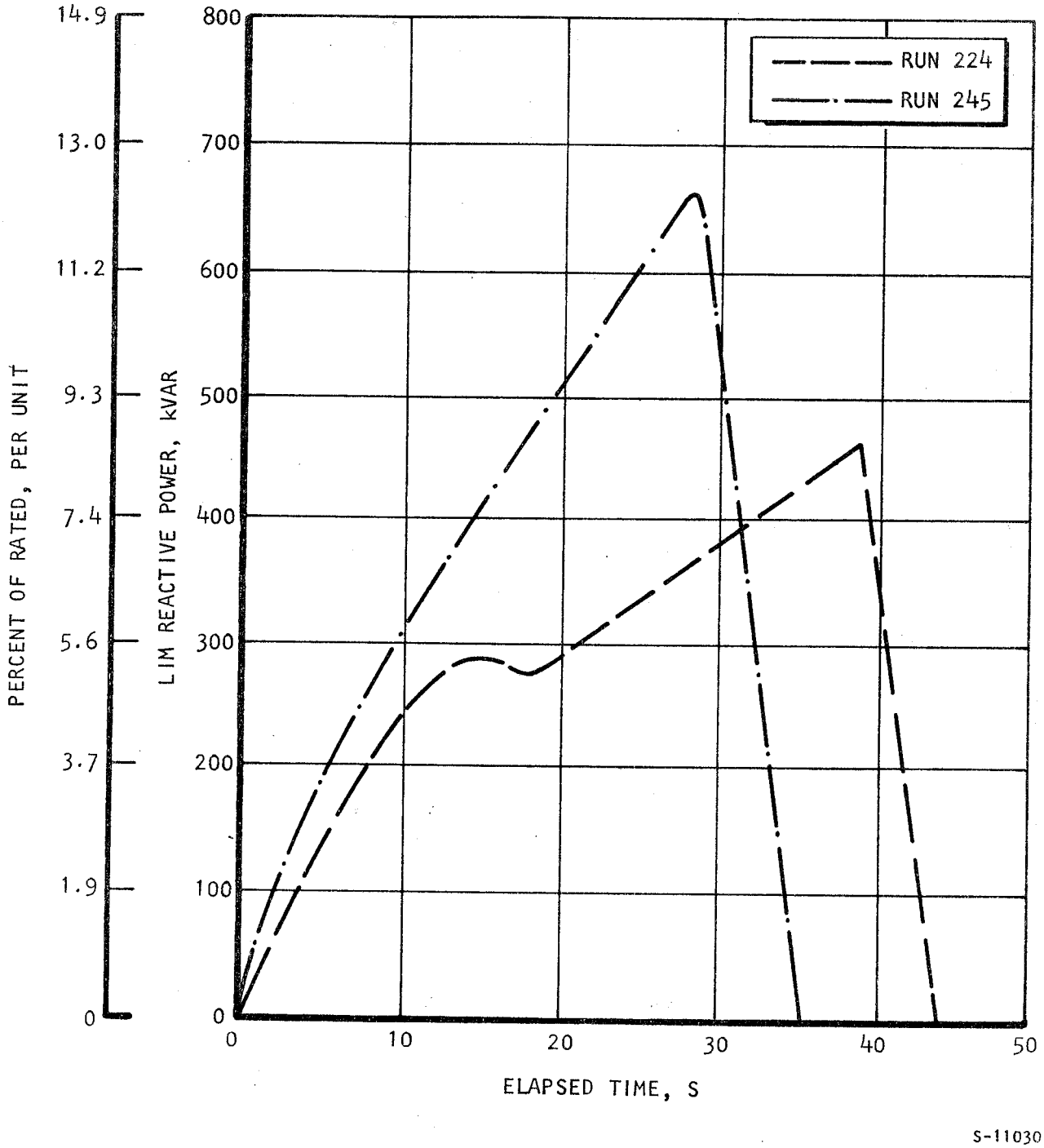

Figure 9-29. Typical LIM Reactive Power Usage

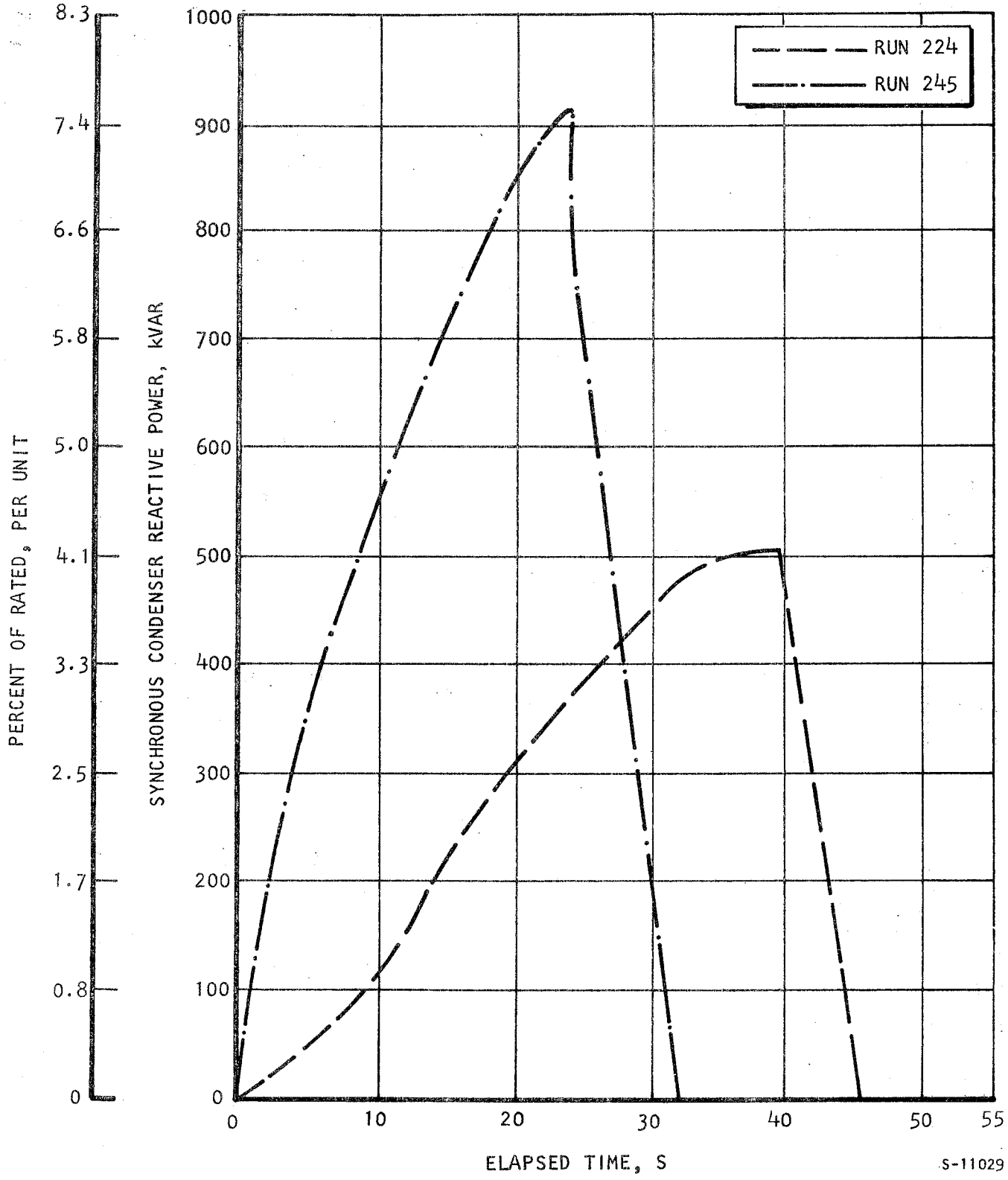

Figure 9-30. Typical Synchronous Condenser Reactive Power Usage

Synchronous Condenser Filtering Capability

As in the start mode, the current harmonics generated by the inverter are absorbed by both the LIM and the synchronous condenser. Their relative sharing, at a given operating point, is illustrated in Figure 9-31, which shows the current waveshape in the inverter, LIM, and synchronous condenser, respectively, and the corresponding harmonic content in terms of the frequency spectrum.

Synchronous Condenser Grounding

In full-wave bridge-connected converters (both in the rectifing and inverting modes) the dc link midpoint oscillates at triple frequency with respect to the electrical neutral of the ac input. To limit circulating currents in the groundloop, the synchronous condenser neutral is grounded through a 10-kilohm resistor. The resulting voltage stress level at the synchronous condenser neutral is given in Figure 9-32, which shows the peak value of the neutral-to-ground voltage as a function of the electrical frequency. Extrapolating to the rated frequency, the maximum additional voltage stress, which affects the ground insulation in the synchronous condenser and in the LIM, is approximately 750 V.

LIM Performance

Figure 9-33 shows calculated LIM thrust vs slip frequency, at constant current, and at four constant electrical frequencies. Note the marked impact of the end effects at the low slip frequencies, as indicated by the significant thrust reduction at increasing speed values. Superimposed on these calculated curves, the test data points are also shown. The experimental data, normalized to the same current values as the calculated curves, is grouped into three frequency groups, 0 to 10, 10 to 20, and 20 to 40 Hz. Results

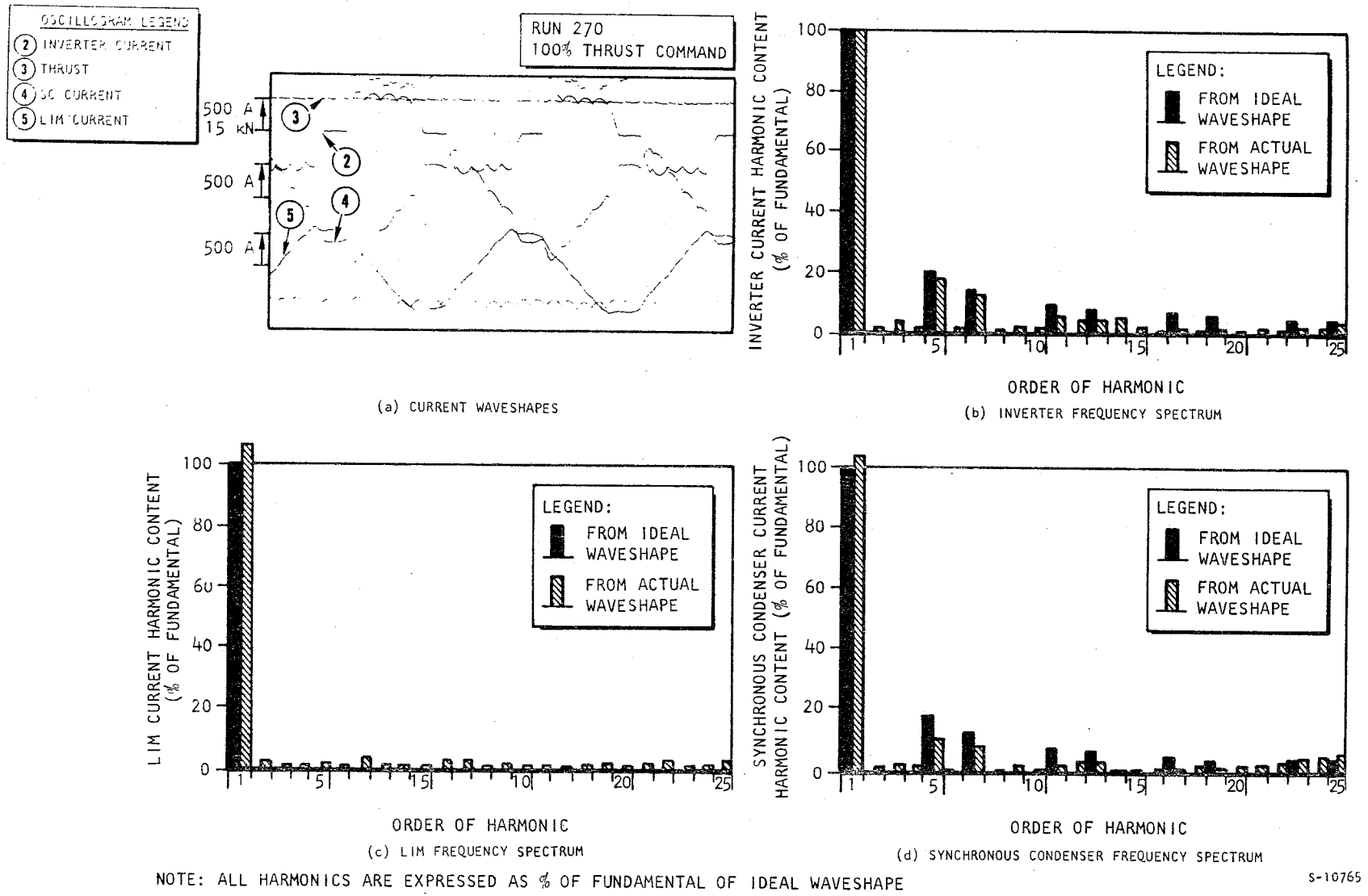

Figure 9-31. Synchronous Condenser Filtering Capability, Run Mode

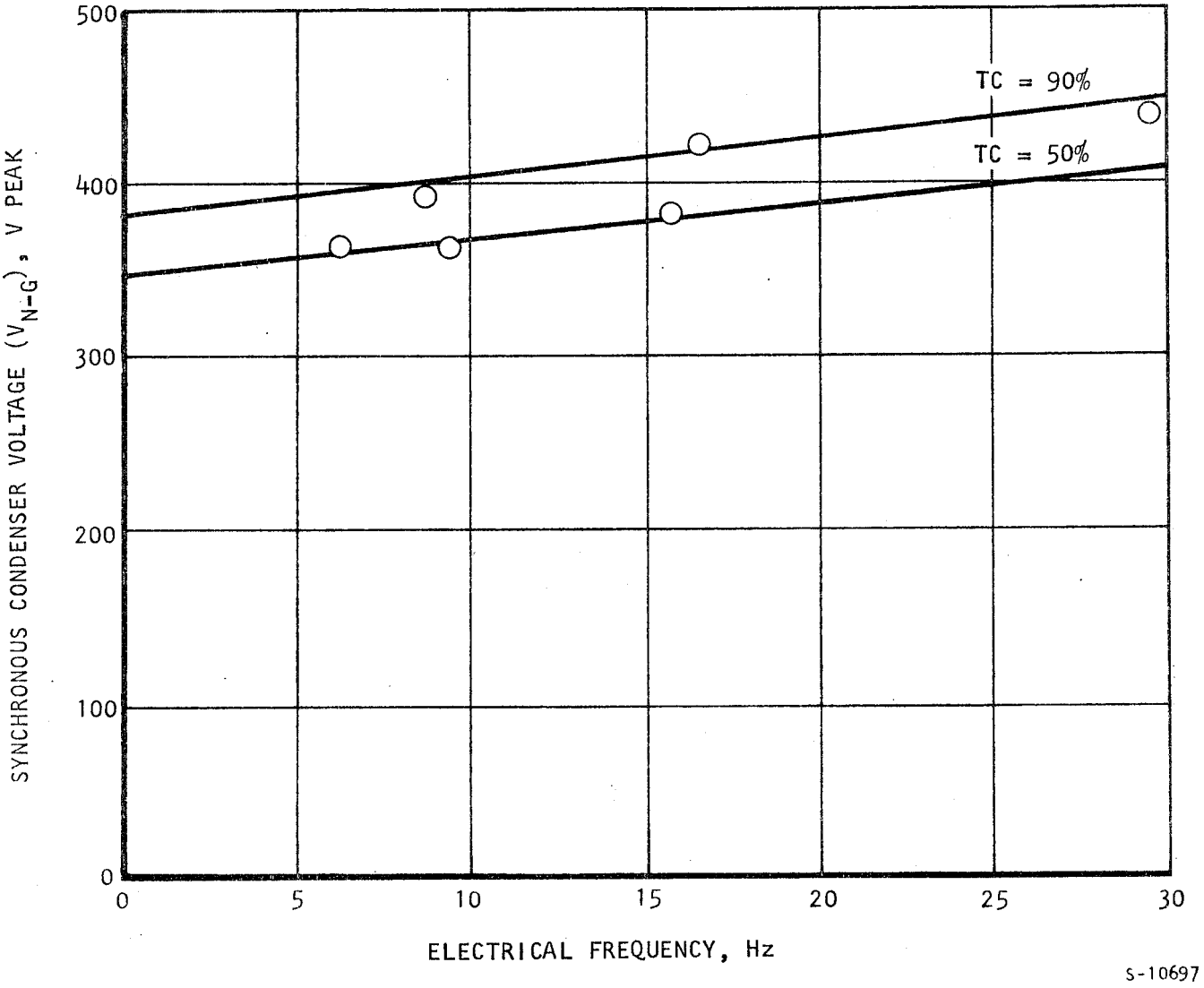

Figure 9-32. Synchronous Condenser Neutral-to-Ground Voltage

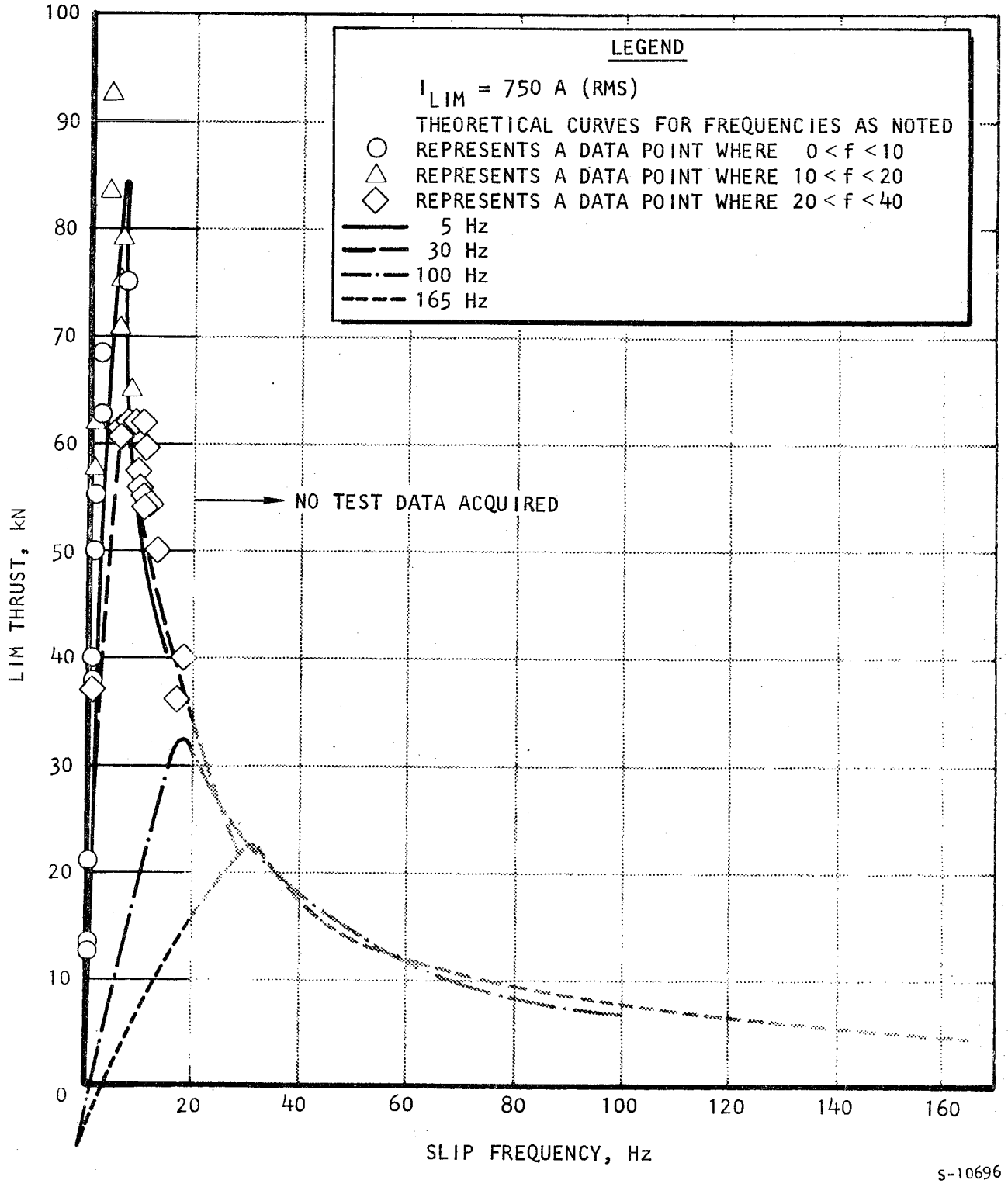

Figure 9-33. LIM Thrust Performance Data

generally agree well with the calculated performance curves. The test data points are all clustered in the low-slip-frequency portion of Figure 9-33 because the field test covered only the low end of the frequency range for which the LIM was designed.

LOW-SPEED BRAKING TESTS

During electrical braking the vehicle speed is greater than the (synchronous) speed of the LIM traveling wave, or in other words the excitation frequency is less than the mechanical frequency. In this mode of operation the LIM develops negative thrust, which acts to decelerate the vehicle. The reduction in vehicle kinetic energy with time manifests itself as mechanical input power to the LIM (i.e., the LIM operates as a generator).

Electrical Braking Characteristics

Two types of electrical braking were observed: regenerative, and dynamic.

1. Regenerative Braking

Electrical braking with regeneration performance data is shown in Figure 9-34. By examining the oscillographic traces of the inverter voltage and current, real power flowing into the inverter, and therefore through the dc link, can be observed. The corresponding phasor diagram is also shown. The power returned through the dc link is quite small, about 22.4 kW, compared with the power input to the LIM, 270 kW. The LIM input power is divided into losses (primary and secondary) of 153 kW and output power of 117 kW. The LIM output power supplies the losses in the synchronous condenser (110 kW) and the regenerated power to the dc link.

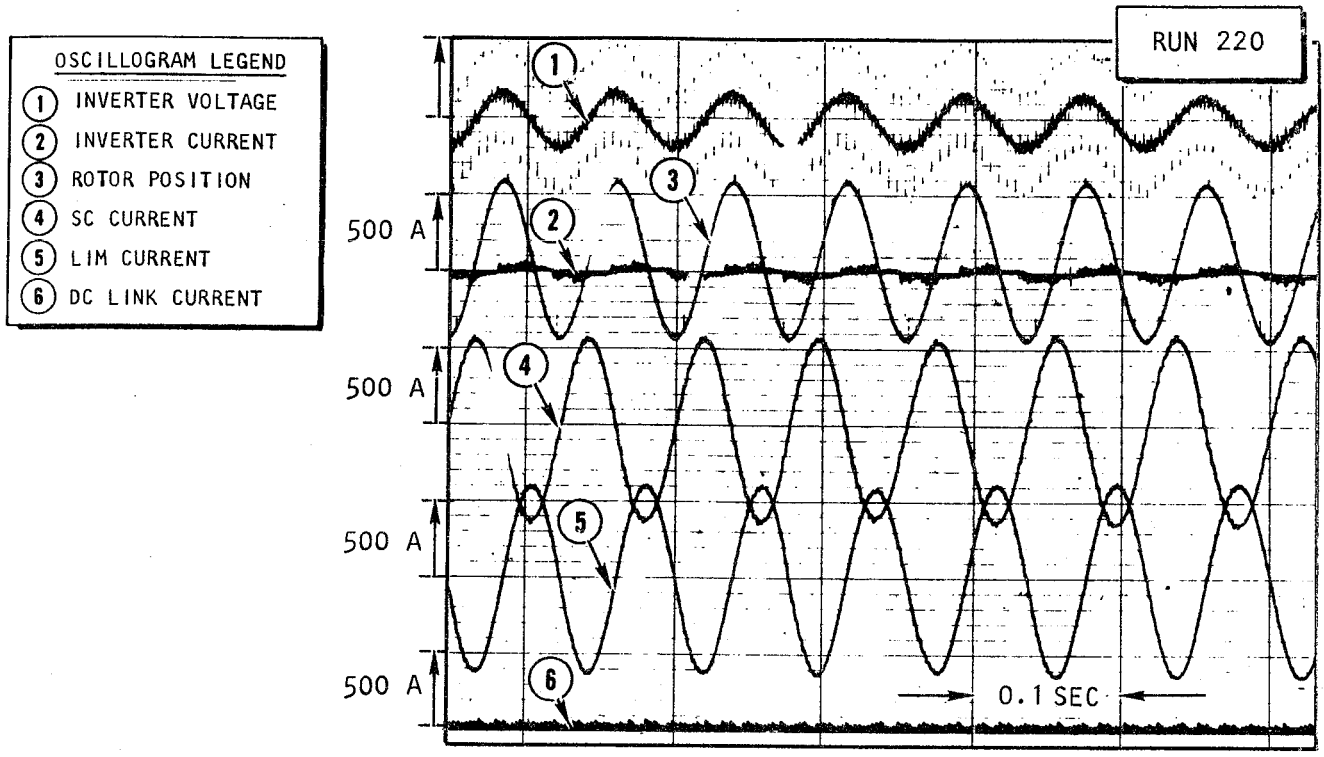

(a) OSCILLOGRAM

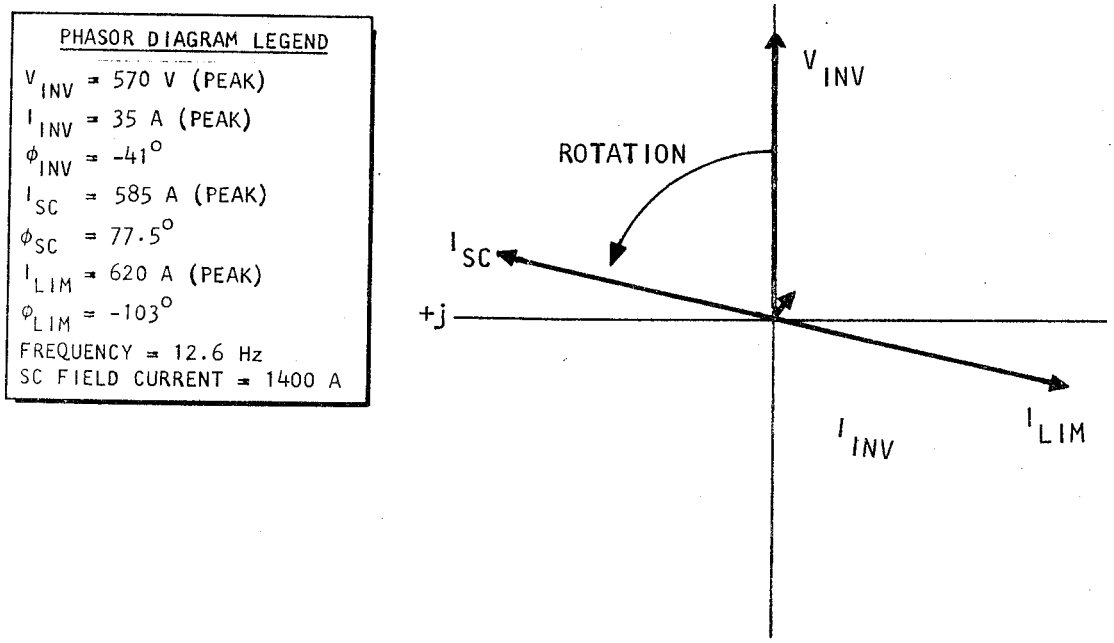

(b) PHASOR DIAGRAM

S-10824

Figure 9-34. Regenerative Braking

2. Dynamic Braking

Because of the losses in the LIM and synchronous condenser, electrical braking does not necessarily mean that electrical power is regenerated into the wayside electrical power system. Such a case, of no power delivery to the wayside, is shown in Figure 9-35 where despite the zero dc link current the LIM still provides a near-rated electrical braking force. This braking mode is referred to as dynamic braking.

The power conditions can be discussed with reference to the accompanying phasor diagram. The LIM developed approximately 14.5 kN negative thrust or braking force, nearly 90 percent of its rated value, which provided a 0.5 m/s^2 average deceleration. Since the vehicle speed at that time was 16.5 m/s, the LIM absorbed the kinetic energy at a 240 kW rate. The losses in the LIM secondary and primary were about 45 kW and 115 kW, respectively, corresponding to a LIM current of 475 A, and a slip frequency of -2.4 Hz.

The voltage and current data also show that at constant (zero) thrust command, as the vehicle speed decreases, the excitation frequency decreases and thereby the LIM slip frequency and thrust remain approximately constant.

Since the inverter current is zero, (1) the LIM and synchronous condenser currents are equal in magnitude, but 180 deg out of phase, and (2) the phase angle between the inverter voltage and synchronous condenser current phasors is approximately 80 deg, which means that real electrical power (about 80 kW) is being transferred from the LIM to the synchronous condenser.

Due to the concurrent slowing of the synchronous condenser, with a rotor moment of inertia of 33.4 Ns^3, the excitation frequency drops at a rate of 0.8 Hz/sec, which corresponds to a small, approximately 4-kW, apparent mechanical power input.

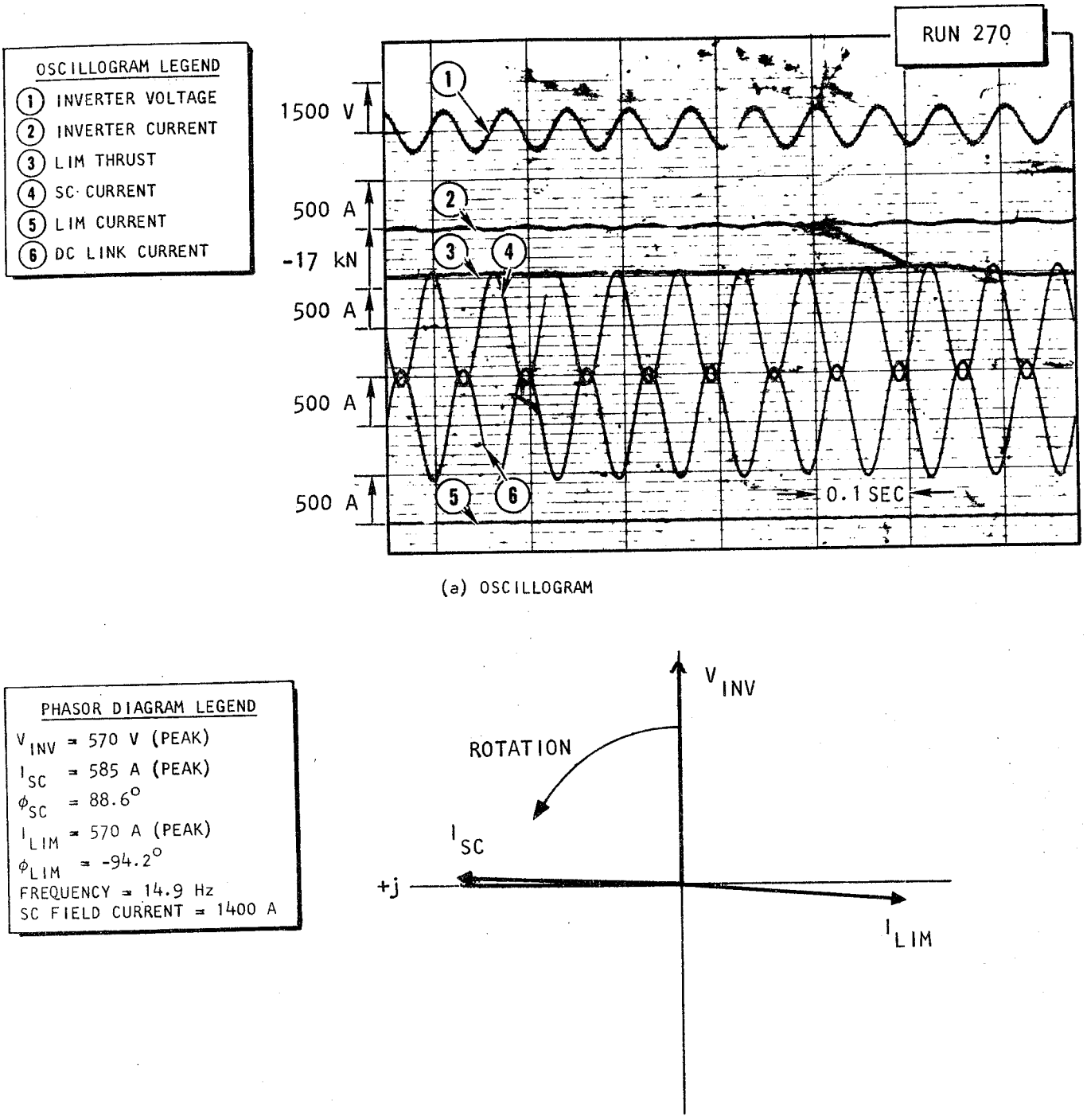

Figure 9-35. Dynamic Braking

REACTION RAIL TEMPERATURE RISE TESTS

Summary

The temperature rise of the reaction rail due to secondary LIM losses is of particular interest during vehicle start. Since the starting segment of reaction rail exposure time can be relatively long at low acceleration rates, it is important to determine if the potential for reaction rail overheating exists under various starting conditions.

To investigate the reaction rail temperature rise, locked-rotor tests were conducted to obtain experimental data. By setting the vehicle mechanical brakes, the LIM was held stationary with respect to the reaction rail. The propulsion system was then energized for periods of up to 5-s duration. The reaction rail temperature was measured directly with a suitably placed thermocouple. In addition, the temperature rise was calculated from LIM electrical data. For most test points, the measured and calculated values are in reasonable agreement.

The test results show that the temperature rise at start is quite low. For a typical starting thrust of 10 kN, the maximum reaction rail temperature rise would be about 3.3°C (38°F).

Test Conducted

The vehicle was positioned on the guideway with respect to two thermocouples mounted on the reaction rail such that one was in the approximate geometric center of the motor and the second was under one of the LIM guidance air cushions. The jet engines were operated throughout the test series to provide air for levitating the vehicle and motor. The mechanical brakes were locked on in order to hold the vehicle in a fixed position on the guideway.

The thermocouple outputs were continuously recorded on a strip chart recorder throughout the test series. In addition, onboard analog recordings of key electrical parameters were also made.

A total of 14 runs were made during the locked-rotor test series. At the start of each run, the LIMPS was energized at fixed thrust command values for periods of up to 5-s duration. Several minutes were allowed between runs such that the reaction rail temperature under the LIM could decay to an ambient value.

Throughout the test series, the reaction rail temperature under the LIM air cushion showed a nearly constant value of 60°C (140°F). This was due to the continuous flow of warm air supplied to the air cushions which acted to stabilize the local reaction rail temperature.

Reaction Rail Temperature Rise

Table 9-9 lists the temperature rise per unit time based on the measured temperature data and on calculations using the analog recordings of selected electrical parameters. The thrust command, which was fixed throughout each run, is also shown. Run 254, conducted at a thrust command of 100 percent, is not shown due to a quick shutdown and restart which rendered the data unintelligible.

A plot of temperature rise per unit time vs thrust command is shown in Figure 9-36. Both measured and calculated points are shown.

Measured Temperature Rise

A typical strip chart recording of the response of the two thermocouples is shown in Figure 9-37. The time, $t = 0$, has been arbitrarily set to coincide with the start of the run. Prior to this time, it can be seen that the temperature under the motor has stabilized to a value of 52°C (125.6°F), which

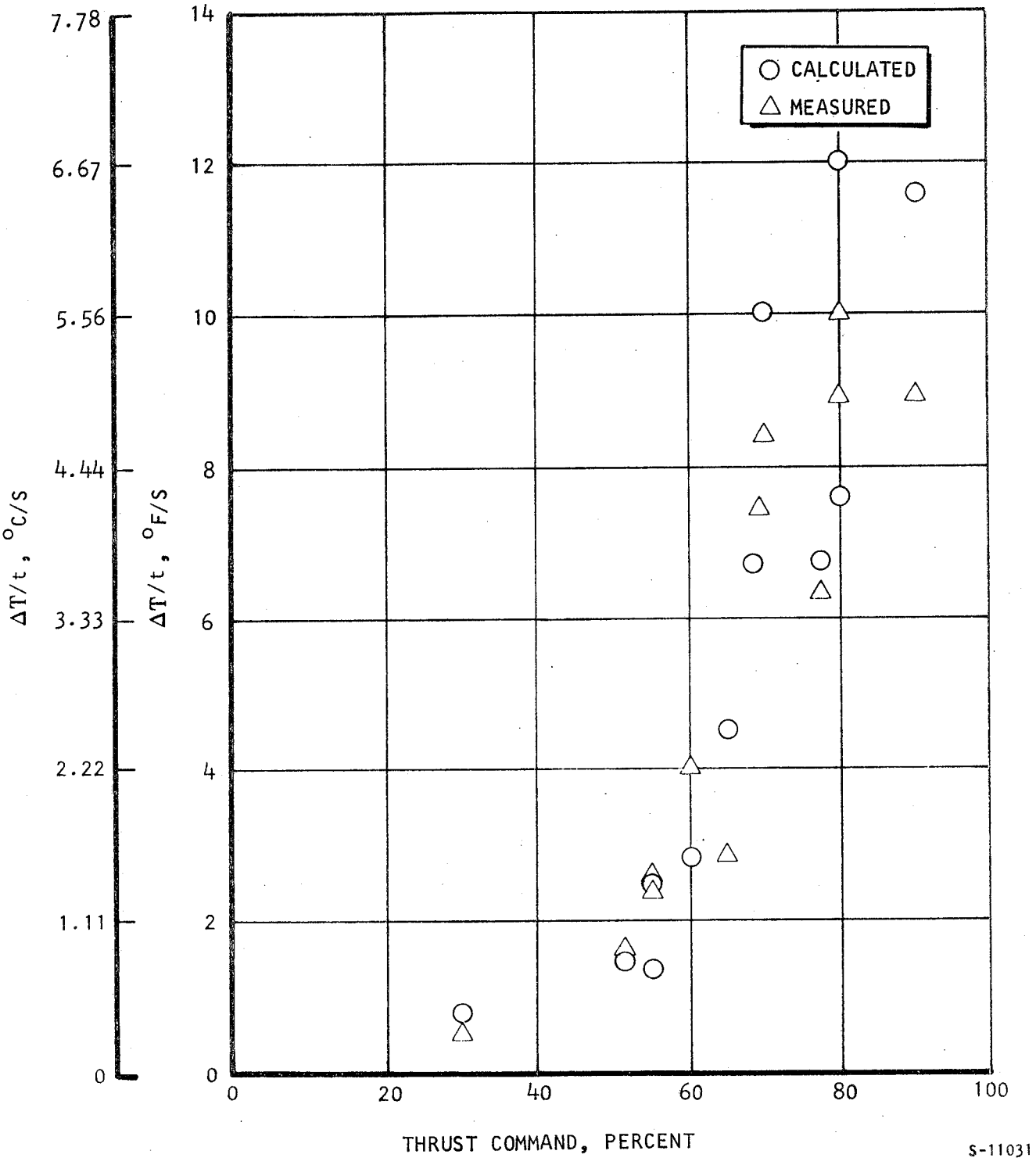

Figure 9-36. Reaction Rail Temperature Rise vs Thrust Command

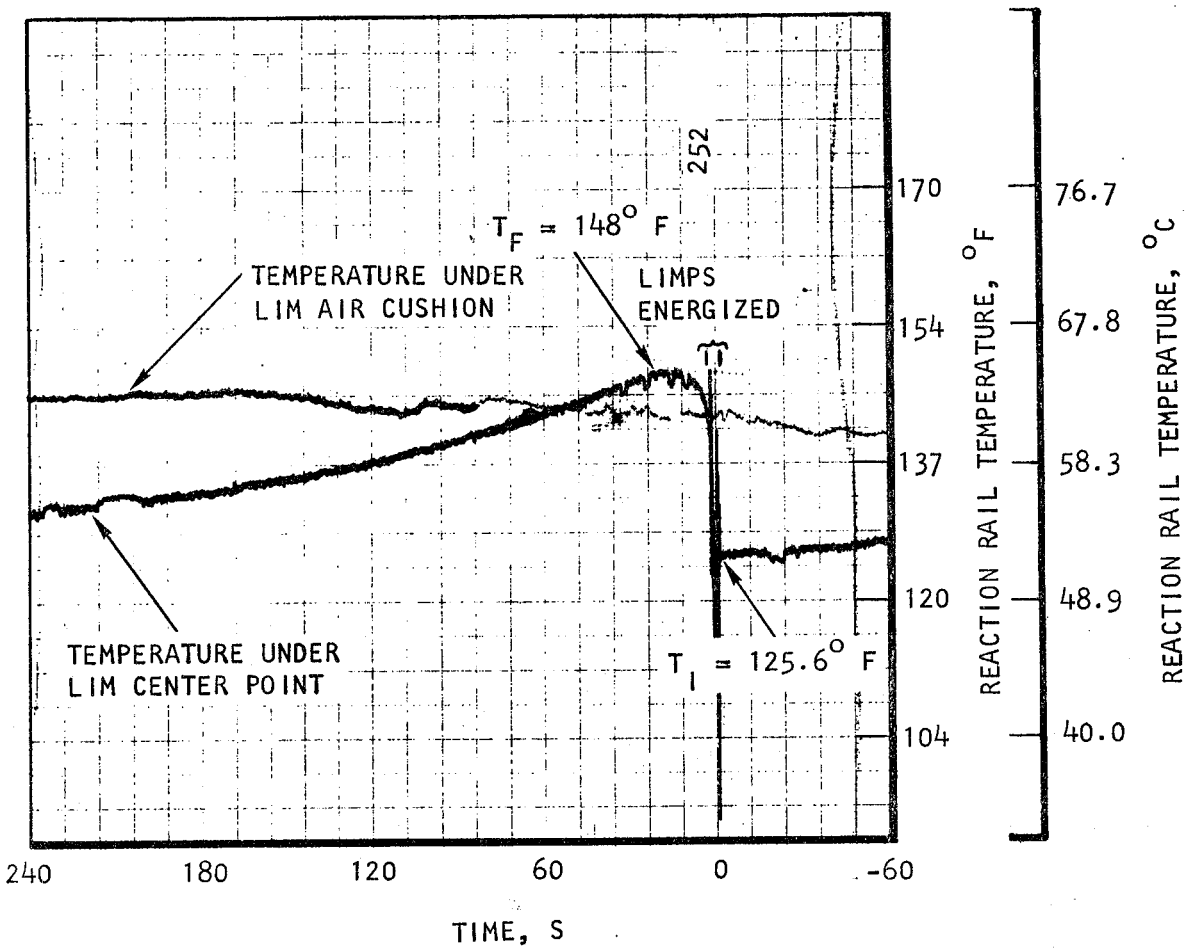

Figure 9-37. Strip Chart Record of Reaction Rail Temperature

TABLE 9-9

MEASURED REACTION RAIL TEMPERATURE RISE

Run No.	$\Delta T/_t$ Measured °C/S	Measured °F/S	Calculated* °C/S	Calculated* °F/S	Thrust Command, Percent
246	0.294	0.53	0.43	0.77	30
247	1.31	2.36	1.62	2.91	55
248	1.56	2.80	2.54	4.57	65
249	0.93	1.67	0.84	1.51	52
250	2.22	4.0	1.55	2.79	60
251	4.17	7.5	3.74	6.73	68
252	4.69	8.44	5.67	10.16	70
255	3.55	6.39	3.74	6.73	77
256	4.93	8.88	4.25	7.65	80
257	0.76	1.36	1.44	2.59	55
258	5.61	10.1	6.69	12.04	80
259	5.0	9.0	6.47	11.65	90

*See page 232 for method of calculation.

is the initial temperature value, T_I, for this run. When the LIMPS is energized, the response of the thermocouple under the LIM shows large oscillations due to the presence of the strong magnetic field. After 5 seconds the LIMPS is deenergized, and shortly thereafter the temperature under the LIM attains a maximum value of 64.7°C (148.4°F), which is the final value of the temperature, T_F, for this run. The temperature continues to drop in a slow decay, as the heat in the reaction rail is dissipated to the surroundings. The temperature of the reaction rail under the LIM air cushion remains approximately constant. This characteristic was typical for all runs.

The initial and final values of the reaction rail temperature under the LIM are given in Table 9-10. The period of time that the propulsion system was energized was obtained from the electrical data.

TABLE 9-10

MEASURED REACTION RAIL TEMPERATURE DATA

Run	Initial Temperature (T_I), °C	Initial Temperature (T_I), °F	Final Temperature (T_F), °C	Final Temperature (T_F), °F	Time, s
246	43.6	110.4	44.0	111.2	1.5
247	45.9	114.6	47.7	117.9	1.4
248	47.2	117.0	50.3	122.6	2.0
249	48.7	119.7	51.6	124.8	4.0
250	49.4	121.0	54.6	130.2	2.3
251	50.6	123.1	60.6	141.1	2.4
252	52.0	125.6	64.7	148.4	2.7
255	53.8	128.8	70.1	158.2	4.6
256	52.9	127.3	72.7	162.8	4.0
257	46.6	115.8	50.3	122.6	5.0
258	49.6	121.2	75.3	167.6	4.6
259	53.6	128.5	72.1	161.7	3.7

Calculated Temperature Rise

During each run, onboard analog recordings of the following selected electrical parameters were made:

LIM voltage, A phase

LIM current, A phase

Dc link current

In addition, the LIM thrust was recorded during the last three runs (257 through 259). The thrust command values were obtained from the test log.

Typically, the LIMPS attained steady-state conditions within one second after being energized. Using the steady state portions of each analog trace, the LIM airgap power was calculated as follows:

$$P_{\text{LIM AIRGAP}} = 3 \times V_{LIM} \times I_{LIM} \times PF - 3I_{LIM}\ R_{PRIMARY}$$

The A-phase values for the RMS LIM voltage V_{LIM}, and RMS LIM current I_{LIM} were based upon the assumption of a balanced 3-phase system. The power factor (PF) was taken from the displacement of the voltage and current traces with respect to each other. The LIM primary resistance per phase, $R_{PRIMARY}$, was evaluated based upon the known LIM characteristics (0.288 ohm at 177°C (350°F) and measured LIM winding temperatures.

In the locked-rotor condition, the total airgap power is dissipated as heat in the secondary. The power input per unit length (1 ft) of reaction rail was calculated by dividing the total airgap power by the number of poles times the pole pitch: (5 x 450.9 mm x 25.4 mm/25.4 mm = 2.254 m).

The reaction rail heat capacity per degree temperature per unit length was evaluated. For the purposes of this evaluation, the reaction rail cross section was broken up into two parts, the vertical section 42.1 cm^2 (6.52 $in.^2$) and the horizontal base section 12.1 cm^2 (1.87 $in.^2$). Only the vertical section was assumed to act as a heat sink for the energy transfered across the LIM airgap. Knowing the specific heat and density of aluminum, one can calculate the temperature rise per unit time as follows:

$$\frac{\Delta T}{\Delta t} = \frac{P_{\text{LIM AIRGAP}}/2.254\ m}{10.18\ \frac{kW \cdot s}{m \cdot {}^oC}} = 4.10 \times 10^{-2}\ P_{\text{LIM AIRGAP}} \times {}^oC/_{kW \cdot s}$$

$$\left(\frac{\Delta T}{\Delta t} = \frac{P_{\text{LIM AIRGAP}}/7.40\ ft}{1.83\ \frac{kW \cdot s}{ft \cdot {}^oF}} = 7.38 \times 10^{-2}\ P_{\text{LIM AIRGAP}} \times {}^oF/_{kW \cdot s}\right)$$

Table 9-11 lists the calculated reaction rail temperature rise per unit time and other pertinent information.

TABLE 9-11

CALCULATED REACTION RAIL TEMPERATURE RISE

Run No.	Dc Link Current, A	LIM Power, kW		Frequency Range, Hz		Remarks	Temperature Rise,	
		Input Power	Airgap Power				°C/S	°F/S
246	160	17.1	9.9	0	1	Transition	0.43	0.77
247	260	70	39.8	0	3.8	No transition	1.62	2.91
248	300	112	61.8	0	3.5	No transition	2.54	4.57
249	250	44.2	20.4	0	1	No transition	0.84	1.51
250	300	88.4	37.5	0	4	No transition	1.55	2.79
251	450	160.6	90.8	0	5	No transition	3.74	6.73
252	530	218	136.8	0	6	Transition and QSD	5.67	10.16
255	412	158	90.7	0	5	No transition	3.74	6.73
256	480	195	102.5	0	6	Transition and QSD	4.25	7.65
257	289	62.7	34.9	0	2	No transition	1.44	2.59
258	525	256	161.1	0	6	No transition	6.69	12.04
259	600	244	156.5	0	6	Transition	6.47	11.65

The maximum reaction rail temperature under typical starting conditions may be estimated by using the data from Run 258. The acceleration rate of the 132,000 kg (60,000-lb) TLRV would be 0.36 m/s (1.18 fps) per the measured thrust of 9.86 kN (2217 lbf). The time of exposure to the airgap power of a point on the reaction rail that is initially in line with the leading edge of the LIM would be:

$$t_{exp} = \sqrt{\frac{2 \times \text{physical motor length}}{\text{acceleration}}} = \sqrt{\frac{2 \times 2.55\ m}{0.36\ m/s^2}} = 3.76\ s$$

Therefore, the total reaction rail temperature rise at this point on the reaction rail would be 25.2°C (45.3°F) based upon the measured reaction rail temperature rise per unit time of 6.7°C/s (12.04°F/s). The maximum rail temperature, if an ambient rail temperature of 65.5°C (150°F) is presumed, would then be only 90.6°C (195°F).

TESTS RELATED TO THE WAYSIDE POWER SYSTEM

In addition to the acquisition of LIMPS performance data, another program objective was compilation of data reflecting the influence of the LIMPS on the wayside.

Harmonics produced by the converter are conducted through the power rails and appear in the supply power system. Further, the harmonics will be radiated from these conductors, and the vehicle as well, potentially producing local electromagnetic interference.

Despite the lower power level of the tests described in this report, some preliminary information was obtained in the following two areas.

Conducted EMI

Figure 9-38 shows the waveshape of the PDR current, which also flows in the power rails. The corresponding frequency spectrum, in bar chart form, shows the amplitudes of the first 25 harmonics. The harmonic content of the measured current is lower than that of the ideal no-load value. This finding is consistent with predictions, since at the measured power level (about 850 kW) the overlap angle is large (about 17 deg), and as the overlap increases the magnitudes of the harmonics decrease, with the higher orders decreasing more rapidly than the lower ones.

Radiated EMI

Broadband radiated emissions were measured in accordance with the procedures outlined in SAE Specification J551c.

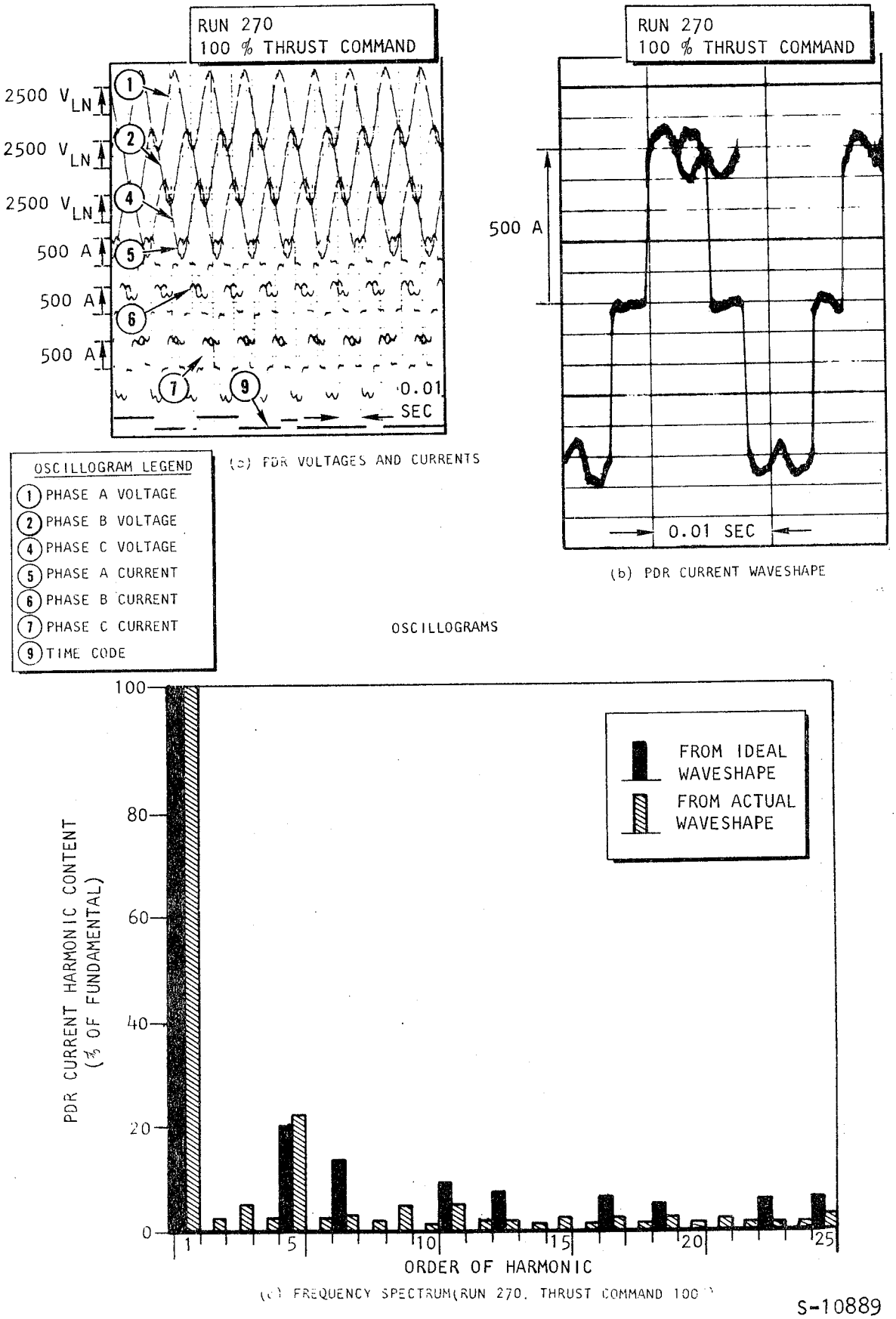

Figure 9-38. Phase Delay Rectifier Current Harmonics

Figure 9-39 shows the measurements of the emissions with all systems deenergized (ambient conditions), with the rail energized and the LIMPS not operating, and with the vehicle traveling at a speed of 15.6 m/s (35 mph).

Of particular interest is the prominence noted at approximately 202 MHz, which occurs with the rail energized, both with and without the vehicle operating. These circumstances lead to the hypothesis that the source of this frequency is external to the LIMPS and the wayside, but that the wayside in this configuration happens to be tuned to this frequency.

It should also be noted that no interference with test site communication facilities or electric power system relaying equipment was reported, either during or following the LIMPS field tests.

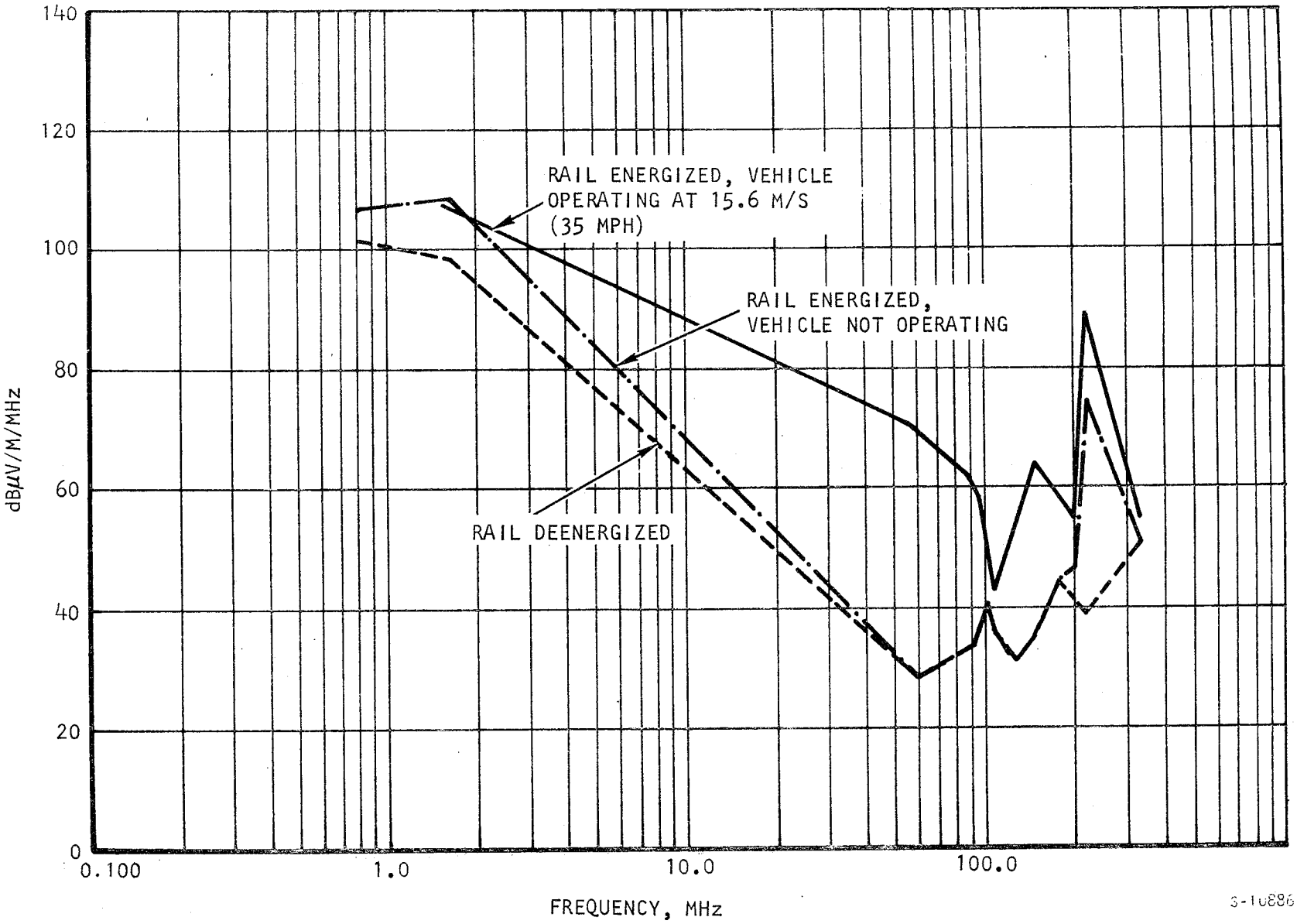

Figure 9-39. LIMPS Broadband Radiated Emissions